

DISSERTATION

**Natural Occurrence of Volatile
Mono-/Polyhalogenated and
Aromatic/Heteroaromatic Hydrocarbons from
Hypersaline Environments**

Torsten Krause

INAUGURAL - DISSERTATION

zur
Erlangung der Doktorwürde
der
Naturwissenschaftlich-Mathematischen Gesamtfakultät
der
Ruprecht-Karls-Universität Heidelberg

vorgelegt von
Diplomchemiker Torsten Krause
aus Preetz

Tag der mündlichen Prüfung: 07.04.2014

**Natural Occurrence of Volatile
Mono-/Polyhalogenated and
Aromatic/Heteroaromatic Hydrocarbons from
Hypersaline Environments**

Gutachter:

Prof. Dr. Heinz Friedrich Schöler

Prof. Dr. Peter Comba

Abstract

Volatile compounds are important substances for tropospheric and stratospheric chemistry. Anthropogenic sources of specific gases causing greenhouse effect, stratospheric ozone depletion, groundlevel ozone formation and aerosol formation are well known. Additionally, many natural sources, like oceans, wetlands and forests, have been investigated and assessed for their atmospheric impact previously.

While emissions from natural sources are often affiliated to biotic mechanisms, model reactions demonstrated also the importance of abiotic reactions. As such furan formation from catechol was successfully accomplished in this work using Fenton chemistry with a well defined biomimetic bispidine Fe^{2+} complex. Furthermore, abiotic formation of ethylfuran from ethylcatechol was demonstrated.

The work in hand also deals with the amalgamation of model reaction and the natural release of volatile compounds from Western Australian salt lakes and the Dead Sea.

On the one hand, Fe^{2+} was determined as the predominant active iron species in most natural hypersaline ecosystems. On the other hand, the release of several aromatic and nonaromatic hydrocarbons, furanoic compounds, sulfur and selenide containing compounds and halogenated compounds was investigated in correlation with geochemical parameters like pH, iron and organic carbon content. Benzene, toluene, ethylbenzene and xylene emissions, normally attributed to anthropogenic sources, correlated significantly with the iron content of Australian salt lake sediments demonstrating their genuine natural abundance. The same was observed for furan and hitherto mostly unnoticed n-alkyl chlorides with a C3-C8 carbon structure. Furthermore, a connection between emissions of methylfurans and their homologous methylthiophenes was observed indicating a mutual precursor and similar formation mechanism in the soils/sediments.

Aside from various known natural chlorinated, brominated and iodinated compounds, new compounds were identified like 3-chlorofuran. Additionally, natural tetrachloromethane formation in acidic salt lakes was postulated supported by various results.

Relevance of these compounds for the atmospheric chemistry was assessed with regard to ultrafine particle formation in Western Australia and reactive IO/BrO over the Dead Sea.

Zusammenfassung

Volatile Verbindungen sind wichtige Stoffe für die Troposphären- und Stratosphärenchemie. Anthropogene Quellen solcher Gase, die verantwortlich sind für den Treibhauseffekt, Ozonabbau in der Stratosphäre, Ozonbildung in der unteren Troposphäre und Partikelbildung, sind weitgehend bekannt. Auch wurden schon natürliche Quellen wie Ozeane, Feuchtgebiete und Wälder untersucht, um deren Bedeutung für die Atmosphärenchemie einzuschätzen.

Während die Emissionen von natürlichen Quellen oft biotischen Mechanismen zugeschrieben werden, zeigen Modellversuche, dass auch abiotische Reaktionen von Bedeutung sind. Als solche wurde die Furanbildung ausgehend von Catechol erfolgreich innerhalb dieser Arbeit mit Hilfe der Fenton-Chemie und einem biomimetischen Fe^{2+} -Bispidin-Komplex durchgeführt. Des Weiteren wurde die abiotische Bildung von Ethylfuran ausgehend von Ethylcatechol demonstriert.

Diese Arbeit stellt zudem eine Verbindung zwischen Modellversuchen und der natürlichen Freisetzung von volatilen Stoffen aus westaustralischen Salzseen und dem Toten Meer her.

Zum einen wurde Fe^{2+} als die vorherrschende Eisenspezies in den meisten natürlichen hypersalinen Ökosystemen bestimmt. Zum anderen wurde die Freisetzung aromatischer und nicht-aromatischer Kohlenwasserstoffe, Furane, schwefel- und selenhaltiger Stoffe sowie halogener Stoffe in Verbindung mit geochemischen Parametern wie dem pH-Wert, Eisen- und Organikgehalt der Proben untersucht. Emissionen von Benzol, Toluol, Ethylbenzol und Xylenen, welche normalerweise anthropogenen Quellen zugeschrieben werden, korrelierten signifikant mit dem Eisengehalt in australischen Sedimenten, was auf eine natürliche Quelle hinweist. Ähnliches wurde für Furan und die bisher wenig beachteten n-Alkylchloride mit einer C3- bis C8-Struktur beobachtet. Weiterhin zeigt sich anhand von korrelierenden Methylfuran- und Methylthiophen-Emissionen, dass diese Stoffe von derselben Vorläuferverbindung abstammen und die Bildungsmechanismen ähnlich sind.

Neben den zahlreichen bekannten natürlichen chlorierten, bromierten und iodierten Verbindungen wurden auch neue gefunden, wie das 3-Chlorfuran. Zudem wird ein natürliches Vorkommen von Tetrachlormethan aufgrund der Daten diskutiert.

Die Relevanz der gefundenen Stoffe für die Atmosphärenchemie wurde mit Bezug auf eine Partikelbildung in Westaustralien und auf reaktive IO/BrO-Spezies über dem Toten Meer erörtert.

Table of Contents

List of abbreviations.....	vi
1 Introduction	1
2 Abiotic processes in natural and model reactions	6
2.1 Fenton chemistry	6
2.1.1 Hydrogen peroxide	8
2.1.2 Redox-sensitive metals	9
2.1.3 Halides	10
2.1.4 Oxidation of organic matter	12
2.2 Model reactions	14
2.2.1 Organic model compounds	14
2.2.2 Iron species	15
2.2.3 Previous results from model reactions	16
3 Volatile organic and inorganic compounds	21
3.1 Aromatic hydrocarbons	21
3.2 Isoprene and monoterpenes	22
3.3 Furans	22
3.3.1 Ground level ozone	23
3.3.2 Secondary organic aerosol	24
3.4 Volatile sulfur and selenium compounds	25
3.4.1 Sulfur cycle	25
3.4.2 Sulfuric acid aerosol	26
3.5 Volatile organohalogens	27
3.5.1 Reactive halogen species in the atmosphere	28
3.5.2 Halogen-induced organic aerosol	30
4 Sampling sites	31
4.1 Southwest Australia	31
4.2 Dead Sea	35
5 Materials and methods	38
5.1 Chemicals	38
5.2 Sampling	39
5.3 Sample preparation	40
5.4 Model reactions	41
5.5 Instruments	41
5.5.1 Volatile compounds (purge and trap GC-MS)	41

5.5.2	Major and trace elements (XRF).....	45
5.5.3	Cations (ICP-OES).....	47
5.5.4	Anions (IC).....	47
5.5.5	Dissolved organic carbon (DOC).....	47
5.5.6	Inorganic carbon (Carbonate bomb)	48
5.5.7	Organic carbon (SC-analyser).....	48
5.5.8	pH, redox potential and conductivity	48
5.5.9	Dissolved oxygen	49
5.5.10	Water redox conditions (Pourbaix diagrams).....	51
5.5.11	Sediment redox conditions (Redox-Sensitive Tapes)	53
5.5.12	On-site detection and quantification of Fe ²⁺ /Fe ³⁺	54
5.5.13	Free and total chlorine.....	55
5.5.14	PTFE chamber.....	56
6	Novel model reactions	57
6.1	Abiotic furan formation from catechol with [Fe ^{II} (N ₂ Py ₂)(OTf) ₂].....	57
6.2	Abiotic ethylfuran formation from ethylcatechol.....	60
7	Soil and sediment profiles – An overview	61
7.1	Western Australia (pH 6-8).....	61
7.2	Western Australia (pH 4-6).....	66
7.3	Western Australia (pH 2-4).....	69
7.4	Sodom, Israel.....	72
8	Water samples – An overview	74
8.1	Western Australia.....	74
8.2	Sodom and the Dead Sea.....	76
9	Chemical parameters of hypersaline environments.....	77
9.1	Geochemical inventory of soils/sediments.....	77
9.2	Geochemical inventory of the aqueous phase	79
9.2.1	pH dependency of soluble constituents.....	81
9.3	Redox milieus and iron speciation	84
9.3.1	Aqueous phase.....	85
9.3.2	Sediments	89
10	Volatile compounds released from hypersaline environments	94
10.1	Overview	94
10.2	Aromatic hydrocarbons	103
10.3	Isoprene and terpenes	106
10.4	Furans.....	111

10.5	Volatile sulfur and selenide compounds	118
10.6	Chloroalkanes.....	122
10.7	Tetrachloromethane.....	127
10.8	Chloroalkenes.....	129
10.9	Bromoalkanes.....	130
10.10	Alkyl iodines	132
10.11	Mixed halogenated alkanes	135
11	Sources of VOX in hypersaline salt lakes.....	139
12	Assessment of aerosol formation over Australian salt lakes	143
13	Assessment of VOX contribution to BrO/IO over the Dead Sea	147
14	Conclusions and outlook.....	149
	References	154
	Appendix A – GC-MS calibration data.....	178
	Appendix B – Locations and pH of Western Australian salt lakes	180
	Appendix C – Soil/sediment sampling locations.....	182
	Appendix D – Water sampling locations.....	184
	Appendix E – Selected emission data	185
	Appendix F – Data obtained during PTFE chamber experiments.....	190
	Acknowledgements.....	201

List of abbreviations

AOP	Advanced oxidation process
ATSDR	Agency for Toxic Substances and Disease Registry
BTEX	Benzene, toluene, ethylbenzene and xylenes
BTX	Benzene, toluene and xylenes
BW	Botswana
CCN	Cloud condensation nuclei
CFC	Chlorofluorocarbons
CRM	Certified reference material
CV	Cap Verde
DFG	Deutsche Forschungsgemeinschaft
DFT	Density functional theory
DO	Dissolved oxygen
DOAS	Differential optical absorption spectroscopy
DOC	Dissolved organic carbon
DOM	Dissolved organic matter
DPD	N,N-Diethyl-p-phenylenediamine
Eh	Redox potential
GC-MS	Gas chromatography-mass spectrometry
GLT	Glass lined tubing
HDPE	High density polyethylene
IC	Ion chromatography
ICL	Israel Chemical Ltd.
ICP-OES	Inductively coupled plasma optical emission spectrometry
IR	Infrared
ISO	International Organization for Standardization
LDPE	Low density polyethylene
LOD	Limit of detection
MIR scale	Maximum Incremental Reactivity scale
MR	Mauritania
NA	Namibia
NASA	National Aeronautics and Space Administration
NDIR	Nondispersive infrared
NIST	National Institute of Technology
NOM	Natural organic matter

OM	Organic matter
PSS-78	Practical salinity scale
PSU	Practical salinity units
PTFE	Polytetrafluoroethylene
PVC	Polyvinyl chloride
RHS	Reactive halogen species
RST	Redox-Sensitive Tapes
RU	Russia
SC	Sulfur/carbon
SOA	Secondary organic aerosol
SVOC	Semi-volatile organic compound
T	Temperature
THM	Trihalomethane
UN	United Nations
UNEP	United Nations Environment Programme
USGS	United States Geological Survey
UV	Ultraviolet
UZ	Uzbekistan
VIS	Visible
VOC	Volatile organic compound
VOX	Volatile organohalogen
VSC	Volatile sulfur compound
VSeC	Volatile selenide compound
VVOC	Very volatile organic compound
WHO	World Health Organization
XOA	Halogen-induced organic aerosol
XRF	X-ray fluorescence

1 Introduction

Mankind has a significant impact on the global climate change observed during the last decades. Deforestation, biomass burning and production of hazardous volatile compounds released to the atmosphere have a negative effect on the biosphere. Non-sustainable land use leads in parts of the world to land degradation, desertification and secondary salinisation (Lal et al., 1989). Increasing release of greenhouse gases, like CO₂ and CH₄, have actuated global warming (Lashof and Ahuja, 1990) accompanied by extreme weather events (Easterling et al., 2000) since the industrial revolution.

Furthermore, emissions of anthropogenic chlorofluorocarbons (CFC) and some chlorinated compounds catalyse depletion of ozone in the stratosphere, which protects life on earth against short-wavelength and most mid-range UV radiation from 210 to 315 nm (Solomon, 1999). With the Montreal Protocol of 1989 production of several halogenated substances, suspected for stratospheric ozone depletion, started to phase out. As a result CFC mixing ratios in the atmosphere are now constant or even decrease again (UNEP, 2009).

In 1992 the non-binding United Nations Framework Convention on Climate Change treaty was negotiated to limit global greenhouse gas emissions and entered force in 1994 (UN, 1992). In 1997 the supplementary Kyoto Protocol was adopted which established legally binding obligations for developed countries to reduce their greenhouse gas emissions (UN, 1997). Not affected by legal restriction of the Kyoto Protocol are developing countries, whereas the USA never signed the treaty and Canada resigned from the treaty in 2011. Other than the effective Montreal Protocol the Kyoto Protocol fell short of expectations as emissions of greenhouse gases like CO₂ still increase (Schiermeier, 2012).

CFC and greenhouse gases are not the only gases that have an impact on the climate (Figure 1). Noteworthy are various compounds that are aerosol precursors, like sulfur containing compounds that are oxidised to acidic H₂SO₄ (Charlson et al., 1987), or volatile organic compounds, like monoterpenes (Lee et al., 2006). Aerosol particles influence the local climate, radiation budget and as cloud condensation nuclei they have an impact on cloud formation and precipitation (Charlson et al., 1992).

Aromatic hydrocarbons, like benzene and toluene, emitted from fuel combustion are not only directly harmful for organisms but are also a source for ground level ozone, which, as a strong oxidant, damages plants, mucus membranes and the respiratory system of organisms (Krupa and Manning, 1988).

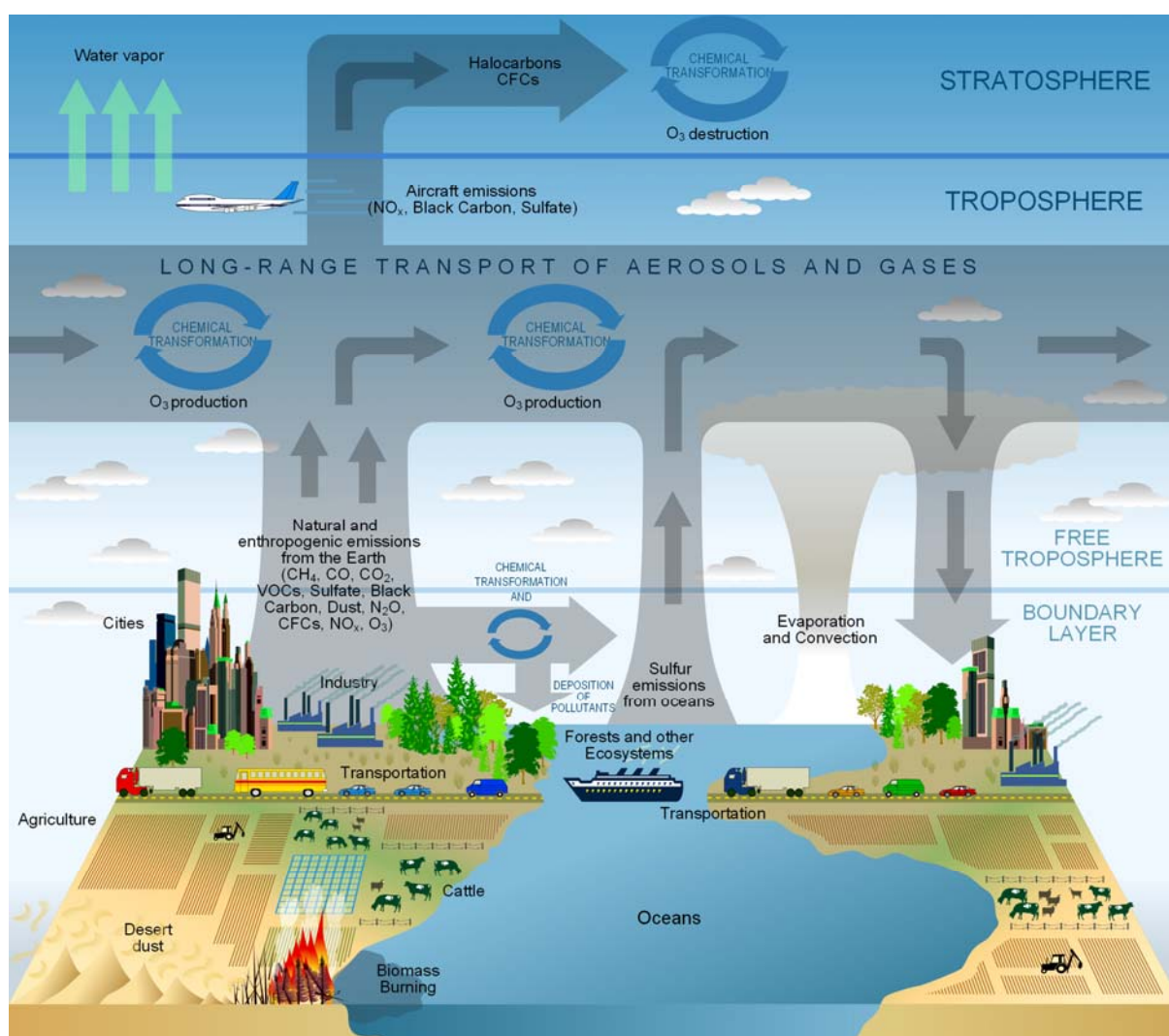


Figure 1. Land air exchange of atmospheric relevant gases and their impact on atmospheric chemistry. Image source: Wikimedia Commons dating from July 15th, 2013. Original illustration by Philippe Rekacewicz (U.S. Climate Change Science Program, 2003). Image resides in the public domain and is reprinted by courtesy of the U.S. Climate Change Science Program.

The majority of these tropospheric and stratospheric relevant gases is of anthropogenic origin, however, there are also natural sources. CO_2 is naturally released via autotrophic and heterotrophic respiration of plants and microorganisms, respectively (Falkowski et al., 2000). Methane is produced by anaerobic organisms (Thauer, 1998) and non-methane volatile organic compounds, most of all isoprene (Sharkey et al., 2008), are emitted by plants among others, while marine algae are an important source for atmospheric sulfur species as they emit dimethyl sulfide (Malin and Erst, 1997). Furthermore, atmospheric abundance of several volatile halogenated compounds (VOX) has been accounted to biotic sources like plants and algae (Gribble, 2010).

Aside from the biotic sources, abiotic formation pathways have drawn attention to the scientific community like iron catalysed Fenton chemistry. Model reactions have

demonstrated abiotic formation of various atmospheric relevant compounds, like halogenated compounds, and were successfully applied to natural soils and sediments (Schöler and Keppler, 2003).

Especially, the natural biotic and abiotic halogenation processes have been in the scientific focus over the last decades. While halogenated compounds were regarded as mostly anthropogenic for some time, a flood of scientific research revealed almost 5000 naturally occurring halogenated compounds from various marine and terrestrial environments (Gribble, 2010). With the expansion of soil salinity in arid and semi-arid regions, like the Aral Sea, natural halogenation processes might become more and more important for the VOX budget in the atmosphere (Kotte et al., 2012).

Investigation of these terrestrial saline to hypersaline ecosystems as sources for natural volatile organic compounds, most of all VOX, and their impact on local atmospheric chemistry has been the goal of the DFG research unit 763 HaloProc. Salt lakes all over the globe from South America to Africa, Asia and Australia were investigated. Samples were collected for analysis of microbiological activity (Emmerich et al., 2012) and the release of volatile compounds. Additionally abiotic formation mechanisms for the observed compounds were investigated. On-site measurements included atmospheric halogen activation (Holla, 2013) and aerosol formation over salt lakes (Kamilli et al., 2013).



Figure 2. Western Australian salt lake photographed in 2012. Image: T. Krause CC BY-SA 4.0.

As part of HaloProc this work deals with the abiotic formation of furans and land-air exchange of various natural volatile compounds from two different hypersaline environments, namely the Dead Sea, Israel and multifarious salt lakes in Western Australia (Figure 2). The analysis of volatile compounds was performed by gas chromatography-mass spectrometry (GC-MS) for which a new purge and trap system was developed to enable accurate and stable measurements of trace gases. Emissions were correlated to various geochemical parameters in

order to unravel important formation parameters and for comparison with model reactions. Analysis of hypersaline samples with regard to their composition is not trivial as high loads of salts need to be diluted prior to liquid injection measurements as used by ion chromatography (IC), for anions, or inductively coupled plasma optical emission spectrometry (ICP-OES), for cations. As a result some constituents cannot be quantified as they are below the limit of detection. Alternatively, solid phase measurements with X-ray fluorescence (XRF) was performed to measure trace elements.

Not less important than the total amount of constituents in a sample are its chemical properties like oxidation state and ligands, especially for iron. Iron speciation is of relevance for mechanistic studies within salt lakes and model reactions alike. To assess the predominant iron species in hypersaline environments various redox milieu studies of salt lakes were performed.

Key aspect of the work in hand is to assess potential geochemical parameters that play a role for emissions of various volatile compounds from hypersaline environments. Furthermore, the release of these compounds is discussed with regard to observed local atmospheric phenomena. On the one hand, there is the formation of ultrafine particles in the vicinity of Western Australian salt lakes which have been postulated to impede cloud formation and thus precipitation over the agricultural land (Junkermann et al., 2009; Kamilli et al., 2013). On the other hand, VOX released from water and soils at the Dead Sea could be an initial source for reactive bromine and iodine species in the boundary layer of the Dead Sea (Hebestreit et al., 1999; Zingler and Platt, 2005).

Structure of this work

The state of knowledge concerning Fenton chemistry, the catalytic decomposition of H_2O_2 by a transition metal, as one of the most important abiotic reaction mechanisms is depicted in **Chapter 2**. Aside from the mechanism behind the reactions, sources of transition metals, most of all iron, and H_2O_2 in natural environments is assessed. A special focus is also devoted to Fenton chemistry in the presence of halides yielding reactive halogen species.

Furthermore, the role of Fenton chemistry for abiotic polar and volatile organic compound formation is discussed exemplary on several model reactions involving catechol as a model compound for natural organic matter. To extend the knowledge about mechanisms involved in natural Fenton model chemistry a well defined bispidine Fe^{2+} complex is employed.

Classes of volatile compounds, such as aromatic hydrocarbons, isoprene and monoterpenes, furans, sulfur/selenide containing compounds and halogenated compounds relevant to this work, are introduced in **Chapter 3**. Common sources are assessed and their impact on atmospheric chemistry as precursors for aerosol, ground level ozone and reactive halogen species is discussed.

Aerosol formation and its impact on the local climate as well as BrO/IO formation is delineated in **Chapter 4** as relevant atmospheric phenomenon for the sampling sites in Western Australia and the Dead Sea, respectively.

Methodical approaches to monitor model reactions and analyse natural samples and model reactions on-site and in the laboratory are summarised in **Chapter 5**. Among others the conversion of the employed purge and trap system for analyte preconcentration prior to GC-MS measurements from dynamic to static cooling is described.

Chapter 6 deals with the results from new model reactions on furan formation employing a biomimetic bispidine Fe^{2+} complex. Furthermore, abiotic ethylfuran formation using Fenton-like conditions is evaluated by employing an ethylated catechol precursor.

Insights from these and previous model reactions are auxiliary for the interpretation of volatile compounds released from natural samples of Western Australia and the Dead Sea introduced in **Chapter 7** and **Chapter 8** and elaborated in more detail within **Chapter 9**. As such emission data is compared in **Chapter 10** with various geochemical parameters to unravel patterns and possible formation mechanisms. Furthermore, novel natural compounds that were identified are introduced.

Separately, natural halogenation processes derived from Fenton chemistry as well as other processes are described in **Chapter 11** to account for the observed VOX emissions.

The importance of emission data obtained from natural samples for local atmospheric chemistry is assessed in **Chapter 12** and **Chapter 13** with regard to particle formation in Western Australia and BrO/IO formation over the Dead Sea, respectively.

The work is concluded by a summary of the obtained scientific insights on natural emissions from abiotic model reactions and hypersaline ecosystems and their role for local atmospheric chemistry. Furthermore, an outlook is presented outlining investigations considered necessary to further unravel formation, emission and atmospheric impact of volatile compounds from hypersaline environments.

2 Abiotic processes in natural and model reactions

Natural organic matter (NOM) as well as anthropogenic organic matter is continuously transformed by abiotic and biotic processes in the biosphere. These reactions include oxidation, i.e. to complete mineralisation, or reduction of organic matter (OM) depending on the redox milieu, which is subdivided into oxic, suboxic and anoxic. At the end of these transformation processes are, among others, volatile products with atmospheric relevance, e.g. CO₂, or organic acids that play a key role in the mobilisation and bioavailability of minerals. One of the key reaction mechanisms is Fenton chemistry as discussed in Chapter 2.1, with its applications in model reactions assessed in Chapter 2.2.

2.1 Fenton chemistry

The Fenton reaction dates back to 1894 and is named after H. J. H. Fenton who discovered the oxidative power of a Fe²⁺ and H₂O₂ mixture in the reaction with tartaric acid (Fenton, 1894). Haber and Weiss postulated a now widely accepted mechanism for the formation of highly reactive free OH radicals (Eq. 1) under the conditions employed by Fenton (Haber and Weiss, 1932).



Furthermore, Fe³⁺ is reduced by H₂O₂ to Fe²⁺ in the so called Fenton-like reaction and thus completes the catalytic iron cycle of the Fenton reaction (Barb et al., 1951). In the Fenton-like reaction hydroperoxyl radicals as well as superoxide radical anions are formed which are less reactive than OH radicals.

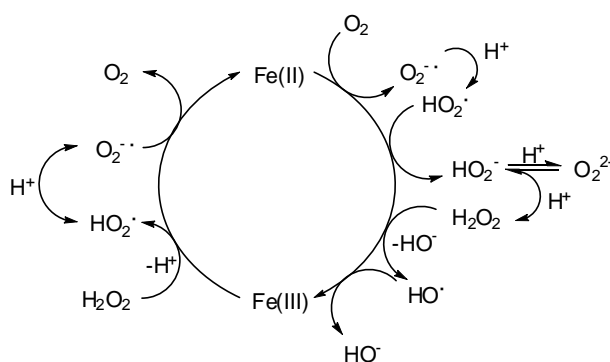


Figure 3. Schematic iron cycle of the Fenton and Fenton-like chemistry.

An overview of the basic iron cycle under Fenton conditions is illustrated in Figure 3. The included autoxidation of Fe^{2+} reducing O_2 to superoxide will be discussed in chapter 2.1.1.

Alternatively to the iron catalysed decomposition of H_2O_2 , photolysis with UV radiation ($\lambda < 400 \text{ nm}$) can be employed to generate OH radicals. Furthermore, radiation of 290-400 nm is employed to enhance the Fenton-like reaction by reducing the Fe^{3+} species $\text{Fe}(\text{OH})^{2+}$ to Fe^{2+} while generating free OH radicals as depicted in Eq. 2 (Kim and Vogelpohl, 1998). This light supported type of Fenton chemistry is known as photo-Fenton reaction.



Depending on reaction conditions the active reactive species may differ from the free OH radicals proposed by Haber and Weiss. One alternative is that iron coordinated by strong chelator ligands binds H_2O_2 to its coordination sphere inhibiting the release of free radicals. Another explanation is that Fe^{2+} is oxidised by H_2O_2 to Fe^{4+} , a transient intermediate which is a more selective oxidant than free OH radicals. Fe^{4+} can be stabilized at circumneutral pH or with the aid of strong ligands (Bray and Gorin, 1932; Yamazaki and Piette, 1991). The different reaction paths are illustrated in Figure 4 according to Gozzo (2001).

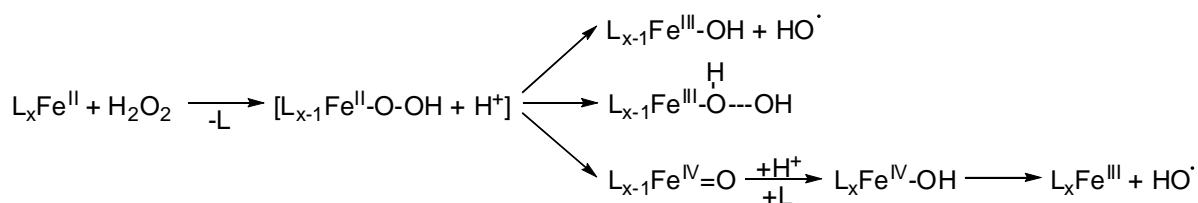


Figure 4. Reaction of Fe^{2+} with H_2O_2 and the formation of three possible reactive oxidation species. Illustration adopted from Gozzo (2001).

To understand the relevance of Fenton chemistry in natural environments the sources of H_2O_2 , the role of transition metals like iron and the influence of halides will be elaborated in the next chapters. Furthermore, the reaction mechanism involving oxidation and halogenation of organic matter will be discussed.

2.1.1 Hydrogen peroxide

Fenton and Fenton-like reactions require H_2O_2 , a substance that has multifarious natural sources in the biosphere as will be discussed in the following paragraphs.

H_2O_2 is abundant in the atmospheric gas phase, clouds and water droplets (Olszyna et al., 1988) and is transported to soils and surface waters by rain (Yoshizumi et al., 1984). Elevated concentrations of H_2O_2 were observed during thunderstorms implying formation through electrostatic discharge (Kok, 1980; Zuo and Deng, 1999; Deng and Zuo, 1999) and near fire plumes (Kok et al., 1978). Additionally, reaction of hydroperoxyl radicals with each other (Eq. 3) is an important atmospheric radical termination producing H_2O_2 (Levy, 1971).



An additional source for atmospheric H_2O_2 is the reaction of ozone with isoprene, monoterpenes and alkenes, as expressed by Eq. 5 (Becker et al., 1990), via a Criegee biradical shown in Eq. 4 (Martinez et al., 1981) with R = protons, alkyl or acyl groups.



Photochemical reactions are a common source for H_2O_2 in terrestrial (Draper and Crosby, 1983), marine (Yocis et al., 2000) and atmospheric (Faust et al., 1993) aqueous environments. The underlying mechanism is the photo ionisation or photo excitation of dissolved organic matter (DOM) by sunlight producing free electrons or excited electrons that can reduce dissolved oxygen (DO) to superoxide as shown in Eq. 6 (Cooper et al., 1988). Alternatively, as depicted in Eq. 7, superoxide is formed by the autoxidation of transition metals like iron (Weiss, 1935; Aust et al., 1985; Voelker et al., 1997) and manganese (Kessick and Morgan, 1975), though this reaction is constrained under acidic conditions and in the presence of chloride (Stumm and Lee, 1961; Millero, 1985, 1989; Trapp and Millero, 2007).



Superoxide either undergoes a disproportionation reaction (Petasne and Zika, 1987) or is reduced further, e.g. by Fe^{2+} (Rush and Bielski, 1985), yielding H_2O_2 as shown in Eq. 8 and 9, respectively.



Additionally, excretion of H_2O_2 by certain fungi species (Koenigs, 1974) and brown algae (Küpper et al., 2002) are known biogenic sources of H_2O_2 in soil and aquatic systems. Furthermore, H_2O_2 plays a significant role in bacterial metabolism (Pardieck et al., 1992).

2.1.2 Redox-sensitive metals

Fenton chemistry was developed on iron chemistry, the fourth most abundant element in the Earth's crust by weight (Taylor, 1964). Iron exists in the biosphere as ferrous iron (Fe^{2+}) and ferric iron (Fe^{3+}) in minerals, in organic complexes and as dissolved iron in aquatic systems. Organic iron complexes play an important role as cofactors in enzymatic biochemistry. Regardless of the species, iron is an important electron transfer mediator in biogenic and abiotic processes between oxygen and reduced organic matter. Figure 5 outlines the general iron cycle in natural environments according to Stumm and Sulzberger (1992).

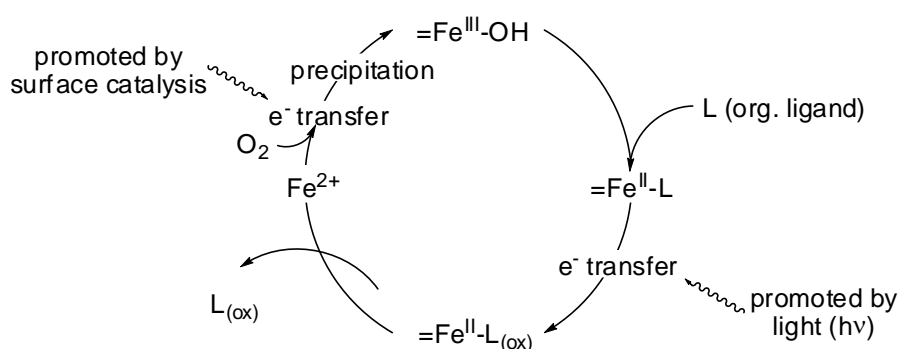


Figure 5. Iron cycle in natural environments adopted from Stumm and Sulzberger (1992).

Furthermore, Fenton chemistry is not limited to iron as redox catalyst but is viable with several redox-sensitive elements. Production of oxidising species in Fenton-like reaction at circumneutral pH increases according to the following order: $\text{Ni}^{2+} < \text{Mn}^{2+} < \text{Fe}^{3+} < \text{Co}^{2+} < \text{Cr}^{3+} < \text{Cu}^{2+}$ (Strlič et al., 2003). In the reaction of Cu^+ with H_2O_2 the formation of OH radicals plays only a subdued role, while the actual active oxidant is Cu^{3+} (Johnson et al., 1985; Pham et al., 2013).

In general, it is postulated that a mixture of low valent transition metals and H_2O_2 showing oxidative properties, called Fenton-like reagents, react via formation of a transient metal-hydrogen peroxide complex. This complex can decompose yielding OH radicals, an oxidised

reactive metal species ($M^{(n+2)}$) or react directly with organic substrates depending on their molecular composition (Goldstein et al., 1993; Goldstein and Meyerstein, 1999).

Aside from Fenton chemistry, these transition metals are also effective catalysts for other redox reactions involving NOM.

2.1.3 Halides

An interesting twist of Fenton chemistry can be observed when halides are abundant in the aqueous reaction mixture. Halides are known to react with OH radicals yielding less reactive halogen species. The general reaction mechanism is shown in Eq. 10-11 with $X = \text{Br}$ (Matheson et al., 1966), $X = \text{Cl}$ (Anbar and Thomas, 1964; Jayson et al., 1973) and $X = \text{I}$ (Weiss, 1937).



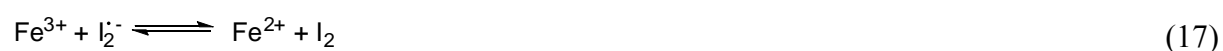
The reactivity of OH radicals with halides decreases from iodine to chlorine (Evans et al., 1952) according to the increasing electronegativity. Furthermore, Matheson et al. (1966) postulated the recombination of bromine radicals, Wu et al. (1980) for chlorine radicals and Weiss (1937), Grossweiner and Matheson (1957) formulated the recombination of iodine radicals (Eq. 12).



More recently, the mechanism for Cl_2 evolution was summarized by Yu and Barker (2003) involving the reactions shown in Eq. 13 and 14.



Additionally, the oxidative power of Fe^{3+} is high enough to oxidise iodide directly through a clock reaction to I_2 (Eq. 15-17) (Fudge and Sykes, 1952).

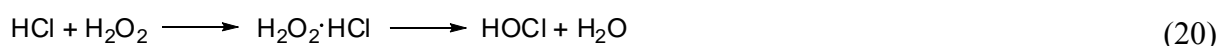


Counteracting reactive halogen species (RHS) formation is their reductive depletion by Fe^{2+} (Jayson et al., 1973) as well as H_2O_2 (Yu and Barker, 2003) to halides.

Moreover, the reaction of H_2O_2 with halides is not restricted to iron catalysed Fenton reaction but halides are also directly oxidised by H_2O_2 yielding RHS. H_2O_2 reacts in the presence of iodide under acidic conditions to hypoiodous acid described by the modified Iodine Clock reaction shown in Eq. 18 (Copper and Koubek, 1998) which is based on the Landolt reaction (Landolt, 1886, 1887). This reaction is probably the main source of iodocarbon in the metabolism of brown algae (Küpper et al., 2008).



A similar reaction mechanism was postulated for the reaction of bromide and chloride with hydrogen peroxide as illustrated in Eq. 19 (Solyanikov and Denisov, 1968) and Eq. 20 (Skudaev et al., 2008), respectively.



Likewise, as in the radical reaction described above (Eq. 10-11), the reactivity between halide and H_2O_2 decreases from I^- to Cl^- (Evans et al., 1952). Furthermore, H_2O_2 is able to reduce the hypohalous acids to hydrogen halides under evolution of oxygen reducing the yield of HOCl (Connick, 1947) and HOBr (Von Gunten and Oliveras, 1997). Hypoiodous acid or iodine even catalyse the decomposition of H_2O_2 as illustrated in Figure 6 (Bray and Liebhafsky, 1931; Peard and Cullis, 1951).

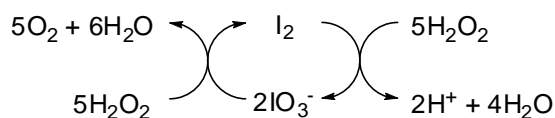


Figure 6. Catalytic decomposition of H_2O_2 by iodine.

This shows the complicated mechanism underlying Fenton reaction and side reactions in the presence of halides yielding RHS like X , X_2^- , X_2 , XOH , XO^- . Additionally, X_2 , XOH and XO^- stand in equilibrium to one another as a function of pH (Eq.21) (Barcellos da Rosa, 2003).



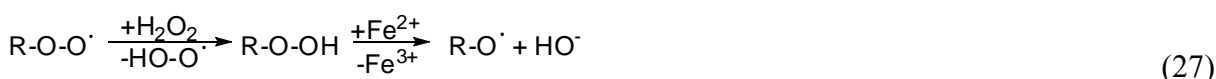
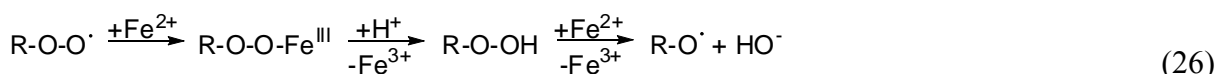
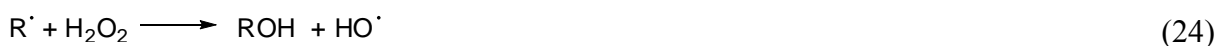
2.1.4 Oxidation of organic matter

The reactive radical species from Fenton chemistry, namely HO₂ and OH radicals (refer to Chapter 2.1) oxidise organic matter eventually to complete mineralisation. Advanced oxidation processes (AOP) make use of this high oxidative power associated with Fenton, Fenton-like and photo-Fenton chemistry to detoxify organic pollutants during water treatment (Kim and Vogelpohl, 1998; Andreozzi et al., 1999). Side reactions appear when AOP are used in the presence of halides, because of RHS formation (see chapter 2.1.3) and subsequent halogenation of OM (Kiwi et al., 2000; Grebel et al., 2010).

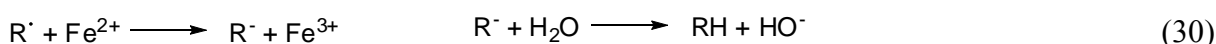
In his review, Gozzo (2001) summarised OM oxidation with initial proton abstraction by a radical (Eq. 22) while Neyens and Baeyens (2003) also mentioned the addition of radicals to unsaturated C-C bonds in their own review (Eq. 23).



The propagation of radical chain reactions are summed up in Eq. 24-28 (Neyens and Baeyens, 2003).



The chain reactions are terminated by iron oxidation or reduction as well as possible dimerisation of carbon radicals (Eq. 29-31) (Gozzo, 2001; Neyens and Baeyens, 2003).



Furthermore, secondary alcohols are oxidised to ketons (Merz and Waters, 1947) while less reactive primary alcohols are converted directly to carboxylic acids (Sato et al., 1997). Figure 7 shows the Fe³⁺ mediated pathway for the oxidation of primary and secondary alcohols.

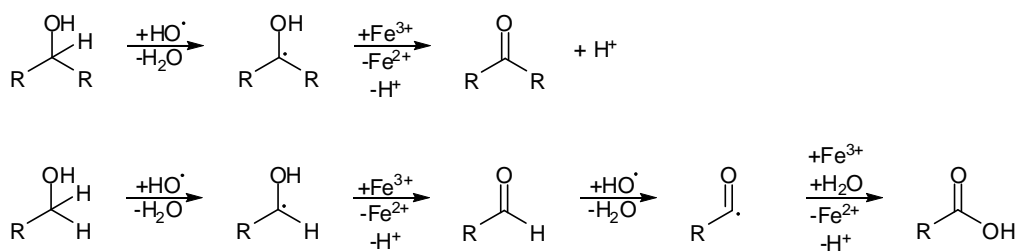


Figure 7. Iron promoted oxidation of secondary and primary alcohols.

In the presence of halides, several halogenation mechanisms are conceivable. Eq. 32 shows the iron mediated ligand transfer of a halide to an organic radical (Minisci and Fontana, 1994), while Eq. 33 takes the formation of halogen radicals, as elaborated in chapter 2.1.3, into account (Kiwi et al., 2000).



Further reactions are electrophilic addition of halogens to alkenes (Eq. 34) (Tarbell and Bartlett, 1937; Roberts and Kimball, 1937; Ruasse, 1990) and, analogous to OH radicals, the addition of free halogen radicals to unsaturated carbon bonds (Eq. 35).



Aside from oxidation by radicals, Fe^{4+} is, under certain conditions as described in chapter 2.1, the main reactive species in the Fenton reaction. A postulated mechanism for the oxidation of hydrocarbons to alcohols (Tung et al., 1992) and halogenation (Barton et al., 1996) by Fe^{4+} are presented in Figure 8 and Figure 9, respectively.

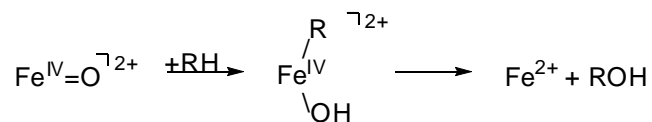


Figure 8. Oxidation mechanism for hydrocarbons to alcohols by Fe^{4+} adopted from Tung et al. (1992).

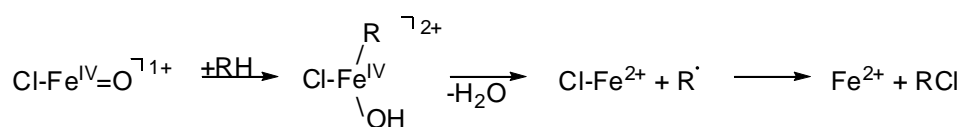


Figure 9. Halogenation mechanism for hydrocarbons by Fe^{4+} adopted from Barton et al. (1996).

2.2 Model reactions

As illustrated in the previous chapters, chemical reactions in soils and aqueous systems are manifold and complicated. To evaluate natural abiotic processes it is inevitable to simulate the reactions under controlled conditions with a reasonable amount of reactants and parameters. In the last two decades the degradation mechanisms of organic model compounds, such as catechol, under Fenton and Fenton-like conditions with a variety of iron species was elaborated. A detailed record of some model systems is given in the following chapters.

2.2.1 Organic model compounds

Organic matter in natural environments is an umbrella term for a diverse array of organic molecules including residues of plants and animals, cells and tissues of various organisms as well as their metabolic excreta. All these substances are found in different stages of decomposition. The major fraction of OM is classified as humic acid, compounds of high molecular weight with a complex structure containing numeral carboxylic and phenolic groups. Humic acids are closely related to fulvic acids which are of lower molecular weight. A model of humic substance is illustrated in Figure 10, composed of lignin, peptide, cellulose and chitin groups as well as chelated minerals (Schöler and Keppler, 2003).

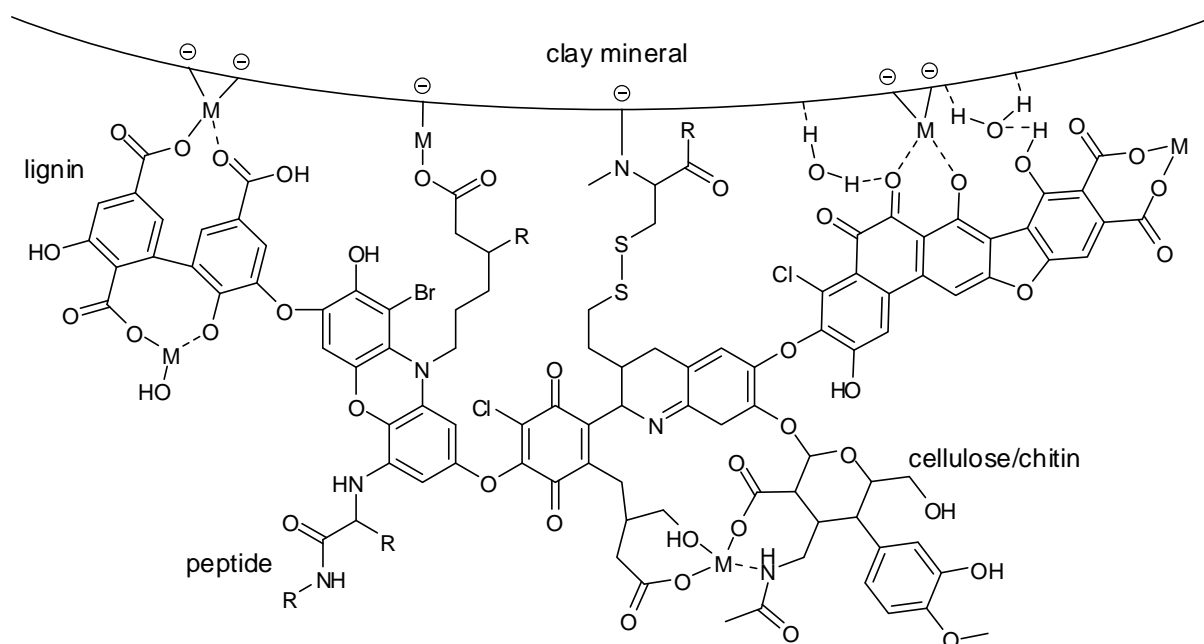


Figure 10. Model of humic acid adopted and modified from Schöler and Keppler (2003).

For model reactions the structure of humic acid is broken down to its phenolic groups with multifarious moieties, including alcohols, halogens, methyl groups and alkyl chains.

2.2.2 Iron species

As outlined in chapter 2.1.2, iron is the fourth most abundant element by weight in the Earth's crust and an important natural redox catalyst for organic matter. Moreover, it is the catalyst in Fenton chemistry producing highly reactive oxidants. Iron can be found in its two main oxidation states $\text{Fe}^{2+}/\text{Fe}^{3+}$ in minerals, like hematite, olivine, pyrite, etc., as dissolved iron and as organic iron complexes, e.g. in humic acid. Furthermore, heme-iron complexes play a key role as active sites in enzymes like catalase and cytochrome.

The most common employed iron species are soluble Fe^{2+} and Fe^{3+} salts, e.g. sulfates. Additionally, there have also been several experiments with iron minerals (Althoff et al., 2010).

A new approach, and part of this thesis, is the evaluation of biomimetic nonheme iron complexes to simulate natural chelating characteristics of OM. One such complex is $[\text{Fe}^{\text{II}}(\text{N}_2\text{Py}_2)(\text{OTf})_2]$ (Börzel et al., 2002). This iron bispidine complex features a well-defined coordination sphere due to its rigid adamantane backbone (Comba et al., 2010). Additionally, the complex has an octahedral coordination sphere with 4 sites occupied by the bispidine ligand restricting reactions to the remaining two sites (Figure 11). Natural bispidine structures are found in various alkaloids like, for example, sparteine (Messer et al., 2005).

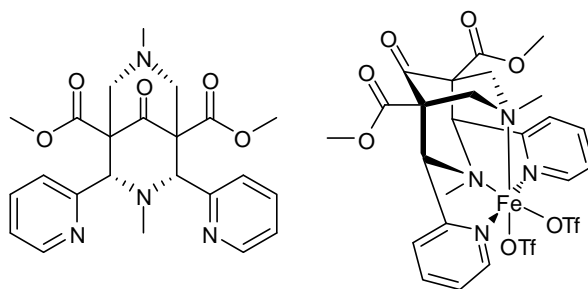


Figure 11. Structure of the bispidine N_2Py_2 ligand (left) and geometry of the $[\text{Fe}^{\text{II}}(\text{N}_2\text{Py}_2)(\text{OTf})_2]$ complex (right).

The $[\text{Fe}^{\text{II}}(\text{N}_2\text{Py}_2)(\text{OTf})_2]$ complex has already been studied on its coordination with catechol (Comba et al., 2011) and its redox reaction with H_2O_2 (Bukowski et al., 2006). Another advantage of the iron complex over iron salts is its stability in solution and anticipated reaction enhancement while impeding side reactions.

2.2.3 Previous results from model reactions

While AOP techniques were intensively studied for hazardous waste water treatment (Huang et al., 1993; Potter and Roth, 1993), their relevance for natural abiotic chemistry was disregarded for a long time. A turning point was, with regard to abiotic formation of halomethanes (Figure 12), a publication by Keppler et al. in 2000. They demonstrated that during oxidation of guaiacol by an electron acceptor, such as iron, halides are alkylated by the methoxy group (Keppler et al., 2000).

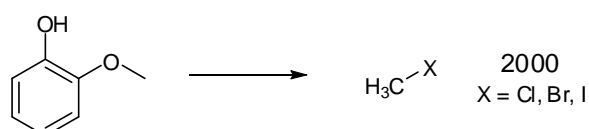


Figure 12. Schematic formation of methyl halides from guaiacol (Keppler et al., 2000).

A suite of investigations on the degradation of phenolic substances, predominantly with catechol, under Fenton and Fenton-like conditions was initiated. Figure 13 illustrates the abiotically formed products of catechol in chronologic order.

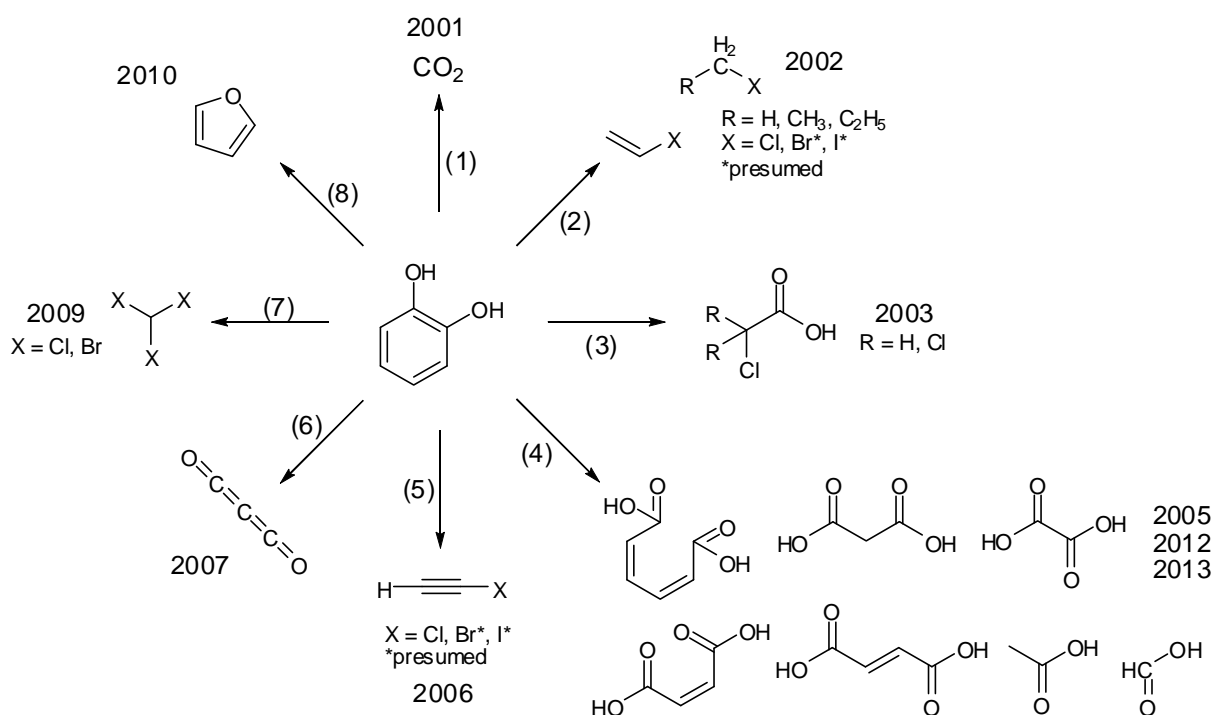


Figure 13. Degradation of catechol by Fe^{3+} or under Fenton and Fenton-like condition to (1) carbon dioxide (Pracht et al., 2001), (2) chloroethene and chloroalkanes (Keppler et al., 2002), (3) chlorinated acetic acid (Fahimi et al., 2003), (4) muconic-, formic-, acetic-, oxalic-, malonic-, fumaric- and maleic acid (Zazo et al., 2005; M'Hemdi et al., 2012; Studenroth et al., 2013), (5) chloroethyne (Keppler et al., 2006), (6) carbon suboxide (Huber et al., 2007), (7) trihalomethanes (Huber et al., 2009), (8) and furan (Huber et al., 2010; Krause et al., 2013).

Pracht et al. (2001) took a closer look on the oxidative capabilities of Fe^{3+} demonstrating that it is able to mineralise catechol to CO_2 while Keppler et al. (2002) proved the formation of chloroethene and chloroalkanes under Fenton-like conditions in the presence of chloride from catechol. Degradation of catechol to di- and mono carboxylic acids was evaluated for AOP under Fenton conditions (Zazo et al., 2005; M'Hemdi et al., 2012) and reinvestigated using Fenton-like conditions under the aspect of natural abiotic chemistry by Studenroth et al. (2013). Furthermore, Fenton-like conditions with abundance of halides yielded chloroethyne (Keppler et al., 2006), carbon suboxide (Huber et al., 2007) and trihalomethanes (Huber et al., 2009).

Based on the evolution of methyl halides from guaiacol (Keppler et al., 2000), Keppler et al. formulated a reaction mechanism that was later adapted to explain emission of different alkyl halides as shown in Figure 14 (Keppler et al., 2003). This mechanism is based on a nucleophilic substitution reaction, most likely $\text{S}_{\text{N}}2$, promoted by the coordination of iron to the oxygen atom linking the aromatic ring with the alkyl group. Additionally, the substitution is assumed to be synchronous with the oxidation of guaiacol to 1,2-benzoquinone by Fe^{3+} , thus decreasing the activation energy.

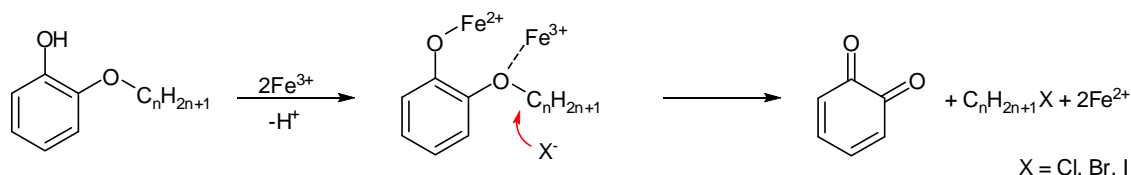


Figure 14. Postulated reaction mechanism for methyl halide formation from guaiacol (Keppler et al., 2000; Keppler et al., 2003).

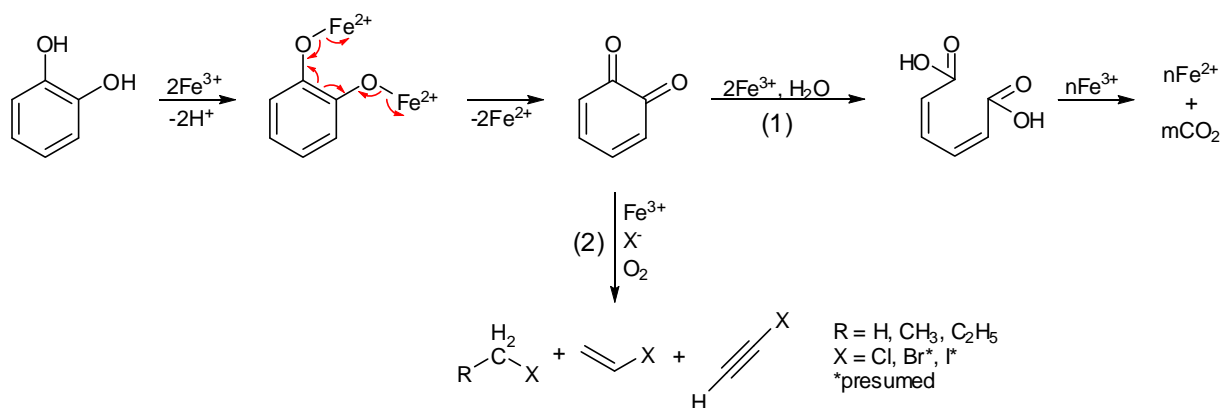


Figure 15. Oxidation of catechol to 1,2-benzoquinone as postulated intermediate during (1) mineralisation to CO_2 (Pracht et al., 2001) and (2) degradation to volatile halocarbons (Keppler et al., 2002; Keppler et al., 2006).

The oxidation of catechol by Fe^{3+} to 1,2-benzoquinone is assumed to be an intermediate state during its mineralisation (Pracht et al., 2001) and the formation of saturated and unsaturated halocarbons (Keppler et al., 2002; Keppler et al., 2006) as shown in Figure 15.

Huber et al. postulated, based on their research with several phenolic derivatives, the formation of 1,2,4,5-tetrahydroxybenzene and, depending on where the C-C bonds in this intermediate is cleaved (Figure 16), the release of carbon suboxide (Huber et al., 2007) and trihalomethanes (Huber et al., 2009).

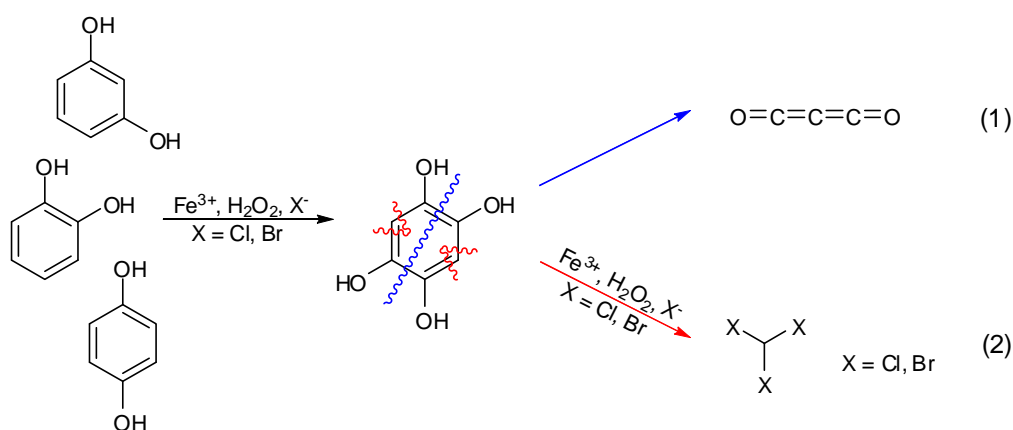


Figure 16. Formation of 1,2,4,5-tetrahydroxybenzene followed by ring cleavage to (1) carbon suboxide (Huber et al., 2007) and (2) trihalomethanes (Huber et al., 2009).

Haloform reaction (Fuson and Bull, 1934) of methyl ketons yielding trihalomethanes after ring fission is ineligible as it presupposes alkaline conditions. Alternatively, Hoekstra et al. (1999) published a reaction mechanism for the degradation of 1,3-dihydroxybenzene to trichloromethane and trichloroacetic acid by direct chlorination of the aromatic structure by HOCl . Adapted to catechol (Figure 17) this mechanism could explain haloacetic acid formation found by Fahimi et al. (Fahimi et al., 2003), but it also presupposes alkaline conditions for the release of trihalomethanes opposed to the conditions employed by Huber et al. (2009).

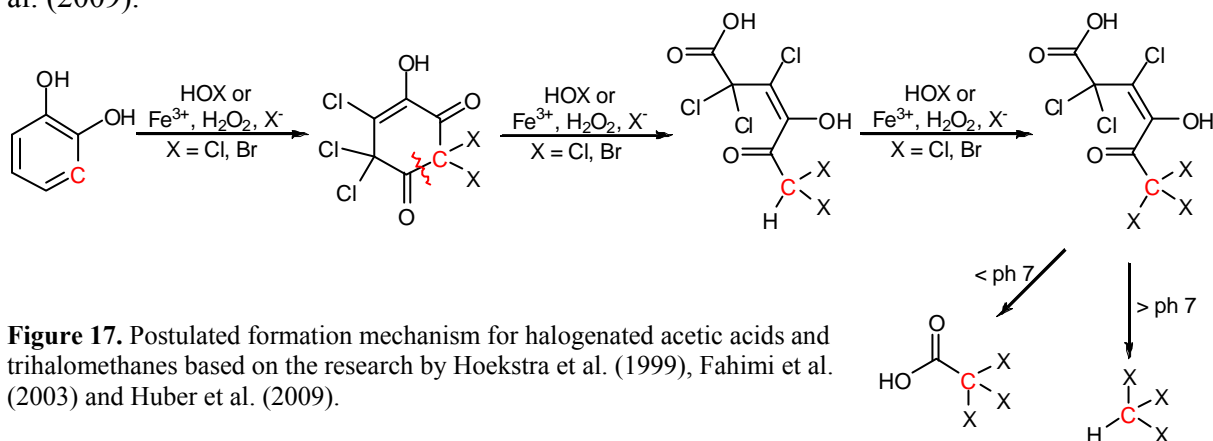


Figure 17. Postulated formation mechanism for halogenated acetic acids and trihalomethanes based on the research by Hoekstra et al. (1999), Fahimi et al. (2003) and Huber et al. (2009).

Additionally, Fenton chemistry is employed as a dechlorination method of chlorinated phenols in AOPs with an excess of H_2O_2 (Potter and Roth, 1993; Tang and Huang, 1995).

A non-halogenated volatile compound stemming from catechol is furan. By means of isotopic labelling, Huber et al. (2010) demonstrated that the oxygen atom in furan stems from H_2O_2 . Their postulated mechanism is depicted in Figure 18.

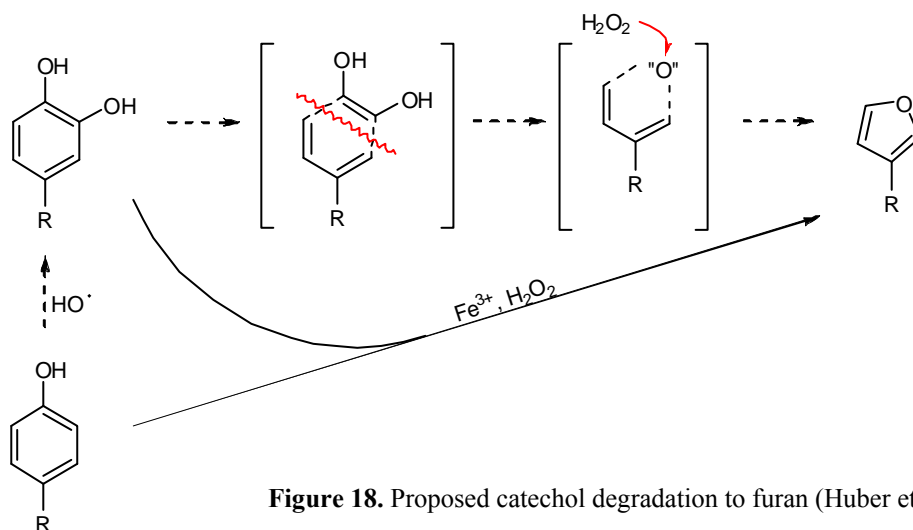


Figure 18. Proposed catechol degradation to furan (Huber et al., 2010).

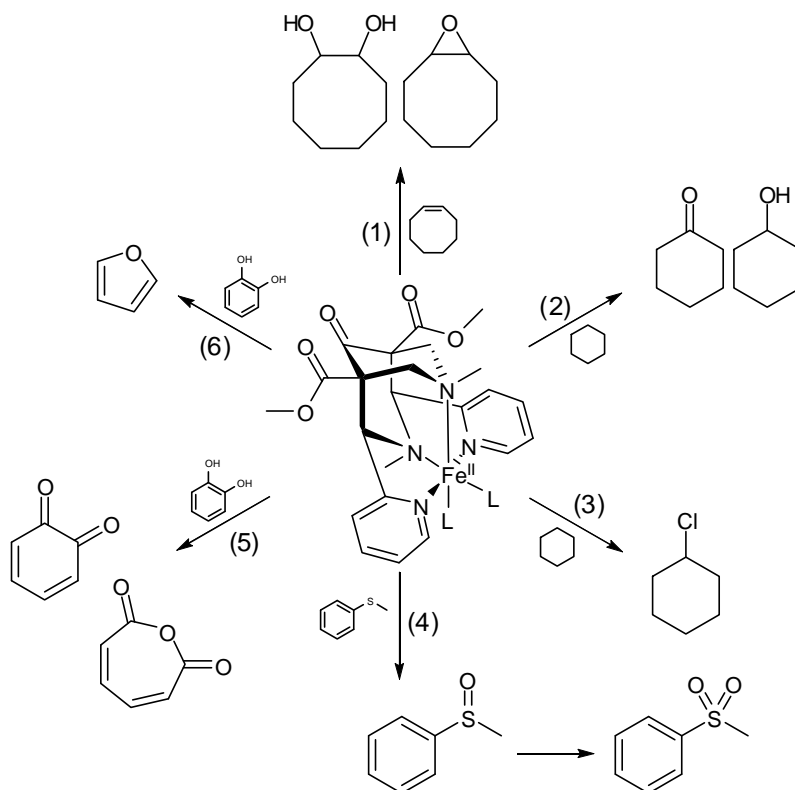


Figure 19. Reactions catalysed by a $[\text{Fe}^{\text{II}}(\text{N}_2\text{Py}_2)(\text{L})_2]$ complex: (1) olefin epoxidation and cis-dihydroxylation (Bukowski et al., 2006; Bautz et al., 2007), cyclohexane (2) oxidation (Comba et al., 2008, 2009) and (3) halogenation (Comba and Wunderlich, 2010), (4) sulfoxidation (Jaccob et al., 2011), (5) catechol oxidation (Comba et al., 2011) and (6) furan formation (Krause et al., 2013).

As part of this thesis the degradation of catechol to furan was revisited employing the non-heme $[\text{Fe}^{\text{II}}(\text{N}_2\text{Py}_2)(\text{L})_2]$ complex (chapter 2.2.2). This iron complex is of particular interest because of its biomimetic catalytic character and well-studied reaction behaviour. The complex was successfully employed in preceding studies (Figure 19) for epoxidation and cis-dihydroxylation of alkenes (Bukowski et al., 2006; Bautz et al., 2007), oxidation (Comba et al., 2008, 2009) and halogenation (Comba and Wunderlich, 2010) of cyclohexane, sulfoxidation (Jaccob et al., 2011) and catechol oxidation (Comba et al., 2011), albeit always in organic solvents, mostly acetonitrile.

Furthermore, the reaction of a $[\text{Fe}^{\text{II}}(\text{N}_2\text{Py}_2)(\text{L})_2]$ complex with H_2O_2 in acetonitrile and small amounts of water was studied by density functional theory (DFT). From those calculations the thermodynamically most likely reaction pathway is illustrated in Figure 20 in which Fe^{2+} is directly oxidised to $\text{Fe}^{\text{IV}}=\text{O}$ as the reactive intermediate species, while no OH radicals are formed (Comba et al., 2007).

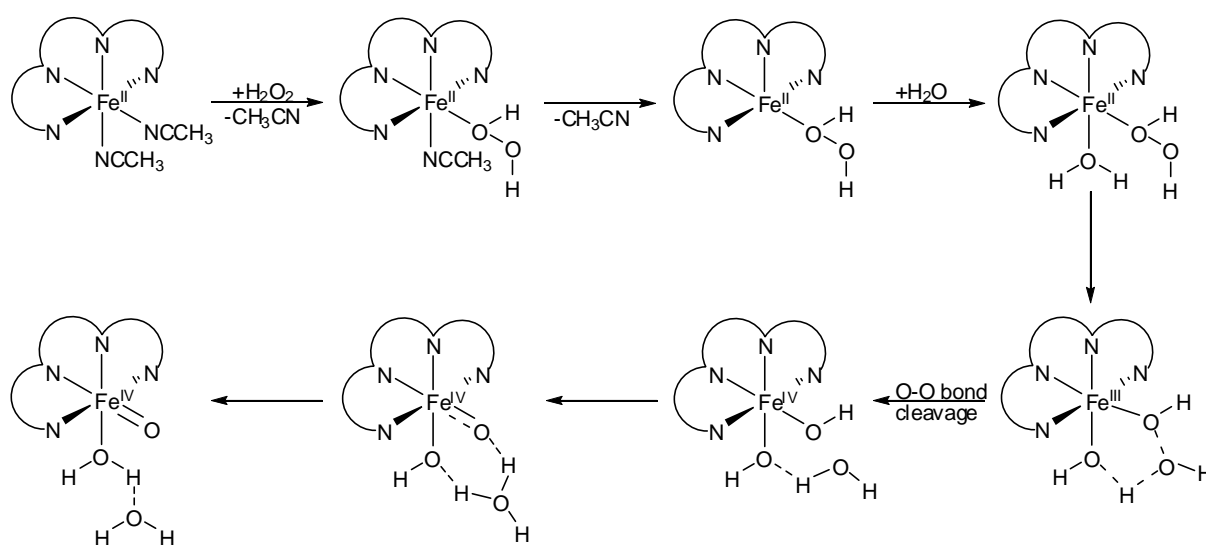


Figure 20. Energetically most favourable formation pathway of $\text{Fe}^{\text{IV}}=\text{O}$ in acetonitrile in the presence of water as calculated by DFT (Comba et al., 2007).

Several products of the presented model reactions are volatile compounds that have also been identified in natural environments. The forthcoming chapter describes sources of various volatile compounds relevant for the work in hand as well as their potential impact on atmospheric chemistry.

3 Volatile organic and inorganic compounds

Volatile organic compounds (VOC), relevant for the work in hand, include all kinds of organic molecules with boiling points up to 240-260 °C. This group can be further subdivided into very volatile organic compounds (VVOC) with boiling points up to 50-100 °C and expanded to semi-volatile organic compounds (SVOC) with boiling points above 240-260 °C (WHO, 1989). A subclass of VOC are the volatile organohalogenes (VOX) as will be discussed in chapter 3.5. With regard to volatile sulfur and selenide compounds (VSC/VSeC) not only organic but also inorganic compounds will be discussed in chapter 3.4.

Before, Chapter 3.1 to 3.2 describe known sources of aromatic hydrocarbons, furans and isoprene/monoterpenes as well as their impact on atmospheric chemistry.

3.1 Aromatic hydrocarbons

The monoaromatic volatile hydrocarbons benzene, toluene, ethylbenzene and xylenes are abbreviated as BTEX.

A major source for BTEX is biomass burning (Andreae and Merlet, 2001). Aside from being naturally abundant in petroleum (Wang et al., 1995), petroleum is also the main industrial source for benzene, toluene and xylenes (BTX) production superseding coke and coal-tar as educts. BTX are mainly used as gasoline additives followed by their common use as solvents, in spite of their carcinogenic character (WHO, 1993, 1985, 1997). Ethylbenzene is produced by a variation of Friedel-Craft alkylation of benzene and is used foremost for the production of styrene and subsequently polystyrene (WHO, 1996). As a result of their use in petrochemistry, BTEX are notorious pollutants, contaminating soils as well as surface and groundwater by leakage from petroleum production, refinery and storage sites, especially after accidents causing spills, e.g. Deepwater Horizon in 2010 (Camilli et al., 2010). Additionally, elevated BTEX concentrations were found at landfills (Durmusoglu et al., 2010). Terrestrial BTEX plumes expand by migration through soil and groundwater aquifers, but also show a significant sorption by organic rich material (Zytner, 1994). In soils and water systems BTEX are degraded by anaerobic (Edwards et al., 1992; Lovley, 1997) and aerobic (Barker et al., 1987) microorganisms. Atmospheric BTEX are degraded by ozone yielding different carboxylic acids (Franco et al., 2012) and by OH radicals yielding furan among other oxidation products (Shepson et al., 1984; Dumdei et al., 1988; Berndt and Boge, 2001).

3.2 Isoprene and monoterpenes

Isoprene and monoterpenes, i.a. pinene and camphor, are significant biogenic VOC emitted especially from terrestrial (Kesselmeier and Staudt, 1999) and maritime vegetation (Shaw et al., 2010). Isoprene is probably emitted to mitigate heat stress and as a protecting agent against reactive oxygen species (Sharkey et al., 2008). Next to methane, isoprene has the highest annual global flux of biogenic VOC to the atmosphere with estimates of 500 to 750 Tg (Guenther et al., 2006).

While the chemical structure of monoterpenes consists of a multitude of isoprene units, the precursors of terpene biosynthesis are isopentenyl pyrophosphate and dimethylallyl pyrophosphate, which are also precursors of isoprene (Sharkey and Yeh, 2001). Isoprene emission from plants depends on the activity of photosynthesis and temperature while the emission of monoterpenes, which can be stored by plants, is nearly independent of radiation (Kesselmeier and Staudt, 1999; Sharkey et al., 2008).

Isoprene and monoterpenes have a significant impact on the lower troposphere, because of their elevated global fluxes and the high reactivity with major atmospheric oxidants. While the atmospheric lifetime for isoprene is a few hours at night and day, some monoterpenes are degraded within half an hour at daytime (Kesselmeier and Staudt, 1999).

3.3 Furans

Furans are heterocyclic aromatic compounds bearing an oxygen atom in the ring. Like BTEX, furans are biomass burning by-products (Christian et al., 2003) also observed during food processing (Rogge et al., 1991). Among others, natural terrestrial sources of furan and several mono- and dialkylated furans are forest soils (Hempfling and Schulten, 1990), while furfural as well as 2-pentylfuran were found in soils containing plant litter (Leff and Fierer, 2008; Jordan et al., 1993). Plant material was confirmed as a source of furans by several studies including living plants (Isidorov et al., 1985), leaf litter (Isidorov and Jdanova, 2002) and solid woods (Risholm-Sundman et al., 1998). Furthermore, catechol and other phenolic compounds are degraded abiotically under Fenton-like (Huber et al., 2010) and Fenton conditions (Krause et al., 2013) to furanoic compounds.

An atmospheric source is the oxidation of 1,3-butadiene and 1,3-pentadiene to furan and 2-methylfuran, respectively (Ohta, 1984), while isoprene is a precursor for 3-methylfuran (Atkinson et al., 1989b).

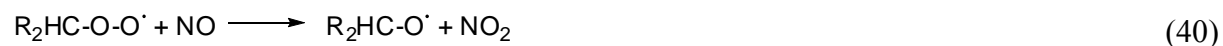
Additionally, furans as sinks for all atmospheric oxidants have an impact on the oxidative budget of the lower troposphere. They react with NO₃ radicals at nighttime (Kind et al., 1996; Berndt et al., 1997) and with OH radicals (Bierbach et al., 1995) or ozone (Atkinson et al., 1983) at daytime. The atmospheric lifetime of furan is about 4 h in the presence of OH radicals. For higher alkylated furans the lifetime decreases (Bierbach et al., 1995; Gu et al., 1985) while the reaction rate of 3-methylfuran with OH radicals is already similar if not even higher than of its precursor isoprene (Atkinson et al., 1989b; Gu et al., 1985). The reaction of furan with atmospheric Cl radicals is even faster than the reaction with OH radicals (Villanueva et al., 2009; Cabañas et al., 2005).

3.3.1 Ground level ozone

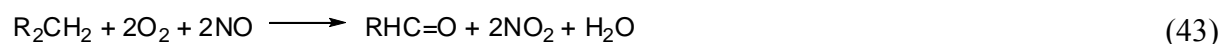
VOC in conjunction with the NO/NO₂ cycle are a source for daytime ozone formation in the lower troposphere, known as ground level ozone. The radical chain reaction as summarised by Krupa and Manning (1988) starts with photolytic depletion of O₃ yielding O₂ and a singlet oxygen atom that reacts rapidly with water yielding two OH radicals (Eq. 36 and 37).



In a cascade of atmospheric reactions, starting with catalytic hydrogen abstraction from VOC by OH radicals and subsequent reaction of the reactive organic species with O₂ and NO, two aliquots of NO₂ are formed (Eq. 38 to 42).



From the net reaction, as shown in Eq. 43, it is evident that OH radicals catalyse the degradation of VOC to aldehydes while NO is oxidised to NO₂.



In the following step, NO₂ is photolytically cleaved to NO again liberating an oxygen atom that reacts with O₂ to O₃ (Eq. 44-45).



One ozone molecule is the precursor for two OH radicals and, neglecting radical termination reactions, each of these can produce two NO₂ molecules or two O₃ molecules, respectively. The optimal net gain of the reaction would be three O₃ molecules.

The efficiency of VOC to participate in ground level ozone formation is described in the Maximum Incremental Reactivity (MIR) scale (Carter, 2009).

An example for anthropogenic induced ground level ozone is the summer smog formation in the Los Angeles basin which is accompanied by secondary organic aerosol formation (Turpin and Huntzicker, 1991).

3.3.2 Secondary organic aerosol

As described in the previous three chapters BTEX, furans, isoprene and monoterpenes, among other VOC, react with atmospheric oxidants and facilitate the formation of ozone. Secondary organic aerosol (SOA) on the other hand describes particles formed by nucleation and condensation of VOC oxidation products. These products are SVOC with low vapour pressure that partition between the gas and aerosol phase (Kroll and Seinfeld, 2008). Schematically this process is illustrated in Figure 21.

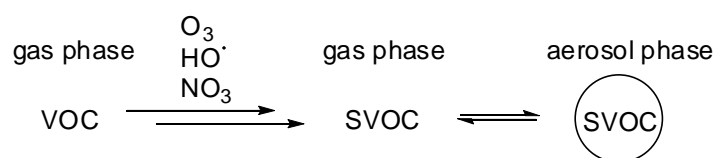


Figure 21. Schematical oxidation of VOC to SVOC and particle formation.

The main contribution to SOA formation of the before mentioned substances comes from isoprene (Carlton et al., 2009) and monoterpenes (Lee et al., 2006), though photooxidation of furans (Gómez Alvarez et al., 2009) and BTEX (Ng et al., 2007) with nitrous acid (HONO) as a precursor for OH radicals also confirmed SOA formation from these compounds.

Aerosols, independent of their origin, have an impact on Earth's albedo as they scatter and absorb solar and terrestrial radiation, leading to surface cooling (Ångström, 1962; McCormick and Ludwig, 1967; Andreae et al., 2005). Especially, a high load of ultrafine particles at nanometre scale is of significant importance for cloud formation and microphysics. They can act as additional cloud condensation nuclei (CCN) (Novakov and Penner, 1993; Pierce and Adams, 2007) increasing the amount of new small droplets in clouds while reducing the size of existing droplets. These smaller droplets are more efficient to reflect light while they are less likely to form rain droplets (Andreae et al., 2005; Khain et al., 2005). This leads to brighter clouds with a higher albedo causing atmospheric cooling, called the Twomey effect (Twomey, 1974, 1977).

Another important aspect for the abundance and distribution of atmospheric trace gases are heterogeneous reactions on solid and multiphase reactions in liquid aerosols, respectively (Ravishankara, 1997). For example, heterogeneous reactions on SOA are a sink for atmospheric RHS, see chapter 3.5.1, in which SOA is physiochemically altered by halogenation to so-called halogenated SOA (Ofner et al., 2012).

3.4 Volatile sulfur and selenium compounds

The term volatile sulfur and selenium compounds (VSC/VSeC) comprises organic as well inorganic species. As a result of the close relationship of sulfur and selenium their chemistry is comparable, but with some notable differences. On the one hand, selenium is mostly toxic for organisms and is metabolically detoxified by methylation (Hassoun et al., 1995). On the other hand, some prokaryotes, eukaryotes and archaeobacteria synthesise the amino acid selenocysteine for enzymes and proteins (Stadtman, 1996).

Volatile sulfur compounds are part of the global sulfur cycle and play a major role in the formation of aerosol and acidic rain as will be discussed in the following subchapters.

3.4.1 Sulfur cycle

Starting from sulfate the cycle begins with assimilative or dissimilative sulfur reduction (Andreae, 1990). On the one hand, there is dissimilative anaerobic respiration of some organisms based on sulfate as electron acceptor for oxidising organic matter. In this process sulfate is reduced via sulfur to sulfide. Sulfide is released as H₂S and can be deposited as

sulfide minerals like FeS or FeS₂ which are important for the formation of acid sulfate soils when exposed to oxygen (Drobner et al., 1990; Smith and Melville, 2004).

On the other hand, sulfate is assimilated by organisms and plants for biosynthesis of different organic sulfur compounds including the amino acids cysteine and methionine. Biosynthesis byproducts as well as biotic and abiotic degradation products of organic sulfur compounds are several volatile sulfur compounds (VSC) such as carbonyl sulfide, methanethiol, carbon disulfide, dimethyl sulfide and dimethyl disulfide (Aneja and Cooper, 1989).

VSC released in aerobic soils and water systems can be reoxidised to sulfate or are assimilated again for biosynthesis of sulfur proteins. In the atmosphere the volatile compounds are oxidised to SO₂ within hours and further to SO₃ within days. SO₃ rapidly reacts with water to H₂SO₄ (Kellogg et al., 1972) which is discussed in the next chapter. The oxidation is enhanced by heterogeneous (Li et al., 2006) and multiphase reactions (von Glasow and Crutzen, 2004) of sulfur species on and in aerosols, respectively. A schematic overview of the natural sulfur cycle is illustrated in Figure 22.

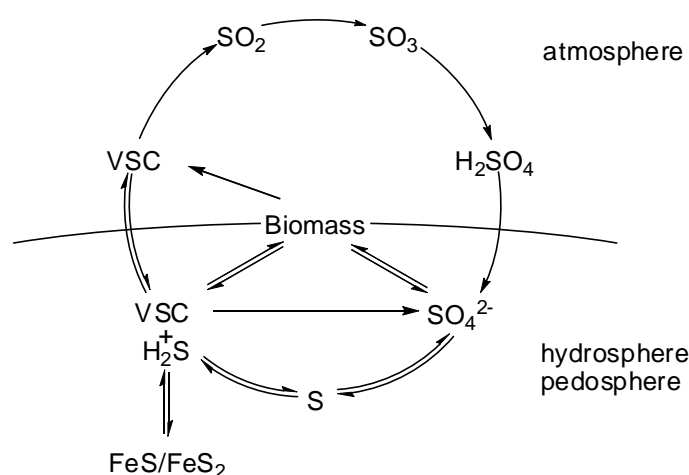


Figure 22. The natural sulfur cycle - a schematic overview (Andreae, 1990; Drobner et al., 1990; Smith and Melville, 2004; Aneja and Cooper, 1989; Kellogg et al., 1972).

3.4.2 Sulfuric acid aerosol

H₂SO₄, the atmospheric oxidation product of VSC, is highly hygroscopic and thus an effective nucleation seed to form fine particles. These particles are attributed to have an important cooling effect on Earth's surface by reflecting extraterrestrial radiation (Kiehl and Briegleb, 1993) and grow into potent CCN (see chapter 3.3.2). Most notably, dimethyl sulfide emission from phytoplankton is the major source for CCN over the oceans (Charlson et al.,

1987). Compared to major abundant natural VOC like isoprene and monoterpenes, oxidation of VSC and thus particle formation is slower (Kellogg et al., 1972).

While water condenses on H_2SO_4 the molecule dissociates unfolding its acidic character allowing unique multiphase reactions. Sulfuric acid aerosol enhances the formation of secondary organic aerosol (Jang and Kamens, 2001), e.g. through aldol condensation (Nozière and Riemer, 2003) or is proposed to cycle atmospheric nitrate via reaction with formaldehyde to NO_2 (Chatfield, 1994). H_2SO_4 does not only form new particles but also acidifies existing aerosols by condensing on them.

Of further importance is halogen activation in acidic aerosols which is discussed in Chapter 3.5.1.

3.5 Volatile organohalogens

For a long time the atmospheric abundance of volatile organic halogen compounds has been mostly attributed to anthropogenic pollution, e.g. chlorofluorocarbons that are responsible for stratospheric ozone depletion. After half a century of intensive research the latest review of Gordon Gribble (2010) states that nearly 5000 halogenated compounds of biogeochemical processes were identified. Biogenic sources are volatile halogenated metabolites from marine and terrestrial organisms, such as microbes, lichen, fungi and plants. Additionally, metabolic semi-volatile organohalogens are biogenically or abiotically degraded to VOX (Gribble, 2010). Moreover, there are abiotic halogenation processes (see also chapter 2.2.3) in soils, sediments and aquatic environments that yield a variety of VOX.

VOX can be divided into chlorinated, brominated, iodinated and fluorinated molecules as well as mixed halogenated species. Moreover, a classification by halogenation grade and carbon structure is reasonable.

An overview of naturally occurring organohalogens and their formation processes involved was compiled in the before mentioned comprehensive review by Gribble (2010) while a review by Schöler and Keppler (2003) emphasised abiotic processes.

VOX are known for stratospheric ozone depletion but also react with tropospheric ozone. The underlying mechanism of ozone depletion, where VOX act as precursors for RHS will be discussed in the next chapter. Furthermore, the relevance of VOX in the formation of halogen-induced organic aerosols will be assessed in chapter 3.5.2.

3.5.1 Reactive halogen species in the atmosphere

Atmospheric RHS include molecular and atomic halogens, hypohalous acid and halogen oxide radicals. These are important gas phase constituents that are abundant in the troposphere as well as the stratosphere. RHS, in the form of molecular chlorine (Spicer et al., 1998), IO (Alicke et al., 1999) and BrO (Hebestreit et al., 1999) were measured in the marine boundary layer. Terrestrial ClO and BrO were observed for example above the hypersaline Great Salt Lake, USA (Stutz et al., 2002).

VOX are one source for atmospheric RHS. By photolysis, the halogen carbon bond (X-C) is cleaved homolytically into a free halogen radical and a free organic radical. Depending on the stability of the X-C bond, VOX are photochemically decomposed in the troposphere or stratosphere (Rattigan et al., 1997; Mossinger et al., 1998). The formed halogen radicals rapidly react in a catalytic cycle with ozone. The depletion products of this reaction are O₂ and halogen monoxide radicals (XO) which are recycled by photolysis or reactions with ozone, oxygen atoms, NO or other halogen monoxides (DeMore et al., 1997). The halogen monoxides can also react with hydroperoxyl radicals to hypohalous acid (HOX), which yields under photochemical fission halogen and OH radicals. Alternatively, XO reacts with NO₂ to XONO₂. Both, HOX and XONO₂ can condense into liquid particles. In the aerosol phase XONO₂ reacts with water to HOX and HNO₃ (Hanson et al., 1996; Platt and Hönninger, 2003). Under acidic conditions, like in sulfuric acid aerosol (chapter 3.3.2), and in presence of halides HOX is transformed into molecular halogens (chapter 2.1.3) including interhalogen molecules, such as ClBr. Released from the aerosol phase these molecular halogens undergo photochemically promoted homolytical fission to halogen radicals (Vogt et al., 1996).

The aerosol reactions are of significant importance because for each halogen atom entering the aerosol phase two halogen atoms are liberated into the gas phase. This reaction path is best known for bromine as the bromine explosion which was observed in the Antarctic (Frieß et al., 2004) and over the Dead Sea (Hebestreit et al., 1999; Matveev et al., 2001; Peleg et al., 2004; Tas et al., 2005; Holla, 2013).

Liberation of RHS from the aerosol phase is furthermore intertwined with NO_x chemistry. As stated before, HNO₃ reacting with formaldehyde is reduced to NO₂ in sulfuric acid aerosol phase (Chatfield, 1994), which is photochemically cleaved to NO and oxygen atoms. Outside the aerosol phase NO either supports ozone depletion cycling back to NO₂ (Logan, 1983) or reacts with OH radicals to form nitrous acid, HONO. A more feasible reaction path for HONO is the reaction of NO₂ with water in the aerosol phase. The different formation

3.5.2 Halogen-induced organic aerosol

Additionally to the catalytic ozone depletion, RHS react with organic trace gases i.a. monoterpenes (Timmerghazin and Ariya, 2001; Cai and Griffin, 2006; Ofner et al., 2013), toluene (Karlsson et al., 2000; Cai et al., 2008) and furans (Villanueva et al., 2009; Zhang and Du, 2011). Likewise to the formation of secondary organic aerosols by the reaction of VOC with O₃ or OH radicals the reaction with RHS is a potential source for organic aerosols, the so-called halogen-induced organic aerosol (XOA) (Cai and Griffin, 2006; Ofner et al., 2013). XOA is the product of VOC reacting with RHS, whereas halogenated SOA describes altering of SOA by subsequent halogenation reactions (chapter 3.3.2). XOA formation was reported from monoterpenes (Cai and Griffin, 2006; Ofner et al., 2013) and toluene (Karlsson et al., 2000; Cai et al., 2008).

Based on their spectroscopic observations Ofner et al. (2013) postulated that the reaction mechanism of XOA formation involves hydrogen abstraction as well as halogen addition to the VOC precursor molecules. Furthermore, they argued that XOA particles are transformed into SOA by chemical aging due to reaction with oxygen-bearing reactants. Moreover, they elucidated that physico-chemical properties, like water solubility and radiative properties of aged XOA differ from normal SOA due to the abundance of solid halogen species in the aerosol phase. For example, a higher water solubility increases the CCN formation potential (Ofner et al., 2013), and with regard to the previous chapter, halides in an aqueous aerosol phase can be liberated again into the gas phase as RHS.

As part of this work, emissions of selected volatile compounds classes was investigated to assess their origin and their atmospheric impact around terrestrial hypersaline environments of Southwest Australia and the Israeli side of the Dead Sea.

4 Sampling sites

Water, soil and sediment samples from several saline environments were collected and analysed as a comparison to model reactions with regard to various geochemical parameters. Additionally, the samples were assessed on their contribution to unique atmospheric phenomena observed in the vicinity of the sampling sites. On the one hand, samples were collected in Southwest Australia in 2011, 2012 and 2013 (Chapter 4.1), with the intention of identifying the source of high and fine aerosol loads over the salt lakes. On the other hand, samples from the Dead Sea in Israel of 2012 (Chapter 4.2) were analysed to further unravel observed BrO and IO formation.

4.1 Southwest Australia

The salt lakes of the Southwestern Australian Wheatbelt are part of the Avon River catchment with an area of about 120000 km². The lakes of this study are situated in the Lockhart sub-catchment, part of the Zone of Ancient Drainage, along the Lockhart River which originates at Lake Bidy north of Newdegate draining north west (Department of Water, 2009a), its tributary the Camm river which originates at Lake King (Department of Water, 2009b) and the Magenta internal catchment north and south of Newdegate (Department of Water, 2009a). Topography is undulated with elevation drops from Lake Bidy to the Camm River confluence of about 28 m over 78 km and from Lake King to the confluence of about 48 m over 197 km. Sluggish drainage of surface waters along the broad and shallow palaeodrainage valleys is only observed after extreme rain events, otherwise water is drained internally (Brambridge and Commander, 2005). The shallow ephemeral lakes are surrounded by sandflats, sand dunes and occasionally rocky outcrops.

The Lockhart catchment area is located on the Yilgarn Craton comprising mostly of Archaean granite and gneiss with patches of greenstone belts and sedimentary rocks in the area of the palaeodrainage. The surface is heavily weathered and contains calcretes and calcareous soils (Lillicrap and George, 2010) as well as acid sulfate soils and sediments (Fitzpatrick and Shand, 2008).

The Lockhart sub-catchment is situated in the so called Wheatbelt, a highly cleared agricultural zone. Extensive clearing started at the turn of the 19th century with increased clearing after each World War. Deep rooted native vegetation called mallee, mainly eucalyptus species, was replaced with pastures and winter growing annual crops, first of all

wheat. As a consequence groundwater recharge by rain increased while mean evaporation through plants decreased leading to a rise of the groundwater table. The rising groundwater passes mineral rich layers, takes up salts and transports these close to the surface, causing secondary salinisation (Hookey, 1987; Nulsen and Catchment Hydrology Group, 1998; Addison, 2001; Ghauri, 2004). Additionally, discharge of saline and mineral rich groundwater into valley floors has an significant impact on endorheic lakes and streams (Rogers and George, 2005). Ephemeral playa lakes, fed by the shallow groundwater and increased run off from rain, expand, while halide concentrations in fresh water lakes and streams increase (Schofield, 1989; Williams, 2001). Dead trees around the lakes bear witness to the recent change of surface salinity illustrated in Figure 24.

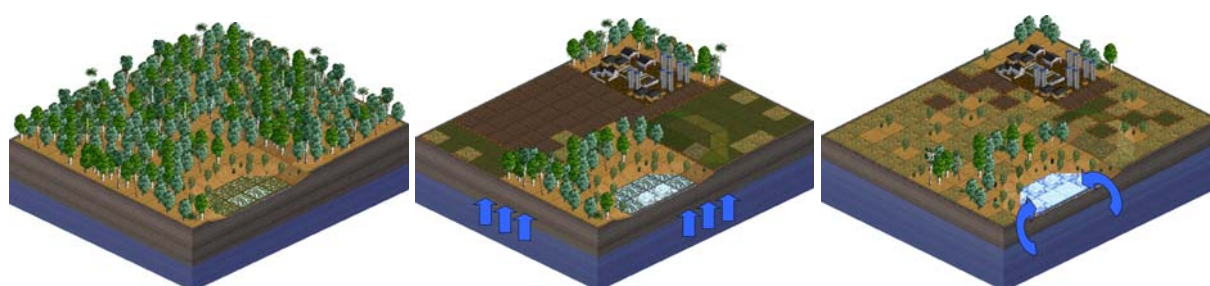
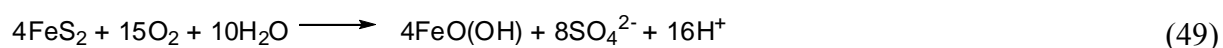
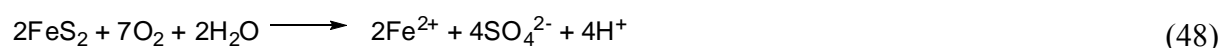
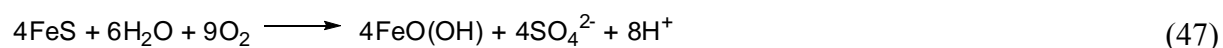


Figure 24. Proposed secondary salinisation after land clearing. Deep rooted native vegetation kept the ground water table low (left), which started to rise after clearing and transported salts toward the surface (middle) discharging into low lying playas (right). Images created with tiles of the © OpenGFX Project published under GNU Public License version 2.

Another environmental hazard is the discharge of acidic groundwater (Degens and Shand, 2010) most likely caused by Fe^{2+} oxidation and hydrolysis, or ferrollysis (Eq. 46) (Mann, 1983; McArthur et al., 1991).



Additionally, the oxidation of iron sulfides in acid sulfate soils could be responsible for acidification as shown in Eq. 47-49 (Shand and Degens, 2008; Fitzpatrick and Shand, 2008).



The Southwestern Australian salt lakes feature a multifarious geochemical inventory with a pH ranging from acidic to alkaline associated with a correspondingly diverse biota (Bowen

and Benison, 2009). Furthermore, geochemistry and biosphere change with the inflow of episodic rain water (Geddes et al., 1981; Timms, 2009). Especially, the hypersaline lakes with a low pH and a high iron content provide a basis for a unique aqueous chemistry.

In addition, the salt lakes of the Wheatbelt were identified to be the source of ultrafine particles which were measured in elevated numbers over the agricultural land by airborne, car based and stationary instruments (Junkermann et al., 2009; Kamilli et al., 2013). This raised the question of the underlying aerosol formation process and whether the salt lakes have a significant impact on the local climate that unambiguously changed over the last decades. As elaborated in chapter 3.3.2 ultrafine particles from SOA are known to modify cloud microphysics changing local albedo and having a direct influence on rain events.

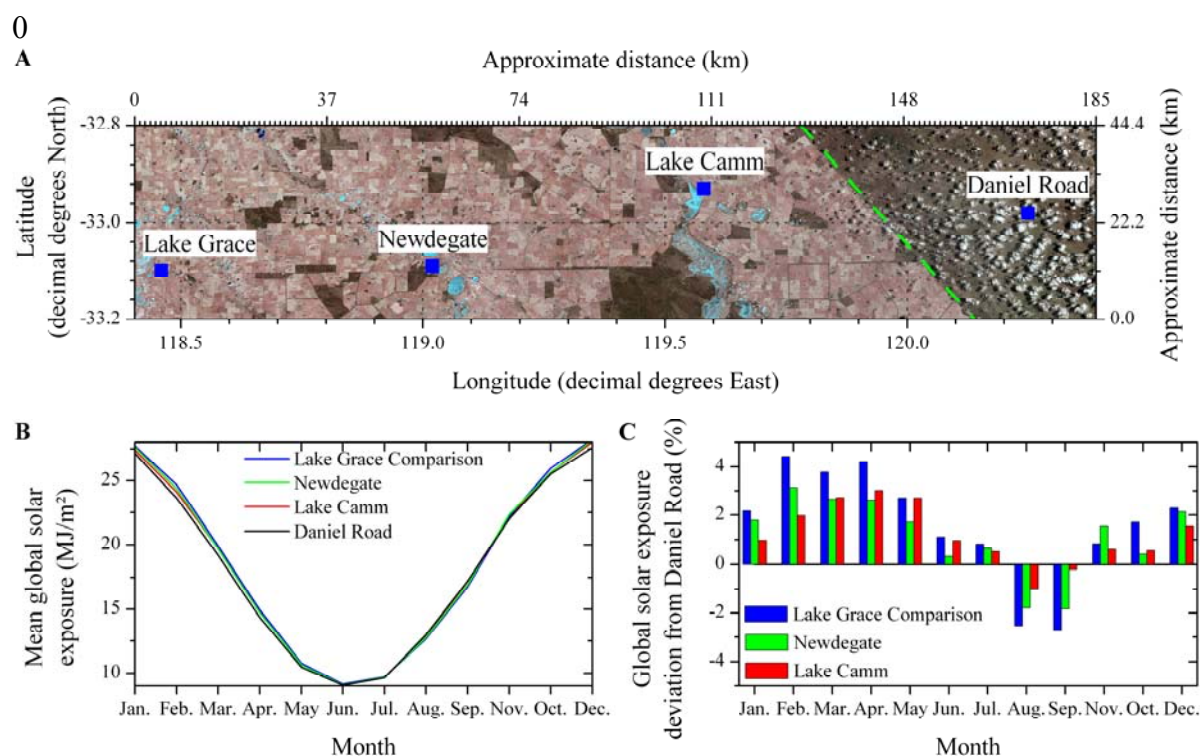


Figure 25. **A** Processed satellite image of the Shire of Lake Grace, showing location of weather stations, a cloudless sky above the agriculture land and small cumulus clouds beyond the state barrier fence (---) above the natural vegetation in the east. Image source: USGS/NASA Landsat Program, 09.12.1989, Landsat TM scene LT51100831989343ASA00. Image resides in the public domain and is reprinted by courtesy of the U.S. Geological Survey. **B** Monthly mean global solar exposure at Lake Grace Comparison, Newdegate, Lake Camm and Daniel Road. **C** Comparison of mean monthly global solar exposure to Daniel Road in percent. Global solar exposure raw data from weather station 010592, 010617, 010606 and 012197, estimated from VIS-IR satellite images, was retrieved from Climate Data Online, Bureau of Meteorology, © Commonwealth of Australia, 2013 and reprocessed and reprinted according the Australian Copyright Act 1968 - Section 40 - Fair dealing for purpose of research or study.

Agriculture and native land are sharply separated by the 1.837 km long State Barrier Fence, formerly known as Rabbit-Proof Fence. This gives the opportunity to directly compare meteorological characteristics of the two different land cover systems and evaluate the impact of deforestation (Lyons et al., 1993).

One difference is the preferred formation of small cumulus clouds east of the fence shown in Figure 25A. On the one hand, planetary boundary layer and sensible heat fluxes are higher over the native land, increasing the chance for cloud formation by an uprise of humid surface air to the lifted condensation level (Xinmei et al., 1995; Lyons et al., 1996; Lyons, 2002; Esau and Lyons, 2002). On the other hand, high numbers of fine particles over the Wheatbelt could favour suppression of cloud formation or their dissipation (Junkermann et al., 2009). Global solar exposure is elevated west of the fence most of the year, except in August and September, when the crops transpire more water than the native vegetation.

Another observed phenomenon is a trend of annual rain patterns (Suppiah and Hennesy, 1998; Haylock and Nicholls, 2000). As depicted in Figure 26 the total amount of rain slightly declined over the last decades in Lake Grace while it slightly increased close to the fence. With about 400-320 mm/a precipitation and about 1800-2200 mm/a evaporation the area is semi-arid (Galloway, 2004).

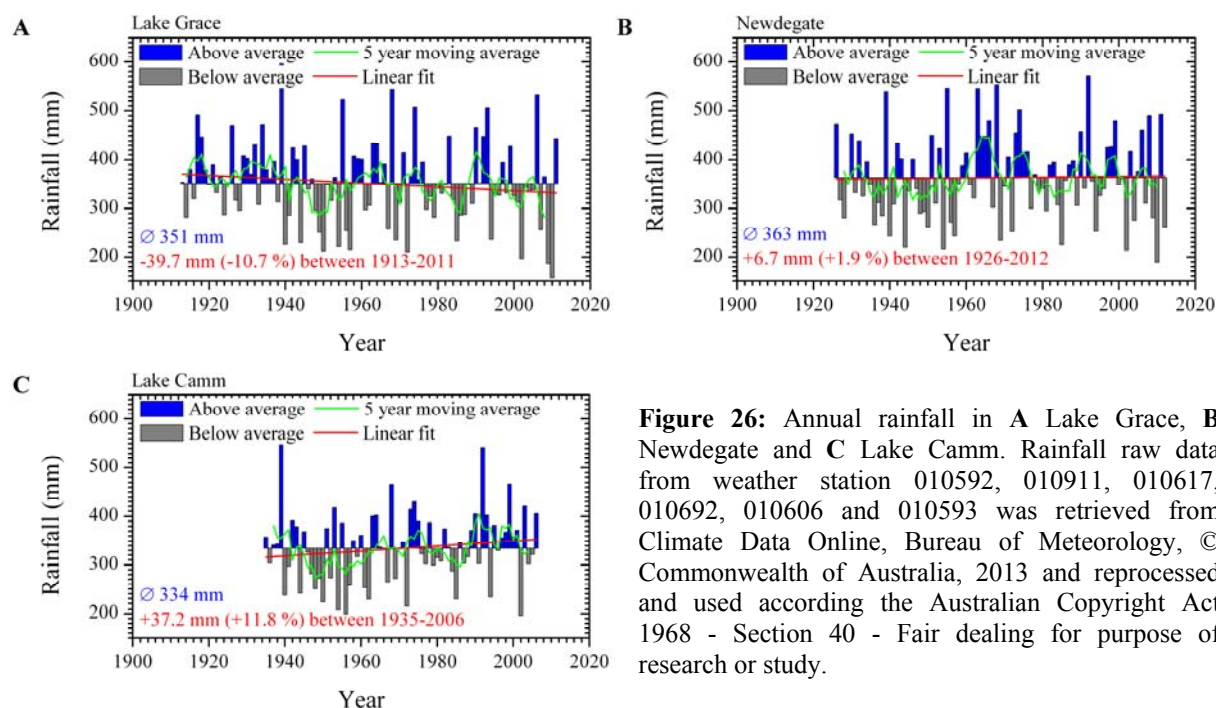


Figure 26: Annual rainfall in **A** Lake Grace, **B** Newdegate and **C** Lake Camm. Rainfall raw data from weather station 010592, 010911, 010617, 010692, 010606 and 010593 was retrieved from Climate Data Online, Bureau of Meteorology, © Commonwealth of Australia, 2013 and reprocessed and used according the Australian Copyright Act 1968 - Section 40 - Fair dealing for purpose of research or study.

More important than the annual rainfalls are the changes of seasonal rain patterns. On the one hand as shown in Figure 27C and D for Lake Grace, a steady decrease of rain was measured during fall and winter months in the time of seeding and crop growing, respectively. On the other hand, heavy summer rain events during and after harvest increased since the middle of the last century.

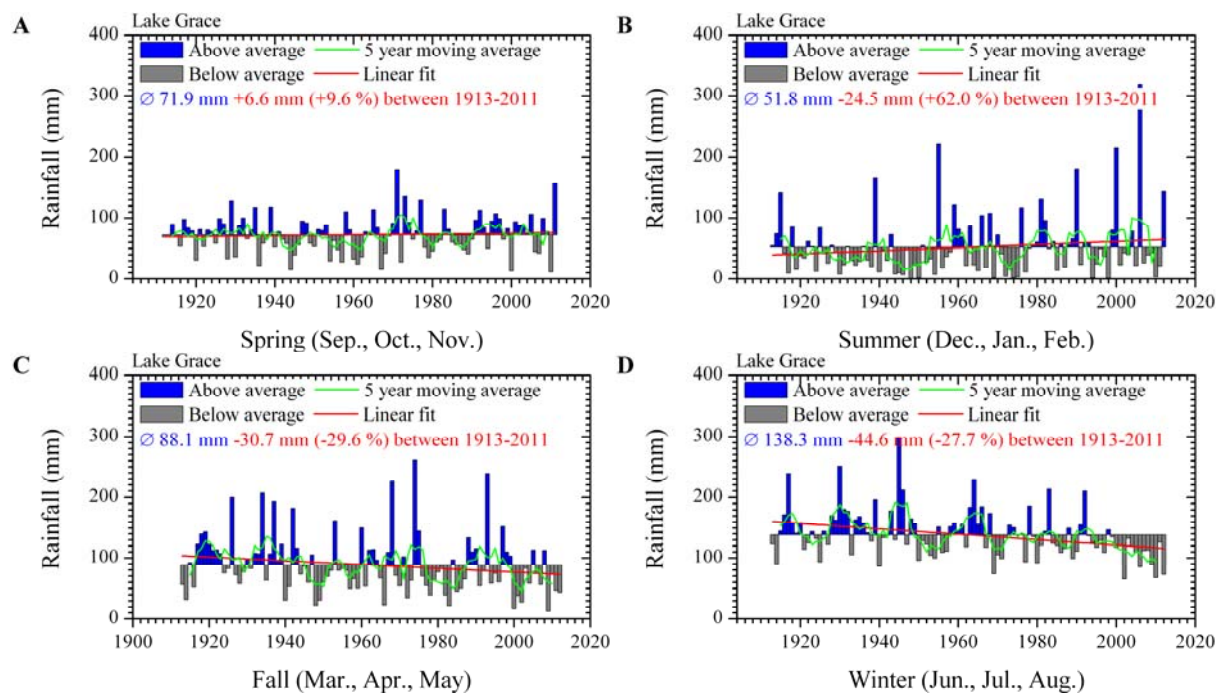


Figure 27: Seasonal rainfall in Lake Grace. Rainfall raw data from weather station 010592 was retrieved from Climate Data Online, Bureau of Meteorology, © Commonwealth of Australia, 2013 and reprocessed and used according to the Australian Copyright Act 1968 - Section 40 - Fair dealing for purpose of research or study.

In conclusion, Western Australia is of scientific interest, because of its geochemical diversity with acidic sulfate soils and the relevance of salt lakes for the local climate which has verifiably changed over the last decades.

4.2 Dead Sea

The Dead Sea is a large endorheic hypersaline lake with the Jordan River as its main tributary situated in the Middle East bordering Israel, Palestinian Territories and Jordan. The area is arid with rainfalls around 75 mm per year, hence the lake is mainly fed by the Jordan River (Enzel et al., 2003). The drainage basin of the Dead Sea covers 40,000 km² (Yeichieli et al., 1998).

The Dead Sea is separated into a deep northern and a shallow southern basin measuring approximately 90 km from north to south in total while its width is no more than 18 km. It is situated in the Jordan Rift Valley with the water table lower than 410 m below sea level and its deepest point at around 730 m below sea level.

Between the northern and southern basin lies the Lisan Peninsula and Lynch Strait with a sill elevation of 402 m below sea level and thus above the Dead Sea water level of today (Klein and Flohn, 1987). With excessive use of the Jordan River since the 1960s the balance between evaporation and water inflow shifted leading to a subsidence of the Dead Sea water table, throttling of the Lynch Strait and a complete separation of northern and southern basin in 1976 (Steinhorn et al., 1979).

The Southern basin is subdivided into several evaporation ponds, additionally bisected into a western Israeli and eastern Jordanian side. The ponds on the western shore are operated by Dead Sea Works, part of the Israel Chemical Ltd. (ICL), to extract minerals, mostly KCl as fertilizer, NaCl, MgCl₂ and CaCl₂ from the Dead Sea which are processed to industrial salts, de-icers, bath salts, table salt and raw materials for the cosmetic industry. Furthermore, the ICL group maintains under the Dead Sea Bromine Group branch chlorine and bromine plants to extract Cl₂ and Br₂ from the halide rich Dead Sea (Kesner, 1999). On the eastern side the Jordan Bromine Company Ltd. is the main producer of Br₂ and bromine based chemicals (Kogel and Society for Mining Metallurgy and Exploration, 2006). Bromine production as of 2011 were 202,000 t/a in Israel and 300,000 t/a in Jordan (U.S. Geological Survey, 2013).

As a result of the subsiding water table and disconnection of the southern basin from the northern basin, the companies started to actively pump water from the northern Dead Sea into the evaporation ponds. Most of the evaporation ponds cover an area that was originally part of the Dead Sea and are therefore connected from north to south. On the Israeli side the evaporation ponds were expanded further to the south build on an upward slope. Therefore, the altitude of the southernmost pond is higher than the northern. Water is pumped from the northern ponds by way of an open canal, passing the Dead Sea Works and bromine plants to the southernmost pond from where it flows back northward. The latest expansion of evaporation ponds was started between 1991-1992.

Figure 28A illustrates the Dead Sea and the sampling sites named En Gedi, En Bokek and Sodom, whereas Figure 28B and Figure 28C show the expansion of the evaporation ponds between 1991 and near the sampling location Sodom in 2012.

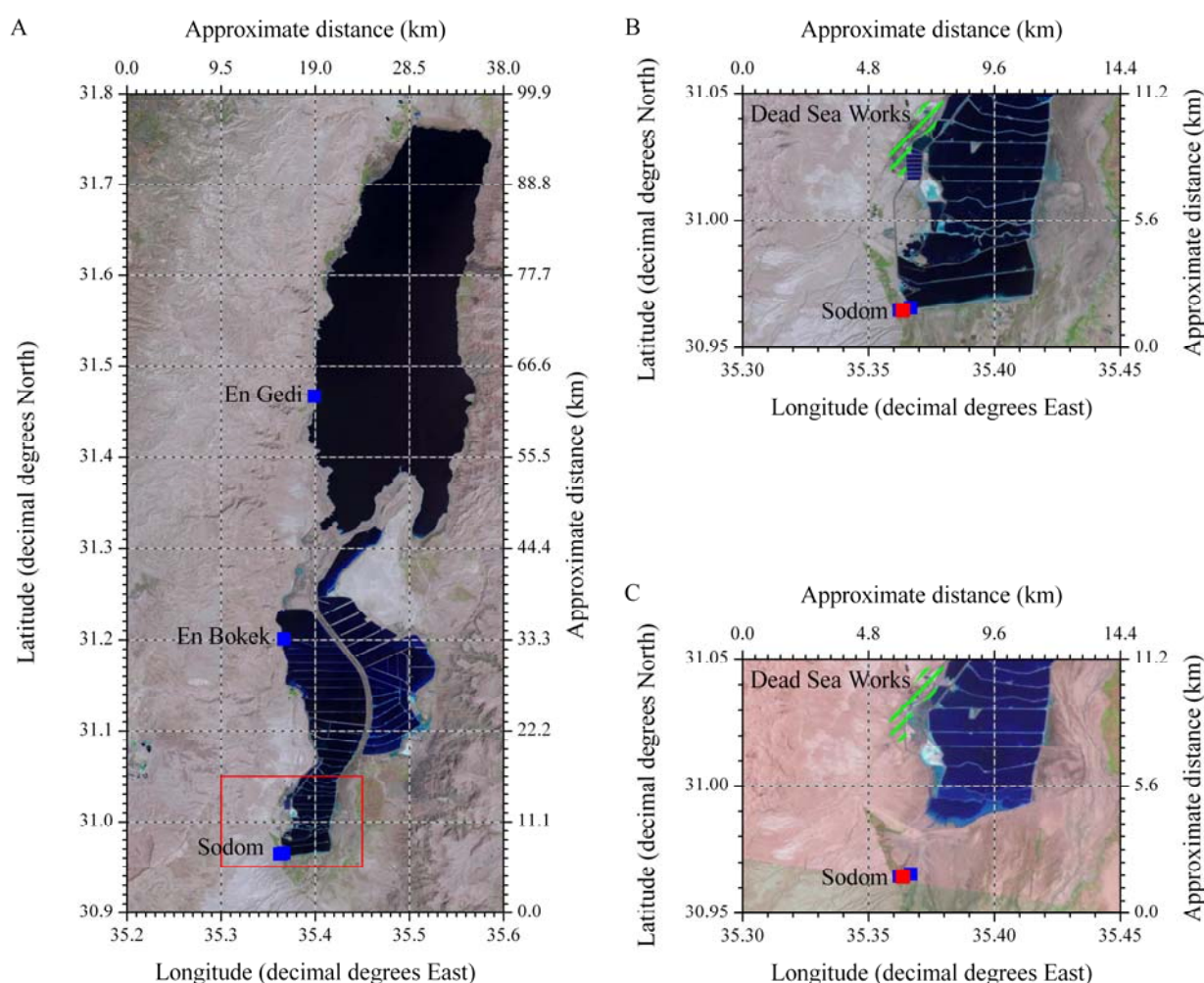


Figure 28. A Northern and Southern Dead Sea Basin in 2013 with ■ water sampling sites. B Southern Dead Sea Basin in 2013 and C in 1991 showing Dead Sea Works Ltd. ///, evaporation pans, ■ water and ■ sediment sampling sites. Image source A and B: USGS/NASA Landsat Program, 2013, Landsat OLI_TIRS_L1T scene LC81740382013249LGN00, USGS, Sioux Falls, 06.09.2013. Image source C: USGS/NASA Landsat Program 1991, Landsat TM L1T, scene LT41740381991181XXX05, USGS, Sioux Falls, 30.06.1991. Images reside in the public domain and are reprinted by courtesy of the U.S. Geological Survey.

The Dead Sea is of scientific importance, because of its unique mineral composition and its impact on atmospheric chemistry. On the one hand, dissolved Ca^{2+} and especially Br^- concentrations are exceptionally elevated (Bentor, 1961). The latter is an important factor for observed atmospheric chemistry. Br^- in Dead Sea waters can be UV activated yielding BrO_3^- , BrO^- and volatile Br_2 depending on the pH (Gratzel and Halmann, 1990). When released to the atmosphere bromine species catalyse ozone depletion through the so called bromine explosion (see chapter 3.5.1) and effecting HO_x and NO_x budgets. Differential optical absorption spectroscopy (DOAS) measurements proved the abundance of BrO in the boundary layer over the Dead Sea (Hebestreit et al., 1999; Matveev et al., 2001; Peleg et al., 2004; Tas et al., 2005; Holla, 2013) but also of another reactive halogen species, namely IO (Zingler and Platt, 2005).

5 Materials and methods

5.1 Chemicals

Model reactions

Catechol (99%; Sigma-Aldrich), 4-ethylcatechol (95%; Aldrich), hydrogen peroxide (30%; Merck), $[\text{Fe}^{\text{II}}(\text{N}_2\text{Py}_2)(\text{OTf})_2]$ (Börzel et al., 2002), $\text{Fe}_2(\text{SO}_4)_3$ (99%; Fe 21-23%; Riedel-de Haën), potassium chloride (99.5%; Merck), sodium hydroxide (99%; Aldrich), sulfuric acid (96%, Riedel-de Haën).

BTEX

EPA 624 calibration mix A (analytical standard; Supelco).

Furans

Furan (99%; Fluka), 2-methylfuran (99%; Sigma-Aldrich), 2-ethylfuran (97%; Aldrich), 2-propylfuran (97%; abcr), 2-butylfuran (98%; abcr), 2-pentylfuran (97%; Aldrich), 2,3-dimethylfuran (99%; Aldrich), 2,5-dimethylfuran (99%; Aldrich), 3-chlorofuran (Zhang et al., 2005), 3-bromofuran (97%; Aldrich).

Isoprene/monoterpenes

Isoprene (99%; Aldrich), (\pm)- α -pinene (98%; Aldrich), camphor (96%; Aldrich), 3-carene (90%; Sigma-Aldrich), sabinene ($\geq 98.5\%$; Carl Roth), p-cymene (99%; Aldrich), (R)-(+)-limonene (97%; Aldrich), eucalyptol (99%; Aldrich).

VSC/VSeC

Sulfur mix (analytical standard; Spectrum Quality Standards), dimethyl sulfide (98%; Aldrich), dimethyl selenide ($\geq 99\%$; Aldrich), dimethyl diselenide (96%; Aldrich), thiophene ($\geq 99\%$; Aldrich), 2-methylthiophene (98%; Aldrich), 3-methylthiophene (98%; Aldrich).

VOX

EPA 624 calibration mix A (analytical standard; Supelco), EPA 624 calibration mix B (analytical standard; Supelco), 1-chloropropane (98%; Aldrich), 1-chlorobutane (99.5%;

Aldrich), 1-chloropentane (99%; Aldrich), 1-chlorohexane (99%; Aldrich), 1-chloroheptan (99%; Aldrich), 1-chlorooctane (99%; Aldrich), 1,3-dichloropropane (99.6%; Fluka), 1,2-dichloropropane (99%; Fluka), 2-chlorobutane ($\geq 99\%$; Aldrich), bromomethane (99%; Aldrich), dibromomethane (99%; Aldrich), 1,2-dibromoethane (p.a.; Acros Organics), 1-bromopentane (95%; Aldrich), bromochloromethane (99.5%; Aldrich), 1-bromo-2-chloroethane (99%; Aldrich), iodomethane (99%; Merck Schuchardt), diiodomethane (99%; Aldrich), iodoethane (99%; Sigma-Aldrich), 1-iodopropane (99%; Aldrich), 2-iodopropane (99%; Aldrich), 1-iodobutane (99%; Aldrich), 2-iodobutane (99%; Aldrich).

Various

Hexafluorobenzene (99%; Aldrich), magnesium perchlorate (anhydrous; ACS grade, Alfa Aesar), nitric acid (65%; Bernd Kraft), calcium carbonate (99%; LECO), hydrochloric acid (25%; Bernd Kraft), methanol (99.8%; Sigma-Aldrich), element standards for ICP-OES (ULTRA SCIENTIFIC), anion standards for IC (CertiPUR; Merck Millipore), total organic carbon standards (Ultra Scientific), buffer capsules 4.01 and 7.00 (Merck).

Type I ultrapure water ($\geq 18 \text{ M}\Omega/\text{cm}$) from a Purelab UHQ System by ELGA LabWater was used in all experiments.

5.2 Sampling

Soil and sediment samples were collected from profile layers with stainless steel putty knives into low density polyethylene (LDPE) plastic bags with zipper locking ordered via neoLab and stored at 4 °C. Sampling was accompanied by determination of soil and sediment colour according to the Munsell soil colour chart, grain size, humidity, temperature and odour.

Plant samples were air-dried and stored at ambient temperatures in paper bags after sampling.

Water samples were collected with disposable syringes. For IC and GC-MS analysis 10 mL were transferred into 20 mL headspace glass vials with air-tight aluminium caps and polytetrafluoroethylene (PTFE) septum obtained via Chromatographie Zubehör Trott. For ICP-OES 15 mL or 50 mL conical centrifuge tubes (falcon tubes) were filled to the rim with the water samples and acidified on site with 50 μL concentrated HNO_3 to stabilize the dissolved cations. All water samples were stored at 4 °C.

For gas samples 2 L electropolished stainless steel canisters were evacuated in the laboratory with a rotary vane pump and a turbomolecular high vacuum pump to less than 10^{-3} mbar. The canisters were closed with bellow valves by Swagelok. At the sampling site the bellow valves were opened for gas to flow into the evacuated canister until equilibrium with atmospheric pressure was reached. In 2013, the sampling method was improved by the use of a compressor pump N814KTDC with a PTFE membrane by KNF to fill the canister with additional 2 bar.

5.3 Sample preparation

In the laboratory soil, sediment and plant samples were frozen at $-26\text{ }^{\circ}\text{C}$ either in the LDPE/paper bags or in high density polyethylene (HDPE) wide neck square bottles by neoLab prior to freeze-drying with a Lyovac GT2 by Steris. The dried samples were then ground with a Pulverisette 5 planetary mill by Fritsch at 250 rpm with agate grinding beakers and balls. Grinding procedure continued until the major particle fraction of the sample was $\leq 315\text{ }\mu\text{m}$ which was then stored in HDPE wide neck square bottles by neoLab under ambient conditions. The powder was subsequently analysed with XRF, carbonate bomb and SC-Analyser by Leco.

Suspensions of 1 g powdered sample and 10 mL ultrapure water were mixed in conical centrifuge tubes for anion analysis with IC and pH measurements or in air-tight headspace vials for additional GC-MS analysis. The suspensions in the headspace vials were shaken on a MTS 2 rotary board by IKA at 500 rpm in the dark at a controlled temperature of $40\text{ }^{\circ}\text{C}$ in a B10 incubator by Memmert for 24 h, while the conical centrifuge tubes were shaken on a KS 501 D vibrating table by IKA at 300 rpm for 24 h under ambient conditions. The tubes, or the vials after GC-MS analysis, were centrifuged with 5000 rpm for 5 min with a Megafuge 1.0 by Hereaus. The pH was directly measured in the supernatant whereas prior to IC analysis the supernatant was filtered through $0.45\text{ }\mu\text{m}$ cartridges and diluted with ultrapure water.

Water samples for IC, ICP-OES and dissolved organic carbon (DOC) were filtered through $0.45\text{ }\mu\text{m}$ cartridges and diluted with ultrapure water. At every dilution step for ICP-OES analysis $50\text{ }\mu\text{L}$ concentrated HNO_3 were added to the samples.

5.4 Model reactions

Model reactions on abiotic furan formations were conducted with catechol representing natural organic matter. Oxidants were a mixture of $[\text{Fe}^{\text{II}}(\text{N}_2\text{Py}_2)(\text{OTf})_2]$ and H_2O_2 . Ethylfuran formation was tested under Fenton-like conditions using $50 \mu\text{M}$ $\text{Fe}_2(\text{SO}_4)_3$ with 0.35 mM H_2O_2 and 0.5 mM 4-ethylcatechol as precursor.

In the experiments with the bispidine Fe^{2+} complex initial catechol concentration was $5 \mu\text{mol}$ in a 10 mL (0.5 mM) aqueous phase whereas iron, H_2O_2 , KCl concentrations as well as reaction time, pH value and temperature were changed subsequently (Table 1) to obtain optimal furan yields.

Table 1. Subsequent optimisation steps for the abiotic furan formation from 0.5 mM catechol under Fenton conditions.

Optimisation step	$[\text{Fe}^{\text{II}}(\text{N}_2\text{Py}_2)(\text{OTf})_2]$ (μM)	H_2O_2 (mM)	Time (h)	pH	Temperature ($^\circ\text{C}$)	KCl (mM)
I $[\text{Fe}^{\text{II}}(\text{N}_2\text{Py}_2)(\text{OTf})_2]$	0-100	1	0.5	4.6	40	5
II H_2O_2	12.5	0-8	0.5	4.6	40	5
III Time	12.5	2	0-24	4.6	40	5
IV pH	12.5	2	0.5	2.1-8.7	40	5
V Temperature	12.5	2	0.5	4.6	20-70	5
VI Chloride	12.5	2	0.5	4.6	40	0-50

5.5 Instruments

The following paragraphs describe the multifarious analytical instruments that were used to characterise natural samples and monitor the model reactions. Standardised instrumental methods are briefly introduced, while the main focus is on adopted and newly developed methods to characterise hypersaline environments.

5.5.1 Volatile compounds (purge and trap GC-MS)

Volatile compounds were qualified and quantified with a Varian gas chromatograph GC 3400 linked by a transferline ($180 \text{ }^\circ\text{C}$) to a Varian Saturn 4D comprising electron impact ionisation ($10 \mu\text{A}$ emission current) and ion trap ($180 \text{ }^\circ\text{C}$, $47\text{-}249 \text{ m/z}$, reconstructed-ion chromatogram modus, scan rate 0.680 s) mass spectrometer. The GC was equipped with a J&W Scientific DB-5 (60 m ; 0.32 mm i.d.; $1 \mu\text{m}$ film thickness) capillary column by Agilent Technologies.

Dynamic headspace technique and analyte preconcentration was performed with a custom made purge and trap system. In general, analytes were purged by helium from the headspace

vials via in- and outlet needle connections and passed through a water trap containing $\text{Mg}(\text{ClO}_4)_2$. Headspace vials, needles and water trap are integral parts of the sampling loop. The analytes were focused and enriched on a glass lined tubing (GLT) by SGE Analytical Science. For preconcentration the GLT was cooled by liquid nitrogen to $-196\text{ }^\circ\text{C}$ and afterwards heated to $\sim 200\text{ }^\circ\text{C}$ by resistance heating to evaporate and transfer the analytes further onto the GC-MS.

The original system used dynamic cooling of the GLT and has been described in detail by Huber (2010). In short, the GLT was implemented horizontally into a cylinder connected by a tube with a cryogenic solenoid valve (P9202053, Norgen) to a self-pressurising cryogenic storage dewar with liquid nitrogen. By opening the valve the cylinder was filled with nitrogen steam to cool the GLT below $-190\text{ }^\circ\text{C}$. After reaching a set temperature the valve was closed to preserve nitrogen and as a result the GLT temperature increased again. Hence, the valve to the liquid nitrogen storage tank had to be reopened in intervals to ensure a sufficient low GLT temperature. This dynamic cooling system consumed a lot of liquid nitrogen while the temperature fluctuations were not favourable for the retention of highly volatile compounds.

In cooperation with S. G. Huber and I. Mulder these problems were solved with the development of an advanced static cooling trap (Mulder et al., 2013). The GLT was bent to be submerged into small a dewar filled with liquid nitrogen for the preconcentration step. Thereby, the amount of liquid nitrogen was limited to 80 mL per measurement and the GLT temperature was kept at constant $-196\text{ }^\circ\text{C}$. At the end of the purge sequence the liquid nitrogen was blown off by a pressurized air stream to allow resistance heating of the GLT.

As the original system was at large elaborated by Huber (2010) only the enhanced system covering a dynamic headspace technique will be discussed here in more detail. Figure 29 outlines the four steps of the preconcentration sequence. In standby (Figure 29A) the helium carrier gas (15 psi) bypasses the sampling loop via pneumatic valves V2, V3 and V4 (65.112 by Kuhnke) directly onto the GLT. The GLT is connected with a tee connector to a retention cap (inactivated GC column) followed by the GC column. Via the tee connector the GLT is furthermore connected to a GFC mass flow controller by ANALYT-MTC, but separated by the closed pneumatic valve V6 (64.024 by Kuhnke). During the 7.5 min of the purge and trap sequence (Figure 29B) a headspace vial is connected to the two needles and the sample loop bypass between valve V3 and V4 is closed. The helium flow is diverted via valve V3 to the headspace vial and via V5 and V4 onto the now cooled GLT. To ensure a steady helium flow during this sequence valve V6 is opened and the flow controller regulates the helium flow

through the system. The flow was set to 10 mL/min for the original setup and to 15 mL/min for the new setup.

The desorption sequence is subdivided into two separate steps. Firstly, the sample loop bypass between V3 and V4 is opened again ceasing further purging of the headspace and V6 is closed routing the carrier gas completely to the GC-MS (Figure 29C). Furthermore, the liquid nitrogen around the GLT is removed by a compressed air stream starting defreezing of the GLT. Secondly, fast and controlled desorption of the analytes on the GLT is supported by resistance heating of the GLT to $\sim 200\text{ }^{\circ}\text{C}$ for 2.4 min controlled with a HKR 139 unit by Newig. At the same time V5 is manually opened to allow a dry helium backflush-stream through the water trap, which is heated to $110\text{ }^{\circ}\text{C}$ controlled by a HS-W-35/M (HS Heizelemente) to regenerate the $\text{Mg}(\text{ClO}_4)_2$.

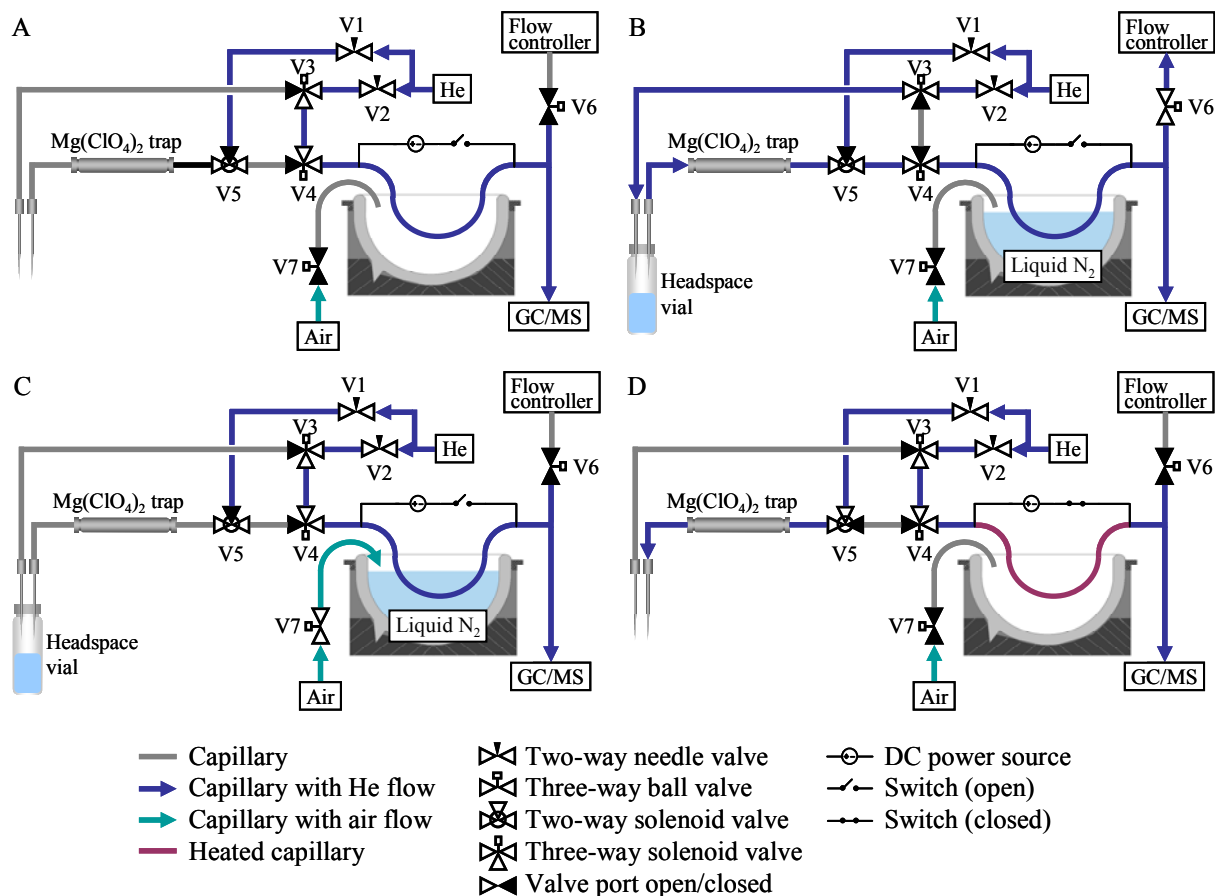


Figure 29. Enhanced purge and trap system with **A** standby mode, **B** analyte preconcentration from headspace vials onto liquid nitrogen cooled GLT, **C** beginning of the desorption sequence by removing the liquid nitrogen with pressurized air and **D** resistance heating and transfer of analytes to the GC-MS.

With the change of the purge and trap system the GC oven temperature program was rewritten to allow faster measurements while improving the separation of very volatile compounds but also to include less volatile compounds such as terpenes into the measurements timeframe. Figure 30 shows the GC oven temperature programs in comparison. With the original program the oven was equilibrated at 35 °C at the beginning of the sequence for 8.5 min and then was heated at 5.5 °C/min to 150 °C and after 5 min to 210 °C at 30 °C/min. The end temperature was held for 15 min. The new program started at 30 °C which was held for 15.5 min before the temperature was risen at 5 °C/min to 114 °C and from there at 30 °C/min to 210 °C which was held for 8 min.

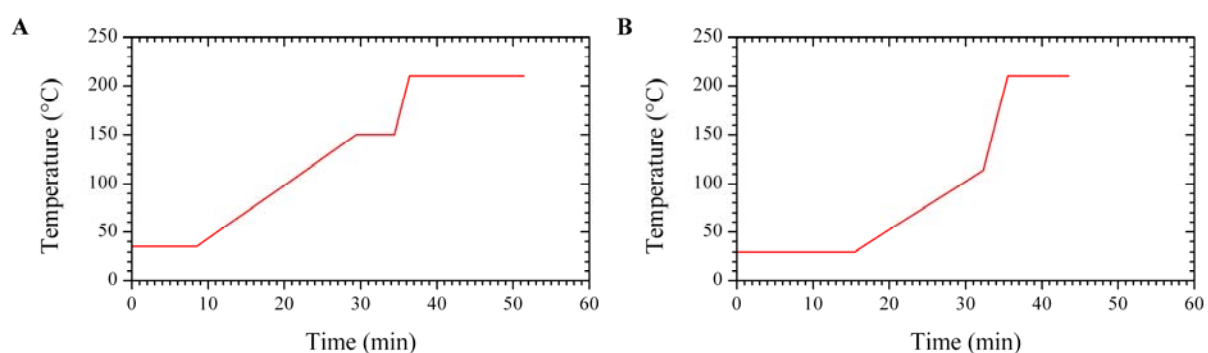


Figure 30. GC oven temperature program for **A** dynamic cooling and **B** static cooling of the GLT trap.

The old system (Huber, 2010) was used to assess the model reaction with the bispidine Fe^{2+} complex, while the new system (Mulder et al., 2013) was used to analyse natural samples.

Analytes in natural samples were identified by retention times and mass spectra with those obtained from commercial standards. In the few cases where no standards were available the mass spectra were compared to the National Institute of Technology (NIST) databases while considering the respective retention times to estimate boiling points.

External multipoint calibration was performed for all commercially available analytes by injection of a methanol based standard with known concentration (Appendix A) into a 20 mL headspace vial filled with 10 mL ultrapure water mimicking conditions applied during the measurements of natural samples and model reactions. In case of 3-methylfuran, 2,4-dimethylfuran and xylenes recovery rates analogous to their isomers were assumed.

Furthermore, all measurements were performed in triplicates and daily performance of the GC-MS was tested with a 0.8 ng/mL hexafluorobenzene (99%; Sigma Aldrich) standard to calculate daily response factors. Additionally, daily blank measurements were performed to subtract eventual analyte background concentrations from actual measurements.

5.5.2 Major and trace elements (XRF)

Major and trace elements in soil, sediment and plant samples were quantified by X-ray fluorescence spectrometry (XRF) using two energy-dispersive multi element analysers. These were custom-made by Andrey Cheburkin using commercially available components. One analyser used a Co X-ray source (17 V, 1 mA) to excite and measure elements between Al and Mn (Z 13-25) with a HPGe-detector called TITAN (Cheburkin and Shotyk, 2005). The other instrument, called EMMA, utilized a Mo X-ray source (37 V, 5 mA) and a Si(Li)-detector for heavier elements from Fe to Y (Z 26-39) as well as Pb (Z 82) (Cheburkin et al., 1997).

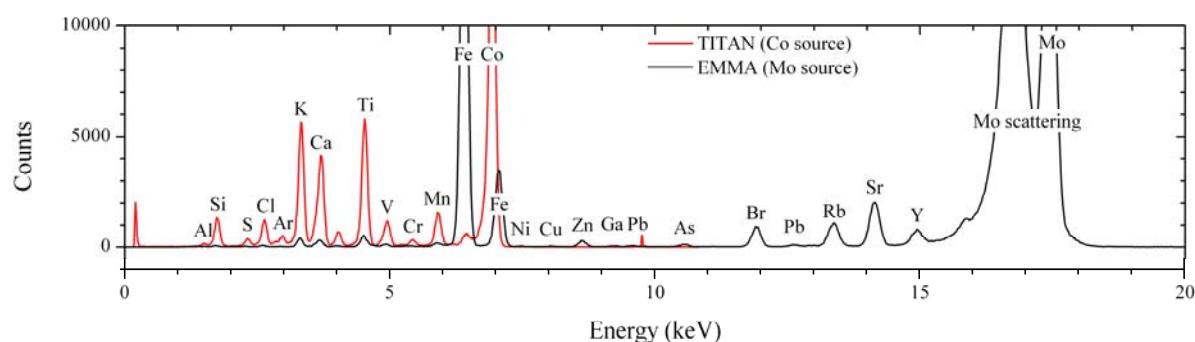


Figure 31. Two fluorescence spectra obtained with TITAN and EMMA.

Table 2. Transition energies of element lines and relative intensity ratios used by the data acquisition software.

TITAN				EMMA			
Energy (keV)	Element	Line	Rel. intensity ratio K_{β}/K_{α}	Energy (keV)	Element	Line	Rel. intensity ratio
1.4862	Al	K_{α}	0.100 K_{β}/K_{α}	5.8981	Mn	K_{α}	0.152 K_{β}/K_{α}
1.7399	Si	K_{α}	0.100 K_{β}/K_{α}	6.3980	Fe	K_{α}	0.159 K_{β}/K_{α}
2.2081	S	K_{α}	0.100 K_{β}/K_{α}	7.4770	Ni	K_{α}	0.166 K_{β}/K_{α}
2.6227	Cl	K_{α}	0.100 K_{β}/K_{α}	8.0470	Cu	K_{α}	0.165 K_{β}/K_{α}
2.9579	Ar	K_{α}	0.103 K_{β}/K_{α}	8.6300	Zn	K_{α}	0.170 K_{β}/K_{α}
3.3133	K	K_{α}	0.122 K_{β}/K_{α}	9.2411	Ga	K_{α}	0.170 K_{β}/K_{α}
3.6914	Ca	K_{α}	0.128 K_{β}/K_{α}	10.549	Pb	L_{α}	1.000 L_{α}/K_{α}
4.5103	Ti	K_{α}	0.182 K_{β}/K_{α}	10.530	As	K_{α}	0.210 K_{β}/K_{α}
4.9520	V	K_{α}	0.139 K_{β}/K_{α}	11.907	Br	K_{α}	0.147 K_{β}/K_{α}
5.4143	Cr	K_{α}	0.192 K_{β}/K_{α}	12.625	Pb	L_{β}	1.220 L_{β}/K_{α}
5.8981	Mn	K_{α}	0.182 K_{β}/K_{α}	13.373	Rb	K_{α}	0.158 K_{β}/K_{α}
6.9304	Co	K_{α}	0.160 K_{β}/K_{α}	14.140	Sr	K_{α}	0.165 K_{β}/K_{α}
				14.931	Y	K_{α}	0.223 K_{β}/K_{α}
				17.441	Mo	K_{α}	0.174 K_{β}/K_{α}

The analysers record photons over time discriminated by energy into different channels. These channels were converted into transition energies by two-point calibration. For TITAN these were normally potassium K_{α} line and Co scattering and for EMMA the iron K_{α} line and Mo coherent scattering, respectively.

Fluorescence emissions of powdered samples were recorded over 10 min for statistical certainty. After calibration of the x-axes peaks were assigned to K and L lines according to transition energies and peak overlaps were compensated by an algorithm based foremost on the relative intensity ratio between elemental K_{α} and K_{β} lines listed in Table 2.

Table 3. CRM for soils, sediments and rocks.

Standard	Description	Supplier
VS-N	Glass standard	ANRT ¹
LKSD-3	Lake sediment	CANMET ²
SY-3	Syenite	CANMET ²
Mica-Fe	Biotite	CRPG ³
Mica-Mg	Phlogopite	CRPG ³
SRM 1633	Coal fly ash	NBS ⁴
SRM 1646	Estuarine sediment	NBS ⁴
SRM 2710	Montana soil	NIST ⁵
SRM 2711	Montana soil	NIST ⁵
GBW07108	Carbonate rock	NRCCRM ⁶
BHVO-1	Basalt	USGS ⁷
G-2	Granite	USGS ⁷
PCC-1	Peridotite	USGS ⁷
MAG-1	Marine sediment	USGS ⁷
W-1	Diabase	USGS ⁷

Table 4. CRM for plants and peats.

Standard	Description	Supplier
BCR No 60	Aquatic plant	BCR ⁸
BCR No 62	Olive leaves	BCR ⁸
SRM 1571	Orchard leaves	NBS ⁴
SRM 1575	Pine needles	NBS ⁴
SRM 1515	Apple leaves	NIST ⁵
SRM 1547	Peach leaves	NIST ⁵
SRM 1573a	Tomato leaves	NIST ⁵
SRM 1632b	Bituminous coal	NIST ⁵
SRM 1635	Subbituminous coal	NIST ⁵
V-10	Hay	IAEA ⁹
CTA-OTL-1	Oriental tobacco leaves	ICH TJ ¹⁰
CTA-VTL-2	Virginia tobacco leaves	ICH TJ ¹⁰
GBW07602	Bush twigs and leaves	IGGE ¹¹
GBW07604	Poplar leaves	IGGE ¹¹
GBW07605	Tea	IGGE ¹¹

¹Association Nationale de la Recherche Technique, ²Canadian Centre of Mineral and Energy Technology, ³Centre de Recherches Pétrographiques et Géochimiques, ⁴National Bureau of Standards now NIST, ⁵National Institute of Standards and Technology, ⁶National Research Center for CRMs, ⁷United States Geological Survey, ⁸Community Bureau of Reference, ⁹International Atomic Energy Agency, ¹⁰Institute of Nuclear Chemistry and Technology, ¹¹Institute of Geophysical and Geochemical Exploration

The XRF-analysers were externally calibrated for a heavy soil/sediment/rock matrix (Table 3) and a light plant/peat matrix (Table 4) with different certified reference materials (CRM) while the coherent and incoherent scattering of the X-ray source elements were used as internal references. Performance of the calibration was constantly verified with at least one of the available CRM.

5.5.3 Cations (ICP-OES)

Cations within water samples were quantified with an ICP-OES Vista MPX by Varian and an Agilent 720. The acidified and filtered solutions were injected via a nebuliser into an argon plasma. Within the plasma the analytes were excited by collisions with electrons and other charged ions and relaxed again by emitting specific electromagnetic radiation. The analytes were identified by their respective electron transition energies in the UV/VIS domain and the ICP-OES was calibrated with standard solutions (ULTRA SCIENTIFIC). All experiments were carried out in triplicates.

5.5.4 Anions (IC)

Anion quantification was performed on an ICS1100 system with an analytical IonPac AS9-HC or AS23 column (4 · 250 mm) by Dionex. Additionally, the system had an AG9-HC guard column (4 · 50 mm) by Dionex and self-regenerating ASRS Ultra II suppressor (45 mA) to enhance measurements with a conductivity detector. Additionally, the system was also equipped with a UV/VIS detector measuring absorbance at 208 nm. A 9 mM Na₂CO₃ eluent was pumped through the system with 1 mL/min. Anions in filtered water samples (Chapter 5.3) were identified by their retention times and quantified with commercial standards (CertiPUR, Merck Millipore). All experiments were carried out in triplicates.

5.5.5 Dissolved organic carbon (DOC)

Inorganic and total dissolved carbon were measured with a TOC-V CPH by Shimadzu. In a first step the total carbon content of a filtered water sample (Chapter 5.3) was determined by means of catalytic combustion in an O₂ stream to produce CO₂ from organic and inorganic carbon. In a second step the aqueous sample was mixed with 25% H₃PO₄ to convert only the inorganic carbon fraction to CO₂. During both steps CO₂ was measured by an NDIR spectrometer. The dissolved organic carbon content of the samples was calculated by subtracting the inorganic carbon concentration from the total organic carbon concentration.

The instrument was calibrated with 1000 mg/L carbon standards by Ultra Scientific. All experiments were carried out in duplicates.

5.5.6 Inorganic carbon (Carbonate bomb)

The inorganic carbon fraction of soil and sediment samples was measured with a carbonate bomb (Müller and Gastner, 1971). Carbon determination is based on the release of CO₂ from carbonate reacting with HCl, as depicted by Eq. 50, in a closed vessel resulting in a measurable pressure increase.



The device was calibrated with a carbonate standard using a one-point calibration. The reliability of the calibration was verified in a bachelor thesis by Pallmer (2010).

For the measurements 2 g of the freeze-dried and ground samples were mixed in the carbonate bomb with 5 mL HCl (25%). All experiments were carried out in duplicates.

5.5.7 Organic carbon (SC-analyser)

Total carbon content was determined with a SC-144DR sulfur/carbon analyser by Leco calibrated with a carbonate standard. Freeze-dried and powdered samples of about 0.1 g were burned in an O₂ stream at over 1200 °C oxidising inorganic and organic carbon alike to CO₂ which was measured by IR spectrometry at 2349 cm⁻¹. The analyser was calibrated with CaCO₃ which equals 12% carbon. The organic fraction (C_{org.}) within natural samples was calculated by subtraction of the inorganic carbon content from the total carbon content. All experiments were carried out in duplicates.

5.5.8 pH, redox potential and conductivity

Several probes were deployed during campaigns and in laboratory measurements to determine pH, redox potential (Eh in mV), electrical conductivity (σ in mS/cm) and temperature (T in °C) of aqueous solutions including eluates from soil and sediment samples (Chapter 5.3). The different utilised probes with the respective pH and multiparameter meters are listed in Table 5 and Table 6. In Australia and at the Dead Sea pH, Eh and conductivity were measured in 50 mL falcon tubes or if sufficient surface water was available directly in the water column of the salt lakes. For the Australian campaign 2013 a flow cell driven by a TP 3005 peristaltic pump (Thölen Pumpen) was used to measure pH, Eh, temperature and dissolved oxygen

(Chapter 5.5.9) during the Teflon chamber experiments (Chapter 5.5.14). The data were logged by a WTW multimeter (Appendix F).

Table 5. Probes for liquid analysis.

Probe	Company	Parameter	Connection
Sentix 940-3	WTW	pH, T	Digital
Sentix 41	WTW	pH, T	Analog
Sentix Mic	WTW	pH, T	Analog
ORP 900	WTW	Eh	Digital
Sentix ORP	WTW	Eh	Analog
TetraCon 925	WTW	σ , T	Digital
TetraCon 325	WTW	σ , T	Analog
FDO 925	WTW	DO, T	Digital

Table 6. pH and multiparameter meters.

Meter	Company	Connection
Multi 3430	WTW	Digital
Multi 3420	WTW	Digital
Multiline P4	WTW	Analog
Toledo Δ -320	Mettler	Analog
pH-Meter 761	Knick	Analog

The pH probes were calibrated on the free hydrogen scale with two buffer solutions by Merck at 4.01 and 7.00. Additionally, the pH probes came with a temperature sensor for internal temperature compensation for the pH calculation. Probes for Eh and conductivity were calibrated with a standard solution by Merck Millipore, respectively. Field campaign experiments were carried out in single or continuous measurements, whereas pH laboratory experiments were carried out in triplicates.

5.5.9 Dissolved oxygen

Dissolved oxygen (DO) was measured at Australian salt lakes within a flow chamber with an FDO 925 probe and corresponding Multi 3430 multiparameter meter from WTW. The oxygen probe was calibrated in water vapour-saturated air provided by an FDO Check calibration vessel. Furthermore, the data from the oxygen probe was automatically corrected for a salinity of 70 PSU (practical salinity units) on the practical salinity scale (PSS-78), which was the maximum available setting but still insufficient to characterise the hypersaline environment. Hence DO values were manually corrected.

In the first step the data was rectified from the automatic salinity correction which is based on the ISO 8514 method according to WTW. This method cites as its source material the International Oceanographic Tables Vol. 2 by the National Institute of Oceanography of Great Britain and UNESCO (1973) which are based on an equation by Weiss (1970). However, these tables were found to be incorrect by Weiss (1980) and the UNESCO updated its tables in 1986 according to Fofonoff and Millard Jr. (1991). The new tables are based on an equation by Benson and Krause Jr. (1984) depicted in Eq. 51 where f_{IOT} is the correction

factor, S‰ is the salinity in ppt and T is the temperature in Kelvin. It is assumed that this equation is also used by the WTW instrument, because it is also endorsed by the USGS (2011) amongst others. Furthermore, it is believed that the instrument equates S‰ with the practical salinity scale as an approximation.

$$f_{\text{IOT}} = \exp\left[-S‰ \cdot \left(0.017674 - \frac{10.754}{T} + \frac{2140.7}{T^2}\right)\right] \quad (51)$$

The measured $\text{DO}_{(T,S‰)}$ values which are a function of temperature T and salinity S‰ were recalculated using Eq. 52. $\text{DO}_{(T,0)}$ and $\text{DO}_{(T,S‰)}$ are dissolved oxygen in mg/L for any temperature T at zero and in this case 70‰ salinity and f_{IOT} is the correction factor from Eq. 51.

$$\text{DO}_{(T,0)} = \frac{\text{DO}_{(T,S‰)}}{f_{\text{IOT}}} \quad (52)$$

To further process the DO values the salinity S‰ of the examined salt lakes was calculated according to Williams and Sherwood (1994) from IC and ICP-OES data and gravimetric density measurements.

The amount of $\text{DO}^*_{(T,S‰)}$ at a given temperature T in Kelvin and salinity S‰ in equilibrium with the atmosphere at 1 atm can be predicted with Eq. 53 for hypersaline NaCl dominated solutions (Sherwood et al., 1991, 1992) with a_i as empirical constants (see Table 7).

$$\text{DO}^*_{(T,S‰)} = \exp\left(a_0 + \frac{a_1}{T} + a_2 \cdot \ln T + a_3 \cdot T + a_4 \cdot T^2 + S‰(a_5 + a_6 \cdot T + a_7 \cdot T^2) + a_8 \cdot S‰^2\right) \quad (53)$$

Table 7. Empirical constants from Sherwood et al. (1992) for Eq. 53.

Constant	Value	Constant	Value	Constant	Value
a_0	$-6.85693750 \cdot 10^4$	a_3	$-4.59371240 \cdot 10^1$	a_6	$2.06161380 \cdot 10^{-4}$
a_1	$1.28038367 \cdot 10^6$	a_4	$2.65097198 \cdot 10^{-2}$	a_7	$-2.68767762 \cdot 10^{-7}$
a_2	$1.32716777 \cdot 10^4$	a_5	$-4.29122353 \cdot 10^{-2}$	a_8	$-3.60557809 \cdot 10^{-6}$

The quotient of $\text{DO}^*_{(T,S‰)}$ from Eq. 53 for any given salinity and zero salinity $\text{DO}^*_{(T,0)}$ gives the respective conversion factors f_{NaCl} (Eq. 54).

^^

$$f_{\text{NaCl}} = \frac{\text{DO}^*_{(T,S‰)}}{\text{DO}^*_{(T,0)}} \quad (54)$$

The $DO_{(T,0)}$ values obtained previously after converting the measured DO with Eq. 51 and 52 are multiplied by the respective conversion factor f_{NaCl} to yield salinity corrected $DO_{(T,S\%)}$ values for the salt lakes (Eq. 55).

$$DO_{(T,S\%)} = f_{NaCl} \cdot DO_{(T,0)} \quad (55)$$

5.5.10 Water redox conditions (Pourbaix diagrams)

Pourbaix diagrams describe phase diagrams of an aqueous electrochemical system as a function of Eh and pH. Transitions from one predominant stable phase to another are defined by the Nernst equation and represented as lines in the plot. On these lines phases are in equilibrium with equal activities of both species.

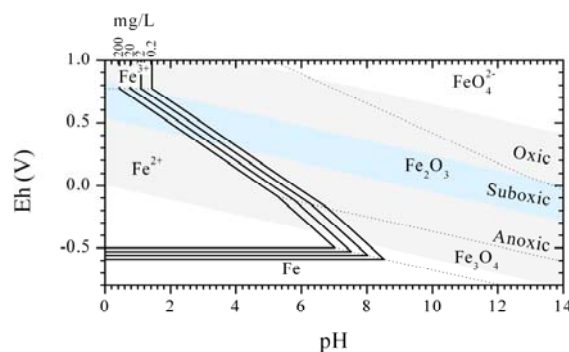
The iron predominance diagrams used to describe the redox systems in salt lakes were constructed according to Verink (2000) with solid lines indicating concentration dependent equilibriums and pointed lines concentration independent equilibriums. The common assumption that molar concentration equals the activity of a species is not valid for solutions of high ionic strength such as hypersaline waters. Reliable calculations of the activity coefficients are limited due to the restriction of the Debye-Hückel equation (Debye and Hückel, 1923), including the extended version, and Davies equation (Davies, 1962) in hypersaline solutions (España and Ercilla, 2008). Only the Pitzer equation (Pitzer, 1973) is feasible at high ionic strength but is limited to a system consisting of only a handful of elements, excluding Fe^{3+} for example, though there have been attempts to fill this gap (Millero et al., 1995; Bozau, 2013). The activity for Fe^{2+} was calculated for a model salt lake with the PHREEQC Interactive software (v. 3.0.6.7757) by the USGS using the Pitzer database and McInnes assumption that the activity of K^+ and Cl^- are equal (Plummer et al., 1988). Input parameters and some output parameters are summarised in Table 8 for different total iron concentrations. For simplicity it was assumed that the activity of Fe^{3+} equals the activity of Fe^{2+} for the same concentrations.

The data from Table 8 was used to create the simplified Pourbaix diagram for different total iron concentrations as illustrated in Figure 32.

Table 8. Calculated activities for various iron concentrations in a model salt lake.

Input parameters	Value	Output parameters	Value
Temperature	25 °C	For 0.2 mg/L Fe ²⁺	
Density	1.204 kg/L	Ionic strength	7.018 mol/L
pH	4.8067	Activity	9.288·10 ⁻³ mol/L
Cl ⁻	5184.588 mmol/L	For 2 mg/L Fe ²⁺	
Br ⁻	5.874 mmol/L	Ionic strength	7.009 mol/L
SO ₄ ²⁻	210.712 mmol/L	Activity	9.263·10 ⁻⁴ mol/L
Ca	11.469 mmol/L	For 20 mg/L Fe ²⁺	
K	52.578 mmol/L	Ionic strength	7.008 mol/L
Mg	538.584 mmol/L	Activity	9.260·10 ⁻⁵ mol/L
Mn	0.203 mmol/L	For 200 mg/L Fe ²⁺	
Na	4161.092 mmol/L	Ionic strength	7.008 mol/L
Sr	0.222 mmol/L	Activity	9.260·10 ⁻⁶ mol/L

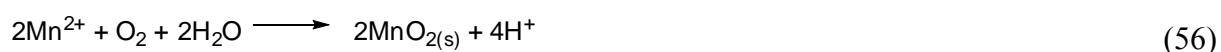
Interpretation of Eh pH plots and the used simplified Pourbaix diagrams underlie some considerations. Firstly, the obtained Eh values do not represent a discrete redox system of one element but of all available elements. Secondly, the Pourbaix diagram only includes equilibria of a limited amount of iron species, neglecting several other possible equilibria. Thirdly, a temperature of 25 °C was used to construct the Pourbaix diagrams neglecting temperature dependency of the potential. Though the whole system is limited by these restrictions it is adequate to discuss redox conditions of hypersaline lake waters and predict the abundance of soluble Fe²⁺.

**Figure 32.** Simplified Pourbaix diagram (Verink, 2000) used for the interpretation of Eh pH plots.

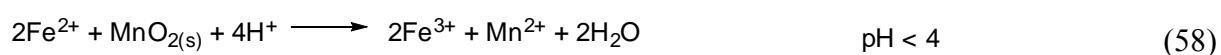
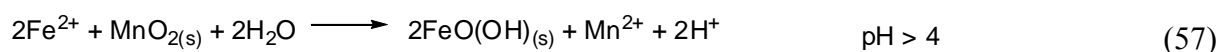
5.5.11 Sediment redox conditions (Redox-Sensitive Tapes)

Redox-Sensitive Tapes (RST), provided by Oeste (2010), were used to classify redox zones of salt lake sediments in Australia. RST are made of synthetic fibre impregnated with various inorganic substances. As such, RST-A contains black MnO_2 , RST-B brown FeO(OH) and RST-C a mixture of MnO_2 , FeO(OH) , BaSO_4 and PbSO_4 . The tapes were fixed to a PVC sheet and submerged into the lake sediments for at least 3 weeks. Depending on the sediment redox conditions the pigments can react with the environment resulting in a colour change. The milieus are separated into four categories: oxic milieu I, suboxic milieu II with Mn(IV)-reducing conditions and Fe(II)-oxidising conditions, suboxic milieu III with Fe(III)-reducing and sulfide-oxidising conditions and anoxic milieu IV with sulfate-reducing to methanogenic conditions.

In the oxic milieu I Mn^{2+} reacts with oxygen to MnO_2 as shown in Eq. 56 (Jones et al., 2011), which has no influence on the colour of the RST.



In the suboxic milieu II MnO_2 on RST-A and RST-C is reduced by Fe^{2+} to soluble Mn^{2+} . At a $\text{pH} > 4$ formed Fe^{3+} precipitates as brown iron oxides, e.g. FeO(OH) (Eq. 57), on the RST or stays in solution below a pH of 4 (Eq. 58) (Postma, 1985).



Milieu III is characterized by Fe^{3+} to Fe^{2+} reduction and sulfide to sulfate oxidation. The half-cell reaction for Fe^{3+} is given by Eq. 59 (Sparks, 2003). Electron donors are organic substances or biogenic processes of anaerobic microorganisms (Lovley, 1987). Hence, Fe^{3+} pigments of RST-B and RST-C dissolve from the tapes as well as iron oxides formed on RST-A in the course of MnO_2 reduction.



In the anoxic milieu IV sulfate is reduced biologically to sulfide as shown in the half-cell reaction depicted in Eq. 60 (Silverman et al., 1964).



The sensitive reaction of H_2S with PbSO_4 (Eq. 61) leaves brown stains on RST-C while at higher H_2S concentrations black FeS formation (Eq. 62) can be observed on the RST.



During drying the FeS on the black RST reacts with oxygen forming brown iron oxides like $\text{FeO}(\text{OH})$ according to Eq. 63 (Schnitker et al., 1980).



5.5.12 On-site detection and quantification of $\text{Fe}^{2+}/\text{Fe}^{3+}$

Fe^{2+} was identified in sediments and salt crusts by a specific test with the chelating agent 2,2'-bipyridine as a red complex (Figure 33A) during the Australian campaigns 2012 and 2013.

The dissolved $\text{Fe}^{2+}/\text{Fe}^{3+}$ ratio of water samples was measured on-site with a Hach-Lange DR2800 spectrophotometer using a Spectroquant iron test kit (100796) by Merck Millipore in 2013. Calibration of the spectrophotometer is shown in Figure 33B. Measuring principle is the formation of a coloured complex of 1,10-phenanthroline and Fe^{2+} with a maximal extinction at 508 nm. In a second step Fe^{3+} is reduced to Fe^{2+} by ascorbic acid to measure total dissolved Fe concentrations. In most cases natural samples had to be diluted to total Fe concentrations of 0.01 to 5 mg/L with acidic distilled water. Prior to measurements a zero adjustment was conducted.

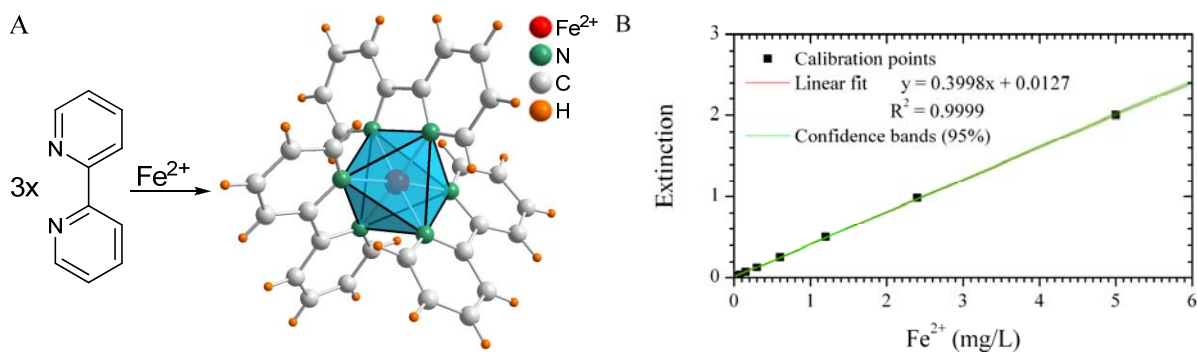
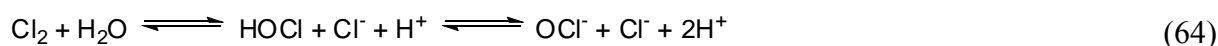


Figure 33. **A** Formation of octahedral tris(2,2'-bipyridine-N,N')-iron(II) complex (Ariyananda and Norman, 2002). **B** Calibration of the Hach-Lange spectrophotometer for Fe^{2+} and Fe^{3+} quantification.

5.5.13 Free and total chlorine

With the 2nd campaign to Australia in 2012 the on-site measurement of free and combined chlorine in hypersaline surface waters with N,N-diethyl-*p*-phenylenediamine (DPD) (Palin, 1957) was evaluated.

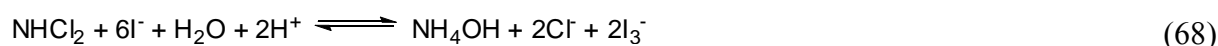
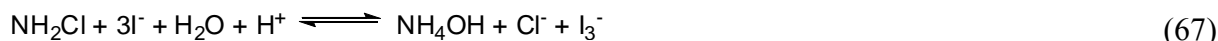
Depending on the pH free chlorine exists as chlorine, hypochlorous acid or hypochloride in aqueous solution (Barcellos da Rosa, 2003). Under acidic conditions molecular chlorine is the predominant chlorine species, while under alkaline conditions it is hypochloride (Eq. 64).



Free chlorine reacts with amines forming reactive mono- and dichloramines, so-called bound chlorine, as depicted in Eq. 65 and 66.



While the interference of chloramines with the DPD method is minimal, they readily react with iodide to form triiodide (Eq. 67-68).



Free chlorine reacts with DPD producing the magenta coloured Würster Dye that can be measured with a photometer. Furthermore, the triiodide from the reactions of chloramines with iodide (Eq. 11-12) can be utilized to measure the total chlorine content of aqueous solutions (Figure 34). At high levels of oxidants the Würster Dye reacts further to a colourless imine.

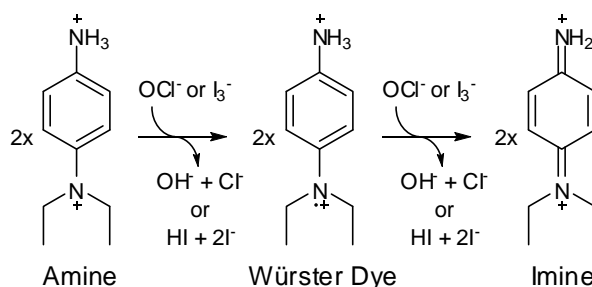


Figure 34. Reaction of hypochlorite and triiodide with the DPD reagent and on-going reaction to an imine.

With an AL 100 photometer by Aqualytic the reaction of chlorine with DPD was monitored at 530 nm (Appendix F). For the measurements the pH of a 10 mL water sample was adjusted to 6-7 with NaOH before it was transferred into the photometer cell. After zero adjustment a DPD No. 1 tablet was added to and crushed in the solution with a plastic pestle and free chlorine content was measured. The procedure was repeated after adding a DPD No. 3 tablet containing iodide into the cell to measure the total chlorine concentration.

Rising the pH of some acidic samples to 6-7 resulted in $\text{Al}(\text{OH})_3$ precipitation which had to be filtered from the solution prior to photometric analysis with the risk of losing free chlorine in the process. Furthermore, the use of tablets in halide saturated water samples was less than optimal. Major known interfering substances for the DPD method are ClO_2 , Br_2 , I_2 , H_2O_2 , Mn^{4+} , Mn^{7+} and Cr^{6+} .

5.5.14 PTFE chamber

In 2012 and 2013, a 1.5 m³ PTFE chamber was set up on several salt lakes in Western Australia to identify sources of particle formation and monitor atmospheric conditions like ozone abundance (Kamilli et al., 2013).



Figure 35. Setup for water analysis and air collection (left) and PTFE chamber on Lake Dune in 2013 (right).
Images: Torsten Krause CC BY-SA 4.0.

Additionally, the temperature of the salt crust and upper sediment layer were logged with a ThermaData TD2F by ETI, water temperature, Eh, pH and DO by the setup described in Chapter 5.5.8 and 5.5.9 and air temperature as well as humidity with a DL-120TH data logger by Voltcraft. Furthermore, a 435-2 multimeter with an IAQ multi-function probe by Testo recorded CO_2 , temperature and humidity within the chamber. Attached to the chamber were PTFE tubes to collect air samples via a N814KTDC membrane pump by KNF and to monitor chlorine with an external pump and X-am 5000 by Draeger (Appendix F).

6 Novel model reactions

The importance of abiotic furanoic compound formation in natural environments was investigated within two model reactions (Krause et al., 2013). The first was a comprehensive series on the Fenton induced furan formation from catechol (Chapter 6.1) and the second was an exemplary study on monoalkylated furan formation with alkylchains exceeding a methyl moiety (Chapter 6.2). These model reactions extend the work of Huber et al. (2010) to understand furan formation in Fe^{2+} predominant environments, like the Australian salt lakes (Chapter 9.3), and the formation of several monoalkylated furans from natural samples (Chapter 10.4).

6.1 Abiotic furan formation from catechol with $[\text{Fe}^{\text{II}}(\text{N}_2\text{Py}_2)(\text{OTf})_2]$

Catechol is converted to furan, by Fenton reaction involving $[\text{Fe}^{\text{II}}(\text{N}_2\text{Py}_2)(\text{OTf})_2]$, comparable to Fenton-like chemistry with $\text{Fe}_2(\text{SO}_4)_3$ (Huber et al., 2010). With initial concentrations of 5 mM catechol the optimal bispidine iron complex concentration for the reaction was 12.5 μM (Figure 36A). Furan was not detected in the absence of iron while higher iron concentrations led to a moderate depletion of furan emissions.

The optimal molar ratio of iron to catechol was 1:40 in these experiments showing the catalytic efficiency of the used iron complex. Furthermore, the turnover numbers for the bispidine iron complex were 8 times higher than for $\text{Fe}_2(\text{SO}_4)_3$ salt with an optimal iron/catechol ratio of only 1:5 (Huber et al., 2010). A plausible explanation is that the bispidine iron complex is stabilised in solution by its ligands, whereas Fe^{3+} from sulfate salts is susceptible to precipitation and thus is removed from the reaction cycle.

Also essential for furan formation was H_2O_2 which is decomposed by iron cycling yielding reactive OH radicals. Optimal H_2O_2 concentration was an excess of 2 mM (Figure 36B) compared to 0.5 mM catechol giving a molar ratio of 4:1. Higher H_2O_2 concentrations can promote side- and follow-up reactions to higher oxidised products like oxalic acid (Studenroth et al., 2013) or to complete mineralisation (Pracht et al., 2001) while furan yields decline.

Of interest is the excess of H_2O_2 compared to catechol needed for optimal furan formation, whereas previous studies with Fe^{3+} sulfate produced optimal yields with less H_2O_2 compared to catechol (molar ratio of 1:1.4) (Huber et al., 2010).

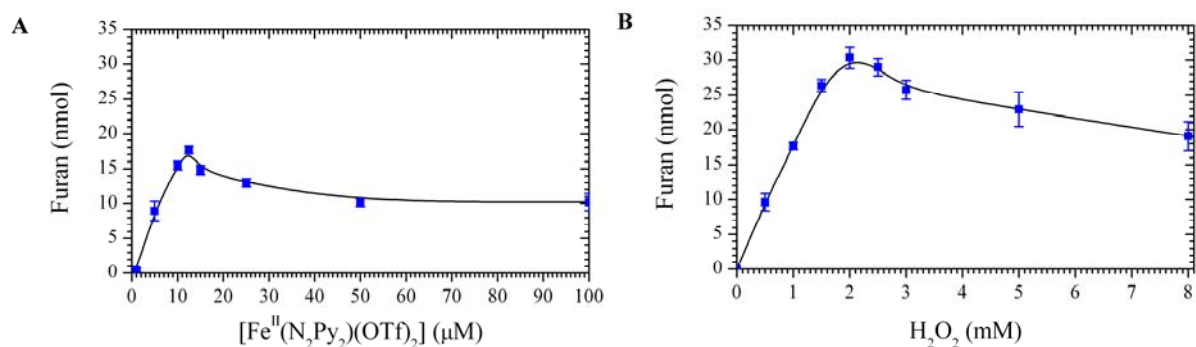


Figure 36. Effects of different parameters on the furan formation from a 10 mL solution. **A** Variation of $[\text{Fe}^{\text{II}}(\text{N}_2\text{Py}_2)(\text{OTf})_2]$: reaction of 0.5 mM catechol with 0-100 μM $[\text{Fe}^{\text{II}}(\text{N}_2\text{Py}_2)(\text{OTf})_2]$, 1 mM H_2O_2 , 5 mM KCl at a pH of 4.6 and 40 °C after 30 min. **B** Variation of H_2O_2 : reaction of 0.5 mM catechol with 12.5 μM $[\text{Fe}^{\text{II}}(\text{N}_2\text{Py}_2)(\text{OTf})_2]$, 0-8 mM H_2O_2 , 5 mM KCl at a pH of 4.6 and 40 °C after 30 min.

Furthermore, with an optimal reaction time of 30 min (Figure 37A) the reaction was slower as compared to the Fenton-like reaction with $\text{Fe}_2(\text{SO}_4)_3$ (Huber et al., 2010). Longer reaction times yielded less furan indicating decomposition reactions within the headspace vial. Soluble furan is probably oxidised within the aqueous phase by radicals generated via Fenton chemistry. A comparable degradation mechanism for furan was described in gas phase chemistry (Gómez Alvarez et al., 2009; Atkinson et al., 1983).

The optimal pH value for the reaction was 4.6. Under more acidic conditions the reaction between $[\text{Fe}^{\text{II}}(\text{N}_2\text{Py}_2)(\text{OTf})_2]$ and H_2O_2 is inhibited while alkaline conditions favour precipitation of iron hydroxide (Remucal and Sedlak, 2011). In both cases OH radical generation is subdued resulting in less furan formation (Figure 37B).

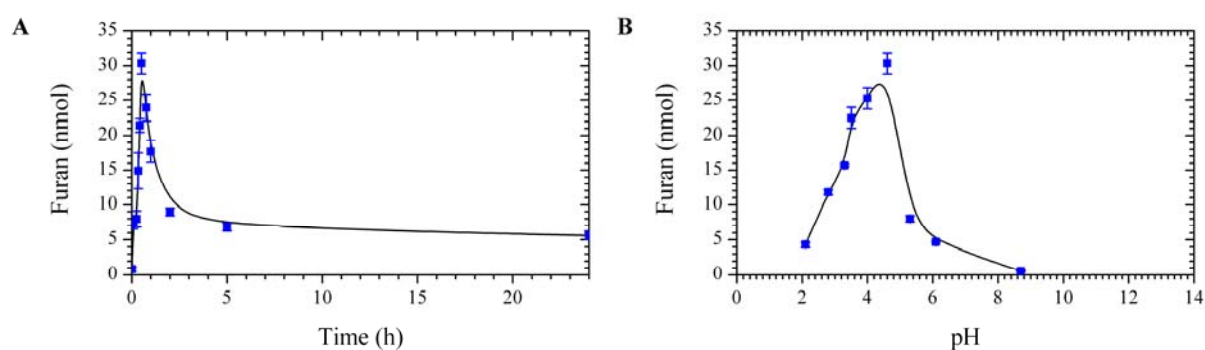


Figure 37. Effects of different parameters on the furan formation from a 10 mL solution. **A** Time dependency: reaction of 0.5 mM catechol with 12.5 μM $[\text{Fe}^{\text{II}}(\text{N}_2\text{Py}_2)(\text{OTf})_2]$, 2 mM H_2O_2 , 5 mM KCl at a pH of 4.6 and 40 °C after 0-24 h. **B** Variation of pH: reaction of 0.5 mM catechol with 12.5 μM $[\text{Fe}^{\text{II}}(\text{N}_2\text{Py}_2)(\text{OTf})_2]$, 2 mM H_2O_2 , 5 mM KCl at a pH of 2.1-8.7 and 40 °C after 30 min.

Elevated temperatures of 40 °C yielded highest furan concentrations (Figure 38A). With less energy input to the reaction, furan concentrations were subdued at lower temperature, and also at higher temperatures which promote side and follow-up reactions.

If chloride was added to the reaction furan formation, employing the bispidine Fe^{2+} complex, was inhibited, most likely due to chloride reacting with OH radicals forming less reactive halogen species (Grebel et al., 2010). As such furan yields declined linearly within the range of investigated chloride amounts (Figure 38B). This phenomenon was not observed with $\text{Fe}_2(\text{SO}_4)_3$ by Huber et al. (2010).

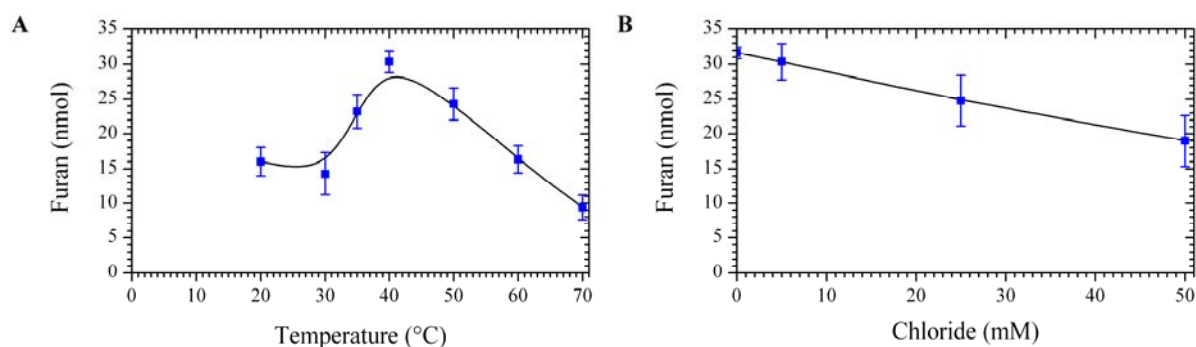


Figure 38. Effects of different parameters on the furan formation from a 10 mL solution. **A** Temperature dependency: reaction of 0.5 mM catechol with 12.5 μM $[\text{Fe}^{\text{II}}(\text{N}_2\text{Py}_2)(\text{OTf})_2]$, 2 mM H_2O_2 , 5 mM KCl at a pH of 4.6 and 20-70 $^\circ\text{C}$ after 30 min. **B** Variation of chloride: reaction of 0.5 mM catechol with 12.5 μM $[\text{Fe}^{\text{II}}(\text{N}_2\text{Py}_2)(\text{OTf})_2]$, 2 mM H_2O_2 , 0-50 mM KCl at a pH of 4.6 and 40 $^\circ\text{C}$ after 30 min.

Under optimal conditions summarised in Table 9, the reaction with $[\text{Fe}^{\text{II}}(\text{N}_2\text{Py}_2)(\text{OTf})_2]$ yielded 31.6 nmol (2.15 μg) furan from 5 μmol catechol. A 0.63% turnover rate from catechol for this reactions is comparable with the previous study employing $\text{Fe}_2(\text{SO}_4)_3$ (Huber et al., 2010).

Table 9. Optimised conditions for the abiotic furan formation from 0.5 mM catechol under Fenton conditions (Krause et al., 2013).

	$[\text{Fe}^{\text{II}}(\text{N}_2\text{Py}_2)(\text{OTf})_2]$ (μM)	H_2O_2 (mM)	Time (h)	pH	Temperature ($^\circ\text{C}$)	KCl (mM)
Optimised conditions	12.5	2	0.5	4.6	40	0

6.2 Abiotic ethylfuran formation from ethylcatechol

Based on model studies employing methylated catechols or phenols as precursors for methylated furans in Fenton-like reactions (Huber et al., 2010) an additional abiotic source for furans with an extended alkyl chain found in various natural samples (Chapter 10.4) was investigated.

The commercially available 4-ethylcatechol was successfully degraded to 3-ethylfuran by Fenton-like conditions employing $\text{Fe}_2(\text{SO}_4)_3$. Proven and postulated degradation pathways of catechol and phenols to furanoic species are shown in Figure 39.

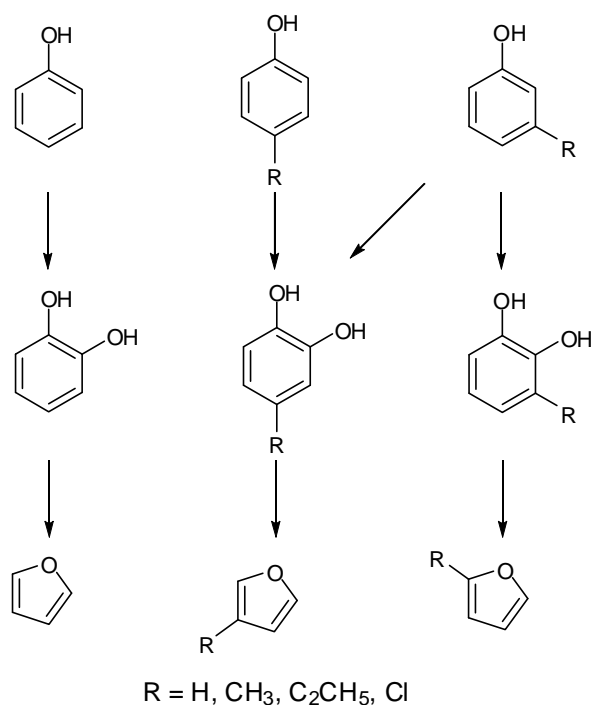


Figure 39. Known and postulated degradation pathways of phenol and catechol derivatives to furanoic species (Huber et al., 2010; Krause et al., 2013).

7 Soil and sediment profiles – An overview

During field campaigns the collected soil/sediment (Appendix C) and water samples (Appendix D) were analysed for elemental composition, pH and organic carbon content as well as the release of volatile compounds. General comparisons of emission distributions in the different collected profiles of 2011 and 2012 are illustrated in the following subchapters. Emissions are grouped by compound classes which are described in Chapter 10.

Based on the Australian salt lake classification outlined in Chapter 9.3, sediment profiles from Australian lakes are grouped by their ground or surface water acidity into acidic (pH 2-4), slightly acidic (pH 4-6) and circumneutral (pH 6-8) lakes.

7.1 Western Australia (pH 6-8)

Circumneutral lake sediment profiles feature a thick dark grey to black layer containing iron sulfides. Dominant volatile emissions by weight were mostly sulfur containing compounds, followed by terpenes, VOX, furans and BTEX. Overall emissions decreased with depth and also slightly correlated with the amount of transition metals and organic carbon.

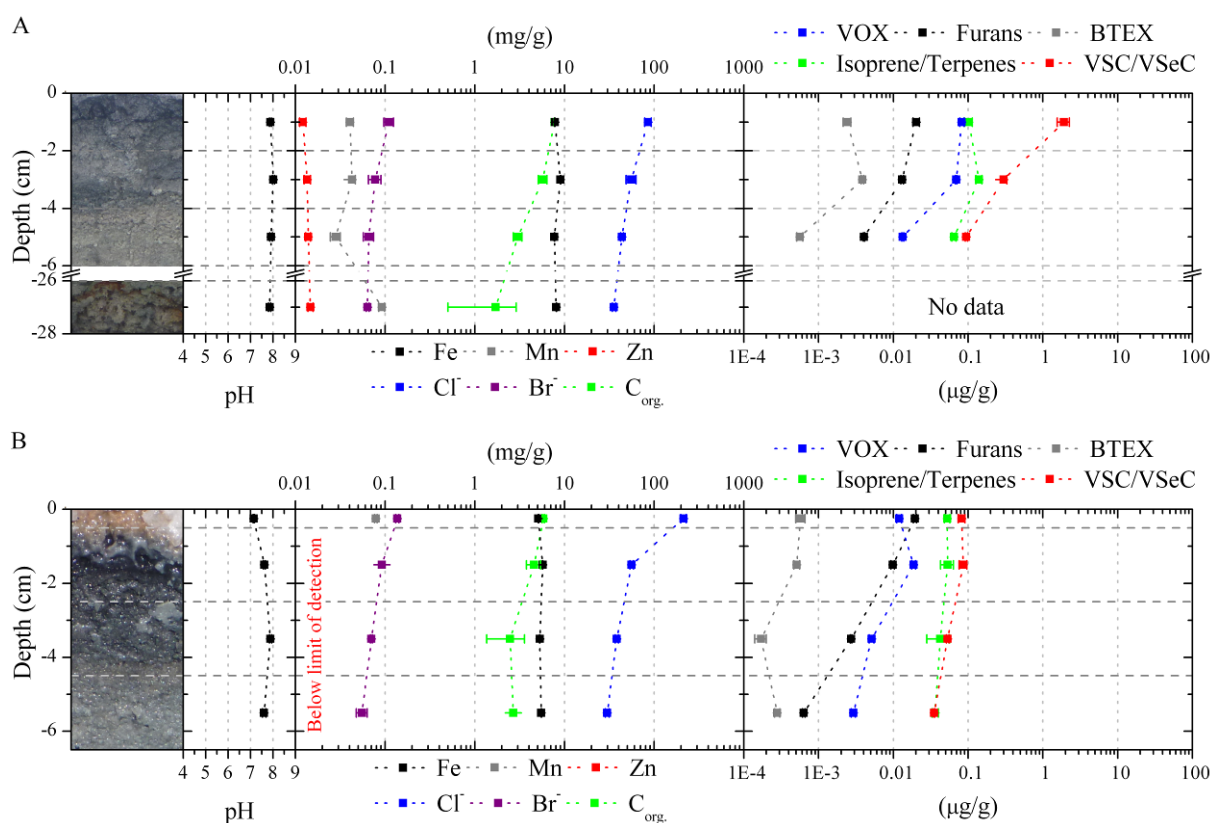


Figure 40. Profiles of **A** Lake King I and **B** Lake King II, both sampled in 2011. Plots show the distribution of important geochemical parameters and volatile compound emissions. Images: T. Krause CC BY-SA 4.0.

Lake King is a large unsymmetrical lake with a north-south expansion of about 24 km and a west-east expansion of 8 km intersected by State Highway 107. Surrounded by low native vegetation the lake itself features small sandy islands with *Salicornia* and other halophytes. Depending on wind directions water and salt content are transported over the lake accumulating near shores or the State Highway causeway. Within the sediment layers halide, transition metal and organic carbon concentrations generally decreased with the exception of manganese. Volatile compound releases also declined with greater depths (Figure 40).

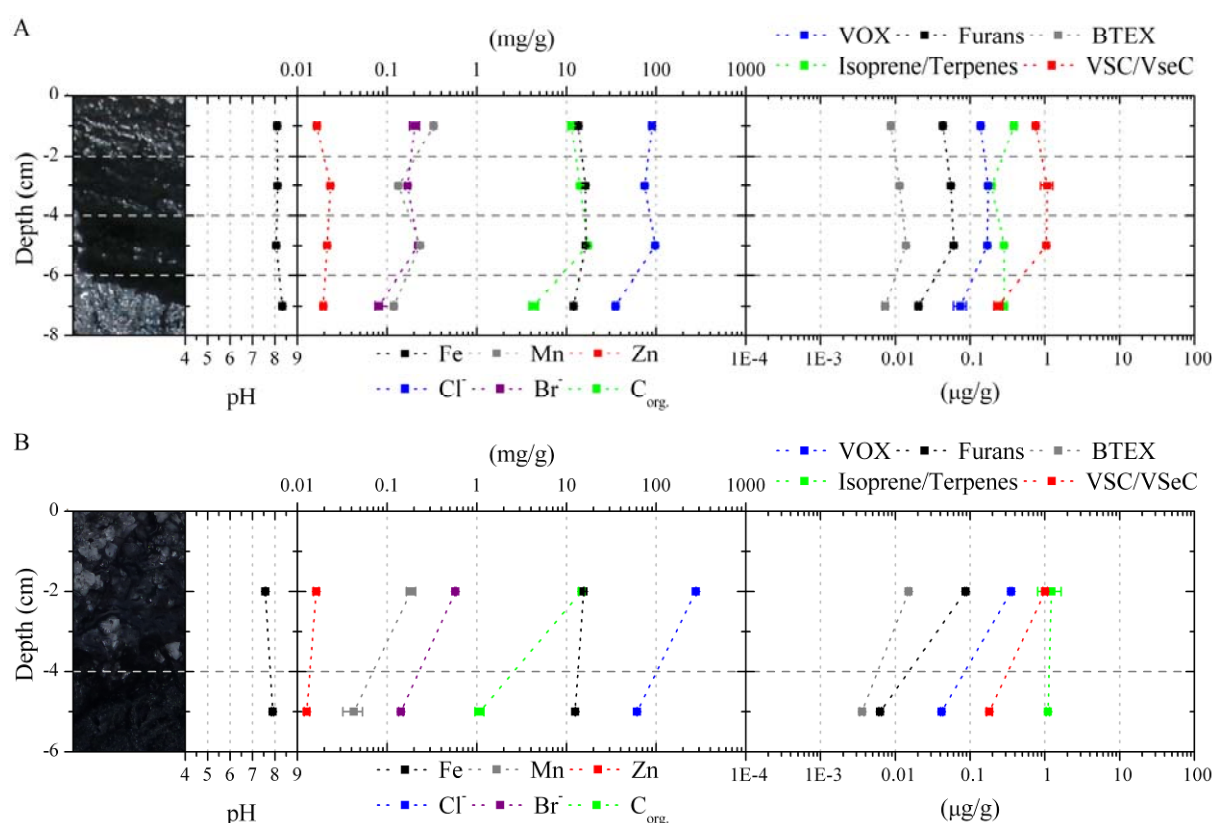


Figure 41. Profiles of Lake Strawbridge sampled in **A** 2011 and **B** 2012. Plots show the distribution of important geochemical parameters and volatile compound emissions. Images: T. Krause CC BY-SA 4.0.

Lake Strawbridge is a remote round salt lake with a 0.6 km diameter and a closed, soft and partly reddish salt crust. Samples were collected in 2011, 2012 and 2013. The lake is surrounded by a broad belt of *Salicornia* and other low growing halophytes. Exoskeletons of crayfish indicate occasional flooding of the lake, probably through the main inlet in the south with a catchment area that expands through native vegetation and fields. As is shown in Chapter 9.3, the lake sediment is anoxic with sulfate reducing conditions. Data plots show generally increasing pH values with depth while transition metal and organic carbon concentrations decreased. Furthermore, the release of volatile compounds decreased with depth, except isoprene/monoterpenes, which remained constant (Figure 41).

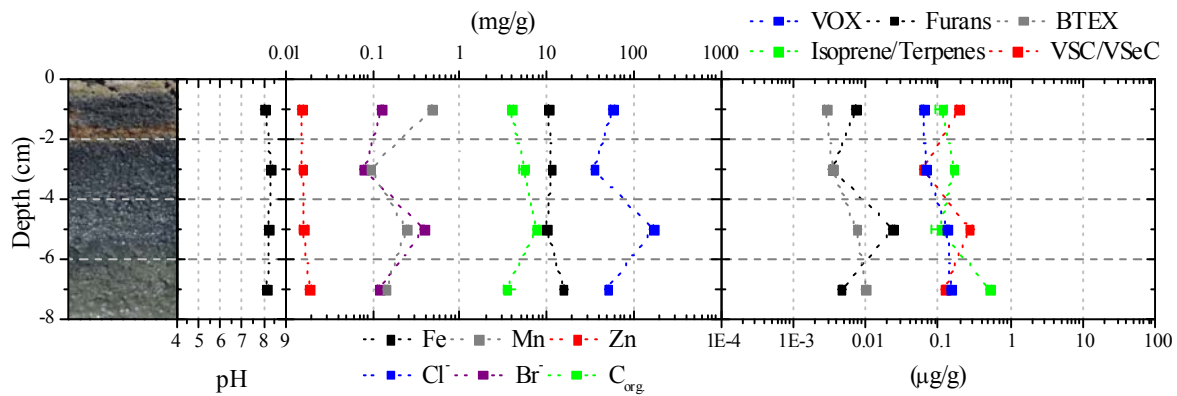


Figure 42. Profile of Lake Stubbs sampled in 2011. Plot shows the distribution of important geochemical parameters and volatile compound emissions. Image: T. Krause CC BY-SA 4.0.

Lake Stubbs is another large lake with a 3 km diameter and a broad sandy shore. Vegetation around the lake comprises mostly *Salicornia* and other small halophytes. The lake is completely covered by a thick salt crust and has an anoxic sediment (Chapter 9.3). Aside from the profile shown in Figure 42 another profile and some single samples were collected in 2011. Contemporary witnesses told of heavy flooding in 1999/2000 and also that the lake was occasionally used for swimming, which shows how dynamic the ecosystem is. Within the depicted profile, Figure 42, a similar trend between Fe, Mn, chloride and the release of furans as well as VSC/VSeC is evident. Contrary is the release of isoprene/monoterpenes.

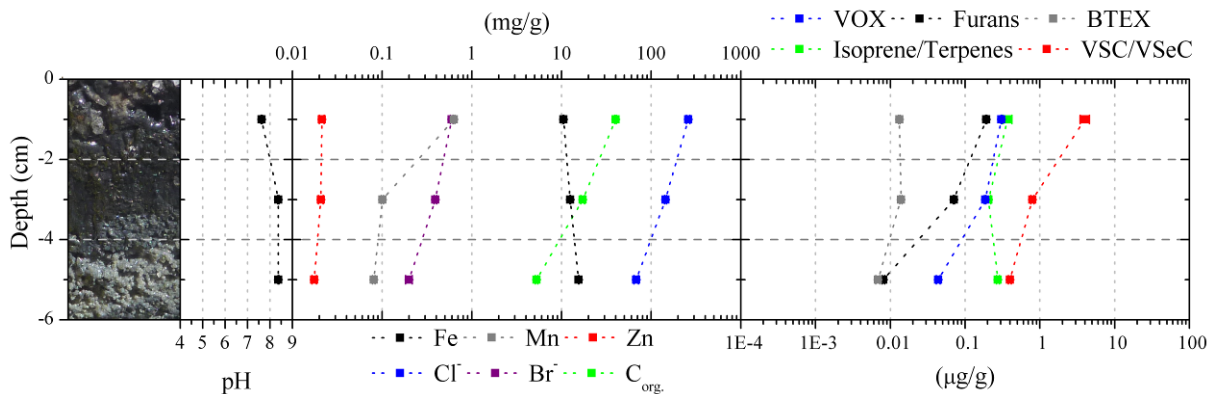


Figure 43. Profile of Lake Hatter Hill sampled in 2011. Plot shows the distribution of important geochemical parameters and volatile compound emissions. Image: T. Krause CC BY-SA 4.0.

Lake Hatter Hill is a small lake with a diameter of about 0.5 km surrounded by shrubs, trees and fields. A broad belt of dead shrubs on the shore bears witness to an advanced state of salinisation. Furthermore, in the anoxic sediment (Chapter 9.3) plant residues were found originating from water plants that grow in the lake after heavy rain events, e.g. at the end of 2011. While the lake had a thick salt crust in 2011, it was filled with water in 2012. This

water column of about 2 m did not completely evaporate until 2013. During this time water plants grew and the lake was habituated by birds. A profile collected in 2011 (Figure 43) showed decreasing trends for sediment parameters and volatile emissions except for the pH and iron content.

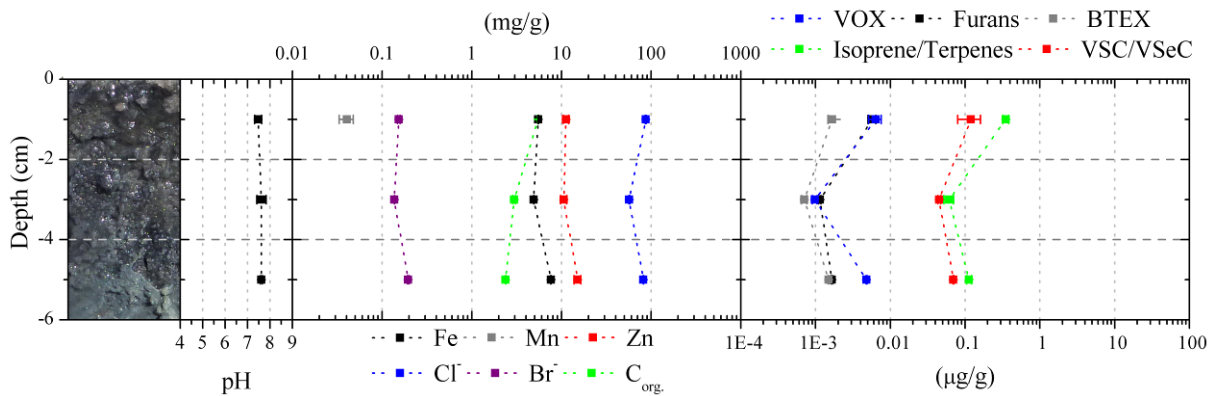


Figure 44. Profile of Lake Newton I sampled in 2012. Plot shows the distribution of important geochemical parameters and volatile compound emissions. Image: T. Krause CC BY-SA 4.0.

Lake Newton again is a larger lake, intersected by isles, with a north-south expansion of 0.5 km and west-east expansion of 3 km. Predominant vegetation is *Salicornia* and other low growing halophytes. An unofficial dumpsite is located on its shore, containing rusted canisters and car batteries among other debris. However, BTEX concentrations were not elevated compared to other lakes. Overall a correlation between inorganic substances and volatile compounds released is evident (Figure 44).

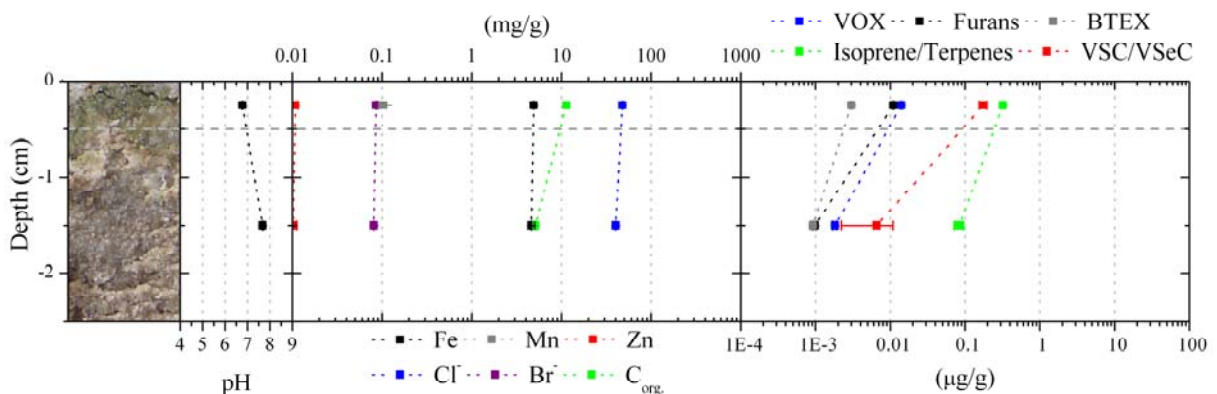


Figure 45. Profile of Lake Newton II sampled in 2012. Plot shows the distribution of important geochemical parameters and volatile compound emissions. Image: T. Krause CC BY-SA 4.0.

Another profile sampled on the shore of Lake Newton in 2012 featured a bright greyish sandy soil with green pigments in the uppermost layer indicating photosynthetic organisms (Figure 45). Plots show that the pH increased from the upper sampled layer to the lower layer while emissions decreased and the other parameters were mostly constant.

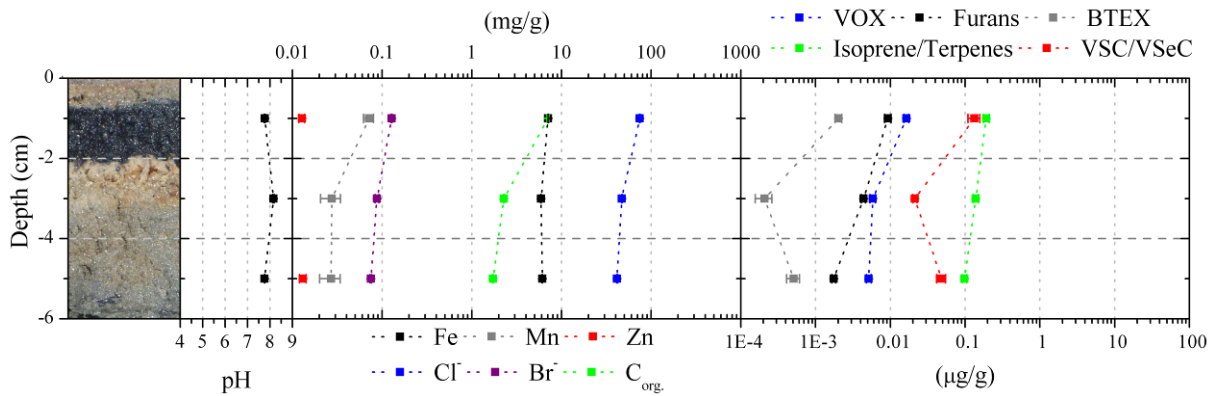


Figure 46. Profile of Lake Gulson sampled in 2012. Plot shows the distribution of important geochemical parameters and volatile compound emissions. Image: T. Krause CC BY-SA 4.0.

Lake Gulson, a saline sand playa with a diameter of about 5 km, was the only lake that did not feature a salt crust, albeit chloride concentrations of the sediment were on par with other salt lakes. The sandy sediment featured a thin black layer between otherwise yellow grey layers (Figure 46). Concentration of halides, transition metals and organic carbon as well as emissions decreased generally to deeper layers.

7.2 Western Australia (pH 4-6)

In a more acidic milieu sulfur compounds contributed less to the total weight of volatile compounds. Instead, isoprene/monoterpenes accounted for the main mass fraction followed by VSC/VSeC and VOX. Lowest emission by mass were again observed for furans and BTEX. Typically emissions decreased with depth and seemed to correlate with transition metal and organic carbon concentrations.

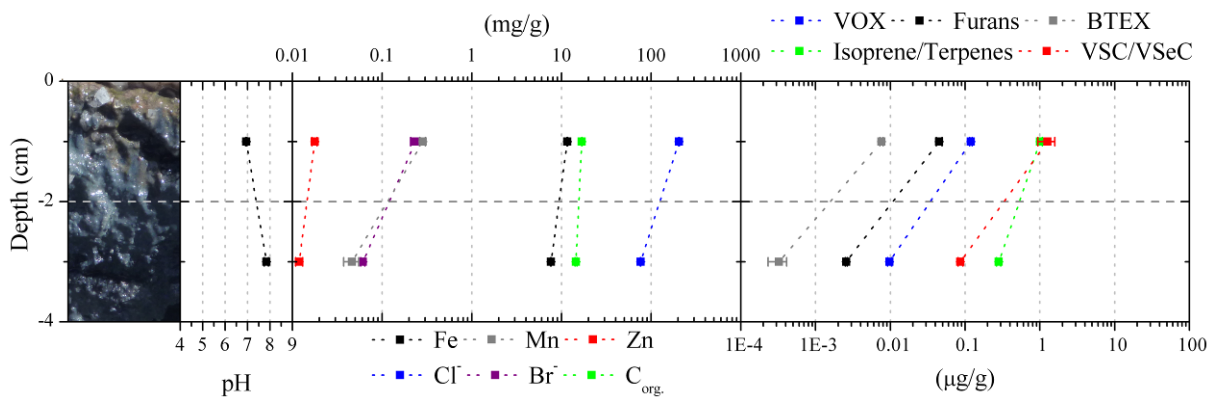


Figure 47. Profile of Lake Emu sampled in 2012. Plot shows the distribution of important geochemical parameters and volatile compound emissions. Image: T. Krause CC BY-SA 4.0.

Lake Emu is a small salt playa with a diameter of 0.5 km, featuring a salt crust and a black grey sediment reminiscence of circumneutral lakes. The lake is surrounded by fields with some trees and shrubs in between. Contrary to a rising pH in deeper layers, other parameters and emissions declined (Figure 47).

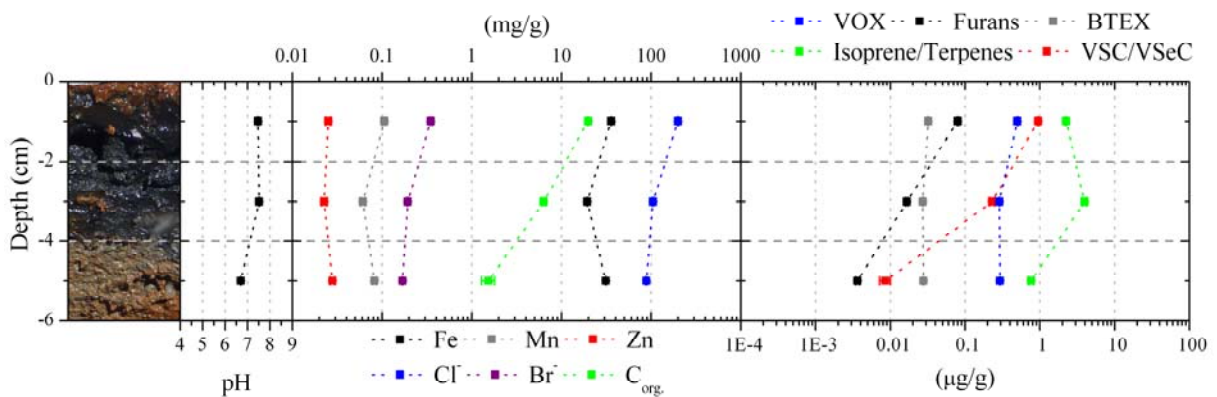


Figure 48. Profile of Lake Golf sampled in 2011. Plot shows the distribution of important geochemical parameters and volatile compound emissions. Image: T. Krause CC BY-SA 4.0.

Lake Golf is a round lake surrounded by a eucalyptus forest and several rocky outcrops. The diameter of the lake is about 1 km. The sediment profile under the salt crust features a thin rusty red iron oxide layer followed by black sediment. Organic carbon as well as furan and VSC/VSeC emissions significantly declined to lower sediment layers while changes of other parameters were less pronounced (Figure 48).

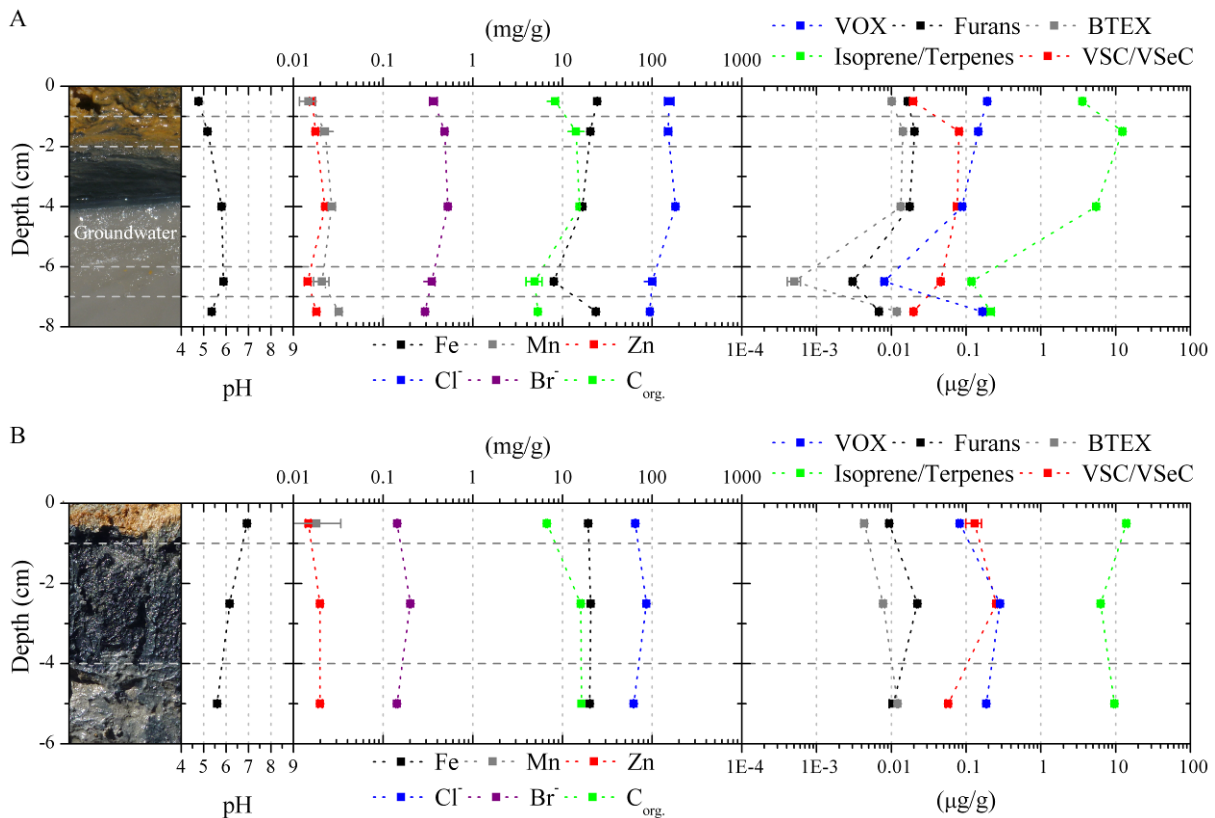


Figure 49. Profiles of Lake Whurr sampled in **A** 2011 and **B** 2012. Plots show the distribution of important geochemical parameters and volatile compound emissions.
Images: **A** H. F. Schöler and **B** T. Krause CC BY-SA 4.0.

Lake Whurr was sampled in 2011 as well as 2012 at different locations. The lake is connected by a run-off with Lake Stubbs. North-south expansion is only 0.3 km while it stretches over nearly 1 km from west to east. The lake is surrounded by a few eucalyptus trees and shrubs as well as farmland in the greater vicinity. In 2011, the groundwater pH was 4.2 while in 2012 surface water had a pH of 3.1. Contrary to the low pH, the sediment profile is typical for slightly acidic lakes with an iron oxide layer and iron sulfides below. Aside from a NaCl salt crust gypsum needles were abundant on and in the sediment. The sediment itself was classified as suboxic in 2013 (Chapter 9.3). In the upper 6 cm geochemical parameters and emissions aside from the pH were similar in 2011 and 2012 (Figure 49).

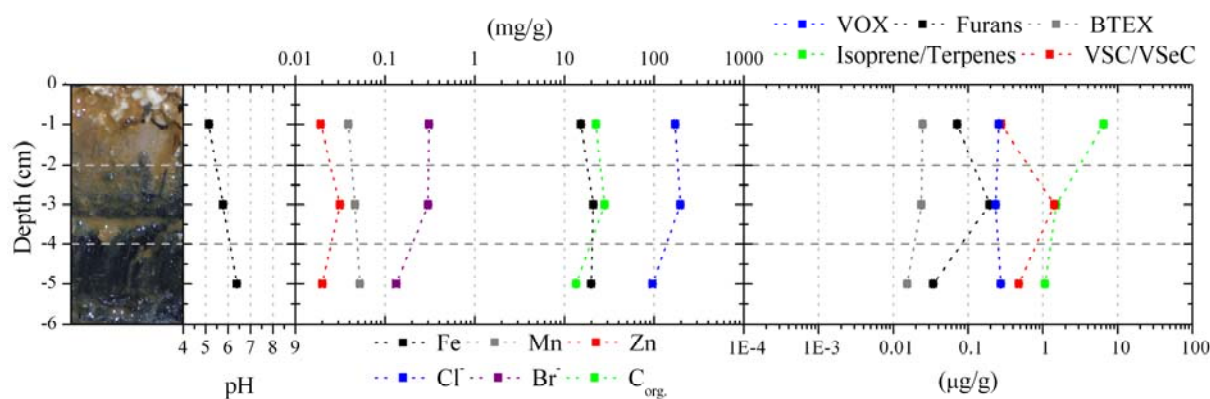


Figure 50. Profile of Lake Springfield sampled in 2011. Plot shows the distribution of important geochemical parameters and volatile compound emissions. Image: T. Krause CC BY-SA 4.0.

The small **Lake Springfield**, with a diameter of 0.3 km, is surrounded by fields and shrubs. Like the other slightly acidic lakes deeper layers are black while the top layer has a reddish brown colour under the salt crust (Figure 50). Between 2 and 4 cm an increase of most inorganic constituents and emission of furans and VSC was observed.

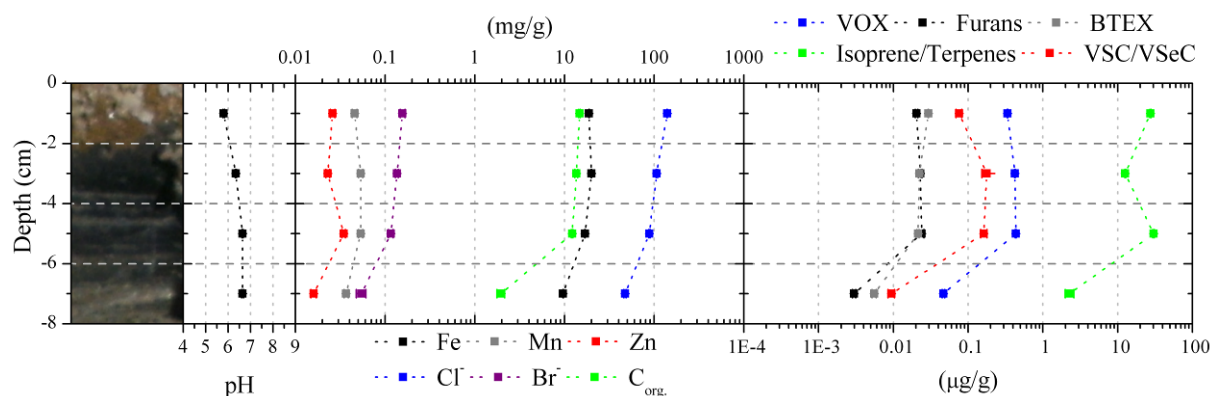


Figure 51. Profile of Lake Orr II sampled in 2011. Plot shows the distribution of important geochemical parameters and volatile compound emissions. Image: H. F. Schöler.

In 2011, two profiles were collected from **Lake Orr**. The lake is 0.6 km in diameter, but is mostly covered by shallow sand dunes giving the lake a crescent form nowadays. The first profile, shown in Figure 51, with the brown top layer and black sediment clearly is reminiscent of slightly acidic lakes. However, ground- and surface water in 2011 to 2013 were always below a pH of 4. Emissions of all compounds as well as transition metal, halide and organic carbon concentrations decreased with depth in this sediment, while the pH increased. The second profile as well as a third profile collected in 2012 are presented in Chapter 7.3 as they are characteristic for acidic lakes.

7.3 Western Australia (pH 2-4)

In highly acidic lakes, the main volatile mass fraction again stems mostly from monoterpenes. Though the significant difference, compared to slightly acidic and circumneutral lakes, is the distinct contribution of VOX as the second most important group of compounds. Sulfur compounds are mostly third by weight followed by furans and BTEX. Emissions are evenly distributed over the analysed sediment layers or even increased with depth. Correlations of emission with transition metals and organic carbon content is evident except for isoprene/monoterpenes. Furthermore, an odour resembling that of chlorinated swimming pool water was observed around the acidic lakes.

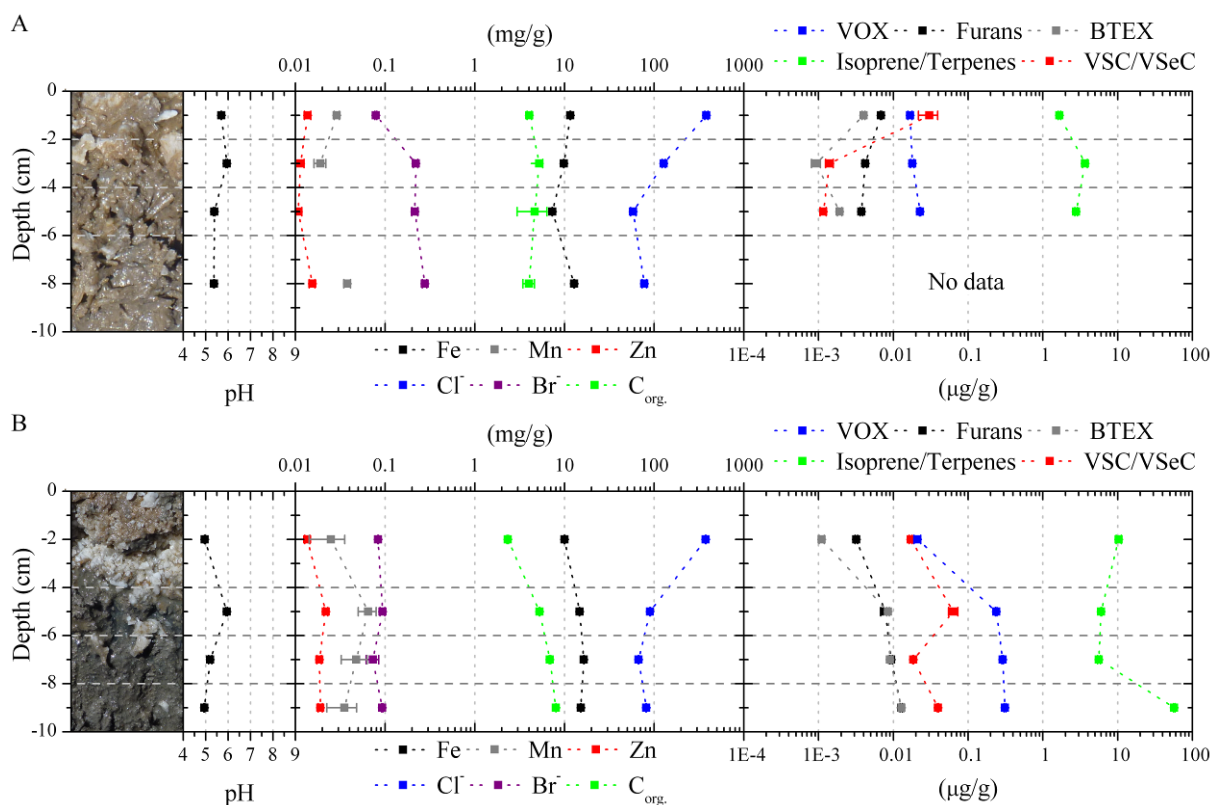


Figure 52. Profiles of Lake Orr sampled in **A** 2011 and **B** 2012. Plots show the distribution of important geochemical parameters and volatile compound emissions. Images: T. Krause CC BY-SA 4.0.

As mentioned before, **Lake Orr** is an acidic lake with a pH of about 3.1. Additional profiles sampled in 2011 and 2012 from the same area show typical brown grey sediments for an acidic lake contrary to the black sediment shown in Figure 51. While geochemical parameters are similar in both years, the emissions were more pronounced in 2012 (Figure 52).

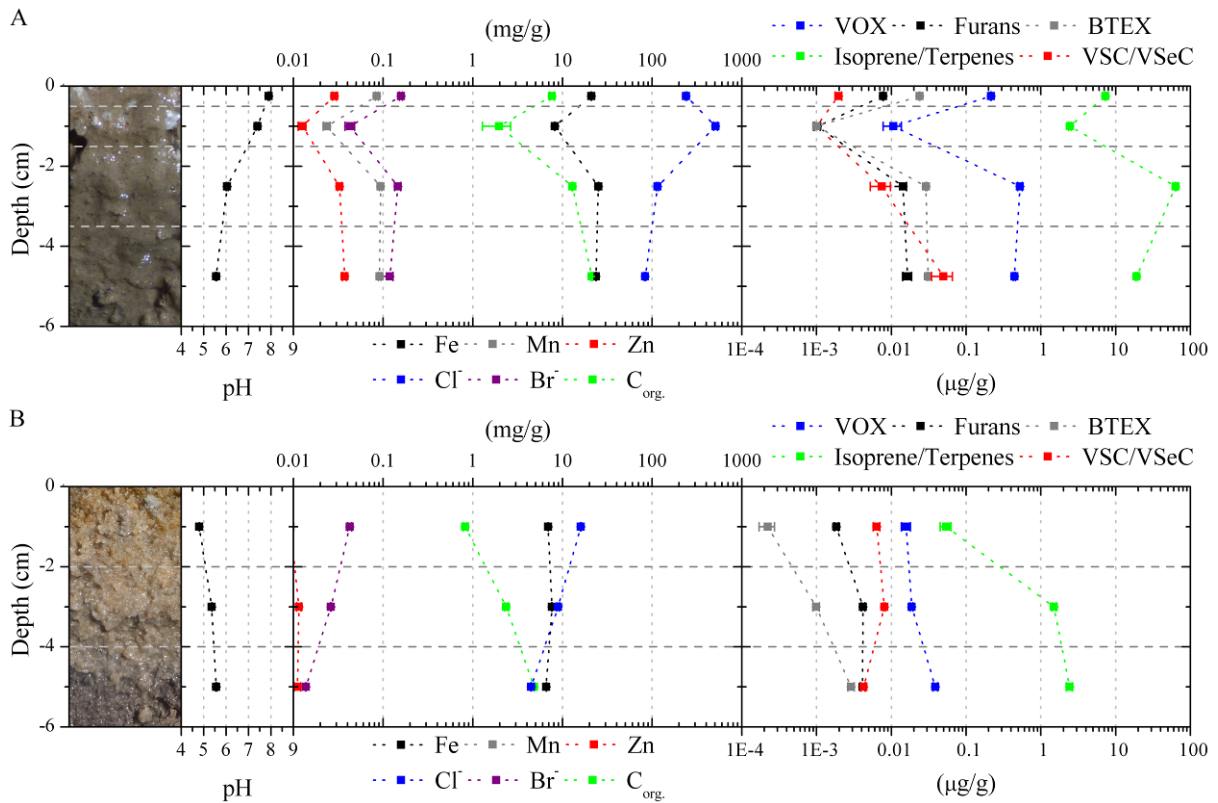


Figure 53. Profiles of Lake Dune sampled in **A** 2011 and **B** 2012. Plots show the distribution of important geochemical parameters and volatile compound emissions. Images: T. Krause CC BY-SA 4.0.

Two profiles from **Lake Dune** were sampled in 2011 and 2012 at different locations. The lake has a diameter of about 0.3 km and is surrounded by eucalyptus trees and low bushes. On the eastern shore rusted canisters with unknown content were disposed of. The brown grey sandy sediments were classified as suboxic/anoxic in 2013 (Chapter 9.3). Emissions were subdued in 2012 and transition metal and organic carbon concentrations were also lower. Samples of 2011 showed a significant trend between emissions of volatile compounds and metal as well as organic carbon concentrations (Figure 53A). Emissions from samples collected in 2012 increased with depth correlating with organic carbon concentrations (Figure 53B).

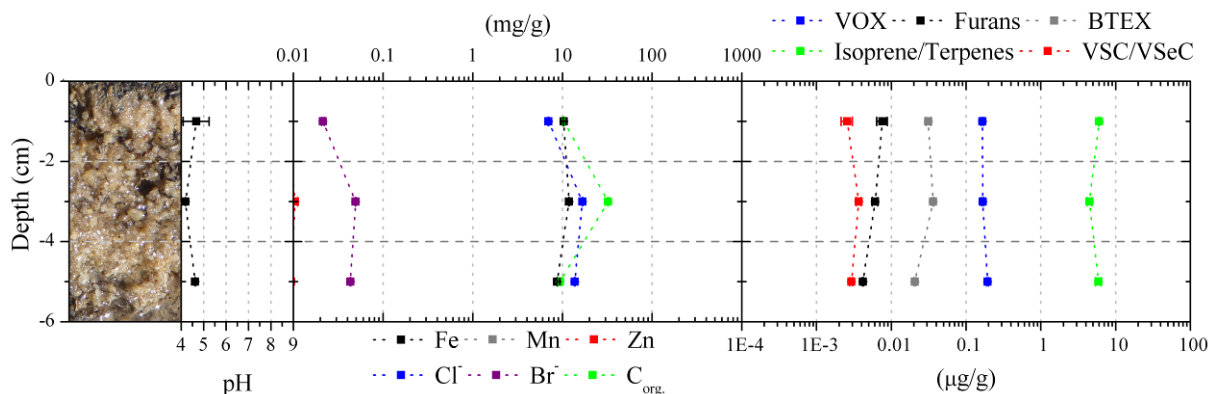


Figure 54. Profile of Lake Boats sampled in 2012. Plot shows the distribution of important geochemical parameters and volatile compound emissions. Image: T. Krause CC BY-SA 4.0.

Lake Boats, the most acidic salt lake under investigation with a pH of 2.3, has a diameter of about 0.3 km and is surrounded by eucalyptus trees and bushes. A thick hard salt crust covers an anoxic sandy sediment. The data plot shows no significant trends in emissions and geochemical parameter distribution (Figure 54).

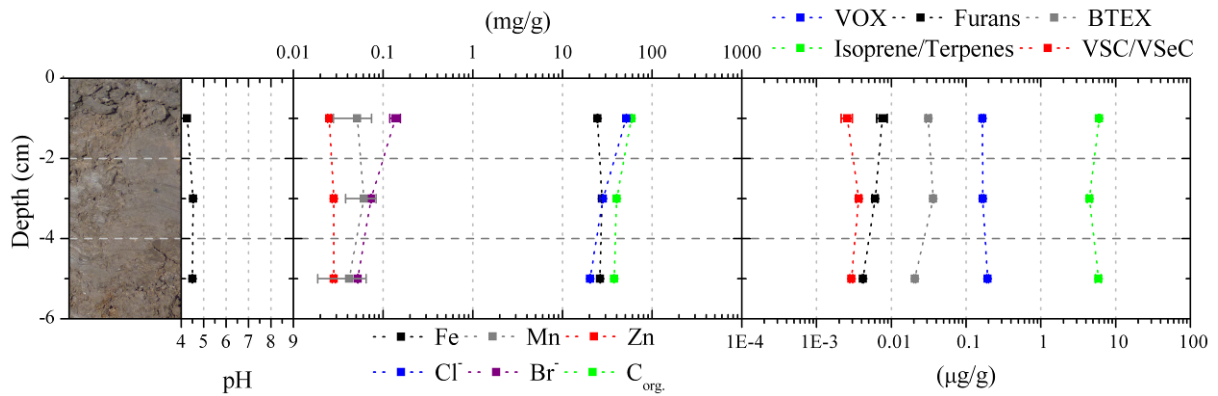


Figure 55. Profile of Lake Boats Claypan sampled in 2012. Plot shows the distribution of important geochemical parameters and volatile compound emissions. Image: T. Krause CC BY-SA 4.0.

In the vicinity of Lake Boats is a small hypersaline claypan which is occasionally fed by rain water. The investigated sediment of **Lake Boats Claypan** had a high organic carbon content as well as high halide concentrations. Like in the sediment of Lake Boats, no significant changes of parameters and emissions were observed in the different sediment layers (Figure 55).

7.4 Sodom, Israel

Three soil profiles were collected in Israel south of the Dead Sea. These soils were brighter compared to Australian sediment samples. Emissions were again dominated by isoprene/monoterpenes and VSC/VSeC followed by VOX, furans and BTEX. Typically emission decreased immediately below the crust and increased again at greater depths with no significant correlation to geochemical parameters (Figure 56).

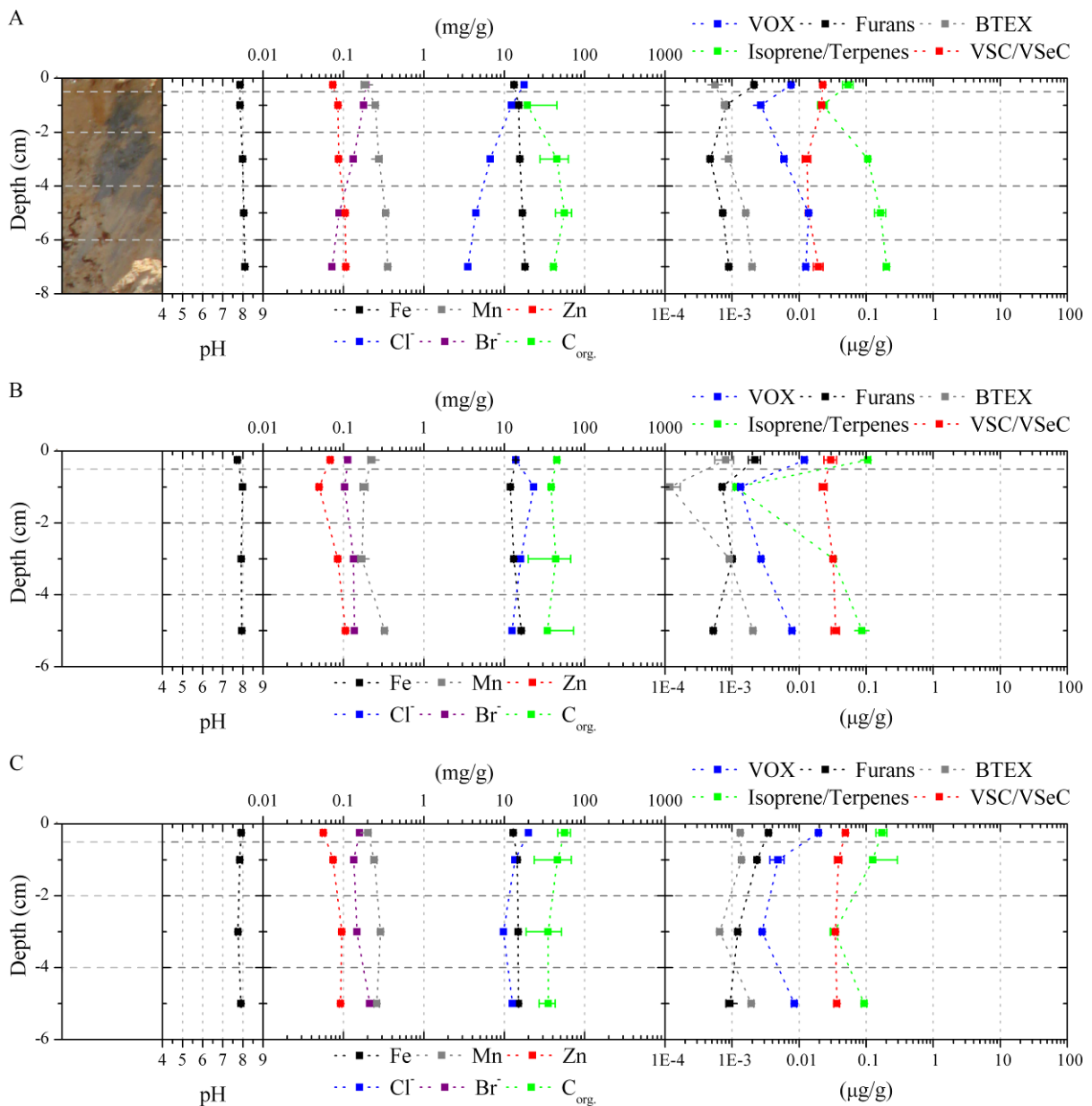


Figure 56. Distribution of pH, halides, Fe, Mn, Zn, organic carbon and emissions of different classes of chemical compounds from profiles of **A** Sodom 1, **B** Sodom 2 and **C** Sodom Plant. Images: C. Tubbesing.

Emissions from the three Sodom profiles are overall lower compared to Australian samples, even though pH, transition metal and organic carbon concentrations are comparable.

In conclusion, emission from Australian sediments and Israeli soils shows a distinct pattern with regard to the pH. In circumneutral lakes emission is dominated by sulfur and isoprene/terpene species though the proportion of the sulfur compounds decline toward acidic lakes with VOX becoming more prominent. Trends between the emission of some compound classes and transition metal as well as organic carbon concentrations are observable within most profile layers.

8 Water samples – An overview

Figure 57 shows pH values and volatile compound emissions, grouped again into chemical classes, from all analysed water samples from Australia 2011 and 2012 as well as the Dead Sea 2012 (Appendix D).

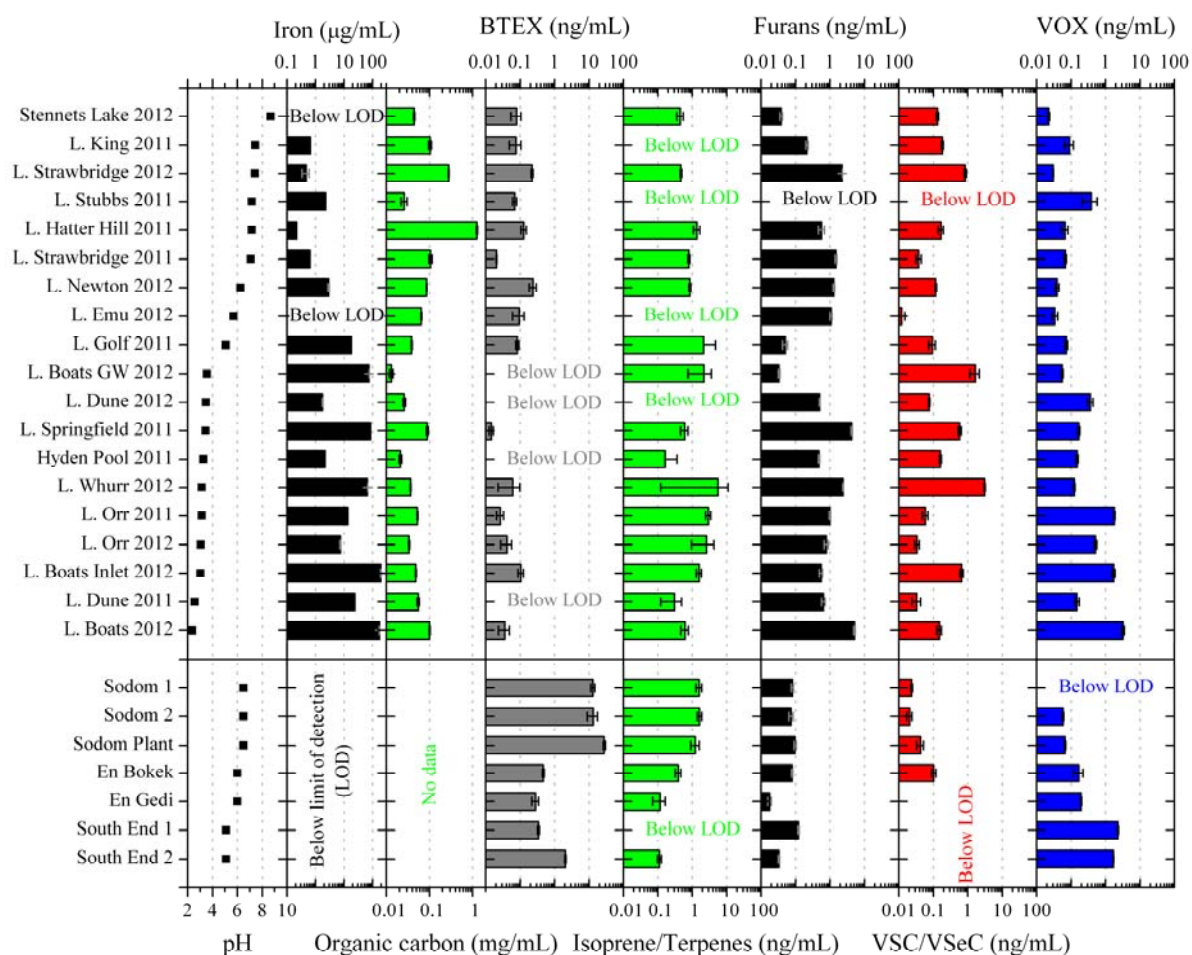


Figure 57. pH, dissolved iron concentration, dissolved organic carbon content and emission data for water samples from Australia (top) and the Dead Sea (bottom).

8.1 Western Australia

The pH of about 100 salt lakes was investigated during the Australian campaigns in 2011, 2012 and 2013 (Appendix B). Figure 58 shows the distribution of acidic to circumneutral lakes in the area around Hyden, Varley, Newdegate and Lake King.

Four water samples were collected from hypersaline environments not mentioned in the previous Chapter 7. One sample was from an artificial hypersaline swimming pool at the Wave Rock Lakeside Resort near Hyden, here named Hyden Pool. The others were collected in the vicinity of Lake Boats comprising groundwater (Lake Boats GW) taken about 30 m

away which eventually discharges via a streamlet (Lake Boats Inlet) into the lake. The fourth sample originates from Stennets Lake, a saline lake with only 5.5 g/L chloride.

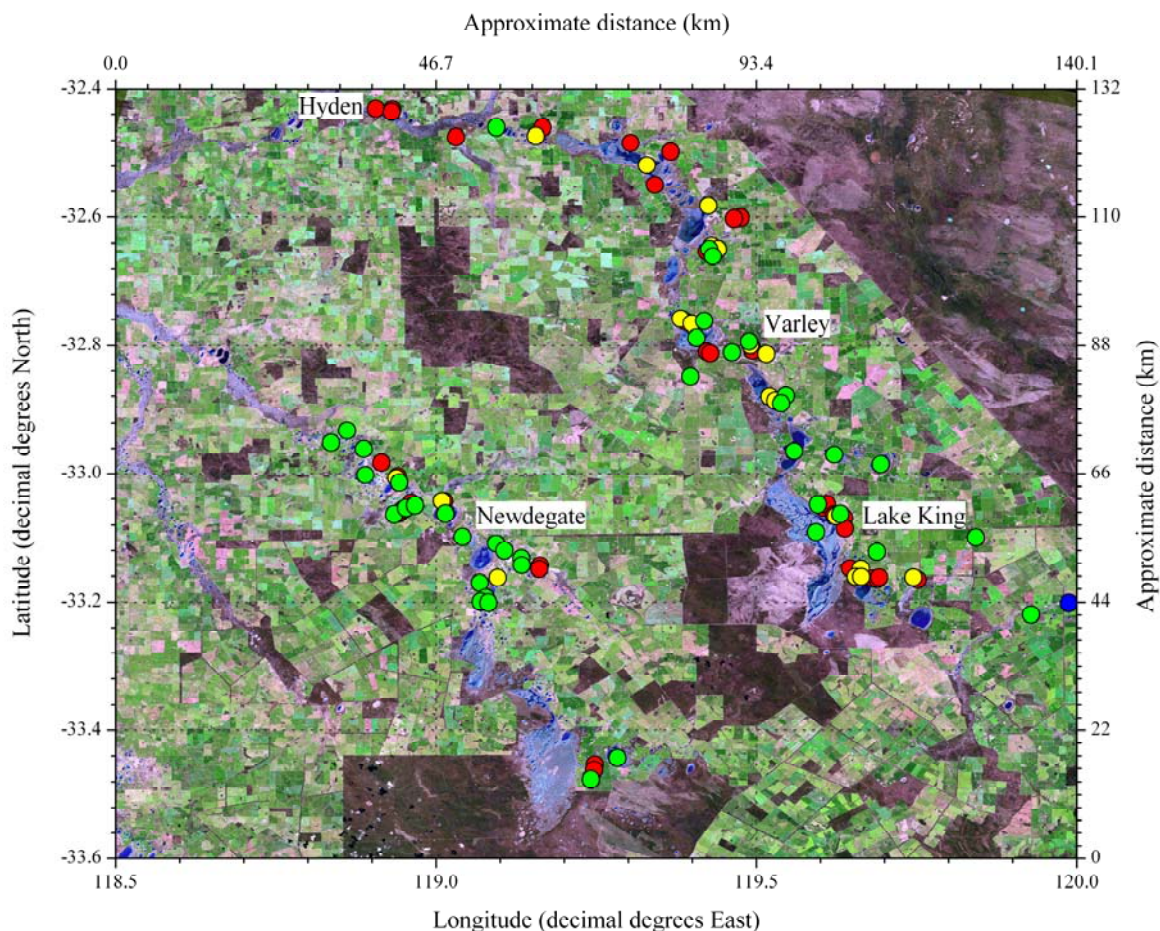


Figure 58. Processed satellite image showing acidic to circumneutral salt lakes around Hyden, Varley, Newdegate and Lake King, Western Australia. Surface or groundwater pH of ● 2-4, ● 4-6, ● 6-8, ● 8-10. Image source: USGS/NASA Landsat Program, 06.09.2013, Landsat OLI_TIRS_L1T scene LC81100832013249LGN00. Image resides in the public domain and is reprinted by courtesy of the U.S. Geological Survey.

The three samples from Lake Boats illustrate the transportation of saline iron rich acidic groundwater into the lake (Figure 59).

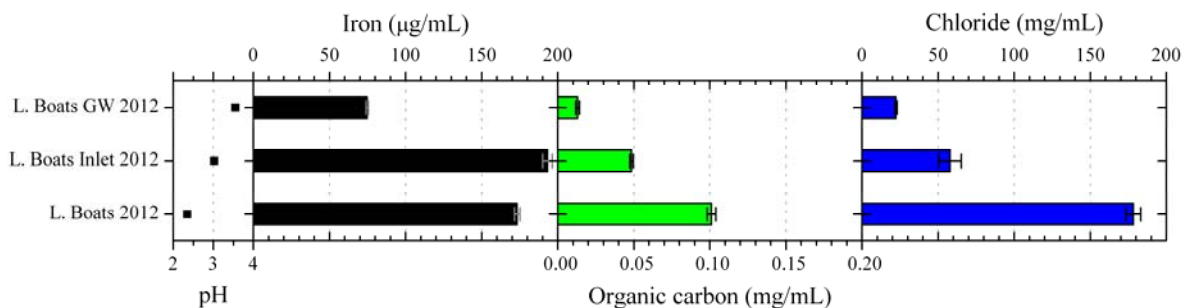


Figure 59. Change of pH, iron, organic carbon and chloride concentrations in groundwater, discharging surface water and Lake Boats.

Furthermore, dissolved iron from discharging anoxic groundwater partly precipitates on contact with oxygen forming iron oxide accumulations and mixed-valent iron films (Grathoff et al., 2007) shown in Figure 60. Such phenomena were also observed at further acidic lakes.

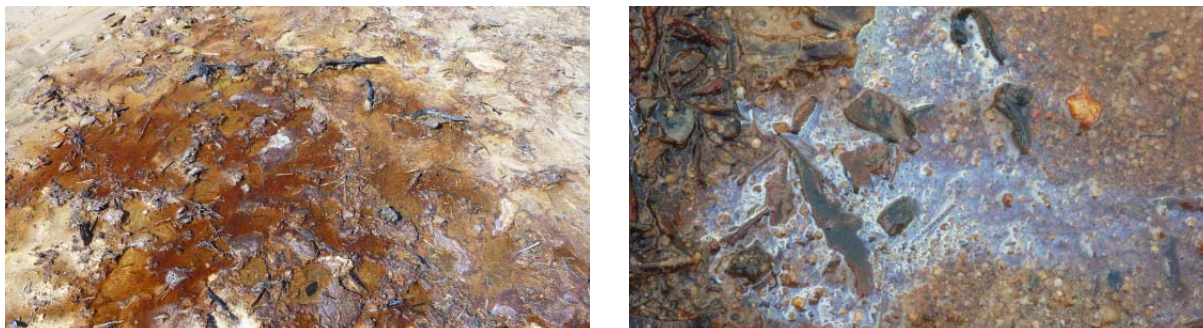


Figure 60. Precipitated iron oxides (left) and mixed-valent iron film (right) at Lake Boats, 2013.
Images: T. Krause CC BY-SA 4.0.

The plotted data show that BTEX emissions decreased with decreasing pH and dissolved iron concentrations, whereas VOX concentrations increased (Figure 57). Furthermore, there was no obvious pattern for isoprene/monoterpenes, furanic compounds and VSC/VSeC emissions. BTEX emission at potentially polluted sites like Lake Newton, Dune and King were not significantly elevated compared to the other locations. Worthy of mentioning was also the absence of isoprene/monoterpenes, furan and VSC/VSeC emissions from Lake Stubbs.

8.2 Sodom and the Dead Sea

Water samples from Sodom were collected from the groundwater at 45-85 cm depth. Additionally, a water sample was collected at En Bokek from the natural part of the Dead Sea, at En Gedi from one of the northern evaporation ponds and two samples named South End from the southernmost evaporation pond. The groundwater samples contained BTEX concentrations 10 to 100 times higher than the Dead Sea surface waters or Australian water samples indicating an anthropogenic source. Isoprene/monoterpenes and VSC/VSeC concentrations were also elevated in the groundwater, whereas VOX emissions were extremely low. Highest VOX concentrations were measured in the samples from the southern pool. While halide enrichment advances from En Gedi to South End and might foster halogenation processes, the water pumped into the southern pond also passes the chlorine and bromine plants of the Dead Sea Works. Hence, water pollution has to be considered.

9 Chemical parameters of hypersaline environments

An overview of transition metals, halides, pH and organic content in soil/sediment and water samples from Western Australian campaigns in 2011, 2012 and from the Dead Sea campaign in 2012 is given in Chapter 9.1 and 9.2. Additionally, first data from the Australian campaign in 2013 are included (Krupp, 2013; Wirth, 2013; Sehls, 2013).

Furthermore, these data are plotted in comparison to other saline environments to highlight the unique characteristics of the sampling sites. The referenced saline environments were investigated by colleagues within the framework of the DFG Research Unit 763. These additional samples were collected at the Brenner Moor in Germany (Lippe, 2011; Furchner, 2011; Hoffmann, 2011), Sua Pan in Botswana (BW), Walvis Bay in Namibia (NA), Lake Baskunchak, Lake Elton and Lake Kasin in Russia (RU), Douemina, Iwik and N'Dramcha in Mauritania (MR), on Sal, Cap Verde (CV) and near the Aral Sea in Uzbekistan (UZ).

Chapter 9.2.1 deals with the pH dependency of dissolved constituents in Australian water samples, which was used to simulate natural conditions in the laboratory, e.g. smog chamber in Bayreuth. Also intertwined with the pH are different redox conditions and abundant iron species as discussed in chapter 9.3.

9.1 Geochemical inventory of soils/sediments

High dissolved halide concentrations (Figure 61) occurred in all soil and sediment samples. The Sodom samples from Israel stand out with low chloride but moderate bromide concentrations. Only the Brenner Moor peat samples and the samples from Lake Kasin had low bromide concentrations.

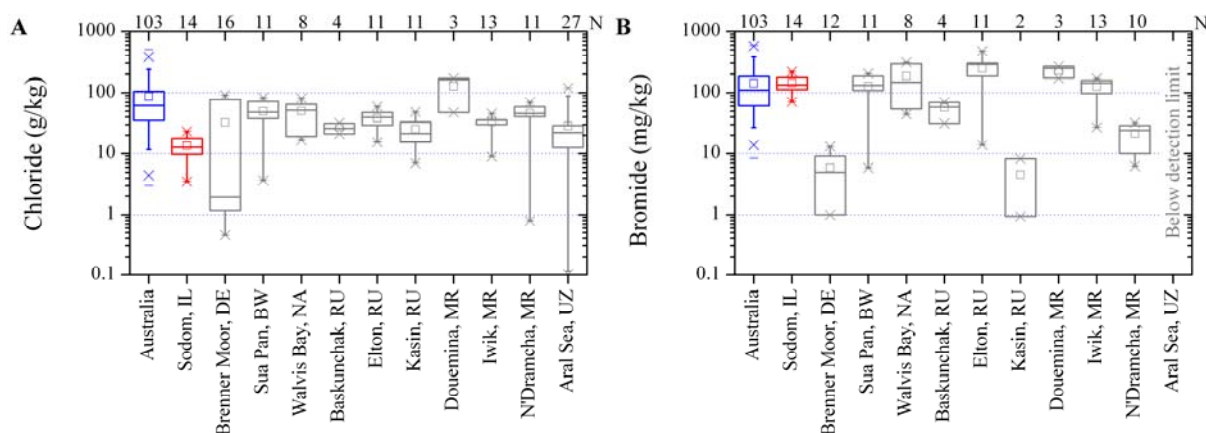


Figure 61. **A** Chloride and **B** bromide distribution in various soil and sediment samples with N being the total available data points from 111 Australian, 14 Dead Sea, 16 Brenner Moor, 11 Sua Pan, 8 Walvis Bay, 4 Baskunchak, 11 Elton, 11 Kasin, 3 Douemina, 13 Iwik, 11 N'Dramcha and 27 Aral Sea samples, respectively.

Figure 62 illustrates the distribution of transition metals in the investigated locations compared to other sample sites. Most abundant is iron, typically in the g/kg range followed by manganese, copper and zinc with concentrations in the mg/kg range.

While mean iron concentrations are mostly similar below 20 g/kg for all sampling sites, they were more widely distributed in the Brenner Moor. The outlier from Australian samples was a sample containing precipitated iron from discharging groundwater (Chapter 8.1, Figure 60). Manganese concentrations were lowest in the Australian samples, while in Sodom samples they were between 100 and 1000 mg/kg comparable to other locations.

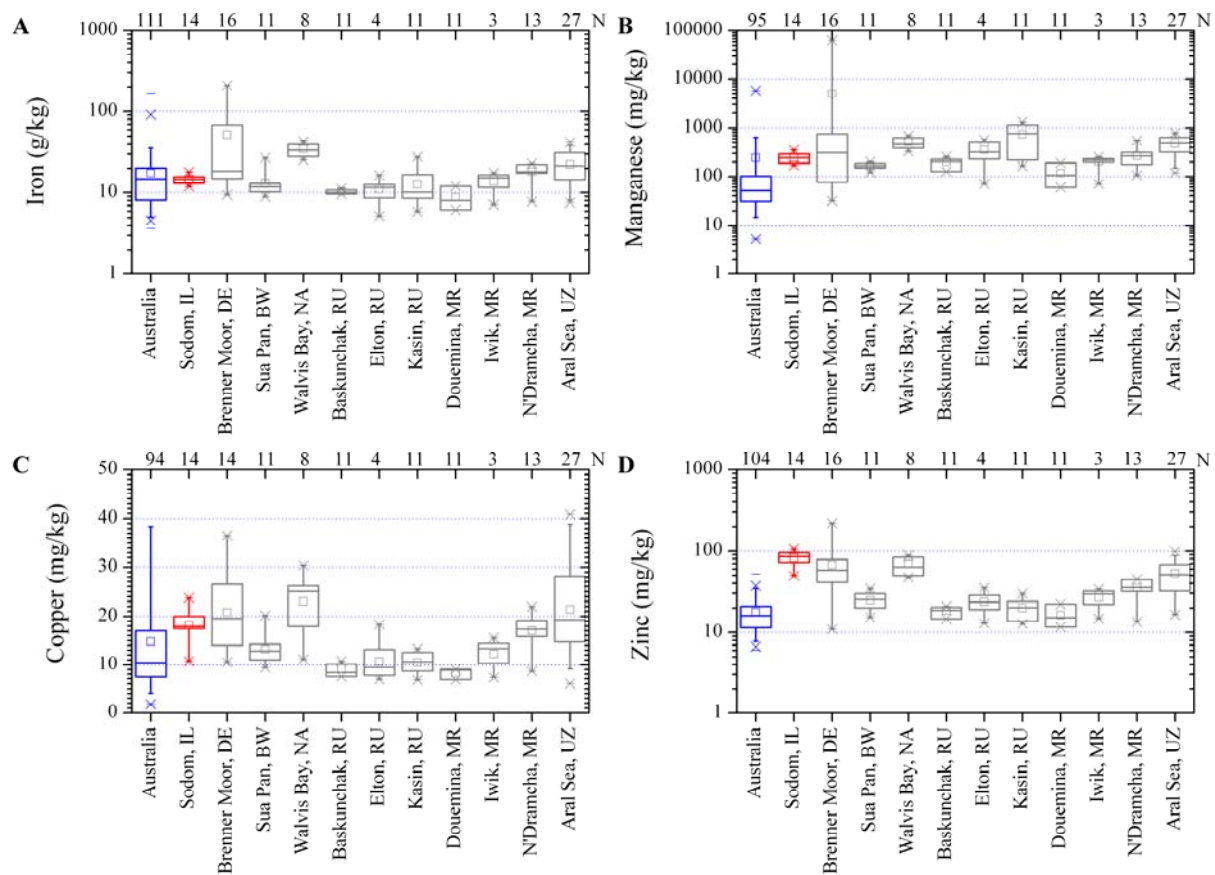


Figure 62. A Iron, B manganese, C copper and D zinc distribution in various soil and sediment samples with N being the total available data points from 111 Australian, 14 Dead Sea, 16 Brenner Moor, 11 Sua Pan, 8 Walvis Bay, 4 Baskunchak, 11 Elton, 11 Kasin, 3 Douemina, 13 Iwik, 11 N'Dramcha and 27 Aral Sea samples, respectively.

Likewise manganese, the zinc content of Australian samples was comparably low while highest overall mean zinc values were measured at Sodom. The copper data showed a similar pattern with mean copper values increasing from Australian to Sodom samples.

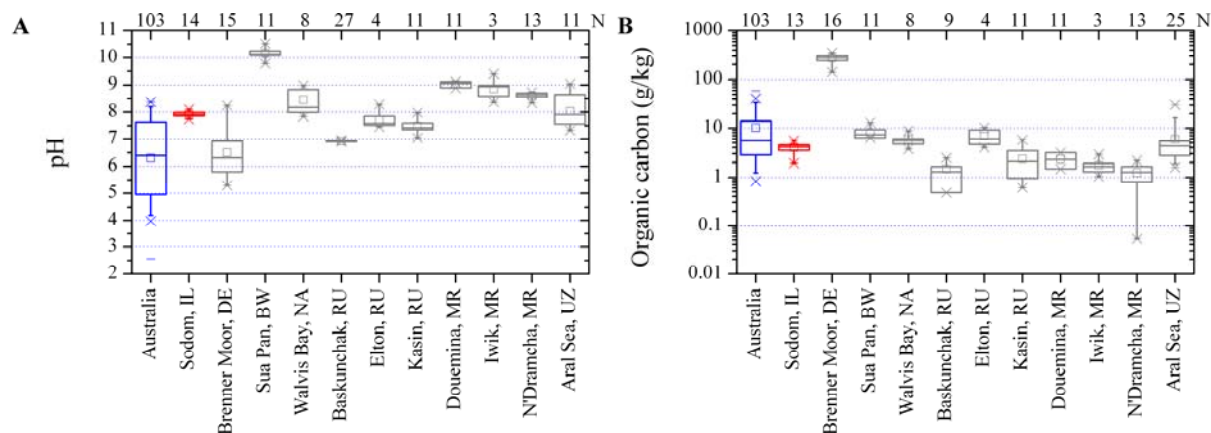


Figure 63. Distribution of **A** pH and **B** organic carbon in various soil and sediment samples with N being the total available data points from 111 Australian, 14 Dead Sea, 16 Brenner Moor, 11 Sua Pan, 8 Walvis Bay, 4 Baskunchak, 11 Elton, 11 Kasin, 3 Douemina, 13 Iwik, 11 N'Dramcha and 27 Aral Sea samples, respectively.

Major differences between the sample locations emerge from pH and organic carbon concentrations as illustrated in Figure 63. Soil and sediments of most sites were neutral to alkaline, whereas samples from the Brenner Moor and Australia were in parts acidic. Australian samples displayed a broad distribution with high concentrations of organic carbon compared to other hypersaline sites, whereas Sodom samples had moderate organic carbon concentrations. Highest organic carbon concentrations were measured in peat samples from the Brenner Moor.

9.2 Geochemical inventory of the aqueous phase

Most water samples had high chloride concentrations, except samples from the Brenner Moor (Figure 64A). While chloride concentrations in all hypersaline waters were about 100-200 g/L, water samples from the Dead Sea showed a large bromide enrichment compared to the other sites (Figure 64B).

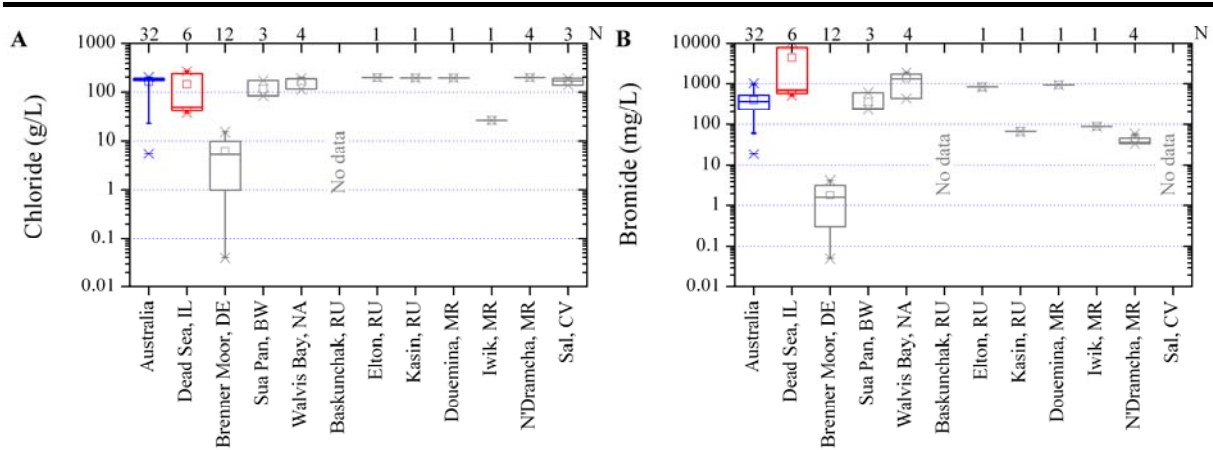


Figure 64. **A** Chloride and **B** bromide distribution in various water samples with N being the total available data points from 32 Australian, 6 Dead Sea, 12 Brenner Moor, 3 Sua Pan, 4 Walvis Bay, 1 Baskunchak, 1 Elton, 1 Kasin, 1 Douemina, 1 Iwik, 4 N'Dramcha and 3 Sal samples, respectively.

Iron and manganese as well as traces of zinc were the only soluble transition metals of note (Figure 65). Their concentrations were highest in the Australian samples, while dissolved iron and zinc were below detection limits in the Dead Sea samples.

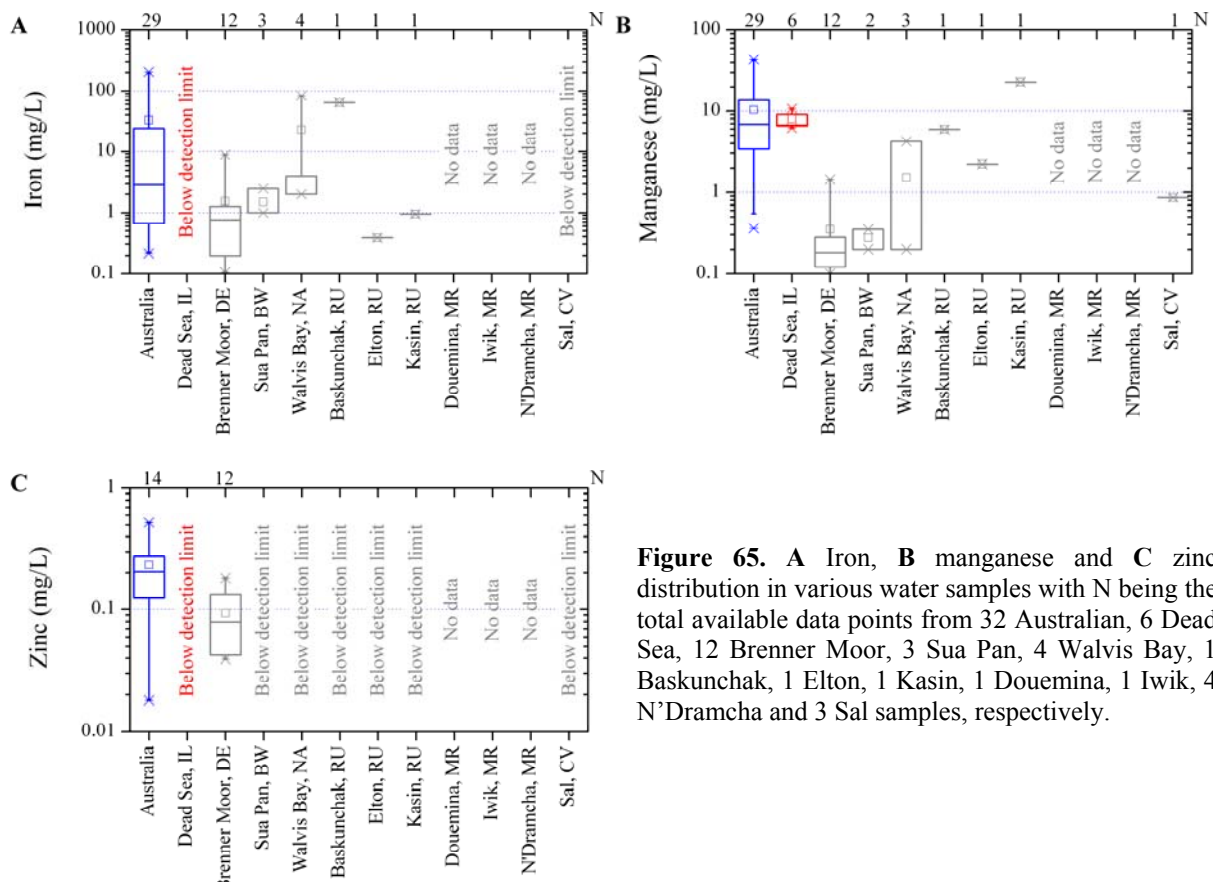
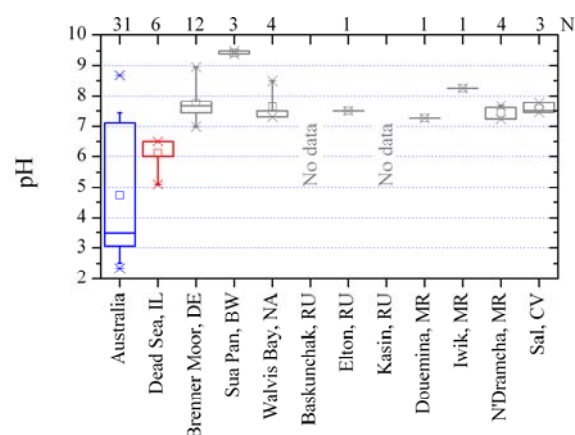


Figure 65. **A** Iron, **B** manganese and **C** zinc distribution in various water samples with N being the total available data points from 32 Australian, 6 Dead Sea, 12 Brenner Moor, 3 Sua Pan, 4 Walvis Bay, 1 Baskunchak, 1 Elton, 1 Kasin, 1 Douemina, 1 Iwik, 4 N'Dramcha and 3 Sal samples, respectively.

Both iron and manganese are important redox-sensitive transition metals and catalysts in Fenton chemistry (see Chapter 2.1). Zinc on the other hand has an anti-oxidative effect on Fenton chemistry inhibiting the production of OH radicals and superoxide (Strlič et al., 2003). The amount of dissolved transition metals correlates with the acidity of the water samples (Figure 66A). The Australian salt lakes have pH values ranging from slightly alkaline to highly acidic, whereas the other samples are circumneutral to alkaline. Only the Dead Sea samples were also slightly acidic with a pH of 5 to 6.5.

Figure 66. Distribution of pH in various water samples with N being the total available data points from 32 Australian, 6 Dead Sea, 12 Brenner Moor, 3 Sua Pan, 4 Walvis Bay, 1 Baskunchak, 1 Elton, 1 Kasin, 1 Douemina, 1 Iwik, 4 N'Dramcha and 3 Sal samples, respectively.



In conclusion, the set of water samples contained halide concentrations ranging from saline to hypersaline. This saline character of the sample sites was also reflected in soil/sediment samples that also contained high halide concentrations. Samples from Australia stand out compared to the other investigated saline environments with regard to their acidity.

The abundance of organic carbon and different transition metals provide the basis for abiotic chemistry as described in Chapter 2.

9.2.1 pH dependency of soluble constituents

To understand the relationship between pH and cations, anions and dissolved organic carbon (DOC) concentrations, 26 hypersaline water samples, collected in Western Australia between 2011 and 2013, were examined.

As can be seen in Figure 67, the abundance of dissolved alkali metals, sodium and potassium, were mostly independent of the water pH.

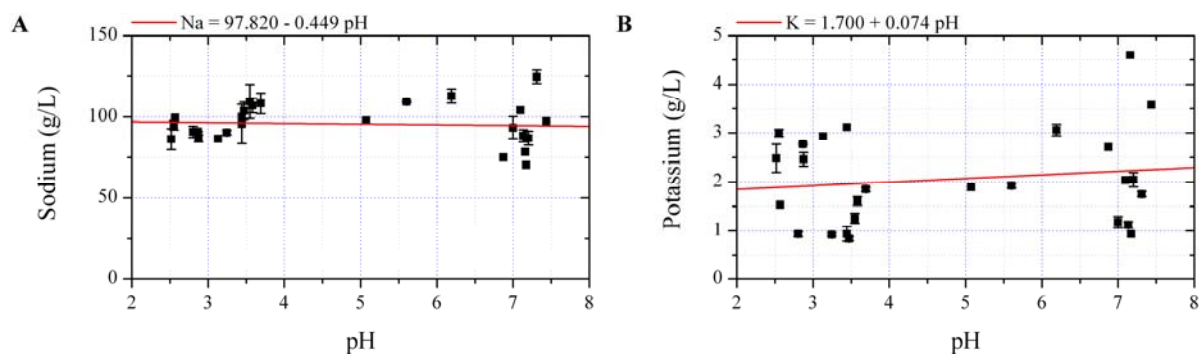


Figure 67. Relationship between **A** sodium, **B** potassium concentrations and the pH in water samples from Australia.

The same was observed for the alkaline earth metals magnesium, calcium and strontium (Figure 68). Though, strontium is less concentrated in acidic lakes (Figure 68C).

An increase of soluble element content at lower pH was measured for the transition metals manganese, iron, zinc and the main group element aluminium. While manganese and zinc concentrations only increased moderately under acidic conditions (Figure 69B and C), the soluble content of iron, mainly Fe^{2+} as demonstrated in chapter 9.3, and aluminium increased exponentially below a pH of 4 (Figure 69A and D).

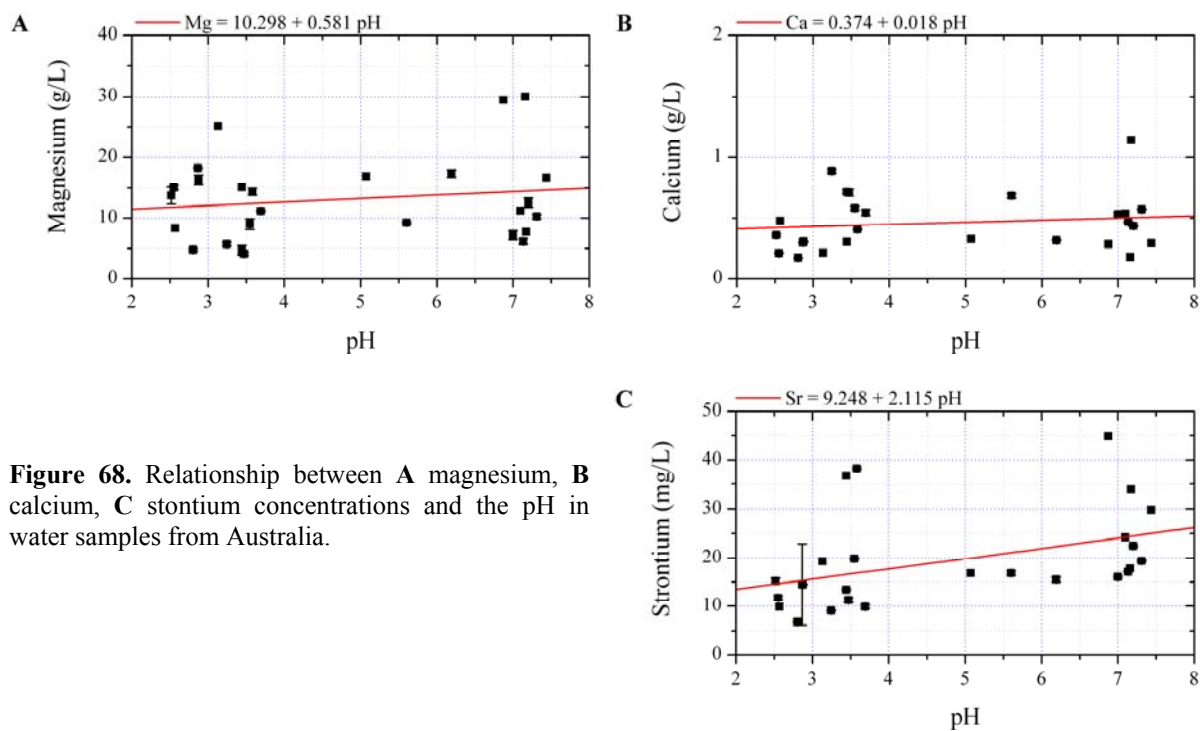


Figure 68. Relationship between **A** magnesium, **B** calcium, **C** stontium concentrations and the pH in water samples from Australia.

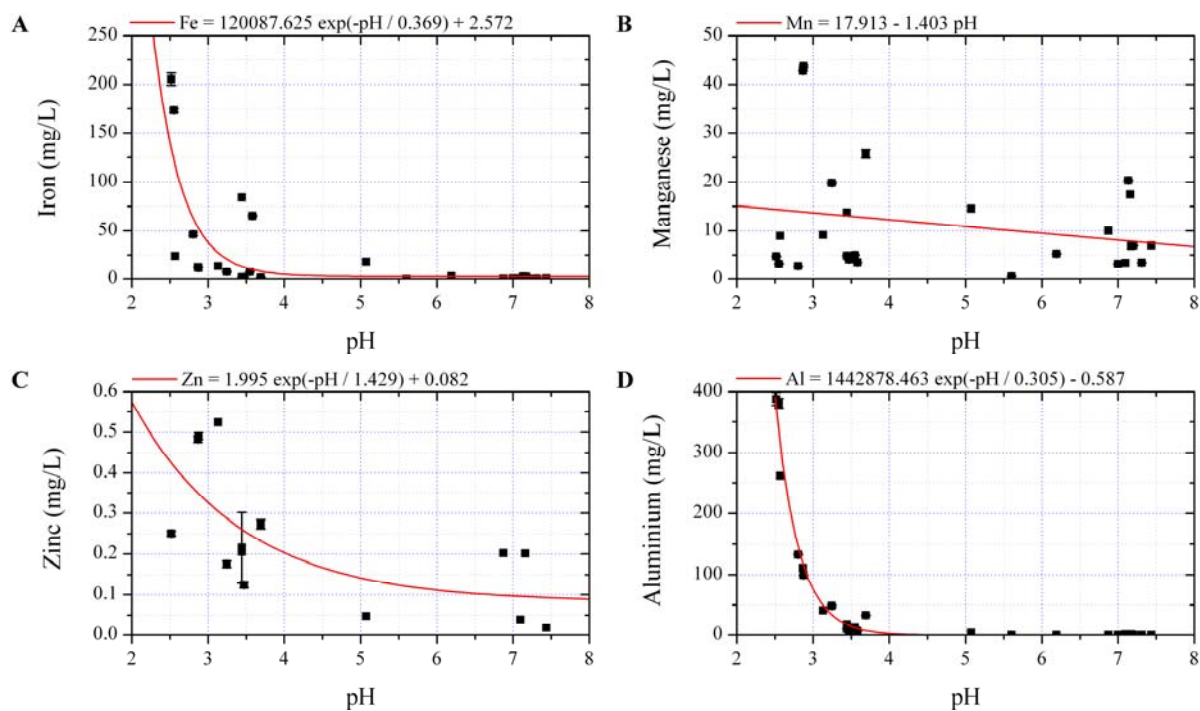


Figure 69. Relationship between **A** iron, **B** manganese, **C** zinc, **D** aluminium concentrations and the pH in water samples from Australia.

By contrast, halides and sulfate as the major anions in the solutions did not show any significant correlation with the pH (Figure 70).

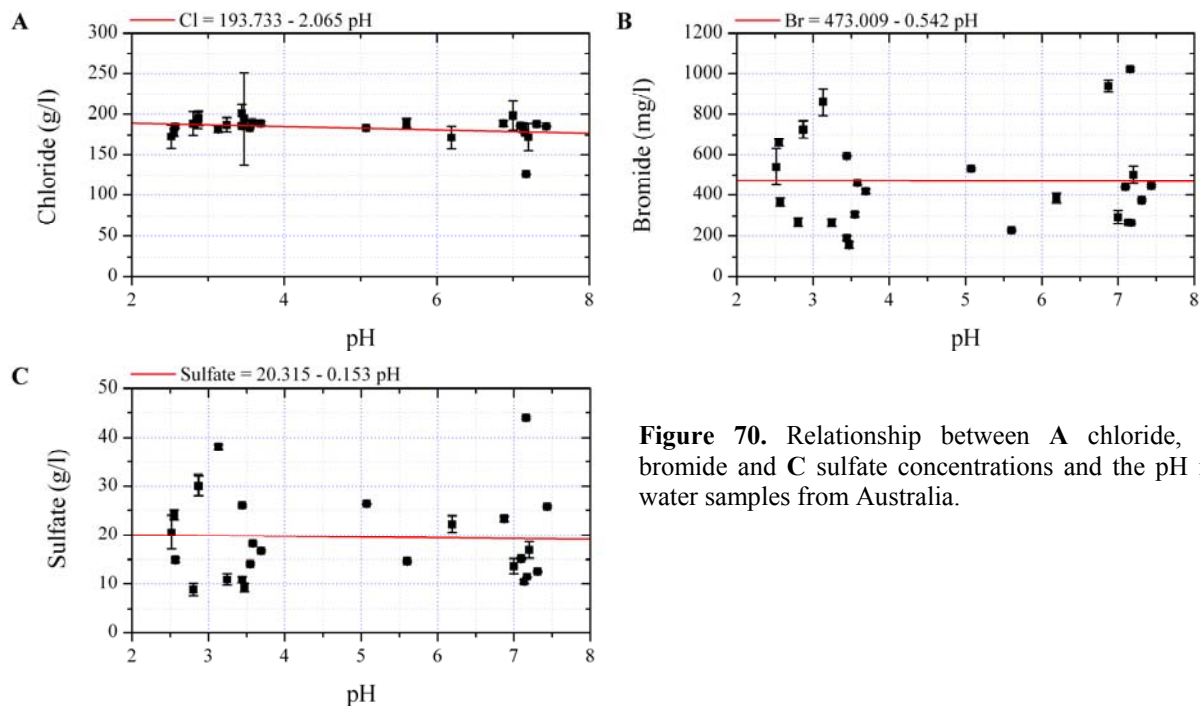


Figure 70. Relationship between **A** chloride, **B** bromide and **C** sulfate concentrations and the pH in water samples from Australia.

Aside from inorganic constituents, dissolved organic carbon was quantified in the water samples. While no chemical speciation for organic carbon is available, the data allows two conclusions.

Firstly, the dissolved organic carbon (DOC) content increased at higher pH values and secondly this could be connected to the observed red tint of circumneutral salt lakes (Figure 71). The colour consists of chromophores, most likely carotenoids from micro-algae, e.g. β -carotene from *Dunaliella salina* (Borowitzka and Borowitzka, 1990), and retinal within the protein bacteriorhodopsin which is produced by *Halobacteria* in large amounts (Stoeckenius and Bogomolni, 1982).

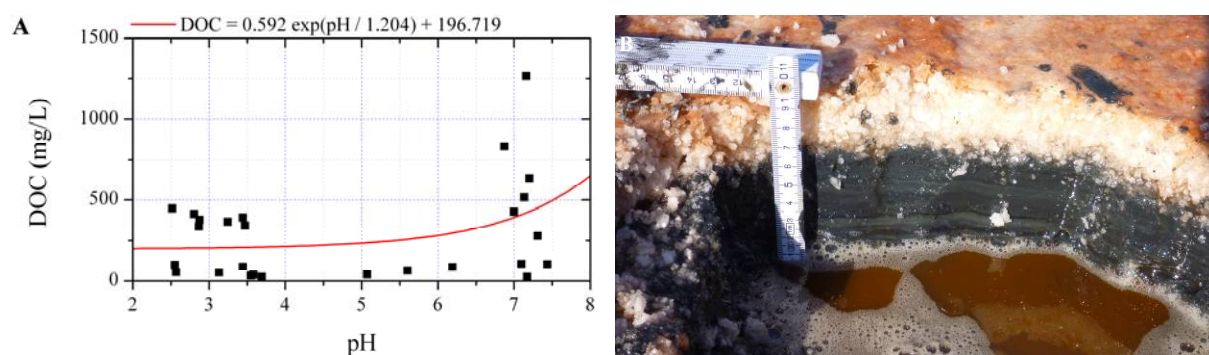


Figure 71. A Correlation between pH and DOC. B Red pigments in the salt crust and aqueous phase of Lake Walker in 2012 (pH 7.1, S 33.053173°, E 118.953010°). Image: T. Krause CC BY-SA 4.0.

The correlation between pH and dissolved compounds was employed within the framework of the DFG Research Unit 763 to simulate various natural geochemical conditions in the laboratory, e.g. in a smog chamber in Bayreuth to comprehend particle formation and growth over salt lakes (Kamilli et al., 2013; Kamilli et al., 2014).

9.3 Redox milieus and iron speciation

The chemistry of salt lakes not only depends on total element concentrations, but also on certain element species, like dissolved or solid Fe^{2+} and Fe^{3+} species. Thermodynamical stability of metal species is defined by pH and redox potential within the medium. The redox potential is determined by the oxidants (e.g. O_2 , Fe^{3+} and aerobes) to reductants (e.g. organic carbon, Fe^{2+} and anaerobes) ratio. Furthermore, the elemental speciation is influenced by the availability of inorganic and organic ligands.

9.3.1 Aqueous phase

One way to define the present redox milieu and predict the predominant iron species in an aqueous solution is to plot the measured redox potential (Eh) against the pH in a Pourbaix diagram (Chapter 5.5.10). Figure 72 shows Eh and pH values in a simplified iron Pourbaix diagram measured in Australian salt lakes in 2011 and 2012, including surface and groundwater. The data plots attribute suboxic and anoxic conditions with soluble Fe^{2+} and solid Fe^{3+} predominance in the salt lakes.

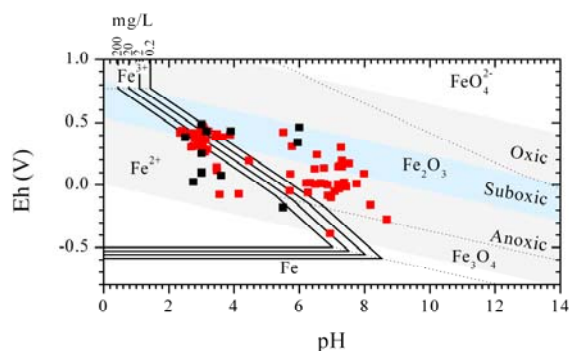


Figure 72. Eh and pH data from Australian salt lakes of 2011 and 2012 fitted into an iron predominance Pourbaix diagram (Verink, 2000). Solid lines indicate concentration dependent (0.2 mg/L, 2 mg/L, 20 mg/L and 200 mg/L iron) and dotted lines concentration independent equilibria between two iron species. Oxidic, suboxic and anoxic conditions are color highlighted.

■ Australia 2011, ■ Australia 2012

Abundance of Fe^{2+} was verified by a sensitive colour reaction in 2012 with the chelating agent 2,2'-bipyridine. The speciation of iron was further improved for the campaign in 2013. With a portable spectrometer the distribution of Fe^{2+} and Fe^{3+} was measured on-site. Simultaneously, Eh and pH as well as dissolved oxygen (DO) were measured in a flow cell.

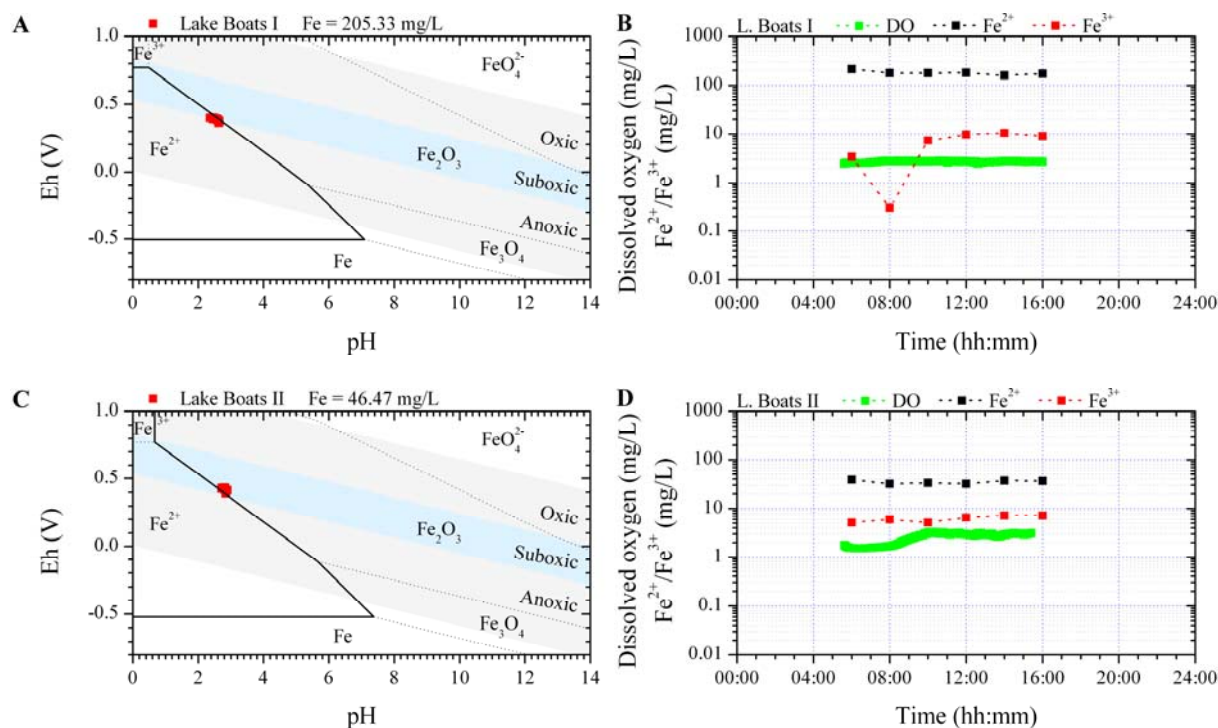


Figure 73. A Pourbaix diagram and B $\text{Fe}^{2+/3+}$ as well as DO concentration for Lake Boats on 08.03.2013. C Pourbaix diagram and D $\text{Fe}^{2+/3+}$ as well as DO concentration for Lake Boats on 18.03.2013.

Figure 73 shows Pourbaix diagrams, DO and iron concentrations for Lake Boats at two days with 51.5 mm precipitation in between. Due to the rain events the water table of Lake Boats had risen and the dissolved iron content was diluted. Furthermore, there is a slight shift of data in the Pourbaix diagrams toward Fe^{3+} species, which is also reflected by the ratio obtained from iron measurements. At the first sampling day the average $\text{Fe}^{2+}/\text{Fe}^{3+}$ ratio was 24:1 while 10 days later after the rain the average ratio was 6:1. Furthermore, both Pourbaix diagrams show that the data plots are in the area of equilibrium between soluble Fe^{2+} and solid Fe^{3+} implying elevated cycling between the two iron species. Moreover, the data in the diagrams are on the transition between suboxic and anoxic conditions.

Measured DO concentrations were close or even above the calculated maximum saturation concentrations while being well below fresh water saturation at that temperature. This difference between measured DO and fresh water saturation was around 3-7 mg/L. Regardless of the rising temperature, the DO values increased after sunrise on both days, which is an indication for photosynthetic processes.

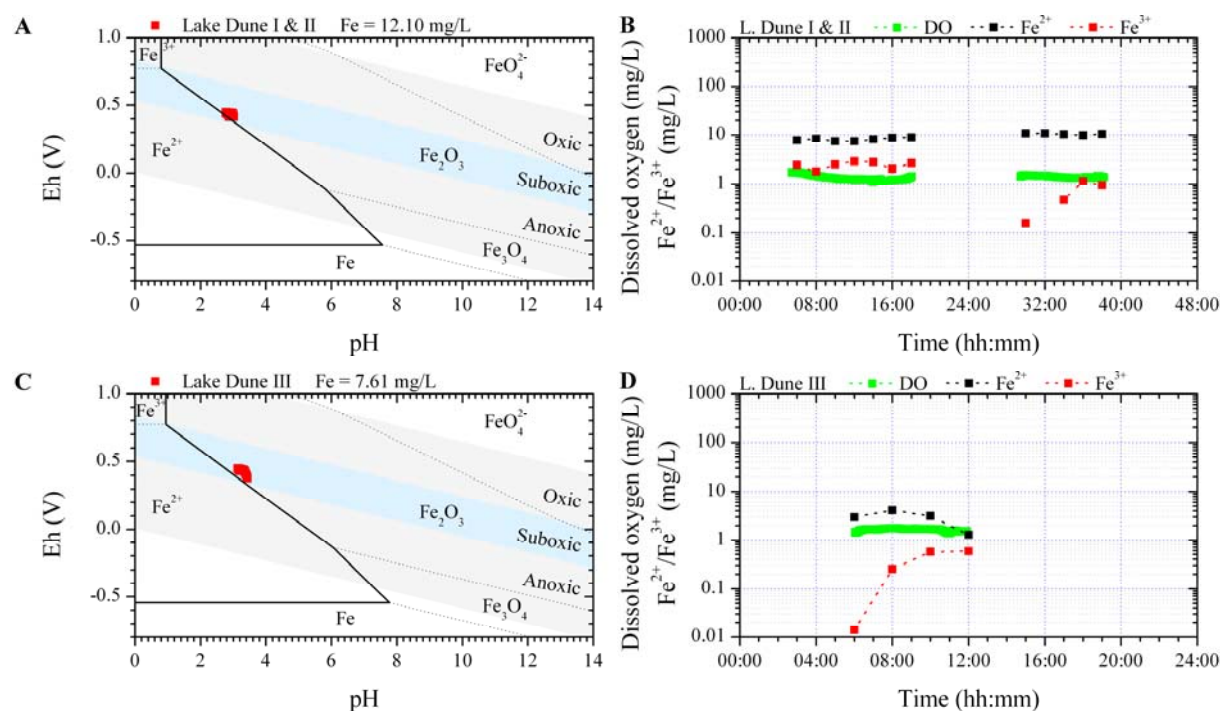


Figure 74. A Pourbaix diagram and B $\text{Fe}^{2+}/\text{Fe}^{3+}$ as well as DO concentration for Lake Dune on 13.03.2013 and 14.03.2013. C Pourbaix diagram and D $\text{Fe}^{2+}/\text{Fe}^{3+}$ as well as DO concentration for Lake Dune on 23.03.2013.

Lake Dune (Figure 74), slightly less acidic than Lake Boats, showed comparable characteristics. Data were collected on two consecutive days (Figure 74A and B) at the same site and 9 days later with 49.5 mm rainfall in an area where groundwater seeped into the lake

(Figure 74C and D). While the total iron content was lower than in Lake Boats, the dominant species was again Fe^{2+} as indicated by on-site measurements, which is also reflected in the Pourbaix diagrams. On the first day $\text{Fe}^{2+}/\text{Fe}^{3+}$ ratio was 3:1, on the second day 19:1 and on the third day 7:1. The difference between the first and second day could be due to wind directions and evaporation.

DO values for Lake Dune were slightly lower than for Lake Boats and at least for the first two days decreased, while the Pourbaix diagrams indicated suboxic conditions.

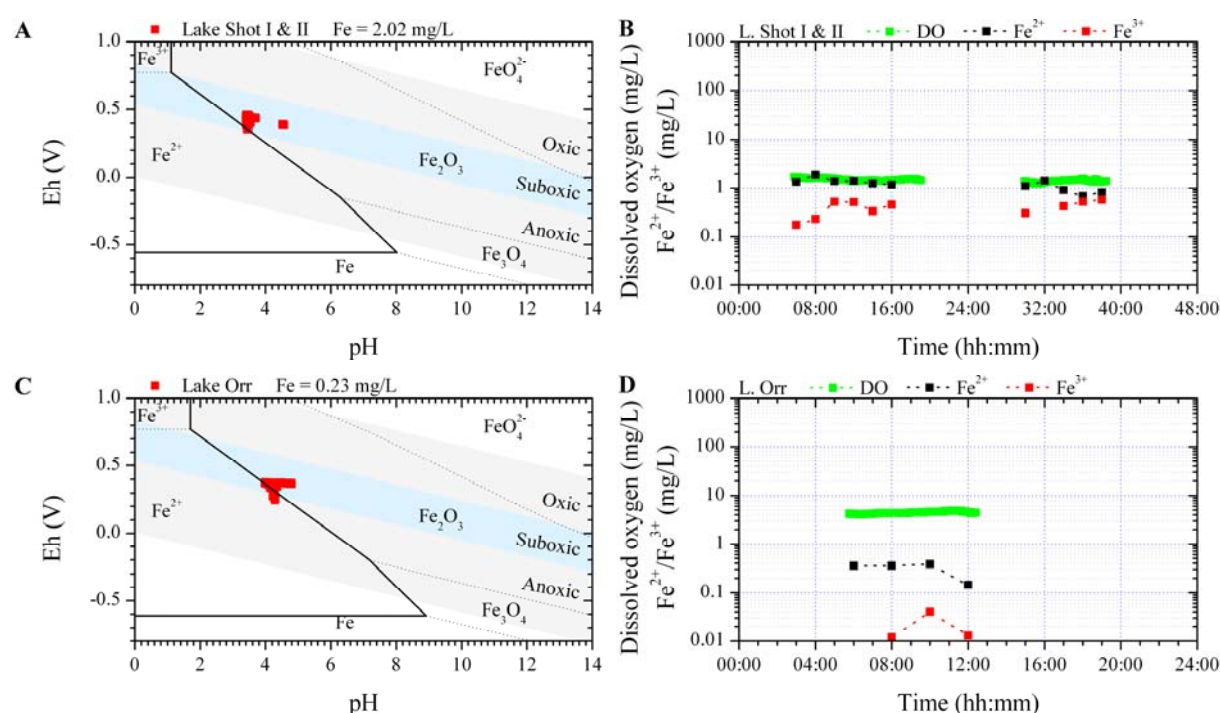


Figure 75. A Pourbaix diagram and B $\text{Fe}^{2+}/\text{Fe}^{3+}$ as well as DO concentration for Lake Shot on 21.03.2013 and 22.03.2013. C Pourbaix diagram and D $\text{Fe}^{2+}/\text{Fe}^{3+}$ as well as DO concentration for Lake Orr on 19.03.2013.

Pourbaix diagrams of Lake Shot, with data from two consecutive days (Figure 75A and B) and Lake Orr (Figure 75C and D) indicated suboxic conditions with an equilibrium between soluble and solid iron shifting more and more to the solid phase. This tendency is seen in the dissolved iron measurements for Lake Shot (max. 2.14 mg/L) and Lake Orr (max. 0.42 mg/L) compared to Lake Dune (max. 11.47 mg/L) and Lake Boats (max. 216.6 mg/L), respectively.

The soluble $\text{Fe}^{2+}/\text{Fe}^{3+}$ ratio was 4:1 and 3:1 for Lake Shot on day one and two, respectively, and 19:1 for Lake Orr.

DO concentration slightly decreased in Lake Shot on the first day until sunset and increased on the second day. Lake Orr, strongly diluted by rain, had the highest measured DO values

due to the lowest salinity. DO concentration increased over the day indicating photosynthetic processes.

The next two lakes were circumneutral during the measurements and clearly differed in their geochemical inventory from the before-mentioned acidic lakes. The Pourbaix diagrams from Lake Bean (Figure 76A) and Lake Kathleen (Figure 76C) indicated solid iron species to be the predominant species in a suboxic environment. Furthermore, dissolved iron measurements showed inversed $\text{Fe}^{2+}/\text{Fe}^{3+}$ ratios of 1:19 and 1:6 for Lake Kathleen and Lake Bean, respectively. Total iron concentrations were again relatively low compared to the strongly acidic lakes, with maximal dissolved iron concentrations of 1.8 mg/L for Lake Bean and 0.48 mg/L for Lake Kathleen, respectively.

While DO concentrations at Lake Kathleen were nearly constant between morning and noon, measurements at Lake Bean showed an increase to about 300% saturation. This could either point to photosynthetic organisms or to an artefact resulting from mechanical degradation of the deployed peristaltic pump.

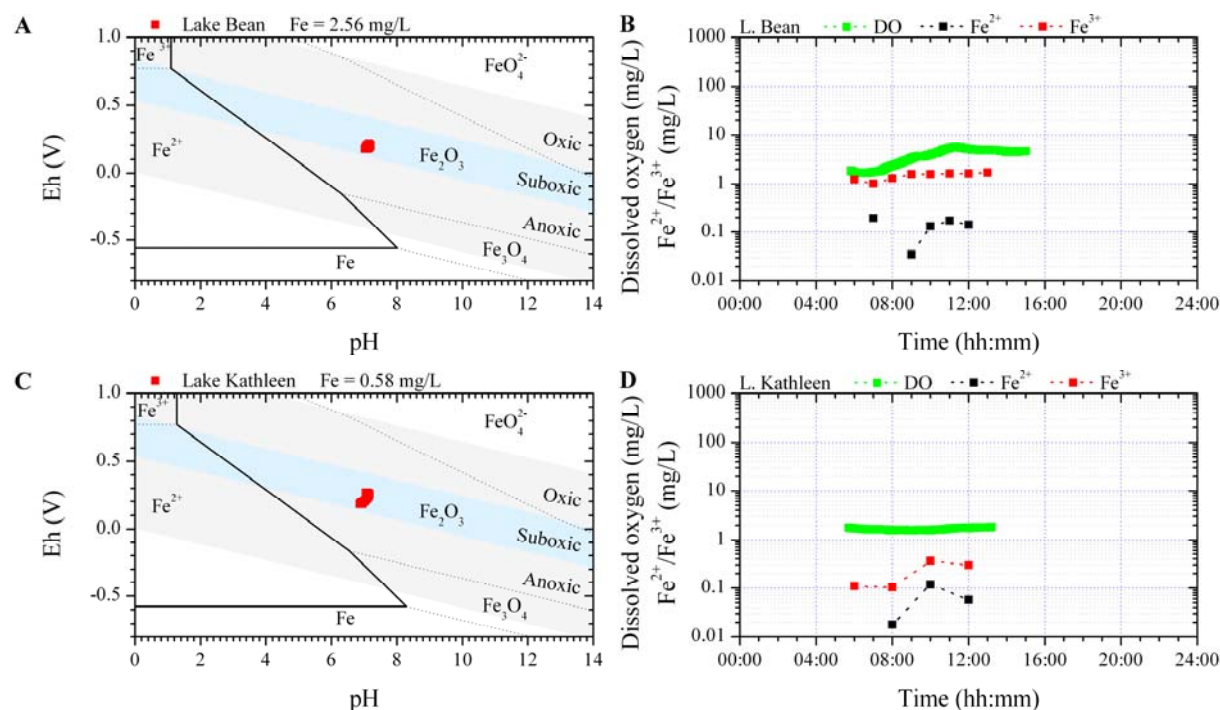


Figure 76. A Pourbaix diagram and B $\text{Fe}^{2+}/\text{Fe}^{3+}$ as well as DO concentration for Lake Bean on 29.03.2013 and 14.03.2013. C Pourbaix diagram and D $\text{Fe}^{2+}/\text{Fe}^{3+}$ as well as DO concentration for Lake Kathleen on 24.03.2013.

The observation of foam on Lake Bean and Lake Boats II (Figure 77) militates for photosynthetic organisms. In both cases a clear increase of DO was measured compared to the other lakes where foam was absent.



Figure 77. Foam on the surface water of Lake Boats. Image: T. Krause CC BY-SA 4.0.

In summary, hypersaline waters can be described as suboxic or even anoxic according to pH-Eh plots. Furthermore, these Pourbaix diagrams can be used to predict the abundance of soluble Fe^{2+} and total soluble iron concentrations. Fe^{2+} and DO are key features for aquatic H_2O_2 formation either by autoxidation (Weiss, 1935; Aust et al., 1985; Voelker et al., 1997; Kessick and Morgan, 1975) or by photochemistry in combination with DOC (Cooper et al., 1988). Additionally, iron is an important catalyst.

9.3.2 Sediments

Redox-Sensitive Tapes (RST) (Oeste, 2010) were deployed to classify the redox zones of sediments at selected Australian salt lakes in 2013.

Figure 78 shows wet and dried RST from lakes with a water pH > 6. These lakes have a fine black sediment layer with a distinguishable odour of VSC in common.

Lake Hatter Hill (Figure 78A) stands out compared to the other two lakes. While it was a hypersaline lake with a salt crust during the campaign in 2011, heavy rains turned it into a brackish water lake with at least 2 m depth in December 2011. Until 2013 the water level did not decline sufficiently to turn the lake back into a hypersaline lake, instead the low brine concentration supported the growth of water plants. Therefore, the upper sediment layer (0-4 cm) contained plant residues. Between 0-4 cm MnO_2 pigments were completely dissolved from RST-A. The absence of $\text{FeO}(\text{OH})$ on RST-A and the bleached RST-B indicated iron-reducing conditions (milieu III) for the upper 0-4 cm layer. Furthermore, bleaching of RST-C indicated PbS formation due to low H_2S concentration. Dark grey to black tinting of all the wet RST between 4-10.5 cm showed the formation of FeS due to sulfate-reducing conditions with high H_2S concentrations (milieu IV) in deeper sediment layers. During drying FeS was oxidised to iron oxides leaving brown stains on all RST.

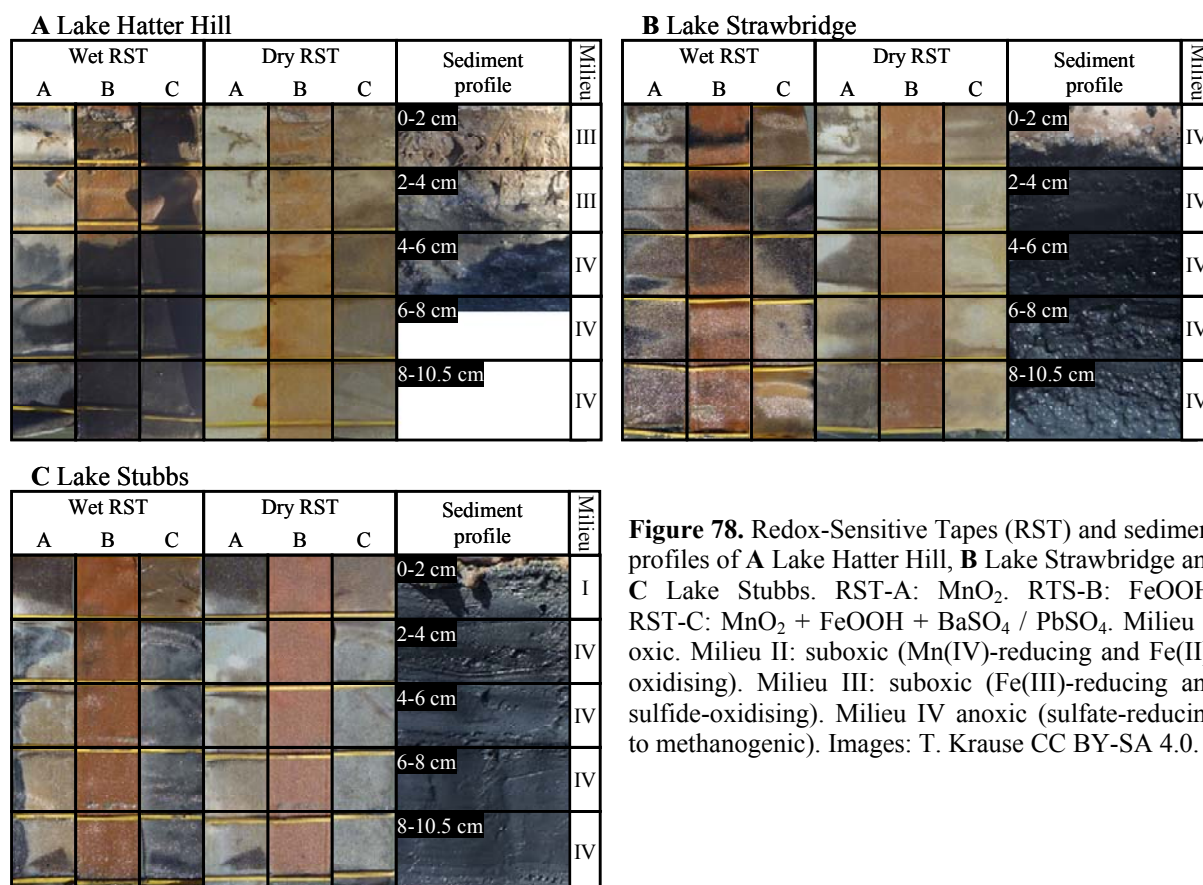


Figure 78. Redox-Sensitive Tapes (RST) and sediment profiles of **A** Lake Hatter Hill, **B** Lake Strawbridge and **C** Lake Stubbs. RST-A: MnO_2 . RST-B: FeOOH . RST-C: $\text{MnO}_2 + \text{FeOOH} + \text{BaSO}_4 / \text{PbSO}_4$. Milieu I: oxic. Milieu II: suboxic (Mn(IV) -reducing and Fe(II) -oxidising). Milieu III: suboxic (Fe(III) -reducing and sulfide-oxidising). Milieu IV anoxic (sulfate-reducing to methanogenic). Images: T. Krause CC BY-SA 4.0.

RST of Lake Strawbridge (Figure 78B) showed an irregular discoloration. Dark grey and black FeS spots between 0-10.5 cm that vanished after drying and leaving brown PbS spots on RST-C point to sulfate reducing milieu IV.

The upper layer of Lake Stubbs (0-2 cm) is classified as oxic milieu I, because of the unchanged RST. In deeper sediment layers grey and black tinting, which bleached during drying, proved the formation of FeS in the black sediment under sulfate-reducing conditions (milieu IV). Light grey tinting of the wet RST-B and grey brownish tinting (PbS) of the dry RST-C indicate low to average H_2S concentrations (Figure 78C).

Formation of black FeS on the RST for these three lakes suggests that the black sediment also contained FeS . Additionally, it can be assumed that the sediments also contained black and more stable FeS_2 as disturbed black sediments only partially bleached when laying in contact with atmospheric oxygen.

Figure 79 shows the RST and sediment profiles of Lake Bean and Lake Whurr, representing lakes with a water pH of 4-6, though pH of lake Whurr decreased below 4 in 2012 and 2013 compared to 2011. In most cases sediments of slightly acidic lakes feature a thin orange layer beneath the crust followed by a black layer above grey yellow sediment layers.

Likewise Lake Stubbs, the RST of Lake Bean (Figure 79A) did not change in the upper 0-1 cm layer pointing to oxic conditions (milieu I). The MnO_2 on RST-A and RST-C was completely dissolved and brown iron oxides dominated the tinge of the tapes. Furthermore, no alteration of RST-B was observed indicating non iron-reducing conditions (milieu II).

A Lake Bean							B Lake Whurr								
Wet RST			Dry RST			Sediment profile	Milieu	Wet RST			Dry RST			Sediment profile	Milieu
A	B	C	A	B	C			A	B	C	A	B	C		
						0-2 cm	I							0-2 cm	II
						2-4 cm	II							2-4 cm	II
						4-6 cm	II							4-6 cm	II
						6-8 cm	II							6-8 cm	II
						8-10.5 cm	II							8-10.5 cm	II

Figure 79. Redox-Sensitive Tapes (RST) and sediment profiles of **A Lake Bean** and **B Lake Whurr**. RST-A: MnO_2 . RST-B: FeOOH . RST-C: $\text{MnO}_2 + \text{FeOOH} + \text{BaSO}_4 / \text{PbSO}_4$. Milieu I: oxic. Milieu II: suboxic (Mn(IV) -reducing and Fe(II) -oxidising). Milieu III: suboxic (Fe(III) -reducing and sulfide-oxidising). Milieu IV anoxic (sulfate-reducing to methanogenic). Images: T. Krause CC BY-SA 4.0.

Interpretation of Lake Whurr (Figure 79B) is analogous to Lake Bean with the exception that suboxic manganese-reducing and iron-oxidising milieu II was assumed for the whole 0-10.5 cm of the sediment.

The redox milieus of acidic lakes (pH 2-4) as shown in Figure 80 cover suboxic (milieu II) to anoxic conditions (milieu IV). While the before mentioned lakes with a pH > 4 normally featured a black FeS layer, the highly acidic lakes (pH 2-4) had plain grey or brown layers with little variances over the investigated depth. Two RST were deployed at Lake Dune: one labelled Lake Dune I/II in the sandy shore sediment and the second, Lake Dune III, in a sediment covered by plant detritus, mainly from Eucalyptus leaves.

RST of Lake Dune I/II (Figure 80A) showed similar changes as mentioned before for Lake Bean and Lake Whurr classifying the sediment from 0-10.5 cm as suboxic with manganese-reducing and iron-oxidising conditions (milieu II). On the other hand Lake Dune III (Figure 80B) was suboxic with iron-reducing conditions (milieu III) as MnO_2 and FeO(OH) were dissolved from RST-A and RST-C, respectively. Additionally, no brown PbS stains on RST-C were observed pointing to the absence of H_2S in the sediment.

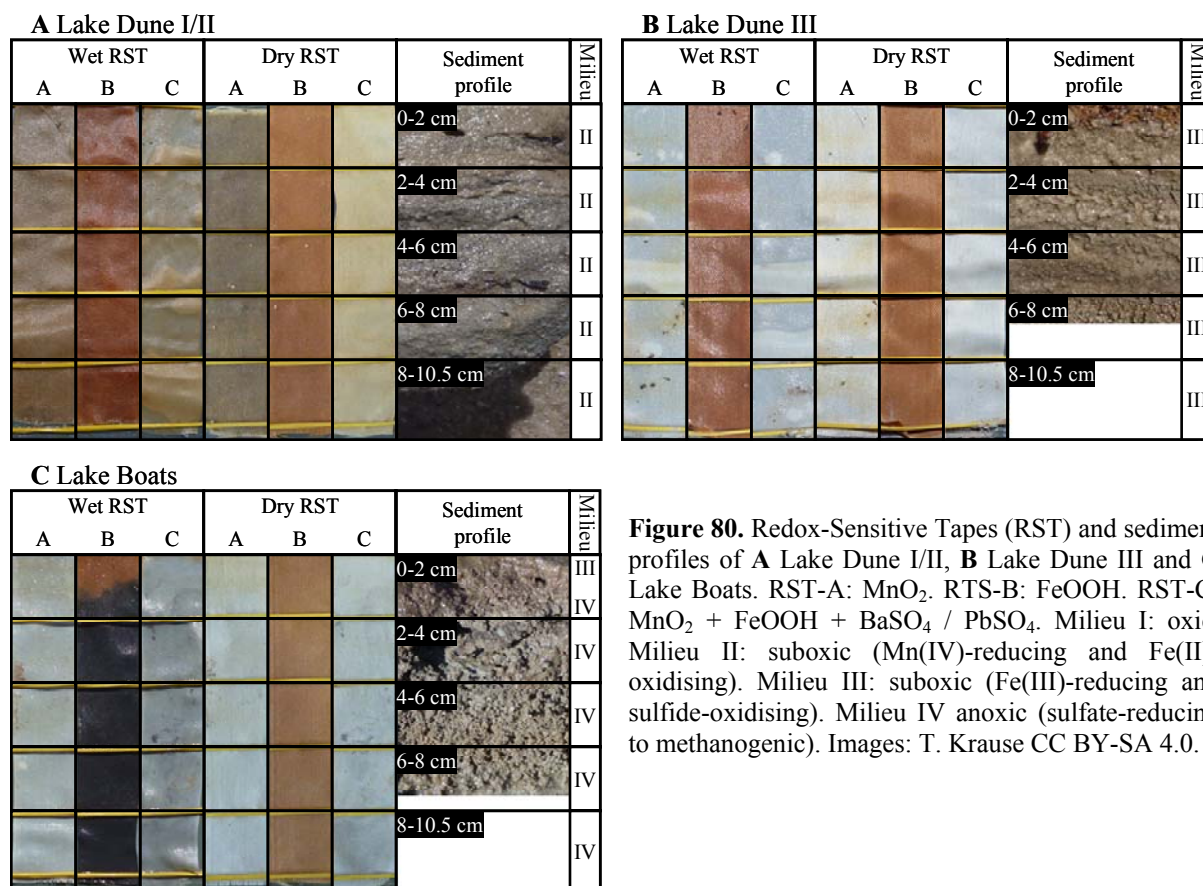


Figure 80. Redox-Sensitive Tapes (RST) and sediment profiles of **A** Lake Dune I/II, **B** Lake Dune III and **C** Lake Boats. RST-A: MnO_2 . RST-B: FeOOH . RST-C: $\text{MnO}_2 + \text{FeOOH} + \text{BaSO}_4 / \text{PbSO}_4$. Milieu I: oxic. Milieu II: suboxic (Mn(IV) -reducing and Fe(II) -oxidising). Milieu III: suboxic (Fe(III) -reducing and sulfide-oxidising). Milieu IV anoxic (sulfate-reducing to methanogenic). Images: T. Krause CC BY-SA 4.0.

Completely bleached RST-A and RST-C from Lake Boats (Figure 80C) clearly showed manganese- and iron-reducing conditions (milieu III) in the upper sediment layer (0-1 cm). Below 1 cm the black stain of the wet RST-B, which turned to brown during drying, proved FeS formation in the sediment under high H_2S concentrations. Although, even small concentrations of H_2S should be indicated by a brown PbS stain on RST-C this was not observed. An explanation is the slow dissolution of lead pigments under acidic conditions over time.

The RST evaluation of suboxic to anoxic milieus was further supported by water content measurements of around 30% in sediment samples. High hypersaline ground and pore waters displace oxygen from the sediments and function as a barrier against atmospheric oxygen penetration.

In conclusion, the black FeS/FeS_2 sediment layers of salt lakes with a water $\text{pH} > 6$ can be classified as anoxic with sulfate-reducing conditions as they contain FeS and FeS_2 , while most of the acidic lakes with a $\text{pH} < 6$ are suboxic with manganese-reducing and in between iron-oxidising and iron-reducing conditions.

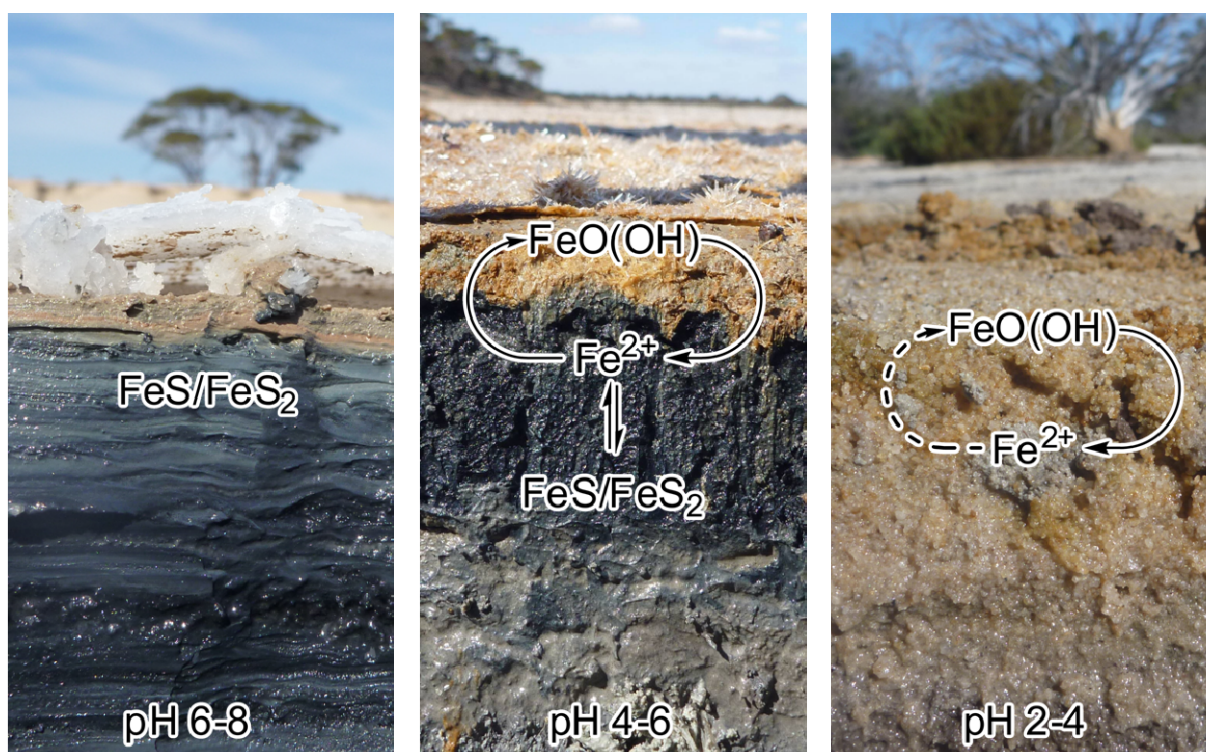


Figure 81. Mobility of iron in circumneutral (left), slightly acidic (middle) and highly acidic (right) salt lake sediments. Images: T. Krause CC BY-SA 4.0.

These results reveal a simple model for iron mobility in Australian salt lakes as a function of pH (Figure 81). In circumneutral to alkaline lakes iron mobility is impeded as iron is mineralised as FeS and FeS₂ under the salt crust. In slightly acidic lakes (pH 4-6), an exchange of iron between the upper anoxic FeS/FeS₂ sediment and surface water in form of Fe²⁺ is likely. In the suboxic to oxic surface water Fe²⁺ is oxidised and precipitates as yellow iron oxides, e.g. FeO(OH), on and within the salt crust. Upon sedimentation the iron oxides are reduced again in the suboxic to anoxic layers beneath the salt crust. In highly acidic lakes, iron mobility between sediments and surface water is mostly unrestricted as soluble Fe²⁺ is the most thermodynamically stable iron species.

Redox milieu investigations demonstrated that the mineral phase within the anoxic sediments are susceptible to oxidation by oxygen. As a consequence, redox equilibria change within collected sediments for laboratory analysis. This process is further enhanced by freeze-drying (Hjorth, 2004), grinding and moistening for the incubation experiments. However, these pretreatments reflect also periodical aridification and moistening in natural environments, while allowing long time storage and reproducible analysis of the samples.

Furthermore, highly volatile compounds are removed from the samples by freeze-drying. Hence, their abundance during soil/sediment incubation experiments can be attributed to de novo formation as is presented in Chapter 10.

10 Volatile compounds released from hypersaline environments

From Australia, 2011 and 2012, as well as the Dead Sea, 2012, 87 soil/sediment (Appendix C) and 27 water samples (Appendix D) were analysed to assess the release of volatile compounds. A total of 69 different volatile compounds was identified and quantified by GC-MS analysis from various saline soil, sediment and water samples. Furthermore, the identity of 26 molecules was postulated by means of their mass spectra and retention times.

An overview of emission data, including measurement frequency and concentration distribution is depicted in Chapter 10.1. A more detailed interpretation of emission patterns in comparison with geochemical parameters is given in Chapter 10.2 to Chapter 10.11.

10.1 Overview

In this chapter concentrations of all quantified compounds regardless of their origin will be presented to give a first impression on emission data from various soil/sediment and water samples. Furthermore, the abundance of each quantified compound in all available samples is given. Their description is divided into the different classes of volatile compounds, namely BTEX, isoprene and monoterpenes, furans, VSC/VSeC and VOX.



Figure 82. Acidic Australian salt lake in 2011. Image: T. Krause CC BY-SA 4.0.

BTEX

Aside from BTEX, some other benzene derivatives (Figure 83) like styrene, methylstyrene, 2-propenylbenzene, as well as trimethylbenzenes, ethylmethylbenzenes and propylbenzene were abundant in several samples according to the obtained mass spectra compared with the NIST mainlib and replib database.

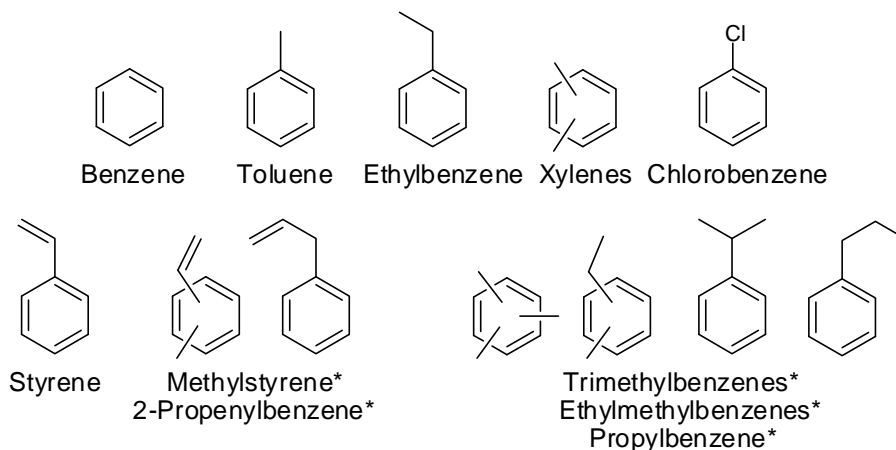


Figure 83. BTEX and other benzene derivatives found in various samples. Postulated compounds are marked with an asterisk.

Most soil and sediment samples contained BTEX with toluene and benzene as the most frequently measured compounds (Figure 84A). While xylenes were not further assigned, it can be assumed that the here called X-xylene is the sum of two xylene isomers that were not properly separated on the used GC column. Boiling points of p-xylene (139.2 °C) and m-xylene (138.4 °C) are almost identical, while o-xylene (144.5 °C) is less volatile (Katritzky et al., 1998) indicating that X-xylenes are the sum of p- and m-xylene. Concentrations in water samples were typically less by a factor of 10 compared to soil/sediment samples in terms of sample weight (Figure 84B).

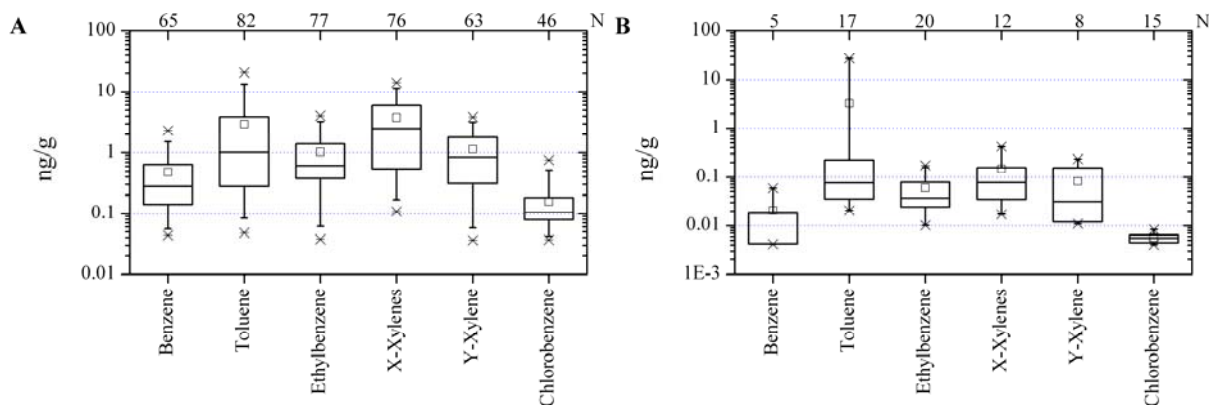


Figure 84. BTEX and chlorobenzene emissions from **A** soil/sediment and **B** water samples with N being the amount of total available data points from 87 soil/sediment and 27 water sample, respectively.

Isoprene and monoterpenes

Chemical structures of isoprene and all identified monoterpenes, including enantiomers, are shown in Figure 85. The non-chiral GC column used in the analytical setup did not allow separation of racemic mixtures and thus identification of a specific enantiomer was not possible.

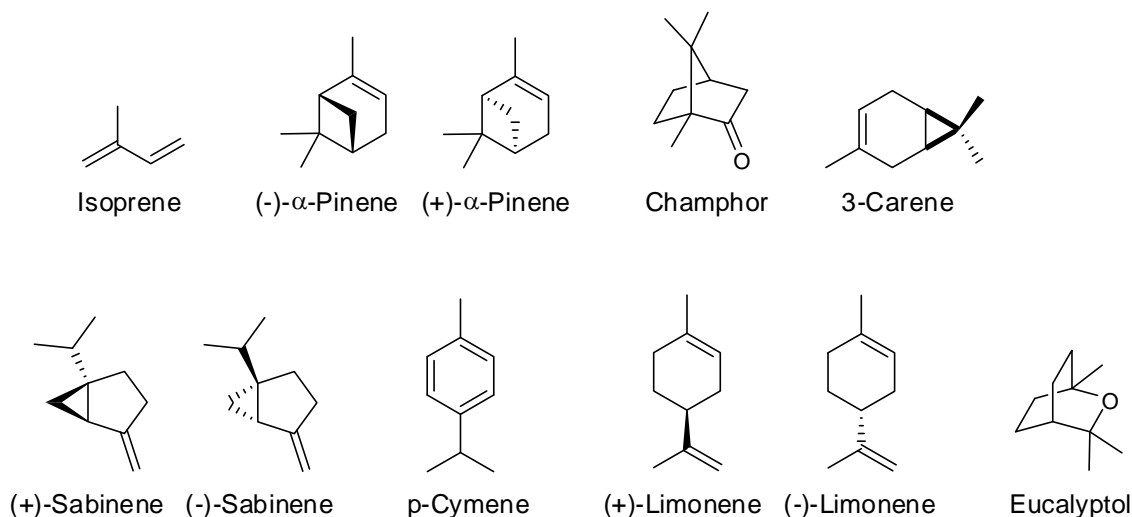


Figure 85. Isoprene and monoterpenes found in various samples.

By far, the highest emissions were observed for several monoterpenes from soil and sediment samples, while isoprene concentrations were significantly lower (Figure 86A). Concentrations above 1 $\mu\text{g/g}$ are extrapolated. In the water samples the concentrations of these hydrophobic compounds were only a small fraction compared to the sediment samples (Figure 86B).

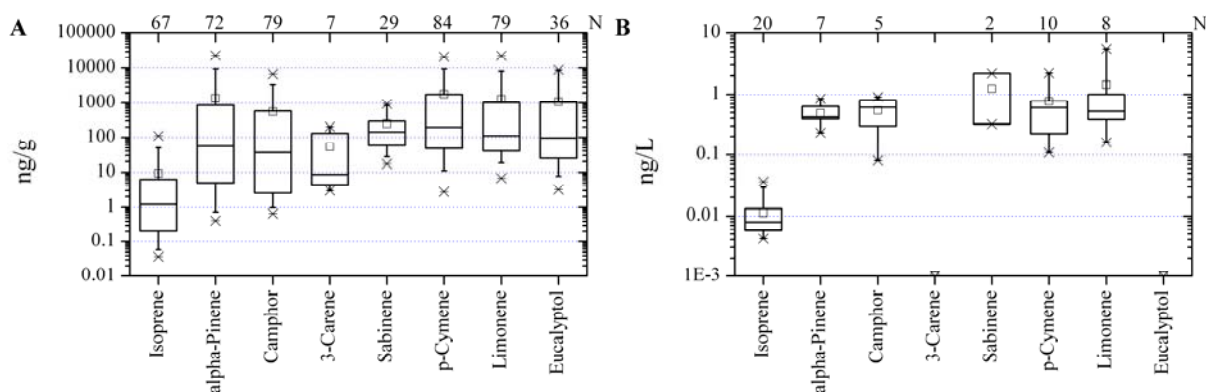


Figure 86. Isoprene and monoterpene emissions from **A** soil/sediment and **B** water samples with N being the amount of total available data points from 87 soil/sediment and 27 water sample, respectively.

Furans

A total of 9 furan derivatives was found in various samples including a chlorinated and a brominated furanoic compound (Figure 87). Another halogenated methylfuran was postulated to be abundant from the obtained mass spectra.

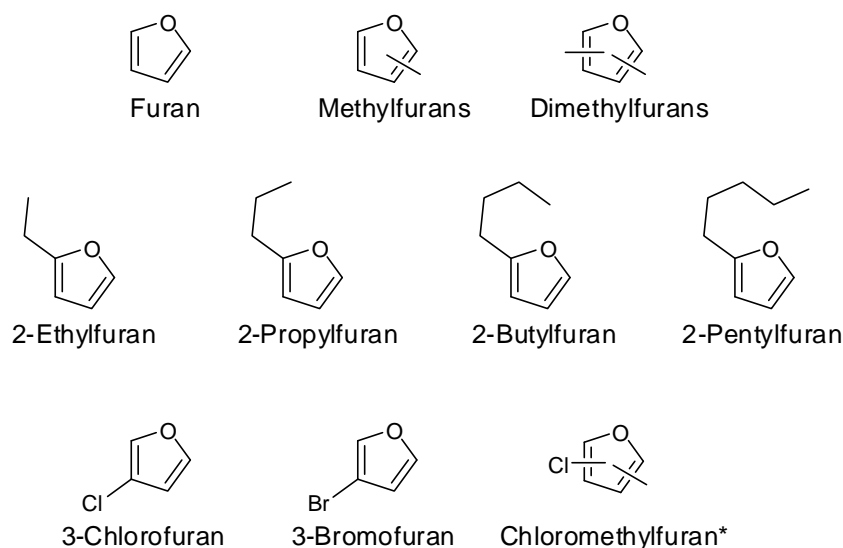


Figure 87. Furanoic compounds found in various samples. Postulated compounds are marked with an asterisk.

Furan and methylated furans were almost ubiquitous in soil/sediment and water samples while higher alkylated furans were less frequently measured (Figure 88). Compared to BTEX concentrations the furanoic compound concentrations were typically higher. Additionally, compared to BTEX and monoterpenes, furans were also found at high frequency and overall at high concentrations in water samples (Figure 88B).

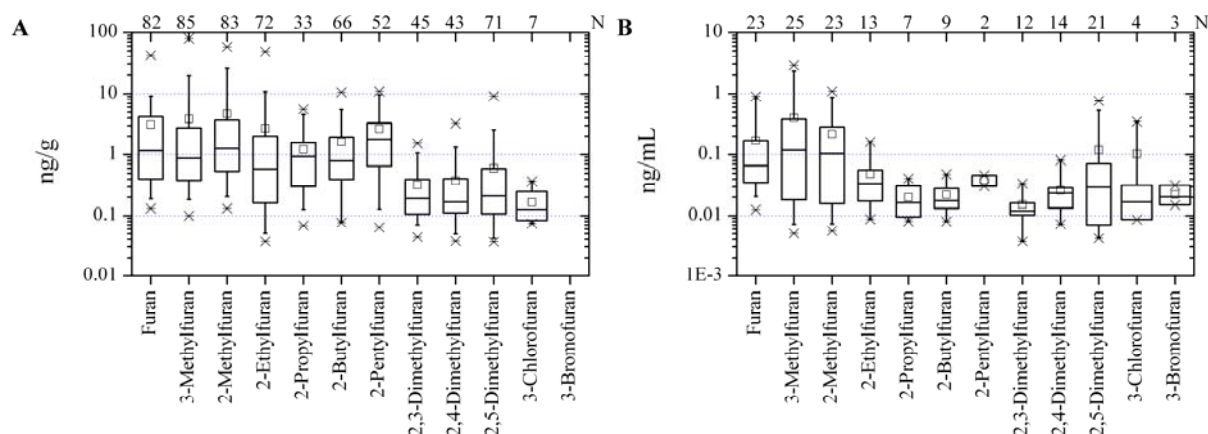


Figure 88. Furanoic compound emissions from **A** soil/sediment and **B** water samples with N being the amount of total available data points from 87 soil/sediment and 27 water sample, respectively.

VSC/VSeC

Identified sulfur compounds include inorganic sulfur species like carbon disulfide and presumably carbonyl sulfide and sulfur dioxide. Furthermore, different methylated sulfur and selenide species were found as well as various heterocyclic thiophenes (Figure 89). From the Australian redox milieu studies (Chapter 9.3) it can be assumed that H₂S is ubiquitous as well.

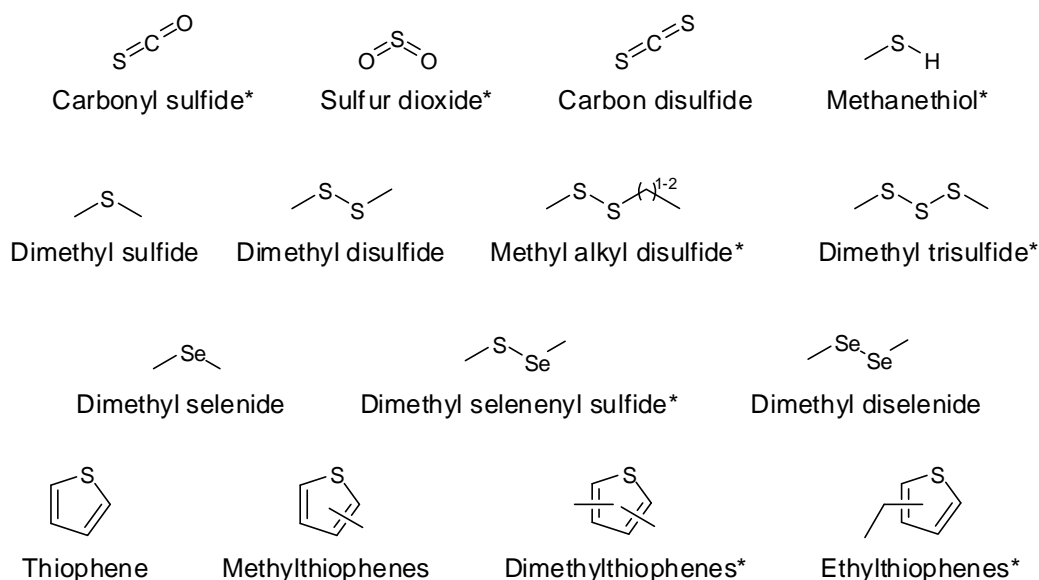


Figure 89. Volatile sulfur and selenide compounds found in various samples. Postulated compounds are marked with an asterisk.

Carbon disulfide and dimethyl disulfide were found with highest concentrations in soil and sediment samples, followed by dimethyl sulfide. A different distribution was observed in aqueous samples with highest concentration of dimethyl sulfide. Overall, sulfur compound concentrations were high (Figure 90) emphasising the anoxic character of the salt lakes described within the redox milieu studies in Chapter 9.3.

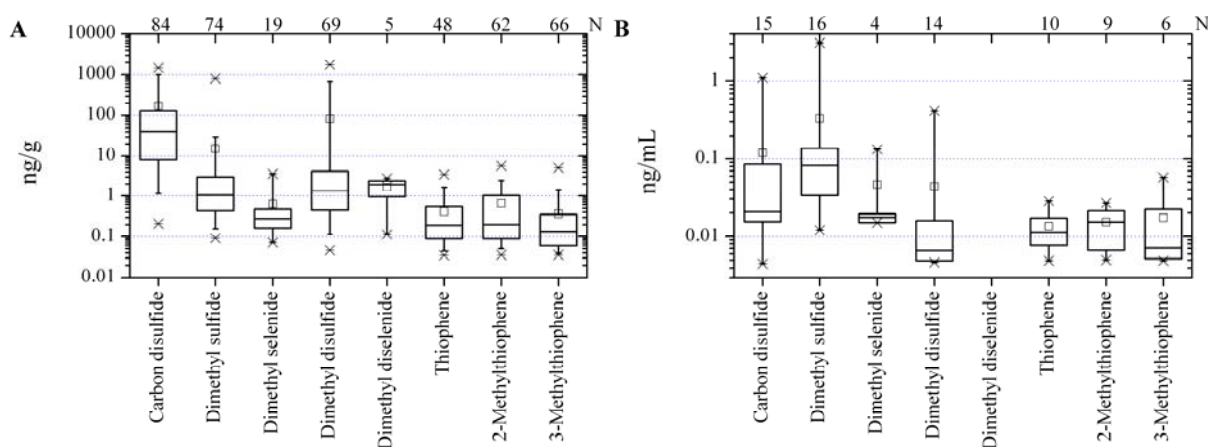


Figure 90. VSC/VSeC emissions from **A** soil/sediment and **B** water samples with N being the amount of total available data points from 87 soil/sediment and 27 water sample, respectively.

VOX

Halogenated compounds represent the most diverse class of volatile compounds that were identified in the samples. Aside from the before mentioned halogenated benzene and furans, various halocarbons were found, i.a. chlorinated alkanes (Figure 91).

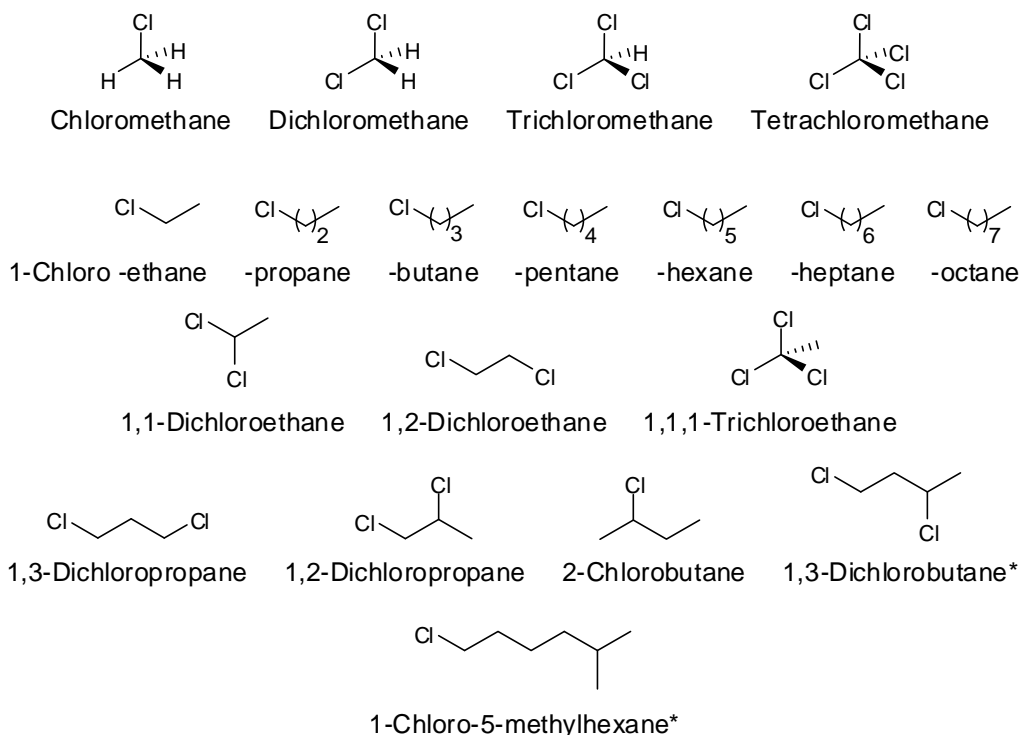


Figure 91. Chlorinated alkanes found in various samples. Postulated compounds are marked with an asterisk.

The main fraction of these compounds were monochlorinated alkanes, mostly terminal chlorinated, which were measured with high concentrations and frequency in soils and sediments. Abundance and concentrations of chloroalkanes in the water samples were overall low.

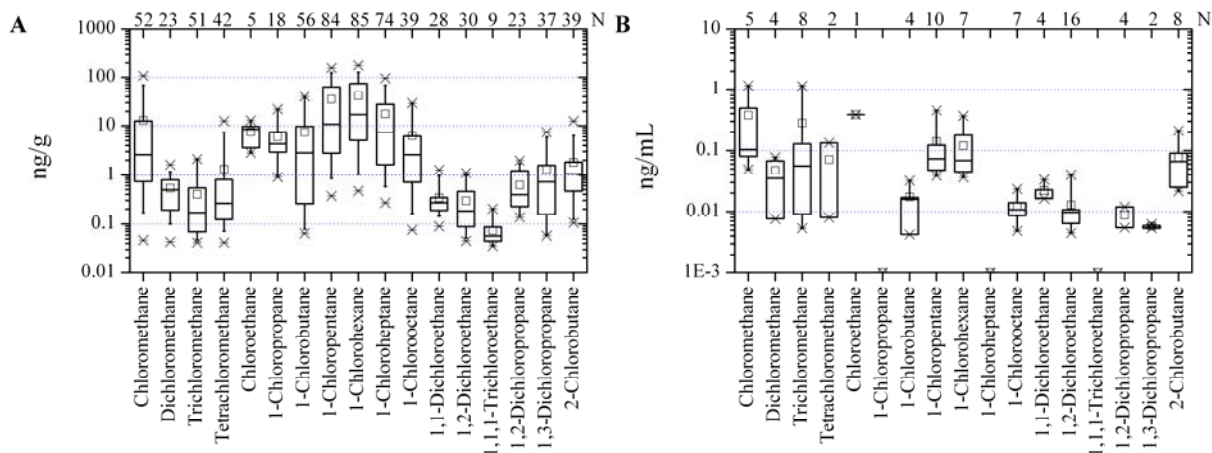


Figure 92. Chlorinated alkane emissions from **A** soil/sediment and **B** water samples with N being the amount of total available data points from 87 soil/sediment and 27 water sample, respectively.

Additionally, a few chlorinated alkenes were found, including polychlorinated ethenes (Figure 93).

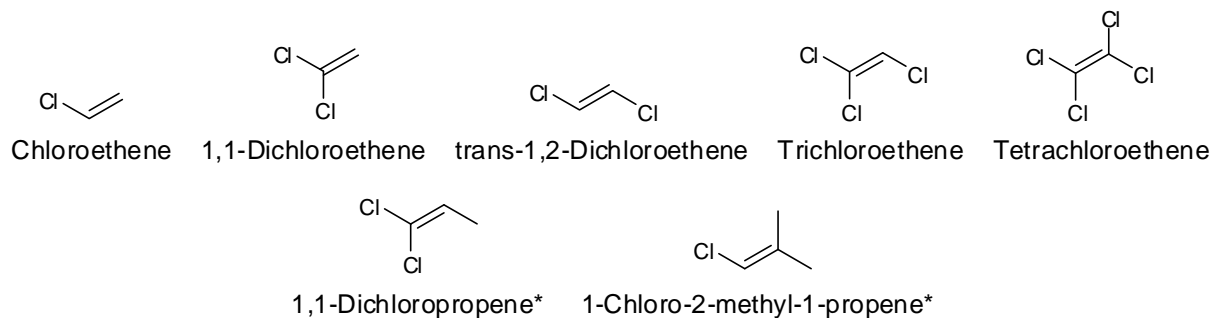


Figure 93. Chlorinated alkenes found in various samples. Postulated compounds are marked with an asterisk.

Concentrations of chlorinated alkenes were lower compared to chlorinated alkanes and aside from tetrachloroethene and trichloroethene, these substances were only found in a few samples.

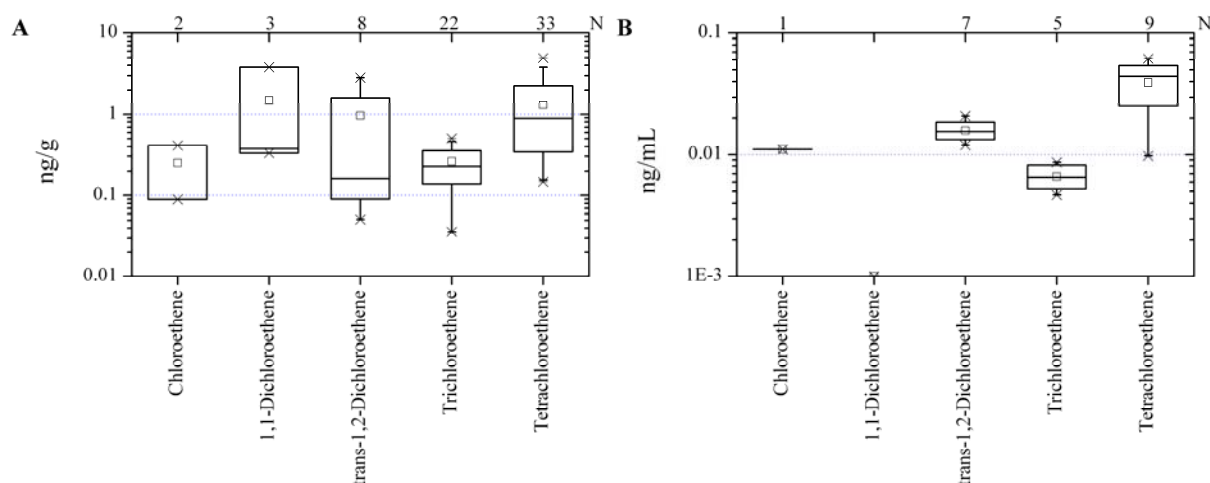


Figure 94. Chlorinated alkene emissions from **A** soil/sediment and **B** water samples with N being the amount of total available data points from 87 soil/sediment and 27 water sample, respectively.

Not only chlorinated hydrocarbons were quantified but also brominated C1, C2 and C4 hydrocarbons (Figure 95).

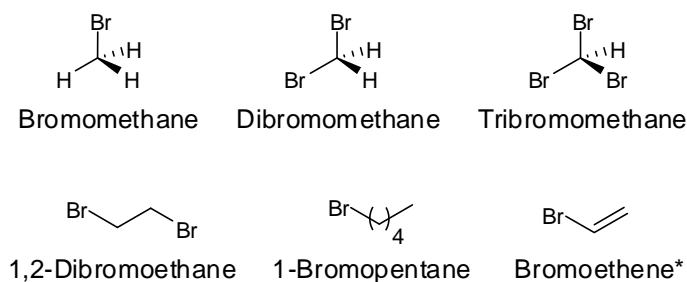


Figure 95. Brominated hydrocarbons found in various samples.

Only tribromomethane was found with higher frequency in several samples while bromomethane was found in 3 and dibromomethane in only 2 soil/sediment samples, respectively (Figure 96). Not quantified were bromoethene found in one water sample, 1,2-dibromoethane in 2 water samples and 1-bromopentane in 4 soil/sediment samples, respectively.

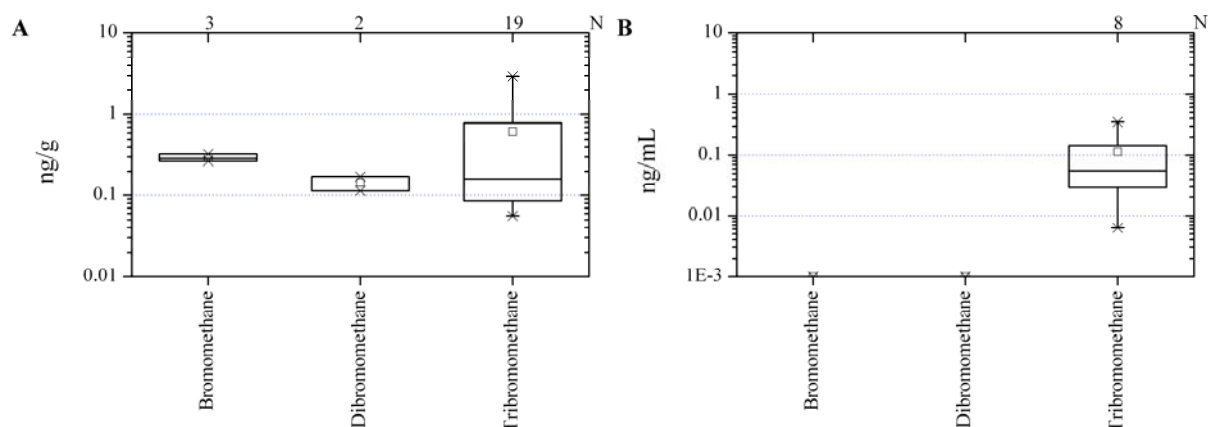


Figure 96. Brominated hydrocarbon emissions from **A** soil/sediment and **B** water samples with N being the amount of total available data points from 87 soil/sediment and 27 water sample, respectively.

Furthermore, some iodinated compounds analogous to chlorinated alkanes were found and quantified (Figure 97). Only for 2-iodopropane no homologous chlorinated or brominated compound was observed.

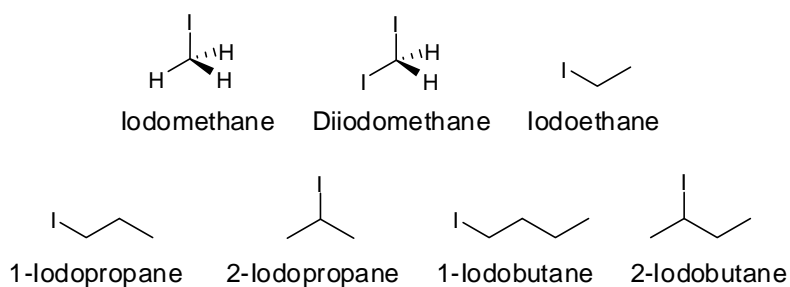


Figure 97. Iodinated alkanes found in various samples.

Like the brominated compounds, iodinated hydrocarbon concentrations and abundances were low in all samples (Figure 98).

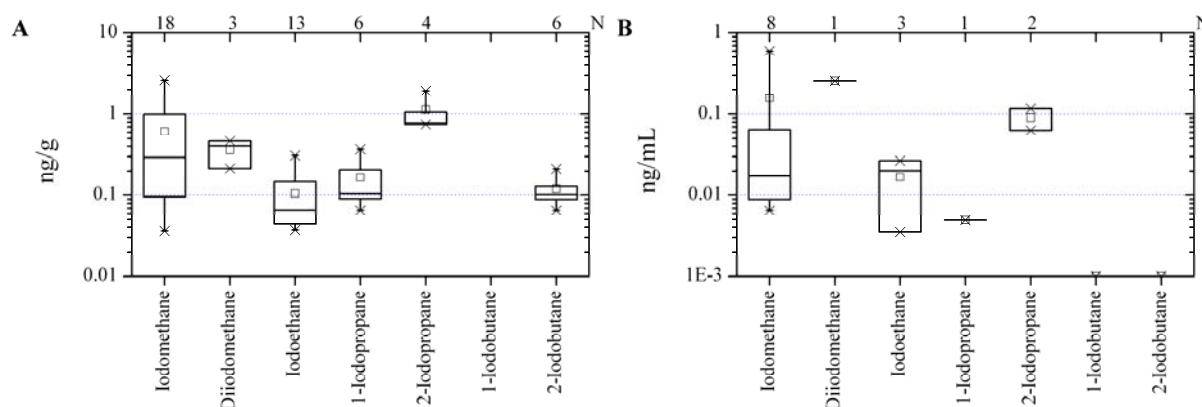


Figure 98. Iodinated alkane emissions from **A** soil/sediment and **B** water samples with N being the amount of total available data points from 87 soil/sediment and 27 water samples, respectively.

Abundance of C3 and C4 chlorinated and iodinated compounds suggested the presence of analogous brominated species. However, unspecific mass fragmentation with subdued bromine isotope pattern overlaid by other volatile compounds restricted the unambiguous identification of brominated species.

Nevertheless, several mixed halogenated compounds were identified (Figure 99), first of all halogenated methane species. Mixed brominated and chlorinated methanes were quantified and the abundance of mixed chlorinated and iodinated methanes is postulated based on mass spectra. Additionally, mixed halogenated ethanes and propanes were postulated.

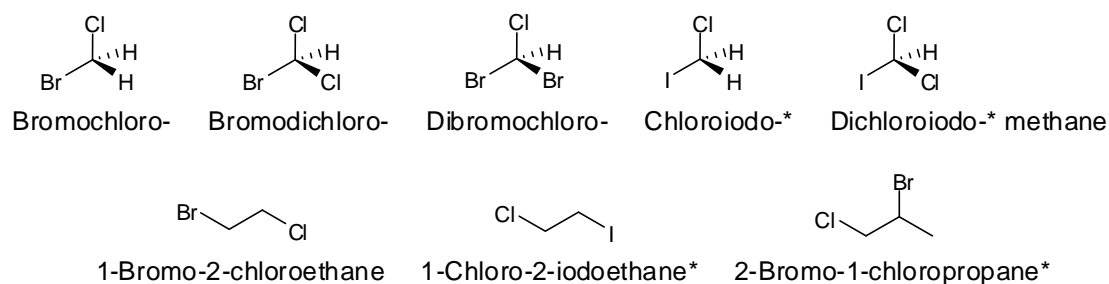


Figure 99. Mixed halogenated alkanes found in various samples. Postulated compounds are marked with an asterisk.

The quantified mixed halogenated methanes were found with low concentrations, but overall moderate frequency in soil/sediment samples and even in a few water samples (Figure 100).

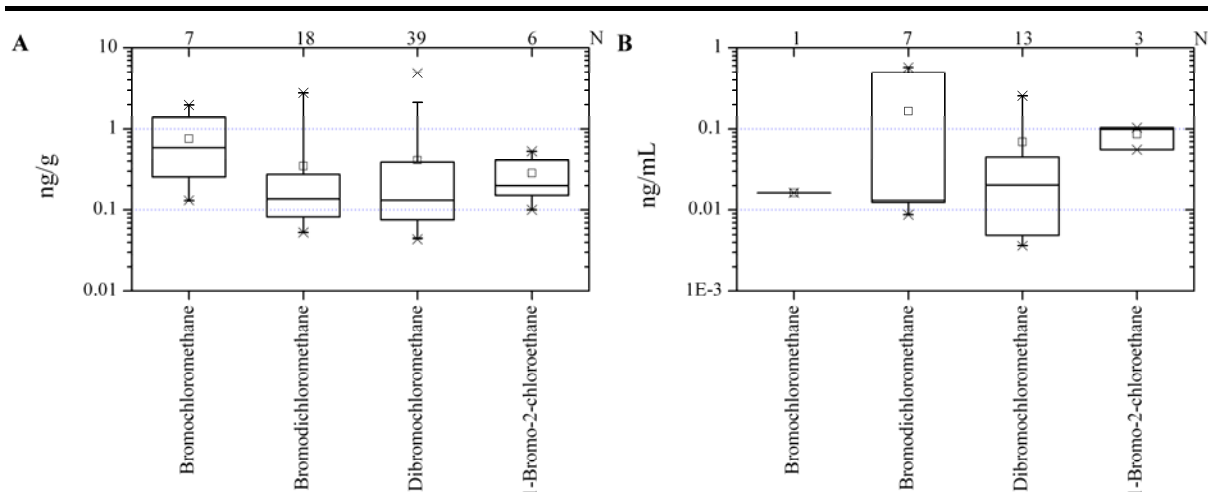


Figure 100. Mixed halogenated methane emissions from **A** soil/sediment and **B** water samples with N being the amount of total available data points from 87 soil/sediment and 27 water samples, respectively.

Monoterpenes, VSC and several VOX were released with high frequency and concentrations from various Australian as well as Dead Sea soil/sediment and water samples. A more detailed analysis of the interplay between geochemical parameters and the emission of selected volatile compounds to unravel their origin will be given in Chapters 10.2 to 10.11.

10.2 Aromatic hydrocarbons

As illustrated in Chapter 10.1 BTEX only made up for a small weight portion of the volatile compounds found in the Australian salt lake sediments. As known anthropogenic substances BTEX are expected to be found in elevated concentrations near major roads or at salt lakes that were abused as dumpsites in the otherwise remote Australian Wheatbelt. Such lakes would be Lake King, which is intersected by State Highway 107, while Lake Dune and Lake Newton were abused for waste disposal. While on the shore of Lake Dune only several unidentifiable rusted metal canisters were deposited, probably used for fuel or pesticides, the dumpsite at Lake Newton was larger containing various debris including rusted canisters and car batteries (Figure 101).



Figure 101. Waste disposal sites at L. Dune (left) and L. Newton (right). Images: T. Krause CC BY-SA 4.0.

Regardless of these possible contamination sources, BTEX emissions from the respective sediments were not elevated compared to other sites as illustrated by Figure 40, Figure 44 and Figure 53 in Chapter 7. BTEX emissions released from Sodom samples in Israel were even unexpectedly low considering the nearby Dead Sea Works industrial complex.

Benzene emission plotted against the soil and sediment pH in Figure 102A shows the before mentioned distribution at the different sampling sites. While there is no correlation between benzene emission and pH there is an obvious correlation with iron and organic carbon content in sediments (Figure 102B and C). Considering benzene to be mostly of anthropogenic origin a correlation with both geochemical parameters is surprising.

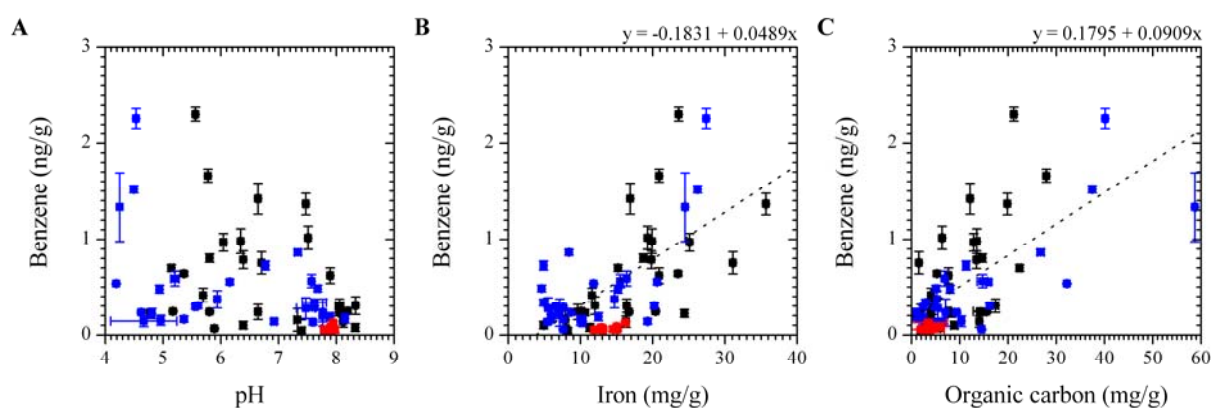


Figure 102. Comparison of **A** pH, **B** iron content and **C** organic carbon content and benzene emissions from soil and sediment samples. ■ Australia 2011 ■ Australia 2012 ■ Israel 2012.

A sole anthropogenic source for the high BTEX concentrations in Australian samples is questionable when comparing the abundance of toluene, ethylbenzene and xylenes with the sediment iron content. In all these cases the emissions clearly increased with higher iron concentrations (Figure 103).

One source for BTEX in the lakes could be iron catalysed decarboxylation of various aromatic acids. Degradation of benzoic acid to benzene in a mixture of Cu^{2+} or Fe^{3+} with ascorbic acid is of relevance in common food chemistry. The hypothesised reaction pathway starts with the reduction of the metals by ascorbic acid with subsequent autoxidation (see Chapter 2.1.1) initiating Fenton chemistry and radical induced decarboxylation of the benzoic acid (Gardner and Lawrence, 1993). Iron reducing conditions of Australian salt lake sediments were determined by redox milieu studies as presented in Chapter 9.3. Moreover, the abundance of Fe^{2+} as iron sulfides or as dissolved iron species was verified by on-site measurements. Oxygen for autoxidation was also available in natural samples (Chapter 9.3)

and in laboratory experiments. Additionally, several aromatic acids are naturally produced by plants, e.g. gallic acid and p-hydroxybenzoic acid were found in different eucalyptus species (Sivagurunathan et al., 1997; Chapuis-Lardy et al., 2002). By way of plant litter these compounds are transported into the salt lakes, where they could undergo radical decarboxylation to benzene derivatives. Furthermore, direct emissions from plants indicate a biosynthetic formation pathway for toluene (Heiden et al., 1999).

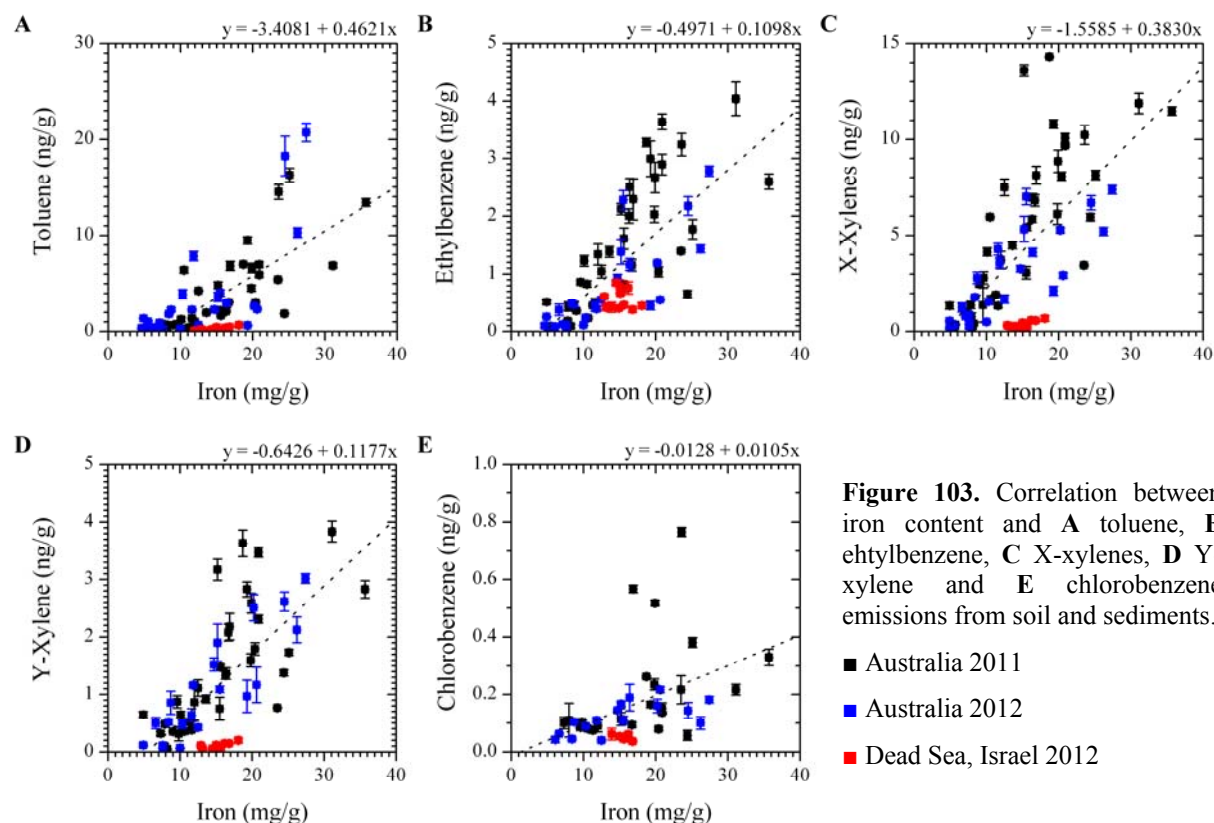


Figure 103. Correlation between iron content and **A** toluene, **B** ethylbenzene, **C** X-xylenes, **D** Y-xylene and **E** chlorobenzene emissions from soil and sediments.

■ Australia 2011
 ■ Australia 2012
 ■ Dead Sea, Israel 2012

Natural formation of chlorobenzoic acid (Niedan and Schöler, 1997) and subsequent degradation, as described above, could be a source for the observed chlorobenzene. However, chlorobenzene is also a known pollutant (ATSDR, 2000) and the low observed concentrations with little variation could also point to background contamination.

The water samples draw a different picture (Appendix E). BTEX concentrations in Australian samples were low, mostly even below the detection limit of 0.005 ng/mL. In contrast, the water samples from the Dead Sea and especially the groundwater samples from the Sodom site, collected at 45-85 cm depth, contained not only elevated BTEX concentrations but also further benzene derivatives illustrated in Figure 83, like styrene and higher alkylated benzene derivatives. The BTEX concentrations of groundwater samples point to anthropogenic contamination of the area.

Additionally to BTEX releases from Australian sediment and water samples, these compounds were measured in air samples collected over Australian salt lakes. Average, though extrapolated mixing ratios for benzene and toluene over Australian salt lakes were 55 pptv and 54 pptv, respectively (Sattler, 2012). These concentration are in the range for remote areas (Nutmagul and Cronn, 1985). However, air samples from the PTFE chamber in 2012 were greatly enriched with toluene. In these samples toluene concentration ranged between 646 to 1727 pptv (Sattler, 2012).

10.3 Isoprene and terpenes

Isoprene and monoterpenes are of higher atmospheric relevance in remote regions than BTEX and furans. Especially, monoterpenes were found in high concentrations in Australian samples where native vegetation, mostly eucalyptus species, is known for their production (Barton et al., 1989).

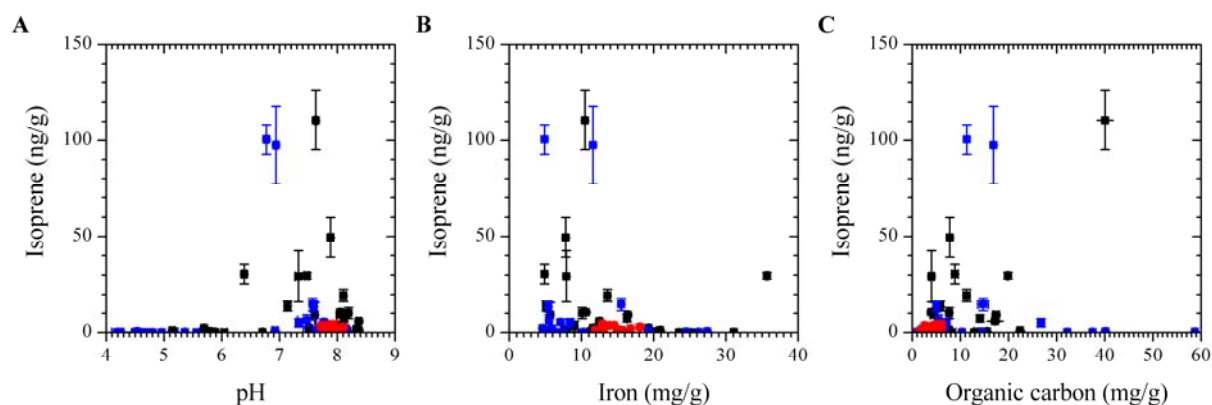
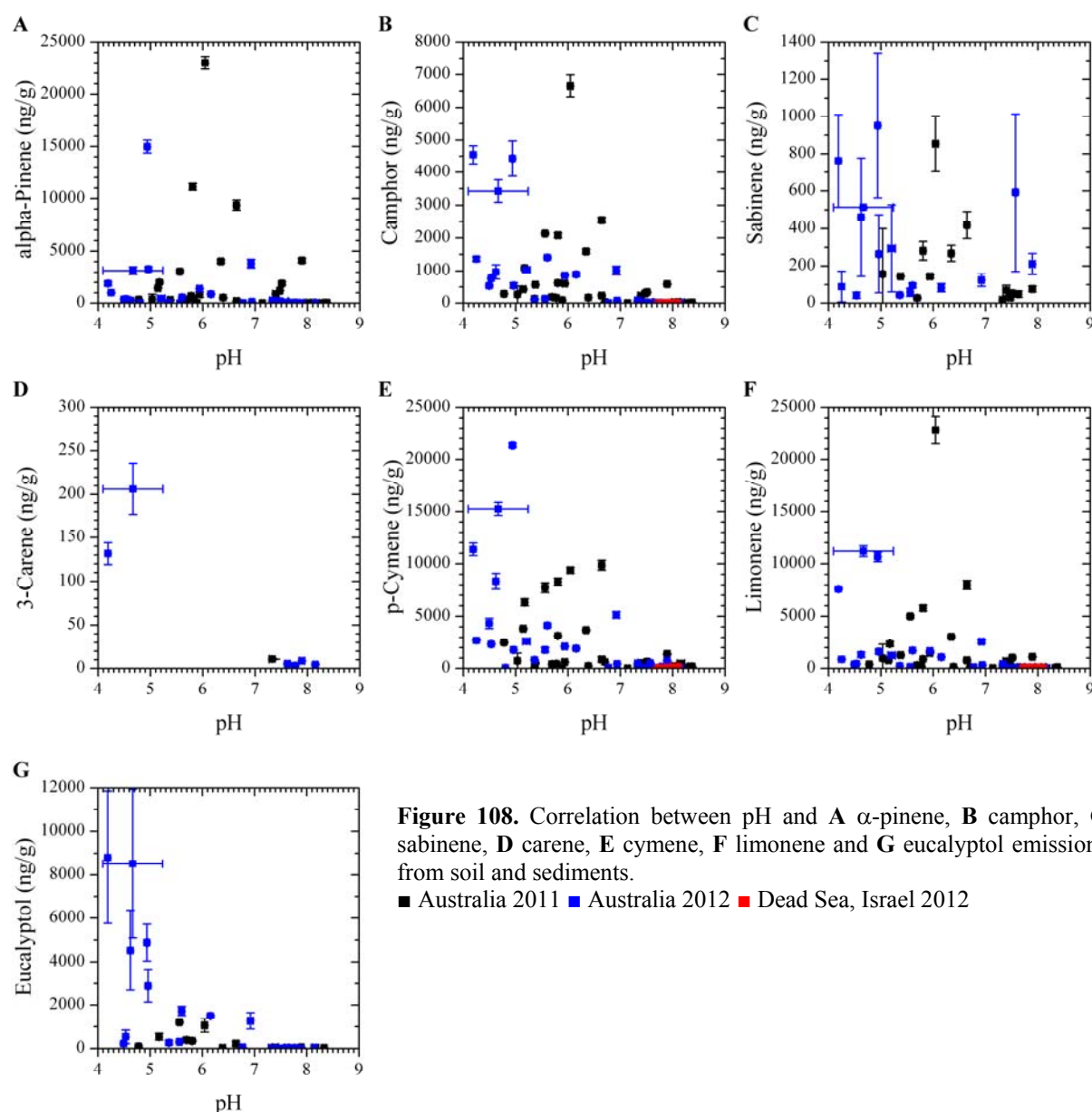


Figure 104. Comparison of **A** pH, **B** iron and **C** organic carbon content with isoprene emissions from soil and sediments. ■ Australia 2011 ■ Australia 2012 ■ Dead Sea, Israel 2012

Isoprene was primarily found at high concentrations in Australian sediment samples, most of all in samples with a high pH and low iron content (Figure 104).

The correlation of isoprene emission with the pH is also evident in the collected water samples as shown in Figure 105.

Further biosynthetic products derived from isoprene units are monoterpenes. Though, with boiling points above 150 °C it must be assumed that releases of monoterpenes from soil/sediment samples were mostly residues not extracted by the freeze-drying process. Nevertheless, there was a slight correlation between the emissions of some monoterpenes and the soil/sediment pH. While α -pinene, sabinene and limonene concentrations were independent of the matrix pH, camphor, 3-carene, p-cymene and eucalyptol concentrations increased under acidic conditions (Figure 108) contrary to the observed isoprene emissions.



An explanation for the elevated monoterpene concentrations under acidic conditions is the close proximity of eucalyptus trees to the mostly small acidic salt lakes, whereas less acidic to alkaline lakes have a more spacious shore with mostly *Salicornia* vegetation. Furthermore,

eucalyptus leaf litter was observed on the shores of several acidic lakes forming large mats (Figure 109).



Figure 109. PTFE chamber on plant litter at lake Dune in 2013 (left) and plant litter on the shore of Lake Holt Rock in 2011 (right). Image: T. Krause CC BY-SA 4.0.

While isoprene and its precursors are probably produced steadily by the observed microorganisms in circumneutral lakes, its main visible source is plant litter in acidic lakes. Low isoprene release rates from acidic lakes can be explained by its volatile nature. The isoprene depot in acidic lakes would decline over time unless new plant litter is transported into the lakes, whereas low volatile monoterpenes in detritus are sedimented into the lakes.

Table 10. Emission data for isoprene/monoterpenes from water samples.

Sampling sites	pH	Isoprene (ng/mL)	α -Pinene (ng/mL)	Camphor (ng/mL)	3-Carene (ng/mL)	Sabinene (ng/mL)	p-Cymene (ng/mL)	Limonene (ng/mL)	Eucalyptol (ng/mL)
Stennets Lake 2012	8.7	0.036	0.421	-	-	-	-	-	-
L. Strawbridge 2012	7.4	0.018	0.457	-	-	-	-	-	-
L. Hatter Hill 2011	7.2	0.013	-	-	-	0.321	0.603	0.437	-
L. Strawbridge 2011	7.1	0.029	-	-	-	-	0.779	-	-
L. Newton 2012	6.3	0.016	0.842	-	-	-	-	-	-
L. Emu 2012	5.7	0.006	-	-	-	-	-	-	-
L. Golf 2011	5.1	0.011	-	-	-	2.165	-	-	-
L. Boats GW 2012	3.6	-	-	-	-	-	2.200	-	-
L. Springfield 2011	3.4	0.004	-	0.080	-	-	-	0.520	-
Hyden Pool 2011	3.3	0.006	-	-	-	-	-	0.159	-
L. Whurr 2012	3.1	0.006	-	-	-	-	-	5.616	-
L. Orr 2011	3.1	0.006	-	0.913	-	-	2.037	-	-
L. Orr 2012	3.1	-	-	-	-	-	-	2.629	-
L. Boats Inlet 2012	3.0	0.014	-	0.810	-	-	0.778	-	-
L. Dune 2011	2.6	0.006	-	0.300	-	-	-	-	-
L. Boats 2012	2.4	0.008	-	0.611	-	-	-	-	-
Sodom 1	6.5	0.008	0.635	-	-	-	0.243	0.725	-
Sodom 2	6.5	0.008	0.414	-	-	-	0.224	1.001	-
Sodom Plant	6.5	0.008	0.231	-	-	-	0.632	0.381	-
En Bokek	6.0	0.010	0.390	-	-	-	-	-	-
En Gedi	6.0	0.008	-	-	-	-	0.111	-	-
South End 2	5.1	0.004	-	-	-	-	0.109	-	-

While water samples verified the release of most monoterpenes from the hypersaline environments, they were less frequently measured and unspecific with regard to geochemical parameters. Exception were 3-carene and eucalyptol which were not observed in any water samples (Table 10).

In 2012, the extrapolated isoprene concentrations from collected air samples ranged between 263 to 382 pptv for the acidic Lake Orr, Lake Dune and Lake Whurr (pH ~3.5). Elevated concentrations of 396 to 475 pptv were found above the circumneutral Lake Newton (pH 6.2) and Lake Strawbridge (pH 7.3) (Sattler, 2012). Highest concentration of 501 pptv (Sattler, 2012) were measured above Lake Emu, which was slightly acidic at that time (pH 5.6) but otherwise showed characteristics of a circumneutral lake.

Furthermore, isoprene mixing ratios were measured beyond the state barrier fence in the Frank Hahn National Park, where native vegetation is still undisturbed and the air nearly devoid of fine particles (Junkermann et al., 2009). Beyond the fence isoprene concentrations of around 822 pptv were found (Sattler, 2012), which is about twice as much as the mean concentration over the salt lakes (Figure 110).

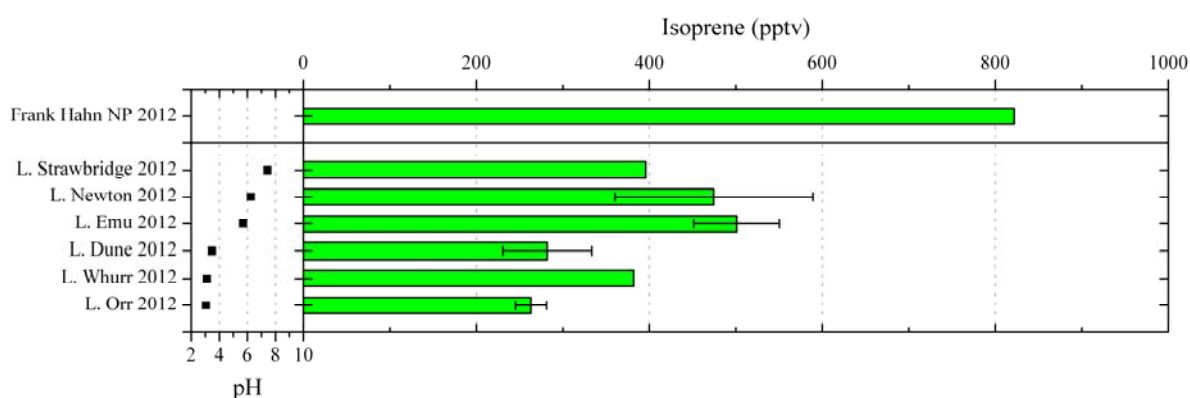


Figure 110. Atmospheric mixing ratios of isoprene over different Australian salt lakes and within the Frank Hahn National Park (NP).

The question arises whether isoprene release rates are less pronounced from salt lakes and adjacent environments compared to native vegetation or whether salt lakes play a significant role as an isoprene sink. In favour of the first assumption is that the air samples were collected after harvest. As a result adjacent fields around the salt lakes were fallow with no significant vegetation as an isoprene source. Another explanation, as outlined in Chapter 12, is the postulated depletion of isoprene by reactions with RHS released from salt lakes.

Isoprene degradation by OH radicals will be also elucidated in Chapter 10.4 as it plays a minor role in atmospheric 3-methylfuran formation.

10.4 Furans

In most soil/sediment and water samples furan and methylfurans and to a lesser extent dimethylfurans were found. Furthermore, the emissions of 2-alkyl furans with ethyl to pentyl moieties as well as three halogenated furan compounds are worth mentioning. An overview of all observed furan species is given in Figure 87.

Compared to geochemical parameters, furan emissions from Australian and Sodom soil/sediment samples correlated with pH, iron and organic carbon content. As such furan emissions increased with higher iron and organic carbon concentrations and at higher acidity of the samples (Figure 111). A similar picture for furan emission can be drawn from water samples (Figure 112). Considering the complicated matrix of natural samples, these correlations are in good agreement with the presented model reactions in Chapter 6 and the literature (Huber et al., 2010; Krause et al., 2013).

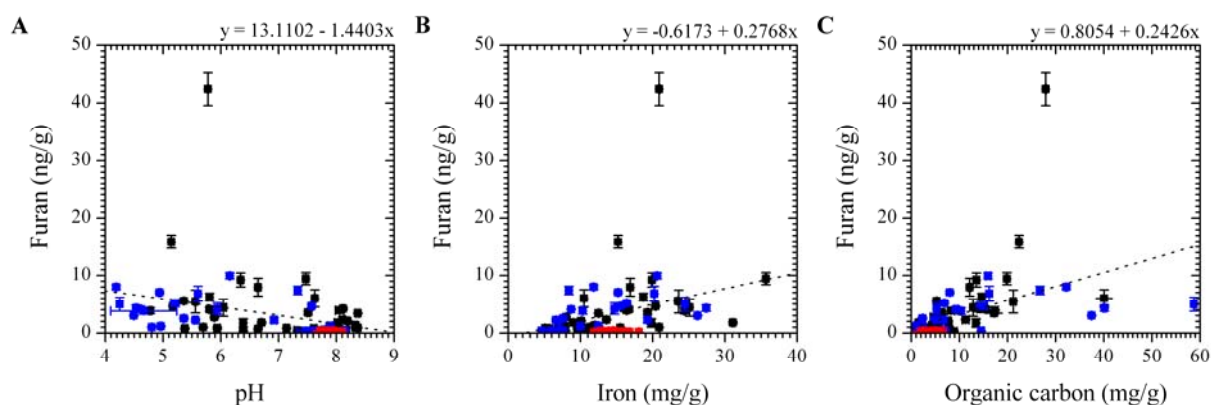


Figure 111. Correlation between furan emission and **A** pH, **B** iron as well as **C** organic carbon concentrations from soil and sediment samples. ■ Australia 2011 ■ Australia 2012 ■ Dead Sea, Israel 2012

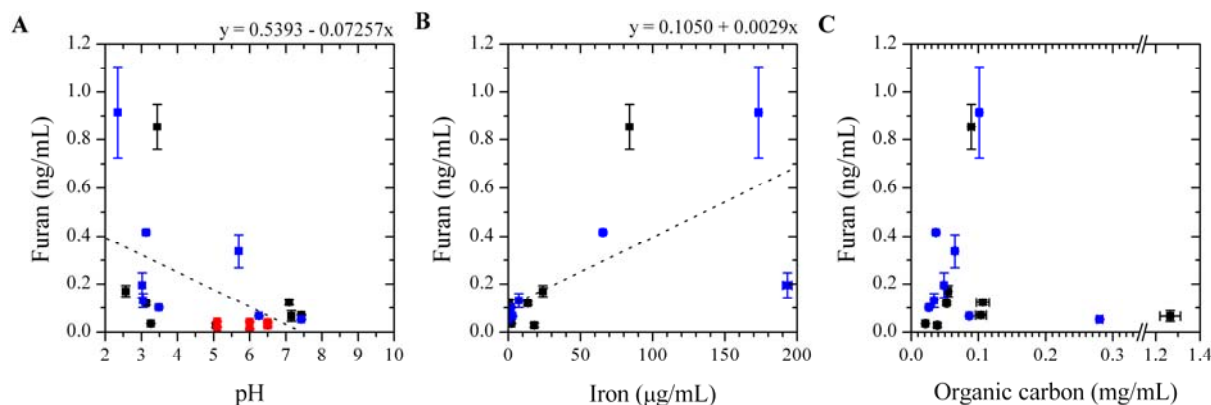


Figure 112. Comparison of **A** pH, **B** iron and **C** organic carbon concentrations with furan emissions from water samples. ■ Australia 2011 ■ Australia 2012 ■ Dead Sea, Israel 2012

Connections between geochemical parameters and the release of other furanoic compounds were less pronounced, especially in water samples. Methylfuran emissions from Australian sediments, most notably from 2011, increased with higher organic carbon concentrations (Figure 114A and B). Albeit, low methylfuran concentrations were measured for samples with an organic carbon concentration > 35 mg/g collected from the salty claypan near Lake Boats in 2012 (Figure 113).



Figure 113. Claypan near Lake Boats, photographed in 2012. Image: T. Krause CC BY-SA 4.0.

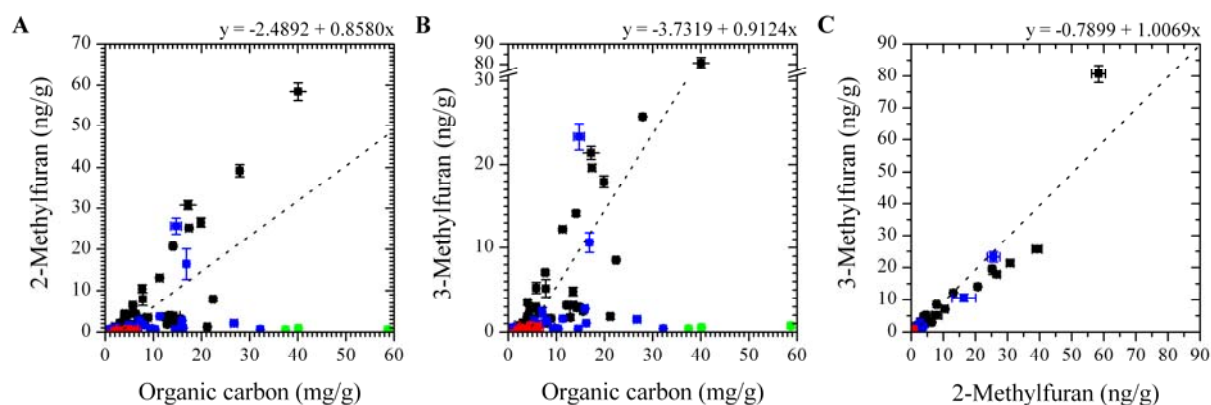


Figure 114. Correlation between organic carbon content and emissions of **A** 2-methylfuran and **B** 3-methylfuran from soil/sediment samples. Lake Boats Claypan samples (organic carbon > 35 mg/g), highlighted green, are excluded from linear regression fittings. **C** Correlation between 2- and 3-methylfuran emissions.

■ Australia 2011 ■ Australia 2012 ■ Dead Sea, Israel 2012

As shown in Figure 114C 2- and 3-methylfuran emissions are nearly equivalent and correlated significantly indicating a mutual precursor and related reaction pathways. One possible precursor for both methylfurans under Fenton-like conditions is 3-methylphenol (Huber et al., 2010).

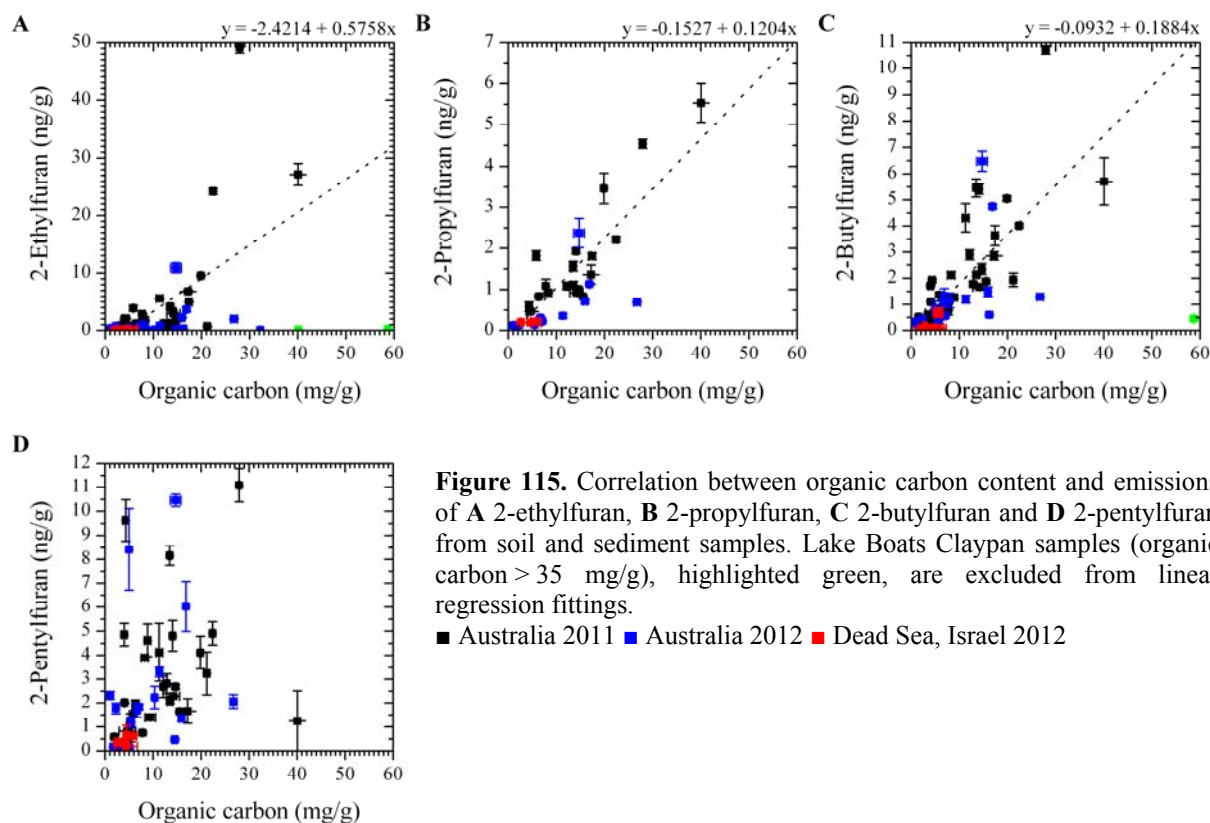


Figure 115. Correlation between organic carbon content and emissions of **A** 2-ethylfuran, **B** 2-propylfuran, **C** 2-butylfuran and **D** 2-pentylfuran from soil and sediment samples. Lake Boats Claypan samples (organic carbon > 35 mg/g), highlighted green, are excluded from linear regression fittings.

■ Australia 2011 ■ Australia 2012 ■ Dead Sea, Israel 2012

Furthermore, the formation process of methylfuran and furans with longer alkyl chain must differ significantly as only 2-substituted alkylfurans were found. 2-Propylfuran and 2-butylfuran emissions notably increased with the organic carbon content of the sediments, whereas a pattern for 2-ethylfuran and 2-pentylfuran was less pronounced (Figure 115). An exception were low alkylfuran releases from the organic rich Lake Boats Claypan sediment.

A source for 2-alkylfurans is the oxidation of polyunsaturated alkenes, especially fatty acids. In food chemistry omega-6 fatty acids are described as precursors for 2-pentylfuran (Min et al., 2003), likewise common omega-3 fatty acids could be precursors for 2-ethylfuran.

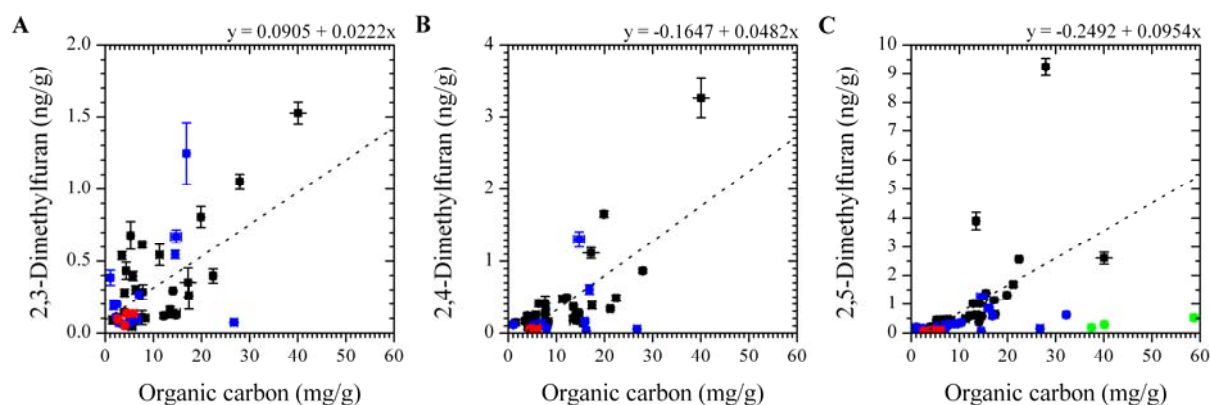


Figure 116. ■ Correlation between organic carbon content and emissions of **A** 2,3-dimethylfuran, **B** 2,4-dimethylfuran and **C** 2,5-dimethylfuran from soil and sediment samples. Lake Boats Claypan samples (organic carbon > 35 mg/g), highlighted green, are excluded from linear regression fittings.

■ Australia 2011 ■ Australia 2012 ■ Dead Sea, Israel 2012

The lowest alkylated furan concentrations were measured for dimethylated furans. Emission of alkylated furans increased more or less with the organic carbon content in soil/sediments (Figure 116).

Table 11. Emission data for furanoic compounds from water samples.

Sampling sites	pH	Furan (ng/mL)	3-Methylfuran (ng/mL)	2-Methylfuran (ng/mL)	2-Ethylfuran (ng/mL)	2-Propylfuran (ng/mL)	2-Butylfuran (ng/mL)	2-Pentylfuran (ng/mL)	2,3-Dimethylfuran (ng/mL)	2,4-Dimethylfuran (ng/mL)	2,5-Dimethylfuran (ng/mL)
Stennets Lake 2012	8.7	-	0.018	0.016	-	-	-	-	-	-	0.004
L. King 2011	7.4	0.070	0.029	0.112	-	-	-	-	-	-	0.005
L. Strawbridge 2012	7.4	0.052	0.830	1.111	0.078	-	0.018	-	0.026	0.081	0.065
L. Stubbs 2011	7.2	-	-	-	-	-	-	-	-	-	-
L. Hatter Hill 2011	7.2	0.066	0.148	0.285	-	-	0.012	-	0.012	0.029	0.024
L. Strawbridge 2011	7.1	0.123	0.355	0.879	0.034	-	0.048	-	0.016	0.027	0.022
L. Newton 2012	6.3	0.066	0.421	0.703	0.044	-	-	-	0.014	0.027	0.030
L. Emu 2012	5.7	0.337	0.047	0.650	0.010	-	-	-	-	0.023	0.014
L. Golf 2011	5.1	0.028	0.008	0.011	-	-	-	-	-	-	0.004
L. Boats GW 2012	3.6	-	0.010	0.007	-	-	-	-	-	-	0.016
L. Dune 2012	3.5	0.101	0.157	0.138	-	-	-	-	-	0.015	0.059
L. Springfield 2011	3.4	0.854	2.306	0.377	0.134	0.041	0.015	0.031	0.034	0.037	0.461
Hyden Pool 2011	3.3	0.035	0.306	-	0.023	0.009	-	-	0.011	0.027	0.071
L. Whurr 2012	3.1	0.417	0.953	0.123	0.056	0.024	0.019	-	0.029	0.022	0.764
L. Orr 2011	3.1	0.118	0.589	0.104	0.034	0.016	0.028	0.046	0.010	0.012	0.042
L. Orr 2012	3.1	0.131	0.382	0.113	-	0.011	-	-	-	0.010	0.096
L. Boats Inlet 2012	3.0	0.194	0.117	0.038	0.009	-	-	-	0.010	0.013	0.173
L. Dune 2011	2.6	0.170	0.312	0.064	0.017	0.008	0.008	-	0.004	0.007	0.062
L. Boats 2012	2.4	0.915	2.879	0.185	0.162	0.031	0.038	-	0.013	0.038	0.536
Sodom 1	6.5	0.040	0.018	0.018	-	-	-	-	-	-	0.004
Sodom 2	6.5	0.027	0.025	0.016	-	-	-	-	-	-	0.007
Sodom Plant	6.5	0.032	0.030	0.013	-	-	0.013	-	0.004	-	0.006
En Bokek	6.0	0.042	0.017	0.013	0.009	-	-	-	-	-	-
En Gedi	6.0	0.013	0.005	-	-	-	-	-	-	-	-
South End 1	5.1	0.043	0.011	0.044	0.024	-	-	-	-	-	-
South End 2	5.1	0.021	0.007	0.006	-	-	-	-	-	-	-

Water samples confirmed the natural abundance of the furanoic compounds released from salt lake sediments, though correlations with pH, dissolved iron and organic carbon content are ambiguous (Table 11). Furthermore, the before mentioned nearly equivalent release of 2- and 3-methylfurans from soil/sediments was not found in the water samples.

Aside from polyunsaturated alkenes there are other sources for furanoic compounds. For example, catechol is abiotically degraded by Fenton (Krause et al., 2013) (Chapter 6.1) and Fenton-like reactions (Huber et al., 2010) to furan. Furthermore, methylated phenols and catechol derivatives yield methylated furans under Fenton-like conditions (Huber et al.,

2010). Degradation of 4-ethylcatechol, the only commercially available ethylcatechol derivative, lead to 3-ethylfuran formation under Fenton-like conditions (Krause et al., 2013) (Chapter 6.2). According to experiments with methylcatechols by Huber et al. (2010) 3-ethylcatechol would yield natural occurring 2-ethylfuran under Fenton-like conditions.

While the abundance of catechol and phenolic derivatives in the salt lakes has not been investigated to this date, other phenyl compounds, namely BTEX, were quantified. In atmospheric chemistry involving OH radicals benzene is a known precursor for furan (Berndt and Boge, 2001) and toluene for 2-methylfuran (Shepson et al., 1984). Likewise, ethylbenzene could be a precursor for 2-ethylfuran. Plotting the benzene emissions from sediments and soils against the respective furan emissions indeed shows a correlation (Figure 117A), whereas a connection between 2-methylfuran and toluene emissions is questionable (Figure 117B). Furthermore, there is no correlation between ethylbenzene and 2-methylfuran emissions (Figure 117C).

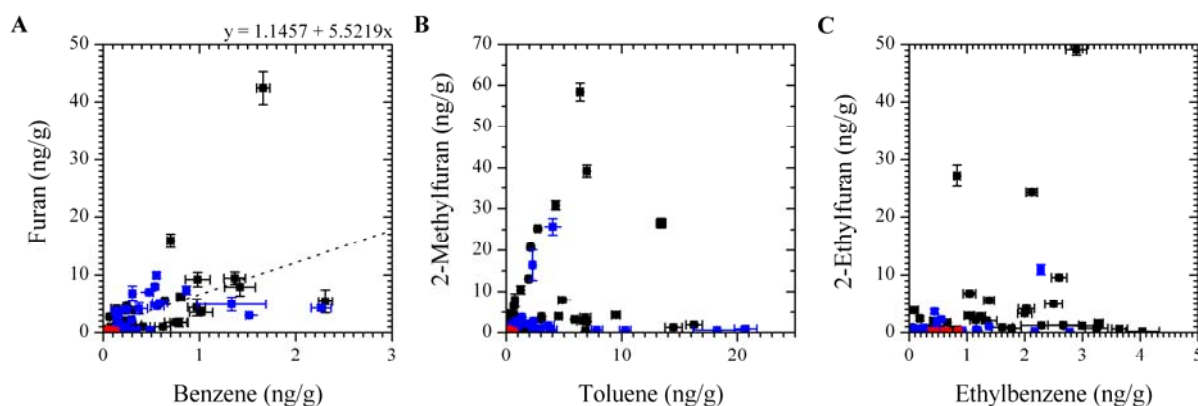


Figure 117. A Correlation between furan and benzene emissions as well as comparison of B 2-methylfuran and toluene and C 2-ethylfuran and ethylbenzene emissions from various soil and sediment samples. ■ Australia 2011 ■ Australia 2012 ■ Dead Sea, Israel 2012

The reaction of isoprene with OH radicals is an atmospheric formation pathway of 3-methylfuran (Atkinson et al., 1989b). While isoprene was found in most soil and sediment samples (see Chapter 10.1) there is no obvious correlation with the abundance of 3-methylfuran (Figure 118).

With a postulated mutual precursor for 2- and 3-methylfuran it is not surprising that neither toluene nor isoprene concentrations correlated with the respective methylfuran releases.

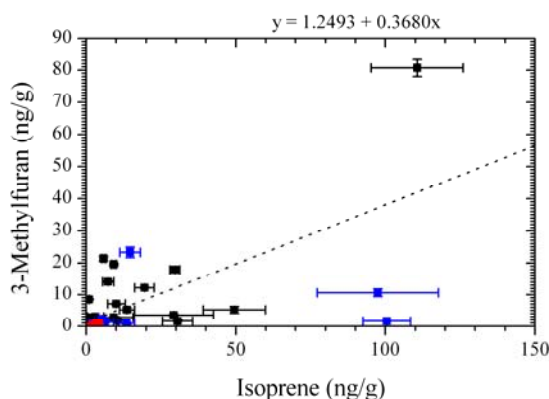


Figure 118. Comparison of 3-methylfuran and isoprene emissions from soil and sediment samples.

■ Australia 2011 ■ Australia 2012 ■ Dead Sea, Israel 2012

Atmospheric mixing ratios of furan were determined with about 100 to 200 ppbtv in 2011 and 2012 (Sattler, 2012). Furthermore, 2- and 3-methylfuran were measured in the air samples. In 2011, 2-methylfuran concentrations were higher than those of 3-methylfuran and vice versa in 2012. This finding stands in contrast to the observed equivalent 2- and 3-methylfuran emissions from sediments (Figure 114C) pointing to additional sources or sinks. Overall methylfuran concentrations were between 45 and 239 pptv for each compound (Sattler, 2012).

Aside from furan and alkylated derivatives 2 halogenated furan compounds were identified in natural soil/sediment and water samples for the first time. A third halogenated furan species is also assumed to be abundant based on obtained mass spectra.

Traces of 3-chlorofuran and of its homologue 3-bromofuran were found in Australian water samples, while 3-chlorofuran was also found in three Australian sediment samples (Table 12 and Table 13).

Table 12. Halofurans in water samples.

Sampling sites	pH	3-Chlorofuran	3-Bromofuran	X-Chloro-Y-methylfuran
		(ng/mL)	(ng/mL)	(counts/mL)
L. Dune 2012	3.5	0.017	0.015	25
L. Whurr 2012	3.1	0.009	-	-
L. Orr 2012	3.1	0.032	0.020	-
L. Boats 2012	2.4	0.348	0.032	157

Table 13. Halofurans released from sediments.

Sampling sites	Layer	3-Chlorofuran	3-Bromofuran	X-Chloro-Y-methylfuran
		(cm)	(ng/g)	(ng/g)
L. Springfield 2011	0-2	0.25	-	-
L. Springfield 2011	2-4	0.13	-	-
L. Whurr 2011	>7	0.37	-	325
L. Strawbridge 2012	0-4	-	-	825

In literature only 3-bromofuran is known to occur naturally as it is emitted from onion bulbs incubated with the *Pectobacterium carotovorum* (Prithiviraj et al., 2004). So far, no natural sources of 3-chlorofuran are known, but Huber et al. (2010) demonstrated its formation from 4-chlorocatechol, 2,4-dichlorocatechol and 4-chlorophenol under Fenton-like conditions.

Traces of another halogenated compound were found in water and sediment samples alike. The mass spectra of the substance from Lake Boats is shown in Figure 119. The NIST library mainlib proposes 3-chlorocyclopent-2-en-1-one with a probability of 70%. While none halogenated cyclopentenone has a boiling point of 150 °C, the retention time of the unidentified chlorinated compound was less than toluene with a boiling point of 111 °C. More likely is a chlorinated methylfuran, which is a structural isomer of the proposed compound, but is not listed in the mainlib or replib database. Aside from the 51 m/z peak all other major peaks and chlorine isotope patterns can be described by the fragmentation of a chlorinated methylfuran. The here presented fragmentation patterns (Figure 119) are based on experiments with furan by Al-Kagali et al. (2008).

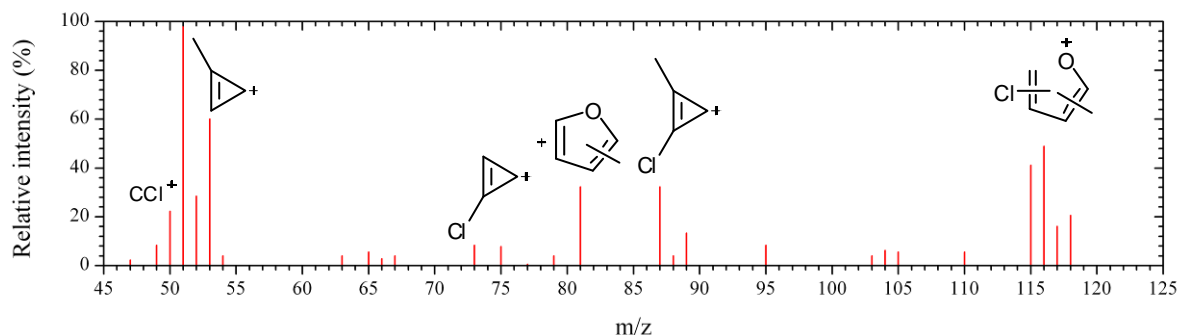


Figure 119. Mass spectrum from an unknown substance obtained from a water sample of Lake Boats, 2012. Suggested fragmentation points to a chlorinated methylfuran.

10.5 Volatile sulfur and selenide compounds

A diverse set of sulfur and selenide compounds was identified by GC-MS measurements in Australian and Israeli samples. The abundance of volatile sulfur compounds in the Australian samples is not surprising considering suboxic to anoxic conditions in the sediments and the presence of reduced sulfur minerals (Chapter 9.3).

With regard to the simple sulfur compounds carbon disulfide, dimethyl sulfide and dimethyl disulfide elevated concentrations were released from several Australian sediment samples, foremost with a neutral to alkaline pH (Figure 121). This observation is consistent with the hypothesis elucidated for isoprene where emissions were linked to microorganism activity such as *Halobacterium* and the algae *Dunaliella salina*. Furthermore, some of the highest concentrations were found in the circumneutral Lake Hatter Hill in 2011. This salt playa is noteworthy as it underwent a significant change to a brackish water lake after sampling in 2011 (Figure 120). The water remained long enough to support growth of aquatic plants and microorganisms as observed in 2012 and 2013.



Figure 120. Lake Hatter Hill in 2011 (top) and after heavy rain events in 2012 (left). Plant residues in the sediment of Lake Hatter Hill in 2011 (right). Images: T. Krause CC BY-SA 4.0.

Plant residues in the sediment found in 2011 indicate that these changes have happened before and might occur periodically. Such evidences for brackish water stages were found at several circumneutral lakes and this observation is in consistency with information from

contemporary witnesses. This is important with regard to volatile sulfur emissions as plants like all organisms produce sulfur containing amino acids. When the lakes dry up and dissolved chloride concentrations increase again, most of these organisms die and abiotic and biogenic degradation of their organic residues lead to the release of volatile sulfur compounds (Watts, 2000).

Furthermore, sulfate-reducing bacteria are likely abundant in the anoxic sediment zones of the salt lakes (Foti et al., 2007).

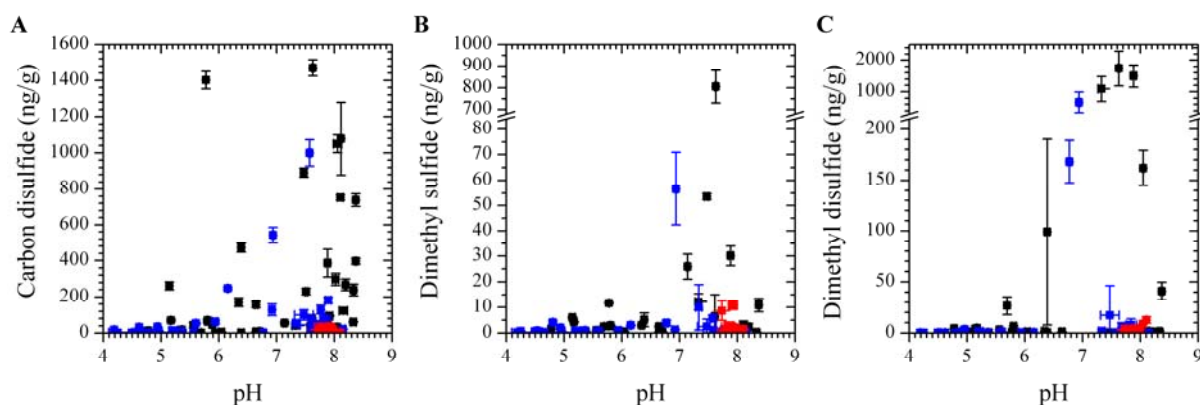


Figure 121. Correlation between pH and emissions of **A** carbon disulfide, **B** dimethyl sulfide and **C** dimethyl disulfide from soil and sediments. ■ Australia 2011 ■ Australia 2012 ■ Dead Sea, Israel 2012

Not only high concentrations of the above mentioned compounds were found in the samples of Lake Hatter Hill, but also higher alkylated disulfides and dimethyl trisulfide as suggested by the NIST databases.

The proposed pH dependency of carbon disulfide release from Australian sediment samples is supported mostly by air samples, whereas no trend for dimethyl sulfide was observed (Sattler, 2012). Additionally, carbonyl sulfide (OCS) was measured in the air samples, which is the degradation product of carbon disulfide in reaction with OH radicals (Hynes et al., 1988).

Normally, OCS is nearly equally distributed over the southern hemisphere with average concentrations of 460 pptv. However, concentrations measured during the Australian campaigns in 2011 and 2012 were almost twice as high. Furthermore, compared to background measurements in the Frank Hahn National Park, OCS was measured at slightly higher concentrations above some acidic lakes pointing to a local source. Moreover, atmospheric mixing ratios of carbon disulfide, a potential precursor for OCS (Hynes et al., 1988), were significantly elevated above several lakes, though mostly above circumneutral lakes. Dimethyl sulfide mixing ratios were slightly lower above the salt lakes compared to

native vegetation background and were almost distributed evenly. The mixing ratios for the three substances are depicted in Figure 122.

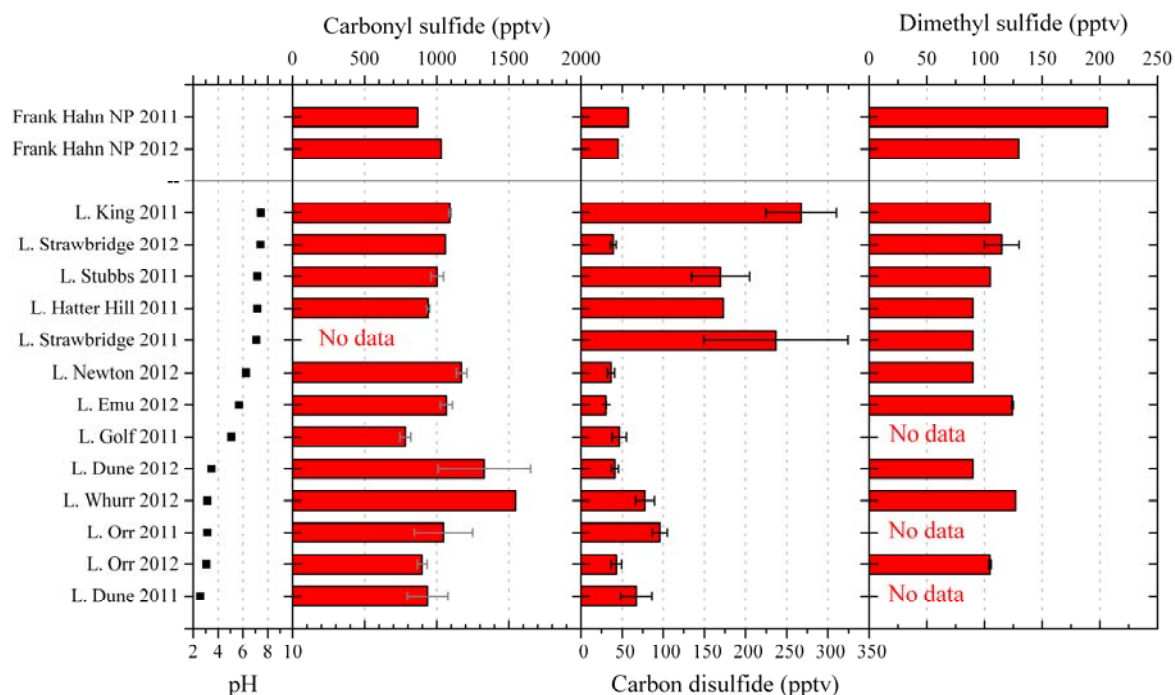


Figure 122. Atmospheric mixing ratios for carbonyl sulfide, carbon disulfide and dimethyl sulfide above Western Australian salt lakes and within the Frank Hahn National Park (Sattler, 2012).

Closely related to dimethyl sulfide and dimethyl disulfide are dimethyl selenide, dimethyl selenenyl sulfide and dimethyl diselenide. These compounds were ubiquitous in soil samples from the Sodom site and also in a few sediment samples from Australia. While selenide competes with sulfide in biosynthesis it is mostly toxic for organisms (Stadtman, 1996). Noticeably for the few Sodom samples is that there is no correlation between selenide compound emissions and respective sulfide compounds (Figure 123). In case of dimethyl selenenyl sulfide quantification was not possible because a standard was not available.

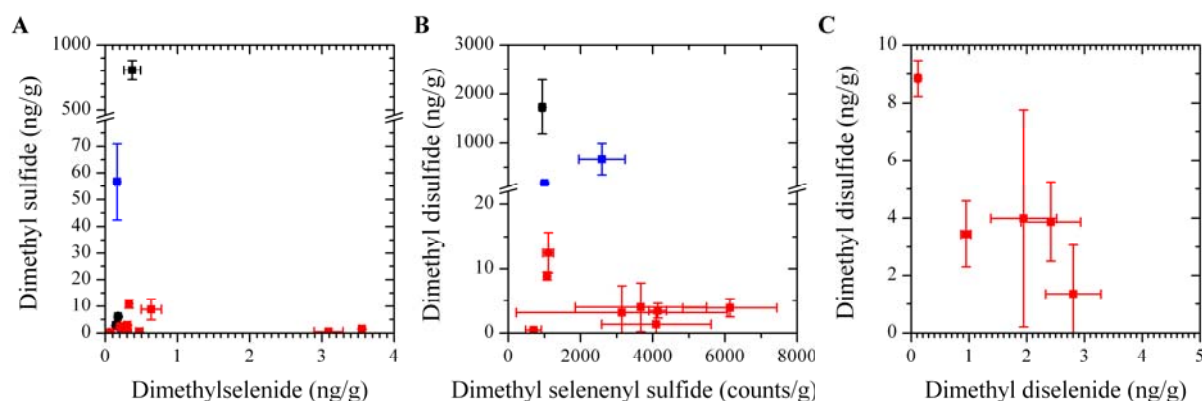


Figure 123. Comparison of **A** dimethyl sulfide and dimethylselenide, **B** dimethyl disulfide and dimethyl selenenyl as well as **C** dimethyl diselenide emissions from soil and sediments. ■ Australia 2011 ■ Australia 2012 ■ Dead Sea, Israel 2012

Emission of methylated selenides could be connected to selenate-respiring microorganisms found in Dead Sea sediments (Switzer Blum et al., 2001).

Furthermore, several thiophene compounds were found in Australian sediment samples and at least methylthiophenes in small quantities at the Sodom site. As shown in Figure 124, emissions correlate with organic carbon content but neither with pH nor iron concentrations of the soils/sediments (not shown).

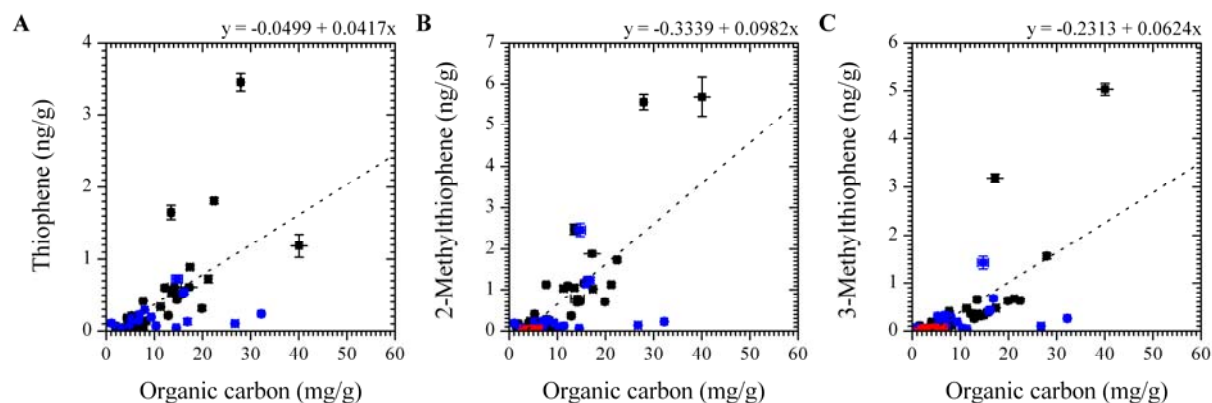


Figure 124. Correlation between organic carbon content with emissions of **A** thiophene, **B** 2-methylthiophene and **C** 3-methylthiophene from soil and sediments. ■ Australia 2011 ■ Australia 2012 ■ Dead Sea, Israel 2012

Furthermore, the emissions of thiophene, 2- and 3-methylthiophene plotted against the respective furanic compounds show a linear dependency (Figure 125A to C). When high emissions of furans were measured the respective thiophenes were also detected at elevated concentrations. This correlation indicates a mutual precursor and a competition between thiol and hydroxyl groups during the formation of heterocyclic aromatic compounds in the soils and the sediments (Krause et al., 2013).

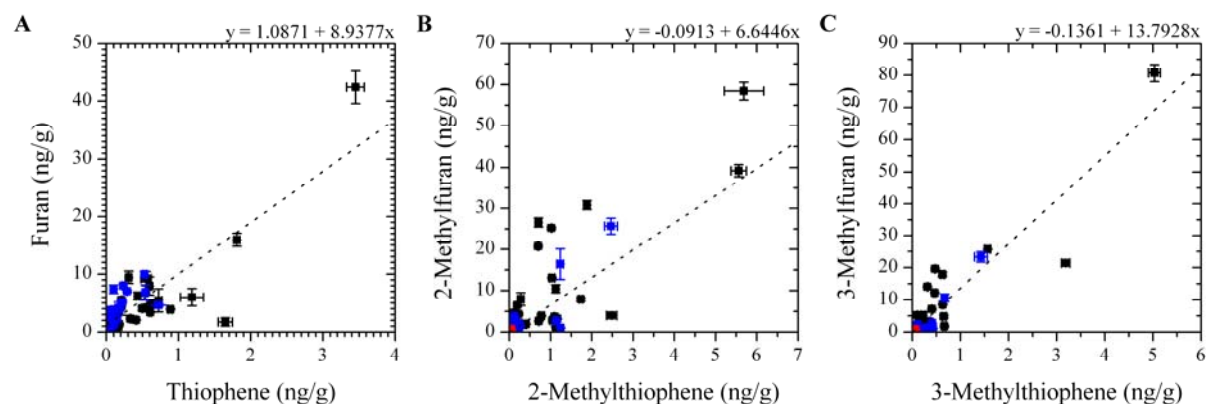


Figure 125. Correlation between emissions of related heterocyclic aromatic compounds. Emissions of **A** furan and thiophene, **B** 2-methylfuran and 2-methylthiophene and **C** 3-methylfuran and 3-methylthiophene from soil and sediment samples. ■ Australia 2011 ■ Australia 2012 ■ Dead Sea, Israel 2012

Aside from the correlations between methylfuran and methylthiophene emissions, a connection between 2- and 3-methylthiophene emissions from soils/sediments is also apparent (Figure 126). These findings point to a mutual precursor and competing formation process for methylfurans and methylthiophenes.

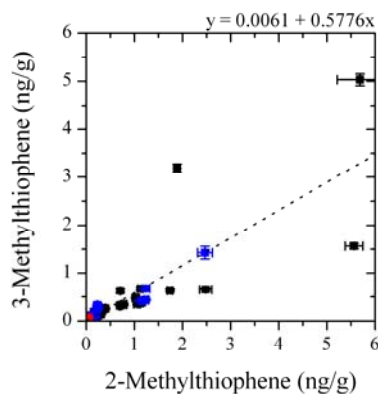


Figure 126. Correlation between 2-methylthiophene and 3-methylthiophene emissions from soil and sediment samples. ■ Australia 2011 ■ Australia 2012 ■ Dead Sea, Israel 2012

10.6 Chloroalkanes

The most diverse group of identified volatile compounds were halogenated compounds. A total of 36 different compounds was quantified, mostly chlorinated but also brominated, iodinated as well as mixed halogenated compounds. The presence of 9 further halogenated compounds was postulated based on mass spectra.

Most abundant were terminal halogenated alkyl chlorides with a non branched carbon chain structure, especially chloromethane and 1-chloropentane to 1-chlorooctane. Chloroethane was only measured in five samples and 1-chlorooctane only with an expanded recording method in samples from 2012. While chloromethane (Gribble, 2010), chloroethane, 1-chloropropane (Keppler et al., 2002) and 1-chlorobutane (Bravo-Linares et al., 2007) were noted prior as of natural origin, no references on the other 1-chloroalkanes were found.

An indication for the natural abundance of 1-chloroalkanes in the soil/sediment samples is the correlation with geochemical parameters. As such chloromethane emissions correlated significantly with the iron concentration (Figure 127).

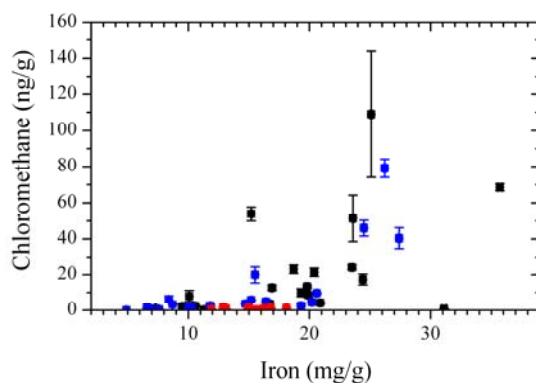


Figure 127. Correlation between iron concentration and chloromethane emission from soil and sediment samples. ■ Australia 2011 ■ Australia 2012 ■ Dead Sea, Israel 2012

The role of iron during alkylation of halides was investigated by Keppler et al. (2000). They showed that Fe^{3+} mediates halomethane formation from methoxy groups, as well as haloethane and halopropane from ethoxy and propoxy moieties, respectively. It can be assumed that this mechanism can be applied to other alkoxy groups as well. While the abundance of chloroethane was too low for statistical evaluation, other 1-chloroalkyl emissions correlated also significantly with the iron content in Australian samples (Figure 128). Samples from Sodom, Israel, fall out of alignment with low quantified emissions contrary to the moderate iron content. This indicates that other geochemical parameters like the low chloride content at the Sodom sites (Chapter 9.1) or the quality and amount of the organic carbon play an important role during formation processes of alkyl halides. Furthermore, alkyl chloride emissions increased at higher chloride and organic carbon concentrations (not shown), though less significantly compared to the presented correlation with iron.

Release of 1-chloropentane to 1-chlorooctane in correlation with iron concentrations demonstrates that these compounds are genuine natural compounds formed after freeze-drying and resuspension. 2-Chlorobutane was also found in several samples, though no correlation of its release with any geochemical parameters was evident (Appendix E).

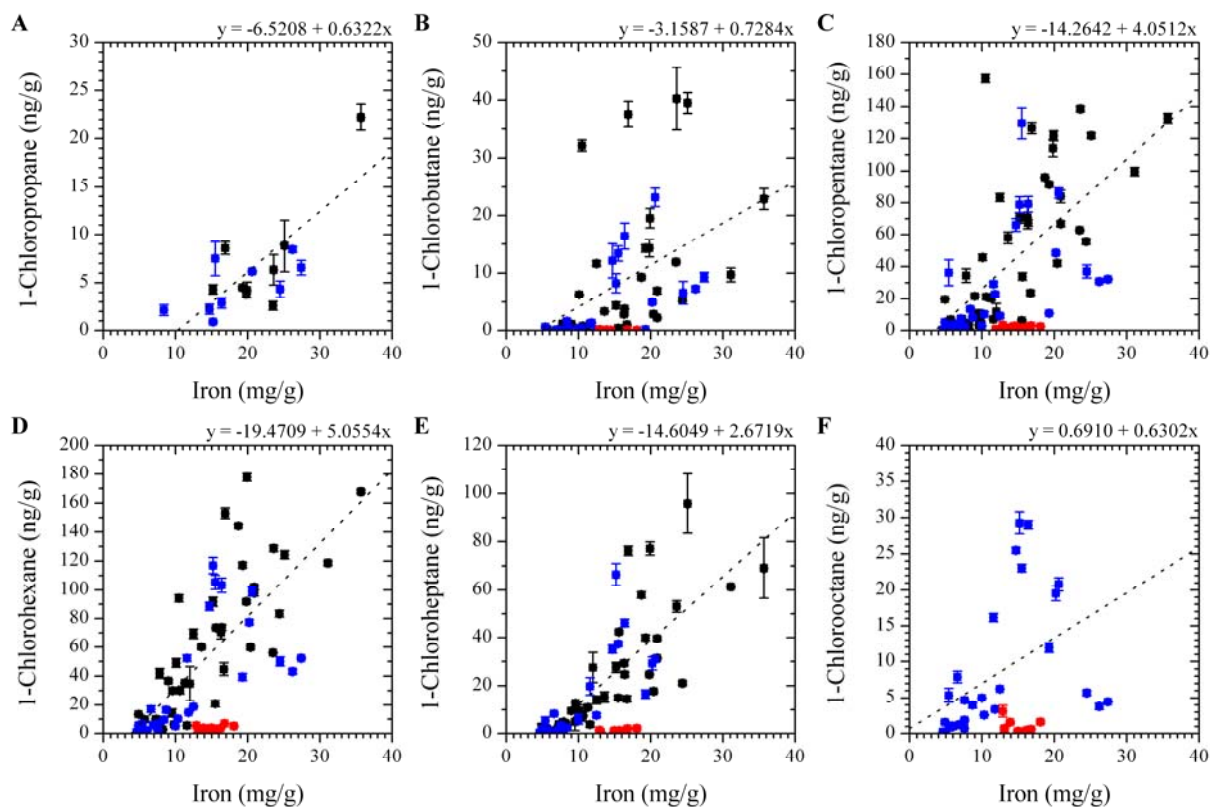


Figure 128. Correlation between iron content and emission of **A** 1-chloropropane, **B** 1-chlorobutane, **C** 1-chloropentane, **D** 1-chlorohexane, **E** 1-chloroheptane and **F** 1-chlorooctane from soil and sediment samples. ■ Australia 2011 ■ Australia 2012 ■ Dead Sea, Israel 2012

Additionally, polychlorinated ethane and propane derivatives were found, but at low frequency and low concentrations in Australian sediments, whereas none of these species was released from Sodom soils. There was a correlation between the concentration of 1,1-dichloroethane, 1,2-dichloroethane as well as 1,3-dichloropropane and the iron content of Australian sediments (Figure 129), but not for 1,2-dichloropropane (Appendix E).

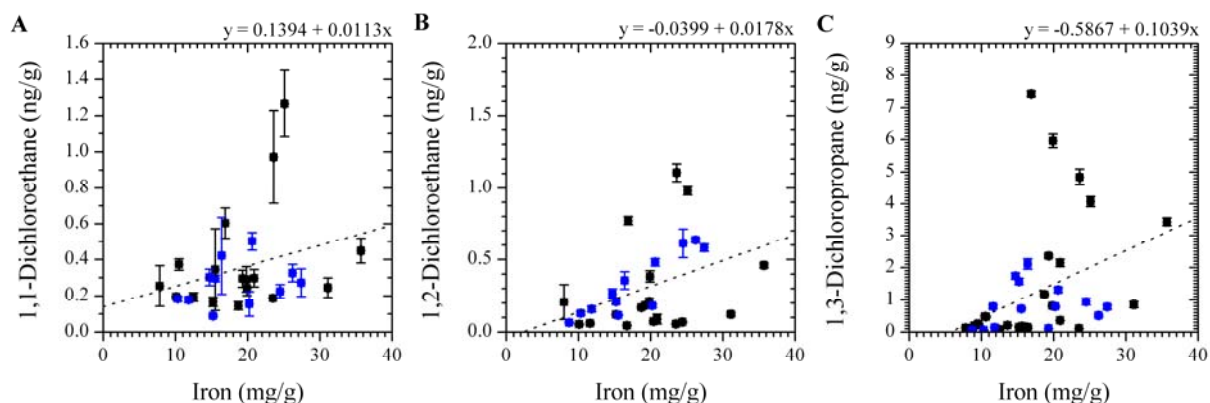


Figure 129. Correlation between iron content and emission of **A** 1,1-dichloroethane, **B** 1,2-dichloroethane and **C** 1,3-dichloropropane from soil/sediment samples. ■ Australia 2011 ■ Australia 2012

Otherwise, abundance of 1,1,1-trichloroethane is ambiguous as it was only measured in 9 samples at low concentrations (Appendix E).

Another chlorobutane derivative was found in 22 of 87 soil/sediment samples. This compound was identified as 1,3-dichlorobutane according to the NIST mainlib database with 78% probability (Figure 130A). Mass spectra interpretation of a further analyte in 37 samples points to the occurrence of 1-chloro-5-methylhexane according to mainlib though with only 28% probability (Figure 130B). The low probability is a result of not recorded but major mass fragments of the compound below 47 m/z.

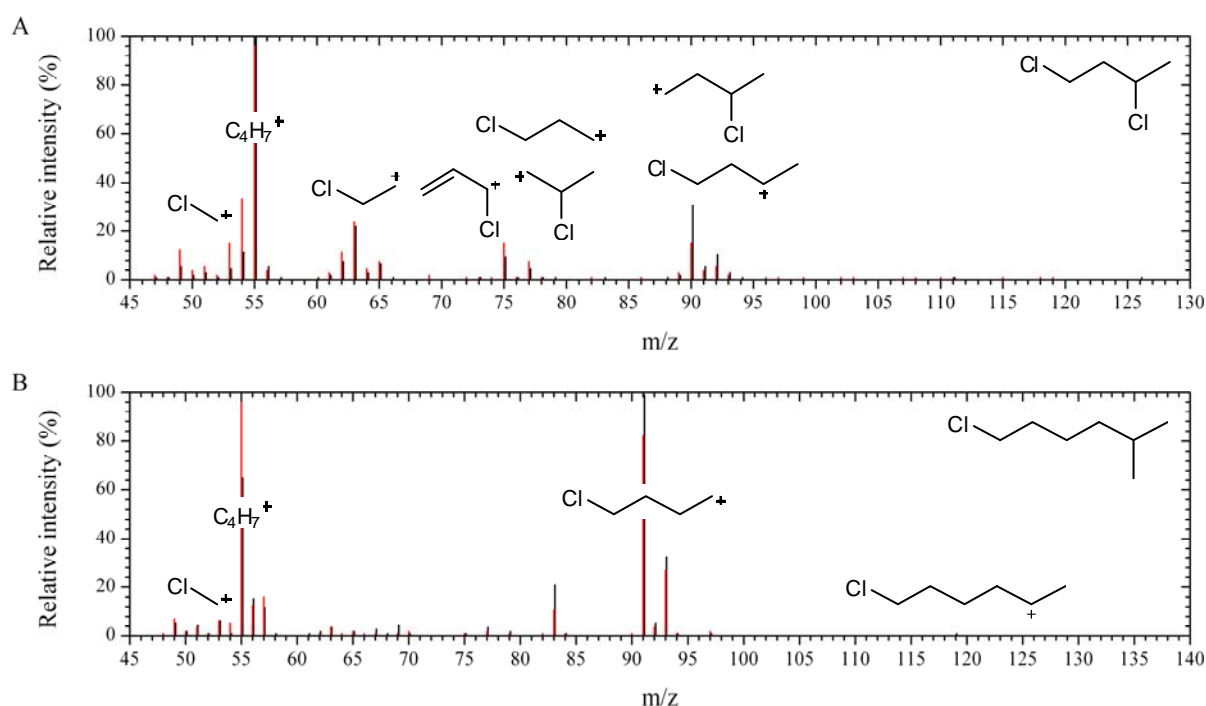


Figure 130. Analyte mass spectra (red) from Lake Golf 0-2 cm (2011) and reference mass spectra (black) from NIST mainlib database (black) for **A** 1,3-dichlorobutane and **B** 1-chloro-5-methylhexane, respectively.

Aside from chloromethane all higher chlorinated methanes (dichloro-, trichloro- and tetrachloromethane) were found in various soil/sediment samples. As described in Chapter 2.2.3 known sources for trichloromethane are among others the haloform reaction (Fuson and Bull, 1934) and degradation of the trichloroacetic acids under alkaline conditions (Fahimi et al., 2003) as well as Fenton-like chemistry under acidic conditions (Huber et al., 2009). Several natural biotic and abiotic sources have been described in literature reviewed by Gribble (2009). Data obtained from the analysed soil/sediment samples showed increasing trichloromethane concentrations at lower pH values which would be in favour for Fenton chemistry.

On the other hand, natural sources for dichloromethane are less known. Gribble quotes biomass combustion, the ocean, macroalgae and volcanoes as sources (Gribble, 2009). Evaluation of the observed dichloromethane is limited due to low emissions from the investigated salt lakes, high standard deviations and a high background. A slight correlation with the organic content of the samples was observed and could mean that the measured values are no artefacts. Furthermore, dichloromethane enrichment was observed in air samples collected from the PTFE chamber on acidic Lake Dune in 2012. Extrapolated mixing ratios of 36 pptv were measured (Sattler, 2012) exceeding the Southern hemisphere background of 17 pptv (Warneck and Williams, 2012). In the same air sample elevated trichloromethane mixing ratios of 51 pptv (Sattler, 2012) were measured as compared to 10 pptv background concentrations (Warneck and Williams, 2012).

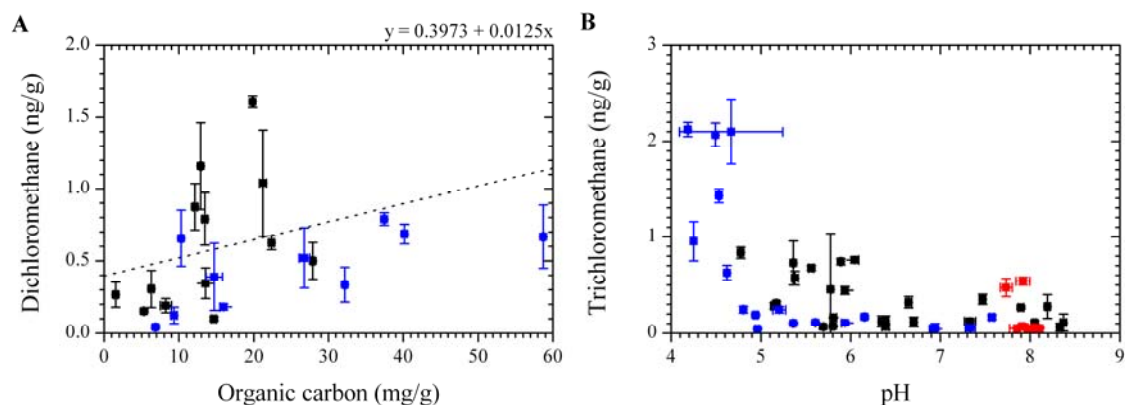


Figure 131. Correlation between **A** organic carbon content and dichloromethane emissions as well as **B** pH and trichloromethane emissions from soil and sediment samples. ■ Australia 2011 ■ Australia 2012 ■ Dead Sea, Israel 2012

For tetrachloromethane the available literature on natural sources is even rarer as compared to dichloromethane. Interpretation of tetrachloromethane will be described in the forthcoming Chapter 10.7 as it might shed new light on an additional novel natural source.

10.7 Tetrachloromethane

Tetrachloromethane is produced abiotically by geothermal processes as it was measured in volcanoes and hydrothermal vents as well as by biomass burning. Furthermore, the seaweed *Eucheuma denticulatum* is able to produce tetrachloromethane via its biogenic metabolism. While it was also found in forest soils it has been assumed that atmospheric tetrachloromethane is in equilibrium with the soil (Gribble, 2009).

The same assumption could be true for salt lakes, e.g. highest amounts measured by Weissflog et al. were only 0.31 ng/g maximum from Southern Russian salt lake sediments (Weissflog et al., 2005). Furthermore, tetrachloromethane mixing ratios over the Australian salt lakes and even in the PTFE chamber did not deviate from the global average in 2011 and 2012 (Sattler, 2012).

However, tetrachloromethane releases from incubated sediments of Australian salt lakes point to a genuine de novo formation in these lakes. Emissions were quantified to be as high as 12.6 ng/g, about 40 times higher than the concentrations reported by Weissflog et al. (2005). Furthermore, emissions significantly increased at lower pH values (Figure 132A), comparable to the trichloromethane emissions. Even a slight correlation between trichloromethane and tetrachloromethane emissions can be interpreted into the data plot (Figure 132B).

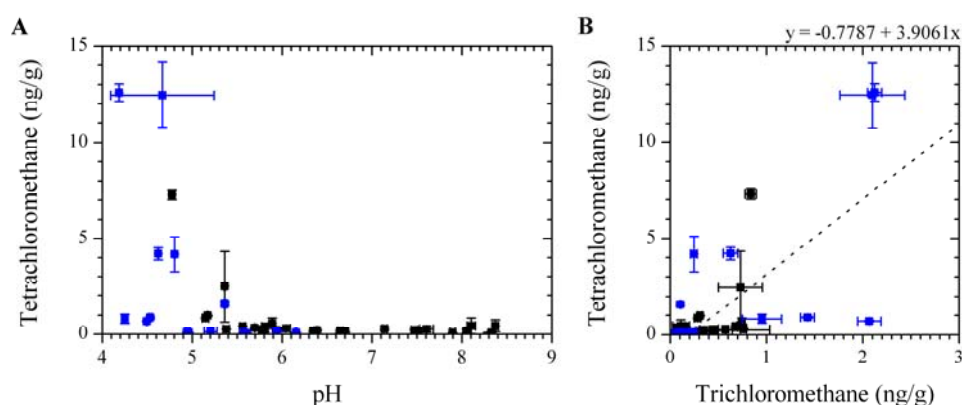


Figure 132. Correlation between tetrachloromethane emissions and **A** pH as well as **B** trichloromethane emissions of soil/sediment samples. ■ Australia 2011 ■ Australia 2012

In 2013, gas enclosed in the sediment under the water table of the highly acidic Lake Boats (Figure 133) was sampled in two headspace vials. Tetrachloromethane mixing ratios of 32 ppbv and 110 ppbv in these samples, respectively, exceeded ambient background

concentration of 96 pptv (Warneck, 1999) by three orders of magnitude. Furthermore, other halogenated compounds were detected at high concentrations in this sediment gas (Table 14).



Figure 133. Lake Boats (top) and gas bubbles emerging from its sediment (button) in 2013.
Images: T. Krause CC BY-SA 4.0.

Table 14. Mixing ratios of VOX in sediment gas from Lake Boats (2013).

		Sample	
		I	II
Chloromethane	(ppbv)	-	48.4
Trichloromethane	(ppbv)	13.2	27.8
Tetrachloromethane	(ppbv)	32.1	110
1-Chlorobutane	(ppbv)	2.57	14.4
1-Chloropentane	(ppbv)	37.2	180
1-Chlorohexane	(ppbv)	24.2	110
1-Chlorooctane	(ppbv)	1.16	2.03
2-Chlorobutane	(ppbv)	7.88	47.6
1,1-Dichloroethane	(ppbv)	7.89	4.55
1,1,1-Trichloroethane	(ppbv)	0.87	2.99
Trichloroethene	(ppbv)	-	0.93
Tetrachloroethene	(ppbv)	4.61	7.66
Iodomethane	(ppbv)	4.82	16.8
Iodoethane	(ppbv)	0.14	0.53

Interpretations of these measurements suggest a high halogenation potential in the sediment. Likely gaseous precursors for the observed halocarbons were also abundant such as methane, ethane and ethene (Benk, 2013).

A possible reaction mechanism for tetrachloromethane formation is subsequent chlorination of methane or chlorinated methanes, like trichloromethane, by atomic chlorine. Chlorination of methane would yield a mixture of mono-, di-, tri- and tetrachloromethanes. In case of the analysed gas samples no dichloromethane was found and less trichloromethane compared to tetrachloromethane. Comparable to sediment samples this indicates that formation of trichloromethane is independent of chloro- and dichloromethane and that trichloromethane is the likely precursor for tetrachloromethane in the salt lakes. Sources for reactive chlorine species in the salt lakes is discussed in Chapter 11.

10.8 Chloroalkenes

From the five detected chloroalkenes only tri- and tetrachloroethene were measured with sufficient frequency for statistical assessments. Furthermore, only trichloroethene was found in one sample from Israel. In the case of tri- and tetrachloroethene emissions slightly correlated with the available iron content of soil/sediment samples (Figure 134), comparable to other chlorinated substances mentioned before. Conspicuous are elevated tetrachloroethene concentrations from samples of 2011 compared to 2012. In addition, tetrachloroethene and trichloroethene were only found in water samples of 2011 (Appendix E). However, high concentration of these compounds were also measured in sediment gas of Lake Boats in 2013 (Chapter 10.7).

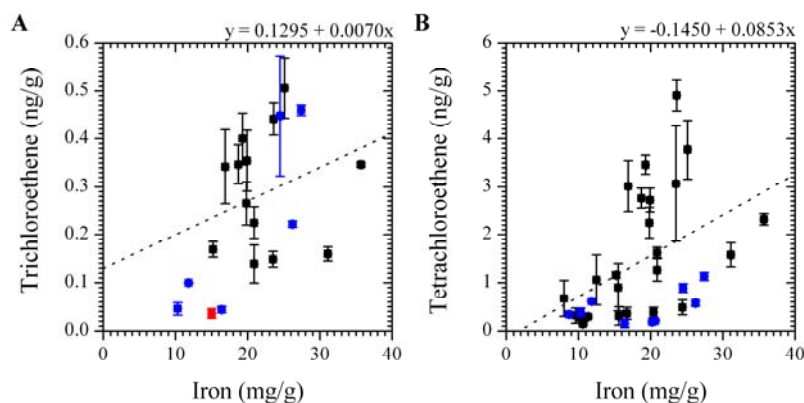


Figure 134. Correlation between iron content and emission of **A** trichloroethene and **B** tetrachloroethene from soil and sediment samples. ■ Australia 2011 ■ Australia 2012 ■ Dead Sea, Israel 2012

Furthermore, 1,1-dichloroethene was only found in 3 samples of 2011, whereas cis-1,2-dichloroethene was only found in 8 samples of 2012 (Appendix E).

One explanation is that geochemical parameters have changed between the years, most likely influenced by heavy rain events in December 2011 prior sampling in March/April 2012. Another factor might be an alteration of organic matter during storage, which was longer for the 2011 samples before measurements. Also a plausible explanation, for tetrachloroethene at least, could be a declining background contamination observed between the measurements of 2011 and 2012. A low background was also detected for trichloroethene, but none for 1,1- and cis-1,2-dichloroethene. While daily backgrounds for all analytes were evaluated and subtracted from sample measurements there is still the possibility of false positive interpretation of these compounds.

Two additional chlorinated ethenes are postulated, again mostly found in Australian samples from 2011. According to NIST mainlib database, the first analyte matches with 69% probability the reference mass spectra of 1,1-dichloropropene and the second with 35% probability could be 1-chloro-2-methyl-1-propene or an isomer of it according to NIST replib database (Figure 135).

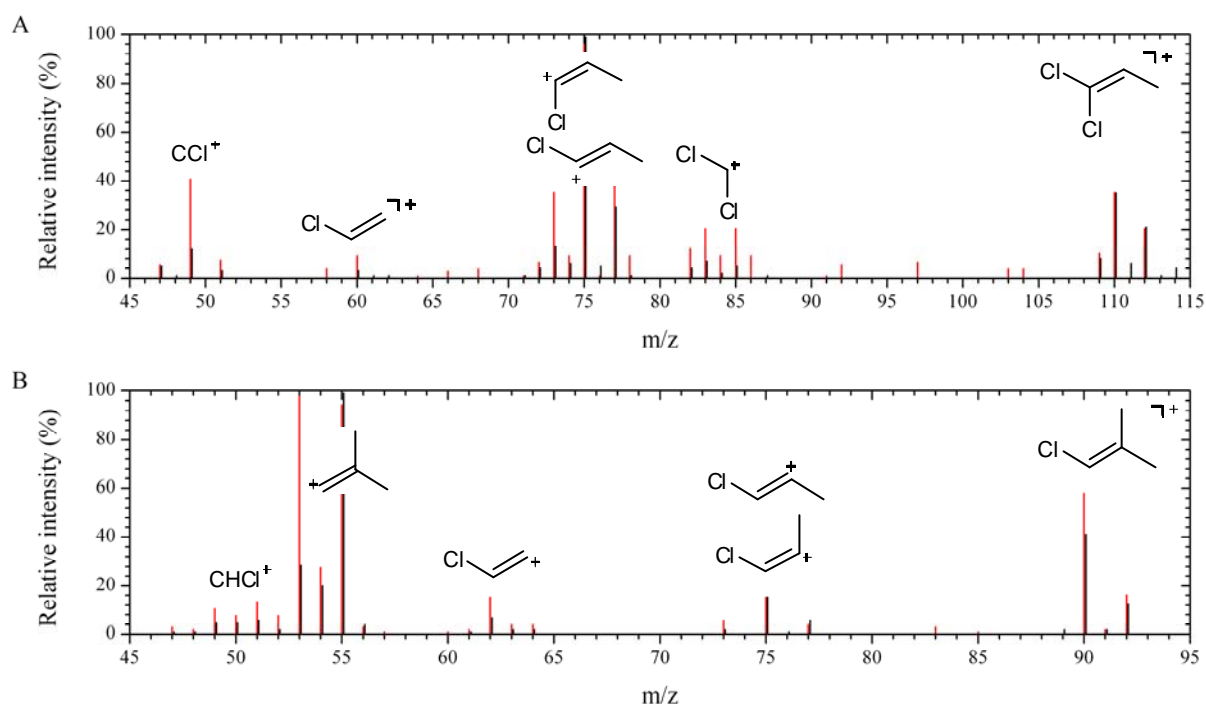


Figure 135. Analyte mass spectra (red) from Lake Golf 0-2 cm (2011) and reference mass spectra (black) from NIST mainlib and replib database (black) for **A** 1,1-dichloropropene and **B** 1-chloro-2-methyl-1-propene, respectively.

10.9 Bromoalkanes

Like volatile organic chlorocarbons, brominated compounds are of importance for stratospheric ozone depletion due to their high stability in the troposphere. Though, Br-C bonds are slightly more photoliable than Cl-C bonds and thus provide a small source for reactive bromine species in the troposphere (Sander et al., 2003). Brominated species were rare though with tribromomethane the most abundant compound. Bromo- and dibromomethane were only found in samples of the acidic saline claypan adjacent to Lake Boats in 2012. Tribromomethane on the other hand was found in various samples of Australia and Sodom including various water samples (Table 15 and Table 16).

While chlorinated compound releases from Australian samples surpassed emissions quantified from Israeli samples, tribromomethane emissions were similar in water samples from both locations and even higher in some Sodom soil samples.

Table 15. Organobromine compound emissions from soil/sediment samples.

Sampling sites	Layer (cm)	Bromomethane	Dibromomethane	1-Bromopentane	Tribromomethane
		(ng/g)	(ng/g)	(counts/g)	(ng/g)
Australia 2011	L. Tay	-	-	-	0.08
	L. Golf	-	-	-	0.07
	L. Dune	-	-	-	0.11
	L. Dune	-	-	-	1.63
	L. Dune	-	-	-	0.78
Australia 2012	L. Gulson I	-	-	207	-
	L. Gulson II	-	-	662	0.06
	L. Strawbridge	-	-	244	-
	L. Newton I	-	-	242	-
	L. Newton II	-	-	-	0.27
	L. Emu	-	-	-	0.11
	L. Whurr	-	-	-	0.24
	L. Whurr	-	-	-	0.32
	L. Orr	-	-	-	0.48
	L. Orr	-	-	-	1.36
	L. Orr	-	-	-	0.16
	L. Boats Claypan	0.27	0.17	-	0.15
	L. Boats Claypan	0.29	0.11	-	0.12
L. Boats Claypan	0.33	-	-	0.09	
Israel	Sodom I	-	-	-	0.07
	Sodom II	-	-	-	2.95
	Sodom Plant	-	-	-	2.72

Table 16. Organobromine compound emissions from water samples.

Sampling sites	pH	Bromoethene	1,2-Dibromoethane	Tribromomethane
		(counts/mL)	(counts/mL)	(ng/mL)
Stennets Lake 2012	8.7	-	-	0.006
L. Dune 2012	3.5	-	-	0.049
L. Orr 2011	3.1	-	-	0.349
L. Orr 2012	3.1	-	-	0.056
L. Boats 2012	2.4	4	-	-
Sodom II	6.5	-	-	0.029
En Gedi	6.0	-	-	0.088
South End I	5.1	-	35	0.186
South End II	5.1	-	5	0.142



Figure 136. Lake Orr with PTFE chamber in 2012. Image: T. Krause CC BY-SA 4.0.

Retention times and mass spectra of commercially available 1-bromobutane and 1-bromopentane were obtained to identify these compounds in natural samples. Typically, the unique isotope pattern of a brominated mass fragment is used for firm identification, though in case of the investigated n-bromoalkanes the relative intensity of these mass fragments was less than 2%. The mass spectra of these compounds consist of one unspecific hydrocarbon fragment for 1-bromobutane and two fragments for 1-bromopentane. Considering the high abundance of 1-chlorobutane it can be assumed that 1-bromobutane is also emitted from the samples, but confident identification was not possible. However, traces of 1-bromopentane were perceived in 4 Australian sediment samples with high probability. Furthermore, 1,2-dibromoethane was found but not quantified in water samples from the southern evaporation

pond of the Dead Sea (South End), the same samples that also contained the highest amount of the homologue 1,2-dichloroethane.

10.10 Alkyl iodines

Even more photoliable than Br-C bonds are I-C bonds (Lin and Bent, 1992). Homolytical cleavage generates reactive iodine atoms. Iodomethane was found in several Australian soil/sediment and water samples most of all under acidic conditions (Figure 137A and B). Other iodinated compounds found mostly at low sample pH in Australia were diiodomethane, iodoethane, 1-iodopropane, 2-iodopropane and 2-iodobutane (Table 17). Only Iodomethane was found in groundwater of the Sodom site near the Dead Sea.

Table 17. Organoiodine compound emissions from soil/sediments.

Sampling sites	Layer (cm)	Iodomethane	Diiodomethane	Iodoethane	1-Iodopropane	2-Iodopropane	2-Iodobutane	
		(ng/g)	(ng/g)	(ng/g)	(ng/g)	(ng/g)	(ng/g)	
Australia 2011	L. Stubbs I	0-0.5	0.46	-	0.05	-	-	-
	L. Stubbs III	0-2	0.07	-	-	-	-	-
	L. Hatter Hill	0-2	-	-	-	-	1.93	0.12
	L. Golf	0-2	-	-	0.04	-	-	-
	L. Springfield	0-2	0.48	-	0.08	-	-	-
	L. Springfield	2-4	0.11	-	0.21	0.10	-	-
	L. Orr II	0-2	0.10	-	-	-	-	-
	L. Dune	1.5-3.5	0.10	-	-	-	-	-
Australia 2012	L. Strawbridge	0-4	-	-	0.04	-	-	-
	L. Dune	0-2	0.21	-	0.04	-	-	-
	L. Dune	2-4	0.33	-	0.05	-	-	-
	L. Dune	4-6	0.34	-	0.04	-	-	-
	L. Orr	0-2	0.04	-	-	-	-	-
	L. Orr	2-4	0.07	-	-	-	-	-
	L. Orr	4-6	0.08	-	-	-	-	-
	L. Boats	0-2	1.71	-	0.12	0.09	0.78	0.09
	L. Boats	2-4	0.99	-	0.07	0.07	-	0.07
	L. Boats	4-6	0.29	-	-	-	-	-
	L. Boats Claypan	0-2	1.24	0.47	0.15	0.21	-	0.10
	L. Boats Claypan	2-4	2.62	0.40	0.31	0.37	1.05	0.21
L. Boats Claypan	4-6	1.79	0.21	0.18	0.17	0.75	0.13	

A correlation between acidic conditions and elevated alkyl iodide releases was also described by Keppler et al. (2003) using humic acid in model reactions. They also described a correlation between the iron content of organic rich soils with alkyl iodide emissions. While data plots did not show an influence of iron content on iodomethane release there is a slight correlation with iodoethane release from Australian sediments (Figure 137C).

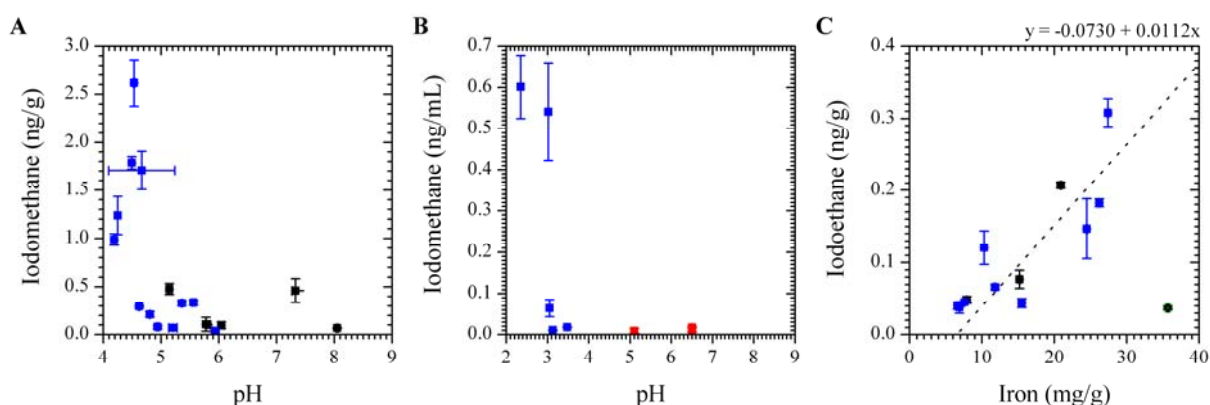


Figure 137. Correlation between iodomethane emissions from **A** soil/sediments and **B** water samples. **C** correlation between iodoethane emissions and iron content of soil/sediments.
 ■ Australia 2011 ■ Australia 2012 ■ Dead Sea, Israel 2012

Iodomethane emissions from sediments did not only correlate with the pH but also with the organic carbon concentration of the sediment (Figure 138A). The same was observed for iodoethane emissions (Figure 138B).

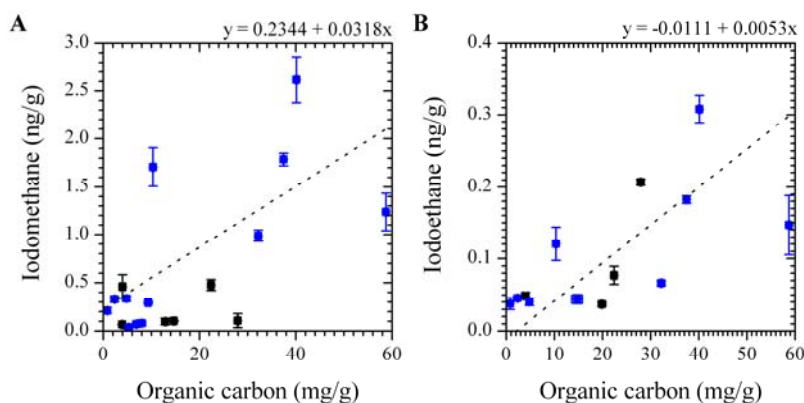


Figure 138. Correlation between **A** iodomethane as well as **B** iodoethane emissions and organic carbon content in the soil/sediments. ■ Australia 2011 ■ Australia 2012

In Chapter 10.3 it was postulated that organic carbon in the acidic salt lakes originates primarily from detritus, most of all leaves from eucalyptus trees. In 2012, two samples of plant litter were collected from the shores of the acidic Lake Dune and Lake Holt Rock (Figure 139). Analysis of the volatile species from the freeze-dried and grounded plant litter showed elevated organoiodine compound emissions compared to sediments (Table 18). From the data a connection between plant litter and volatile iodine species is evident, though the nature and reaction mechanism need to be further unravelled.



Figure 139. Close-up picture of detritus at Lake Holt Rock. Image: T. Krause CC BY-SA 4.0.

Keppler et al. (2003) also demonstrated that organic rich soils emit the same alkyl iodides as released from the detritus. Additionally, they observed that 2-iodopropane emissions were higher than 1-iodopropane emissions which also agrees with the data from eucalyptus detritus (Table 18).

Table 18. Organoiodine compound emissions from detritus.

Sampling sites	Iodomethane (ng/g)	Diiodomethane (ng/g)	Iodoethane (ng/g)	1-Iodopropane (ng/g)	2-Iodopropane (ng/g)	1-Iodobutane (ng/g)	2-Iodobutane (ng/g)
L. Dune Detritus	20.72	2.14	2.65	1.22	9.27	2.20	0.55
L. Holt Rock Detritus	137.61	-	6.68	2.33	53.51	3.09	1.65

From all iodinated compounds only iodomethane was found in water samples from the Dead Sea and Sodom. All organoiodine releases from water samples are listed in Table 19.

Table 19. Organoiodine compound emissions from water samples.

Sampling sites	pH	Iodomethane	Diiodomethane	Iodoethane	1-Iodopropane	2-Iodopropane
		(ng/mL)	(ng/mL)	(ng/mL)	(ng/mL)	(ng/mL)
L. Stubbs 2011	7.2	-	0.255	-	-	-
L. Dune 2012	3.5	0.018	-	0.004	-	-
L. Whurr 2012	3.1	0.011	-	-	-	-
L. Orr 2012	3.1	0.065	-	-	-	-
L. Boats Inlet 2012	3.0	0.541	-	0.020	0.005	0.117
L. Boats 2012	2.4	0.601	-	0.027	-	0.063
Sodom I	6.5	0.007	-	-	-	-
Sodom Plant	6.5	0.017	-	-	-	-
South End II	5.1	0.009	-	-	-	-

10.11 Mixed halogenated alkanes

With the abundance of chlorinated, brominated and iodinated volatile compounds in soil/sediment and water samples from Australia and Israel mixed halogenated compounds are also expected. Indeed, di- and trihalogenated methane as well as dihalogenated ethanes with mixed halogens were observed. The presence of bromochloromethane and postulated chloriodomethane consolidate assumptions for a natural source of dichloromethane (Chapter 10.6) in Australian salt lakes. Bromochloromethane was only found in Australian sediment samples of 2011, and emissions correlated with those of dichloromethane (Figure 140).

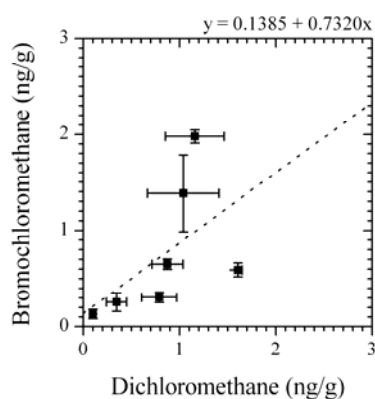


Figure 140. Correlation between Bromochloromethane and Dichloromethane emissions from sediments.
 ■ Australia 2011

Chloriodomethane on the other hand was found in water samples of Australia and the Dead Sea, though data points are too scarce for interpretation. Postulated chloriodomethane abundance is based on a mass spectra comparison with NIST replib database that calculated 99% probability (Figure 141A). Another substance that is assumed to be present in some samples is dichloriodomethane. Theoretical mass fragments of this substance significantly fit into the mass spectra of the analyte in question (Figure 141B).

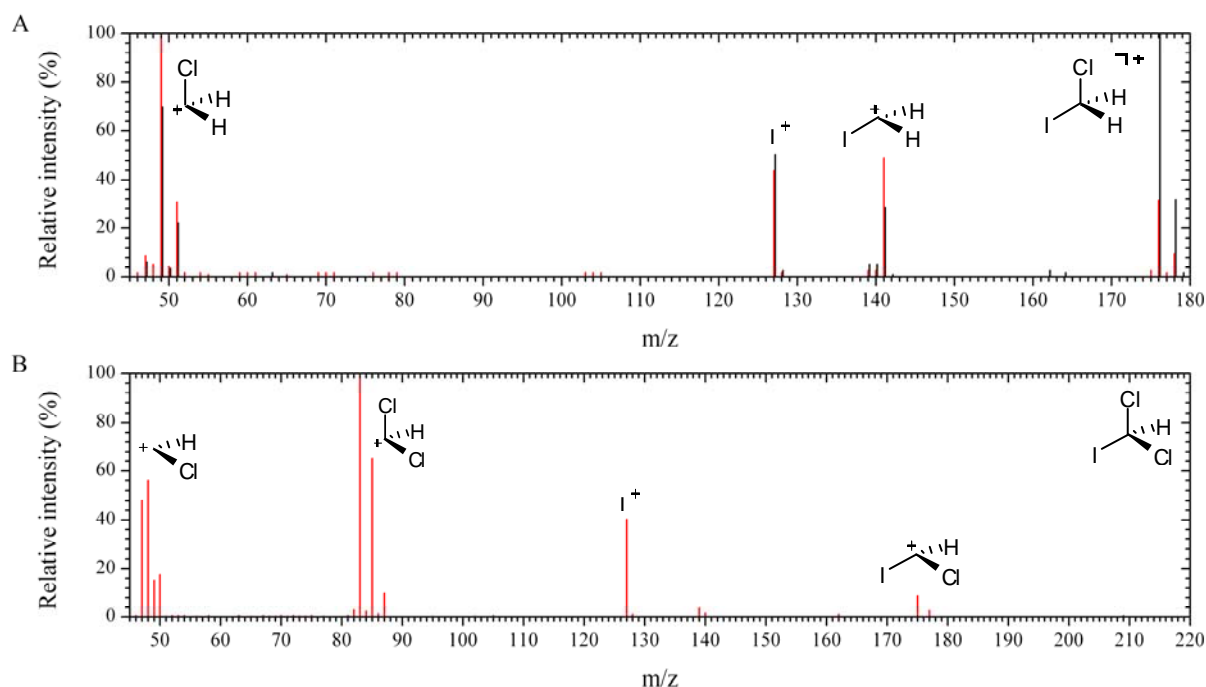


Figure 141. **A** Analyte mass spectrum (red) from a Lake Stubbs water sample (2011) and reference mass spectrum (black) from NIST replib database for chloriodomethane with possible mass fragments. **B** Analyte mass spectrum from a South End water sample (2012) and possible mass fragments of dichloriodomethane.

Further observed trihalomethanes (THM) are bromodichloro- and dibromochloromethane in samples from Australia and Israel.

The homologue to 1,2-dichloroethane and 1,2-dibromoethane, 1-bromo-2-chloroethane was quantified and 1-chloro-2-iodoethane was postulated. The latter was assumed from the mass spectrum of an unknown analyte based on plausible mass fragmentation patterns (Figure 142A).

Based on mass spectra comparisons with NIST replib database the abundance of 2-bromo-1-chloropropane with 75% certainty is also expected (Figure 142B) which is a homologue to 1,2-dichloropropane found in several samples.

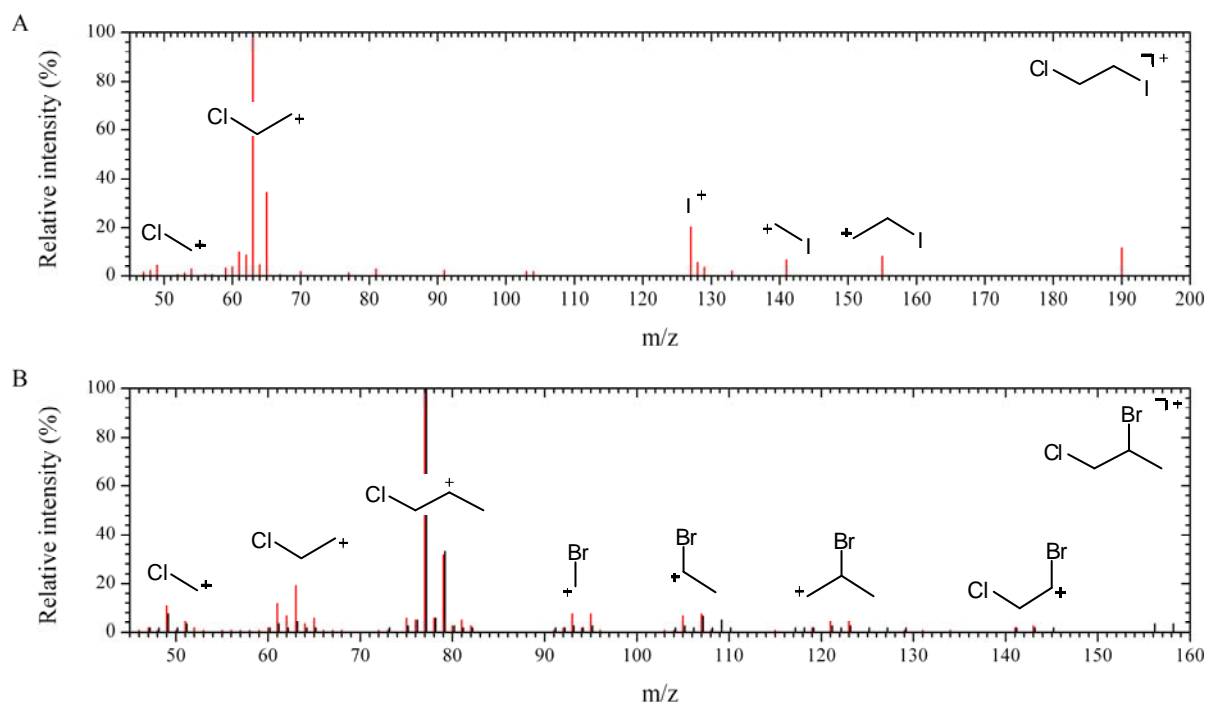


Figure 142. **A** Analyte mass spectrum from a Lake Boats water sample (2012) and possible mass fragments of 1-chloro-2-iodoethane. **B** Analyte mass spectrum (red) from a Lake Orr water sample (2011) and reference mass spectrum (black) from NIST replib database for 2-bromo-1-chloropropane with possible mass fragments.

Table 20. Emissions of mixed halogenated compounds from various water samples.

Sample site	pH	Bromochloromethane	Bromodichloromethane	Dibromochloromethane	Chloriodomethane	Dichloriodomethane	1-Bromo-2-chloroethane	1-Chloro-2-iodoethane	2-Bromo-1-chloropropane
		(ng/mL)	(ng/mL)	(ng/mL)	(counts/mL)	(counts/mL)	(ng/mL)	(counts/mL)	(counts/mL)
L. Stubbs 2011	7.2	-	-	-	741	189	-	-	-
L. Strawbridge 2011	7.1	-	-	0.004	-	-	-	-	-
L. Newton 2012	6.3	-	-	0.005	-	-	-	-	-
L. Emu 2012	5.7	-	-	0.005	-	-	-	-	-
L. Dune 2012	3.5	-	0.013	0.036	-	-	0.099	133	166
L. Whurr 2012	3.1	-	-	0.004	-	-	-	-	-
L. Orr 2011	3.1	-	0.054	0.257	13	-	0.056	-	568
L. Orr 2012	3.1	-	0.012	0.045	-	-	0.103	114	127
L. Boats Inlet 2012	3.0	-	-	-	14	-	-	-	-
L. Dune 2011	2.6	-	-	0.008	34	-	-	-	-
L. Boats 2012	2.4	0.016	-	-	61	-	-	159	-
Sodom I	6.5	-	-	-	12	-	-	-	-
Sodom II	6.5	-	0.009	0.020	63	12	-	-	-
Sodom Plant	6.5	-	-	0.006	-	-	-	-	-
En Gedi	6.0	-	0.013	0.040	-	-	-	-	-
South End I	5.1	-	0.573	0.240	-	611	-	-	-
South End II	5.1	-	0.494	0.230	-	1354	-	-	-

Concentration or relative emission data for mixed halogenated compounds found in Australia and Israel water samples are listed in Table 20. Emission data from soils/sediments is listed in Appendix E.

The variety and amount of halogenated compounds found in the hypersaline environments of Australia and Israel raise the question of formation pathways and their impact on the local atmosphere. Assessments of these questions are given in the next Chapters 12 to 13.

11 Sources of VOX in hypersaline salt lakes

In Chapter 2.2.3 several iron based reaction mechanisms, mostly involving Fenton chemistry, were presented. Products of these reactions were also found in various natural samples from Australia and Israel. On the one hand, Fe^{3+} mediates formation of terminal halogenated n-alkanes from alkoxy groups (Keppler et al., 2000; Keppler et al., 2003) and, on the other hand, Fenton chemistry yielded chloroethene (Keppler et al., 2002) and trihalomethanes (Huber et al., 2009).

As shown in Chapter 9.3 Fe^{2+} and Fe^{3+} are abundant with varying concentrations in the solid and aqueous phases and an active redoxcycling is evident. As described in the literature an increase of n-alkyl halide release from soil/sediment samples was observed at higher iron concentrations (Keppler et al., 2000; Keppler et al., 2003), which is in agreement with the release of chloroalkanes from Australian sediments (Chapter 10.6).

There are also considerable indications for a significant role of Fenton chemistry in the investigated hypersaline environments yielding RHS. First of all THM emissions under acidic conditions, most of all chloroform, are in accordance with model reactions (Huber et al., 2009). Secondly, semiquantitative hydrogen peroxide measurements (Quantofix 25 test sticks by Macherey-Nagel) pointed to photochemical formation (Cooper et al., 1988) after sunrise and decline in the late afternoon (Figure 143) (Appendix F).

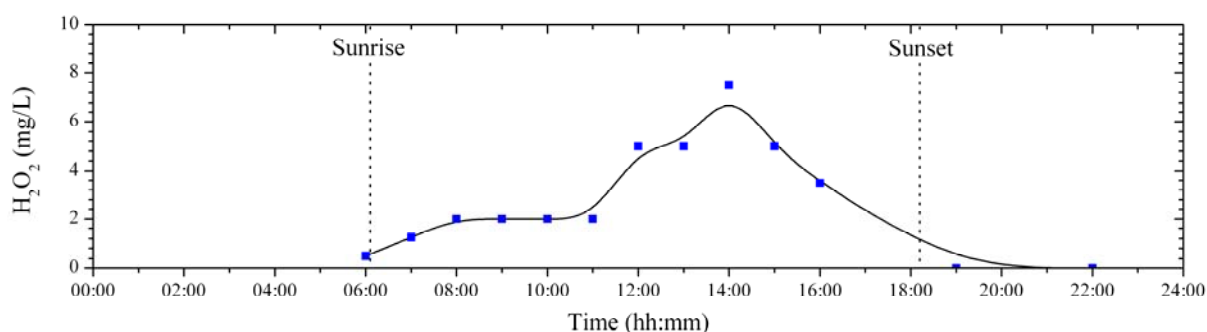


Figure 143. Semiquantitative H_2O_2 measurement showing its photochemical formation at Lake Shot on the 21st of March, 2013.

Further hydrogen peroxide sources are e.g. rain (Yoshizumi et al., 1984) and eventually autoxidation of Fe^{2+} (Weiss, 1935; Aust et al., 1985; Voelker et al., 1997). A general formation pathway for RHS and VOX in the salt lakes is postulated taking into account the abundance of $\text{Fe}^{2+}/\text{Fe}^{3+}$, average dissolved organic matter concentrations of 200 mg/L, high solar radiation and thus the presumed formation of H_2O_2 (Figure 144).

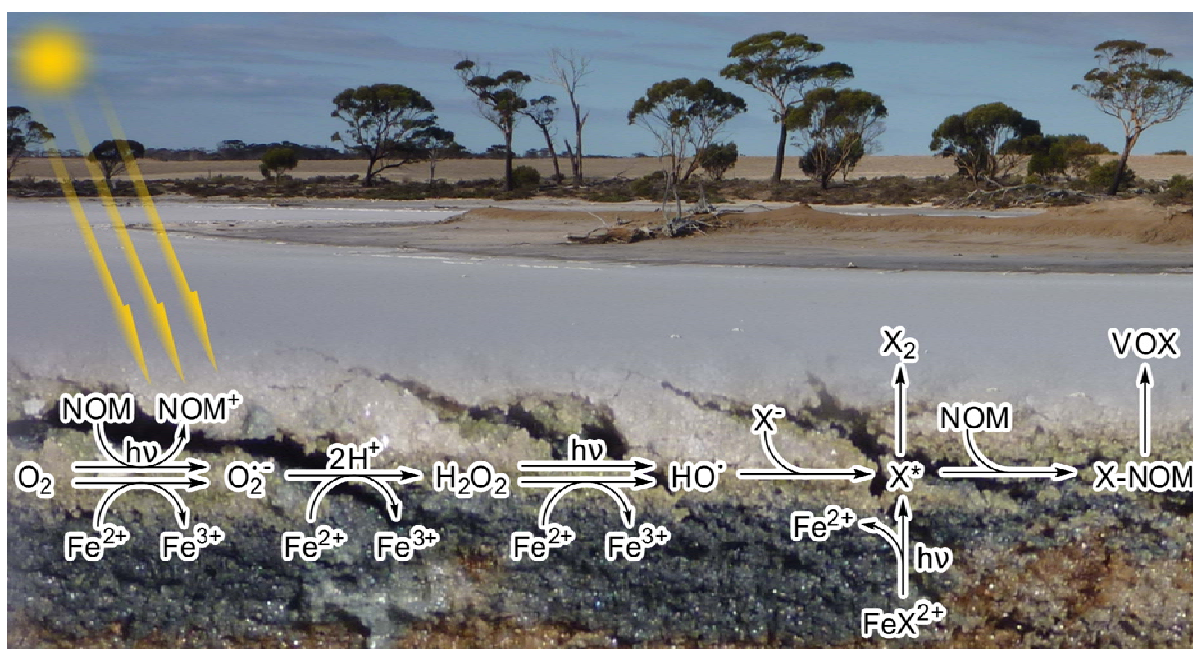


Figure 144. Postulated formation pathway of RHS and VOX in salt lakes, based on superoxide formation (Weiss, 1935; Aust et al., 1985; Voelker et al., 1997; Cooper et al., 1988), Fenton chemistry (Haber and Weiss, 1932) and photochemical activation of FeX^{2+} (Nadtochenko and Kiwi, 1998a; Nadtochenko and Kiwi, 1998b; Machulek Jr et al., 2009) yielding RHS with $\text{X} = \text{Cl}, \text{Br}, \text{I}$. Image: T. Krause CC BY-SA 4.0.

Autoxidation could also be a source of free radicals in the laboratory soil/sediment incubation experiments, especially of alkaline samples (Welch et al., 2002). Furthermore, previous experiments with supplementary hydrogen peroxide during incubation experiments led to increasing organohalogen releases (Keppler et al., 2002; Keppler et al., 2006; Huber et al., 2009; Huber et al., 2010).

Preliminary free and total chlorine measurements with a spectrometer using the DPD method (Chapter 5.5.13) pointed to the abundance of these compounds in Australian salt lakes (Appendix F). However, measurements were constricted under acidic conditions and by high salinity.

Exemplary, time based measurements on the release of volatile compounds from the acidic Lake Boats 0-2 cm layer also showed an exponential emission increase for most analytes within 24 h. Compounds like chloromethane, dichloromethane, trichloromethane and tetrachloromethane increased exponentially within the error margin (Figure 145) pointing to de novo formation of these compounds. However, tetrachloromethane concentrations were already elevated in the gas phase after 1 h incubation, indicating that the compound was not completely removed from the samples during freeze-drying. Furthermore, the liquid-gas

phase equilibrium has to be considered for all compounds (solubility and volatility of dichloromethane > chloroform > chloromethane > tetrachloromethane (Gossett, 1987)).

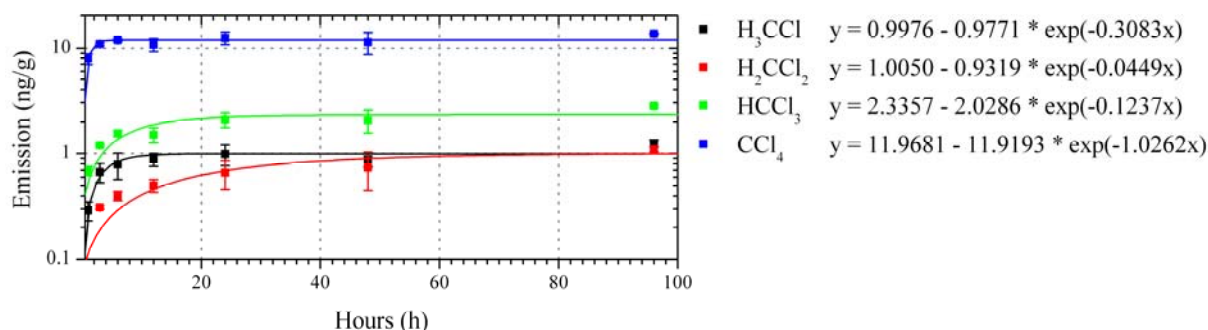


Figure 145. Release of various chlorinated methanes from Lake Boats 0-2 cm sample collected in 2012.

In natural environments, Fenton chemistry is not the only plausible source for RHS. For example, photochemical activation of FeCl^{2+} at low pH values yields free chlorine radicals (Nadtochenko and Kiwi, 1998a; Nadtochenko and Kiwi, 1998b; Machulek Jr et al., 2009).

Further insight into salt lake chemistry is revealed by the distribution between homologous halogenated hydrocarbons with chlorine, bromine and or iodine moieties. From a thermodynamic standpoint iodide is the most favourable halide to be oxidised by the reaction with OH radicals forming reactive iodine species followed by bromide and chloride (Evans et al., 1952). While aqueous reactive chlorine species are better oxidants than bromine or iodine species, bromine reacts faster with organic matter compared to chlorine at a pH of 5-11 (Westerhoff et al., 2004). Mechanistic halogenation of organic compounds by RHS involves the addition to double bonds (Tarbell and Bartlett, 1937; Roberts and Kimball, 1937; Ruasse, 1990), radical chain reactions (Kiwi et al., 2000) or decarboxylation (Larson and Rockwell, 1979), as a variation of the Hunsdiecker reaction (Hunsdiecker and Hunsdiecker, 1942).

Furthermore, iodide is a better nucleophile but also a better leaving group compared to bromide and chloride in substitution reactions within aqueous solutions (Anslyn and Dougherty, 2006). This is also of importance for halogen exchange via substitution reactions, known as Finkelstein reaction, in the aqueous phase (Finkelstein, 1910).

Based on these assumptions brominated or iodinated compounds should be the predominant released species from salt lakes, though the product distribution is also influenced on the concentrations of the respective halides. With an excess of chloride in Australian samples chlorinated compounds comprised the main fraction of VOX, whereas brominated compound releases were more pronounced from bromide rich Dead Sea samples. The Br^-/Cl^- ratio was

0.09-0.6% and 1-4% for the investigated Australian lakes and the Dead Sea, respectively (Figure 146).

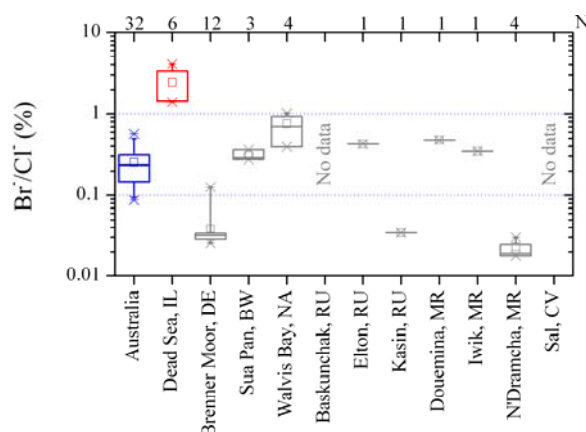


Figure 146. Br⁻/Cl⁻ ratios for surface and groundwater of various saline environments.

Furthermore, biosynthesis of halogenated metabolites, similar to marine algae for example (Paul and Pohnert, 2011), have to be considered to assess VOX release and halogen distribution.

Aqueous chemistry, discussed so far, explains the formation of various VOX and the abundance of homologous compounds with different halogen substitutions. The postulated formation of tetrachloromethane though needs additional attention.

The most likely scenario for its formation is a radical induced tetrachloromethane formation involving chlorine. Homolytical cleavage of molecular chlorine would propagate in a radical chain reaction resulting in subsequent chlorination of methane to tetrachloromethane. The reaction can be initiated and controlled by high temperatures above 250 °C (Pease and Walz, 1931), which is unlikely for Australian sediments, photolysis (Winning, 1951) or by the formation of organic radicals and RHS by Fenton chemistry. Chlorination starting from methane yields a mixture of chloro- dichloro-, trichloro- and tetrachloromethane (McBee et al., 1942). While all these compounds were observed in various Australian samples a correlation was evident only between the abundance of tri- and tetrachloromethane. Hence, chloromethane which correlated with the abundance of iron in the soil/sediments is not the precursor for trichloromethane which negatively correlated with the pH. More likely is a trichloromethane formation in the course of Fenton chemistry (Huber et al., 2009) with subsequent chlorination to tetrachloromethane as described above.

12 Assessment of aerosol formation over Australian salt lakes

As addressed in Chapter 10, several volatile compounds were released from Australian samples that act as potential aerosol precursors. First of all monoterpenes (Lee et al., 2006) and isoprene (Claeys et al., 2004; Carlton et al., 2009) but also BTEX (Ng et al., 2007), furans (Gómez Alvarez et al., 2009) and volatile sulfur compounds, like dimethyl sulfide (Charlson et al., 1987), are known for aerosol formation.

Table 21. Tropospheric lifetimes of volatile compounds with regard to OH radical degradation.

Compound	Lifetime ¹	Reference for rate constants
Isoprene	2.9 h	(Atkinson, 1997)
α -Pinene	5.2 h	(Atkinson, 1997)
Champhor	2.5 d	(Reissell et al., 2001)
3-Carene	3.2 h	(Atkinson, 1997)
Sabinene	2.4 h	(Atkinson, 1997)
Limonen	1.6 h	(Atkinson, 1997)
p-Cymene	18.4 h	(Corchnoy and Atkinson, 1990)
Eucalyptol	1.0 d	(Corchnoy and Atkinson, 1990)
Benzene	9.4 d	(Atkinson et al., 1989a)
Toluene	1.9 d	(Atkinson et al., 1989a)
Ethylbenzene	1.5 d	(Atkinson, 1986)
o-Xylene	22.8 h	(Atkinson and Aschmann, 1989)
m-Xylene	12.1 h	(Atkinson and Aschmann, 1989)
p-Xylene	21.4 h	(Atkinson and Aschmann, 1989)
Furan	6.6 h	(Bierbach et al., 1992)
2-Methylfuran	4.5 h	(Bierbach et al., 1992)
3-Methylfuran	3 h	(Atkinson et al., 1989b)
2-Ethylfuran	2.6 h	(Bierbach et al., 1992)
2,5-Dimethylfuran	2.1 h	(Bierbach et al., 1992)
OCS	3.6 a	(Khalil and Rasmussen, 1984)
Carbon disulfide	5.8 d	(Jones et al., 1983)
Dimethyl sulfide	1.2 d	(Atkinson et al., 1984)
Dimethyl disulfide	1.4 h	(Wine et al., 1981)
Thiophene	1.2 d	(Atkinson, 1986)
SO ₂	10.5 d	(Müller, 1980)
Chloromethane	321.5 d	(Sander et al., 2006)
Chloroethane	27.6 d	(Markert and Nielsen, 1992)
Chloropropane	14.1 d	(Markert and Nielsen, 1992)
Chlorobutane	7.5 d	(Markert and Nielsen, 1992)
Chloropentane	3.8 d	(Markert and Nielsen, 1992)
Chlorohexane	3.0 d	(Markert and Nielsen, 1992)
Trichloromethane	115.7 d	(Sander et al., 2006)
Tetrachloromethane	> 63.4 a	(Sander et al., 2006)
Bromomethane	1.1 a	(Sander et al., 2006)
Dibromomethane	96.5 d	(Sander et al., 2006)
Tribromomethane	77.2 d	(Sander et al., 2006)
Iodomethane	160.8 d	(Sander et al., 2006)

¹With $1 \cdot 10^{-6}$ molecules cm^{-3} OH radicals as global average (Spivakovsky et al., 2000) and ambient reaction conditions.

Exemplary atmospheric lifetimes of these compounds as well as selected halogenated compounds are listed in Table 21. Lifetime calculations are based on reactions with OH radicals under ambient conditions and with average OH radical concentrations of $1 \cdot 10^{-6}$ molecules cm^{-3} (Spivakovsky et al., 2000).

Highly reactive and known sources for aerosol formation are isoprene and several monoterpenes, like limonene and α -pinene. However, atmospheric mixing ratios of isoprene and probably of the monoterpenes were lower at the salt lakes as compared to Frank Hahn National Park (Sattler, 2012). This is of interest, because no significant particle formation was observed at Frank Hahn National Park (Junkermann et al., 2009) even though precursors were abundant. This means the concentrations of atmospheric oxidants over the salt lake or of other volatile aerosol precursors at the salt lakes differ from the National Park.

Furans with increasing alkylation and longer alkyl chains are even more reactive with regard to OH radicals. These compounds were released from most sediment and water samples and the mixing ratios over the salt lakes surpassed the concentrations in the Frank Hahn National Park (Sattler, 2012).

With regard to BTEX, toluene was the only compound found with high mixing ratios within the PTFE chamber (Sattler, 2012). On the one hand, toluene is known as a precursor for secondary organic aerosol (Hurley et al., 2001; Hamilton et al., 2005). On the other hand, the atmospheric half-life of toluene is approximately 13 h (ATSDR, 2000) and thus insufficient to significantly contribute to the fast particle formation observed shortly after sunrise (Kamilli et al., 2013). Likewise unreactive are the other benzene derivatives.

From the volatile sulfur compounds only dimethyl disulfide and probably dimethyl trisulfide, which were released from several sediments, react with OH radicals to SO_2 within hours. However, subsequent oxidation to aerosol forming sulfate needs days (Kellogg et al., 1972).

Depending on the number of halides in the molecule, VOX have lifetimes of several days to years, making them relevant for stratospheric ozone depletion (Rowland, 2006), but less for local tropospheric chemistry. Then again, photolysis of iodine containing volatile compounds could be of importance for the abundance of atmospheric reactive atomic iodine in the vicinity of the salt lakes (Ross and Johnston, 1995; Roehl et al., 1997). Additionally, photooxidation of diiodomethane, which was partially released from various samples, leads to rapid nucleation and thus ultrafine particle formation (O'Dowd et al., 2002; Jimenez et al., 2003).

Postulated RHS releases from salt lakes in the Wheatbelt, as described in Chapter 11, could be the main difference in atmospheric chemistry compared to the Frank Hahn National Park. The hypothesis is supported by kinetic studies of various volatile compounds with atmospheric chlorine. Smog chamber experiments demonstrated that chlorine readily reacts with α -pinene forming SOA (Cai and Griffin, 2006) and even XOA (Ofner et al., 2013). Toluene also yielded aerosol in the reaction with chlorine (Karlsson et al., 2000; Cai et al., 2008).

Furthermore, chlorine reacts with other observed volatile compounds like furans (Cabañas et al., 2005; Villanueva et al., 2009), benzene, ethylbenzene, xylenes and alkenes (Wallington et al., 1988), dimethyl sulfide (Stickel et al., 1992) and carbon disulfide (Nicovich et al., 1990). However, the aerosol formation potential of these reactions have not yet been evaluated. Furthermore, DOAS measurements of some RHS over the salt lakes in 2011 could not prove their abundance (Holla, 2013).

Another important oxidant is ozone, though it is less reactive than OH radicals or chlorine. Atmospheric mixing ratios of ozone were 5 to 50 ppbv over salt lakes as well as east of the State Barrier Fence (Holla, 2013). Typically, ozone mixing ratios increased from sunrise to noon pointing to groundlevel ozone formation (Chapter 3.3.1).

Preliminary results from time resolved air sampling in the PTFE chamber on Australian salt lakes in 2013 indicated that aldehydes and ketones seemed to be involved in the particle formation process. As such, a decline of atmospheric mixing ratios of these compounds was measured in the same time frame as the initial particle formation was observed (Figure 147).

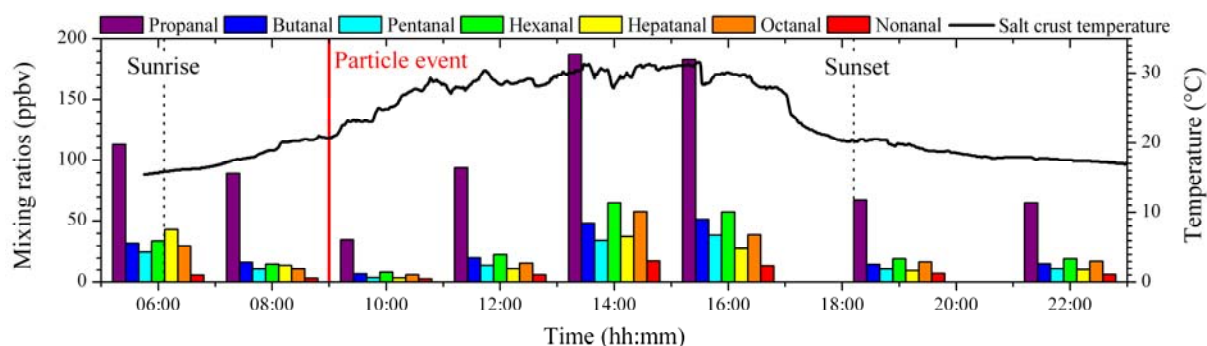


Figure 147. Atmospheric mixing ratios for aldehydes in the PTFE chamber and salt crust temperature at Lake Shot, 21.03.2013 (Krause and Sattler, 2013).

Kinetic rate constants for these compounds with OH radicals yield lifetimes of several hours for aldehydes (Papagni et al., 2000) and days for ketones (Atkinson et al., 1982) which is too slow for rapid particle formation. However, SOA formation and growth is promoted by an uptake and heterogenous reactions of aldehydes on existing, mostly acidic, aerosol seeds (Jang and Kamens, 2001; Jang et al., 2002).

Based on these evidences the mechanism for rapid ultrafine particle formation over natural salt lakes needs to be further investigated. This includes aerosol analysis as well as smog chamber experiments simulating the here presented geochemical and atmospheric conditions.

13 Assessment of VOX contribution to BrO/IO over the Dead Sea

Reactive halogen species were detected at elevated concentrations over the Dead Sea with atmospheric mixing ratios of about 100 pptv BrO (Hebestreit et al., 1999; Tas et al., 2005; Holla, 2013) and 10 pptv IO (Zingler and Platt, 2005).

Additionally to RHS measurements, air samples were collected and analysed for the abundance of bromo-, dibromo- and dibromochloromethane (Matveev et al., 2001). The first two compounds were not observed in natural samples collected in 2012, whereas soil samples and especially water samples from the southern evaporation pond are a source for dibromochloromethane (Chapter 10.9). As shown in Chapter 10.9 and 10.11 additional brominated compounds, mainly tribromomethane were released from soil and water samples.

Organobromine species are relatively stable in the atmosphere and a significant contribution to atmospheric RHS formation is unlikely as no diurnal variation in the mixing ratios of bromo- and dibromomethane was observed (Matveev et al., 2001). However, Tang and McConnell (1996) postulated that even slow photodissociation is sufficient to initiate a rapid bromine release via the autocatalytic bromine explosion.

Models suggest that the bromine explosion, in conjunction with the formation and heterogeneous decomposition of BrONO₂, is the major source for BrO in the Dead Sea boundary layer (Stutz et al., 1999; Tas et al., 2006). However, other models indicated that the release of bromine from the aerosol phase is insufficient and that a direct release of bromine from the Dead Sea is essential to explain the BrO mixing ratios (Smoydzin and von Glasow, 2009), e.g. by photolytic activation of bromide in the Dead Sea (Gratzel and Halmann, 1990).

BrO mixing ratios were highest at the evaporation ponds in the south (Tas et al., 2005), which correlated with increasing bromide concentrations and the observed release of brominated compounds from water samples (Chapter 10.9 and 10.11). However, this evaporation pond is fed by a canal passing through the Dead Sea Works complex and an anthropogenic pollution needs to be considered. A significant contribution to atmospheric bromine from the industrial Dead Sea Works complex as well as its Jordanian counterpart were considered unlikely by Hebestreit et al. (1999) based on their observations.

While organobromine compounds do not significantly contribute to local reactive bromine species, photoliable organoiodine compounds are a potential source for IO in the boundary layer (Carpenter et al., 1999). Furthermore, the formation of reactive iodine species can

promote the photochemical release of bromine and chlorine from the aerosol phase (Vogt et al., 1999).

Organoiodines were also discussed as precursors for atmospheric IO at the Dead Sea (Zingler and Platt, 2005). However, only dichloroiodomethane was detected in water samples from the southern evaporation pond (Chapter 10.11). Additionally, iodomethane was measured in groundwater from the Sodom location (Chapter 10.10). As such, a significant contribution by iodinated compounds to IO formation has to be ruled out based on the collected samples.

14 Conclusions and outlook

While the man-made climate change represents a major challenge in the future it is also necessary to comprehend natural processes that lead to volatile compound emissions and their impact on atmospheric chemistry. In this context, the contribution to global VOC, VSC and VOX fluxes from expanding saline and hypersaline ecosystems, due to secondary salinisation, needs to be assessed. Sources for volatile compounds from salt influenced soils and sediments are diverse and even hypersaline ecosystems are biotically active. Furthermore, model reactions demonstrated the ability of abiotic reactions to generate climate relevant gases like carbon suboxide or trihalogenmethanes (Huber et al., 2007; Huber et al., 2009).

While previous model reactions often used $\text{Fe}_2(\text{SO}_4)_3$ salt as catalyst in Fenton chemistry, investigation of redox zones and determination of dissolved organic carbon content prompt to the abundance of Fe^{2+} complexes in natural hypersaline environments. These findings were adopted within model reactions with a biomimetic bispidine Fe^{2+} complex to degrade catechol under Fenton conditions to furan, a reactive volatile compound with an atmospheric lifetime of some hours and a possible SOA precursor. Conversion of catechol to furan was previously demonstrated with $\text{Fe}_2(\text{SO}_4)_3$ and a yield of 0.68% (Huber et al., 2010). With the bispidine Fe^{2+} complex furan yields of 0.63% were similar, albeit the complex is a better catalyst as the molar ratio of catechol/iron decreased from 1:1.4 for $\text{Fe}_2(\text{SO}_4)_3$ to 4:1. However, optimal H_2O_2 consumption and reaction time increased with the bispidine Fe^{2+} complex compared to $\text{Fe}_2(\text{SO}_4)_3$.

Additionally, a second model reaction was performed to demonstrate that Fenton chemistry is not only feasible for abiotic furan and methylfuran formations but also for higher alkylated furans observed in natural samples. Under Fenton-like conditions with $\text{Fe}_2(\text{SO}_4)_3$ 4-ethylcatechol was successfully degraded to 3-ethylfuran.

Aside from model reactions, a comprehensive study on volatile compounds released from natural samples, comprising 87 soil/sediment and 27 water samples, under controlled laboratory incubations was performed. Samples were collected at salt lakes in Western Australia and the Dead Sea, Israel.

A total of 69 different compounds was reliably identified and additional 26 were postulated by the obtained mass spectra, not including simple hydrocarbons from C1 to C4. Compounds observed were aromatic hydrocarbons, isoprene and monoterpenes, furan derivatives, sulfur and selenide containing compounds, as well as various halogenated compounds.

Geochemical classification of the investigated Australian salt lakes into circumneutral (pH 6-8), slightly acidic (pH 4-6) and acidic (pH 2-4) lakes exposed characteristic emission trends. Sulfur compound emissions were prominent at circumneutral conditions while halogenated compound emissions under acidic conditions. The latter trend was also observed in water samples. Overall, highest emissions from soils/sediments were determined for isoprene and monoterpenes and lowest for BTEX.

A more detailed analysis between the geochemical inventory and the emission of individual compounds brought significant correlations in good accordance with model reactions, but also some unsuspected results, which are listed in the following.

BTEX, attributed as mostly anthropogenic substances in the biosphere, were also released from soils/sediments during incubation experiments. A comparison with geochemical parameters revealed that BTEX emissions significantly increased with the iron content in Australian sediments. This connection demonstrates a possible natural BTEX formation, probably from benzoic acid derivatives.

Isoprene and monoterpene emissions were linked to plant litter, mostly eucalyptus, and halophilic microorganisms as well as algae based on on-site observations. Detritus of plants was evident on the shore of several small acidic lakes surrounded by trees and shrubs, whereas larger circumneutral lakes often featured reddish water and salt crusts resulting from biosynthesis of β -carotene and retinal chromophores.

Emissions of furanoic compounds correlated mostly with the organic carbon content of the soil/sediment samples. Notable correlations with pH and iron content were only observed for furan with increasing emissions under acidic conditions and elevated iron concentrations, which are in agreement with model reactions.

Additionally, a significant linear correlation of 2- and 3-methylfurans was observed indicating a mutual precursor and related formation pathways for these substances. Contrary to methylfurans, only 2-alkylfurans were found in natural samples indicating that their precursors are not related to the methylfuran precursor.

Comparison of 2- and 3-methylfurans with the homologous methylthiophene emission further revealed a linear emission relationship. As such a presumed mutual precursor for methylfurans would also be the precursor for the homologous methylthiophenes. Emissions of other sulfur compounds, like carbon disulfide, dimethyl sulfide and dimethyl disulfide were pronounced in circumneutral Australian lakes, where bioactivity was clearly evident as shown

by the red colour. Especially in soil samples from Sodom, Israel, the competitive formation of organosulfur and -selenide compounds was evident from dimethyl selenide, dimethyl selenenyl sulfide and dimethyl diselenide emissions.

Various volatile halogenated compounds were released from the natural samples, most prominent were mono-chlorinated n-alkanes with a C1-C8 carbon chain. The emissions of chloroalkanes, like BTEX, correlated positively with the iron content of the soils/sediments proving a genuine natural abundance. Aside from chloromethane, all polychlorinated methanes, namely dichloromethane, trichloromethane and tetrachloromethane, were found. While the natural abundance of dichloromethane based on the obtained data is ambiguous, tri- and tetrachloromethane were determined at elevated concentrations within acidic Australian sediments. Furthermore, the analysis of sediment gas collected in 2013 from a highly acidic lake in Australia revealed high mixing ratios of chlorinated compounds, including tetrachloromethane. These findings suggest a natural abundance within the acidic salt lake sediments of Western Australia that can not be explained by an anthropogenic input of tetrachloromethane via the gas phase to the sediments. Therefore, acidic salt lakes in Western Australia could be a second genuine non-thermal natural source for tetrachloromethane.

Furthermore, emissions of several chlorinated alkenes were observed from the natural samples. However, only tri- and tetrachloroethene were measured with sufficient frequency for statistical assessments showing a slight correlation with the iron content of the soils/sediments.

Additionally to chlorinated compounds, several brominated, iodinated and mixed halogenated compounds were released from natural samples.

Brominated compounds were especially prominent in the bromide rich soil and water samples of the Dead Sea. In particular, Dead Sea water from the southernmost evaporation pond with highest bromide concentrations was identified as a source for previously detected dibromochloromethane in the Dead Sea boundary layer (Matveev et al., 2001). Additionally, 1,2-dibromoethane, bromodichloromethane and tribromomethane were found to originate from the Dead Sea waters.

Several iodinated compounds were found foremost in Australian sediment samples. A likely source of these compounds was plant detritus found on the shore of smaller lakes, as analysis of this detritus revealed elevated organoiodine emissions.

During the comprehensive study on emissions from natural hypersaline samples, several compounds were identified that had not been found in natural soil/sediment and water samples before. Most notably are measurements of 3-chlorofuran in any kind of natural samples and 3-bromofuran in natural soil/sediment and water samples. Additionally, the abundance of a third halogenated furan species, a chlorinated methylfuran, is postulated based on mass spectra.

Based on natural environment assessments, abiotic halogenation processes by Fenton chemistry are plausible. The hypersaline ecosystems featured mostly Fe^{2+} as the predominant iron species and preliminary semi-quantitative H_2O_2 measurements revealed the formation of this strong oxidant during daytime.

With regard to new particle formation over the Australian salt lakes, the release of atmospheric reactive isoprene, monoterpenes and furans was observed. Additionally, emission of organoiodines mostly from plant detritus could be a source for reactive iodine species over the salt lakes during daytime. First interpretations of time resolved gas sampling within the PTFE chamber suggest that aldehydes and ketones are also involved in particle formation.

As described before several brominated compounds were found in samples of the Dead Sea and Sodom. Photolytic fission of a few brominated molecules could initialise a bromine explosion leading to elevated BrO concentrations in the Dead Sea boundary layer. Although, dichloriodomethane was released from waters of the southern evaporation pond, no significant sources were found for iodinated compounds to explain IO formation over the Dead Sea.

The obtained results provide several starting points for further promising follow up experiments, which are outlined briefly below. Model reactions demonstrated the importance of abiotic reactions yielding volatile compounds and could be further used to unravel underlying mechanisms. As such, the bispidine Fe^{2+} complex with its rigid adamantane backbone and defined coordination sphere is suitable for density functional theory modelling to calculate energetically favourable transition states of the iron species within the investigated reaction.

To further intertwine model reactions and incubation experiments of natural samples, it is conceivable to specify the organic content or at least moieties to select other feasible model compounds. However, these analyses will not be trivial considering the highly saline matrix of the samples. Furthermore, the evolution of the iron species in both experiments is of interest to assess and compare the mechanisms involved.

Emission correlations with geochemical parameters provide additional starting points to investigate a natural formation of compounds like BTEX and chlorinated n-alkanes. Especially, formation of tetrachloromethane under acidic conditions is worth to be investigated in more detail. Preliminary tests by acidification of a circumneutral sediments, not shown here, were promising with regard to increasing chlorination products including tetrachloromethane.

While a total of 69 emitted compounds from natural samples was identified, there are still many unknown volatile compounds recorded by GC-MS analysis.

Furthermore, the fluxes of compounds from the investigated salt lakes under natural conditions need to be assessed to determine their relevance to atmospheric chemistry. So far, incubation experiments, considering elevated temperature common for salt lakes in arid and semi-arid regions (Appendix F), neglected the influence of solar radiation. That solar radiation is an important factor for iron redox cycling and the production of H_2O_2 is not only described in literature, but also evident from the semi-quantitative H_2O_2 measurements on-site. In this regard, on-site measurements of aqueous oxidants like H_2O_2 or RHS are desirable, but not yet available for high saline and acidic solutions with sufficient detection limits. Also the role of microorganisms in natural hypersaline environments as well as in the incubation experiments demands further investigation.

Data on the geochemical inventory and emissions obtained within this work can be further evaluated within smog chamber studies to understand the mechanisms behind ultrafine particle formation over Western Australian salt lakes. Additional insights are likely to be obtained from interpretations of gas samples collected during the campaign in 2013.

Model reactions are a feasible way to assess the potential of abiotic reactions and the mechanisms involved within natural samples. The analysis of natural samples from hypersaline ecosystems is a challenging but very promising task that offers further insights into hitherto less considered areas of the Earth that will become more important with proceeding climate change and secondary salination. This comprehensive study on volatile compounds emitted from Western Australian salt lakes and the Dead Sea demonstrates the potential of hypersaline ecosystems and connects emissions with various geochemical parameters. These milestone results will trigger future investigations in extreme ecosystems to comprehend soil processes in more detail and the interplay between soil and atmosphere.

References

- Addison, D.: Groundwater study of the Lake Grace townsite, Resource Management Technical Report 212, Agriculture Western Australia, Rural Towns Program, 2001.
- Al-Kahali, M. S. N., Ridley, T., Lawley, K. P., Donovan, R. J., Al-Kahali, M. S. N., Ridley, T., Lawley, K. P., and Donovan, R. J.: On the fragmentation of furan molecule and its dependence on the laser wavelength, *Arab. J. Sci. Eng.*, 33, 51-54, 2008.
- Alicke, B., Hebestreit, K., Stutz, J., and Platt, U.: Iodine oxide in the marine boundary layer, *Nature*, 397, 572-573, doi:10.1038/17508, 1999.
- Althoff, F., Jugold, A., and Keppler, F.: Methane formation by oxidation of ascorbic acid using iron minerals and hydrogen peroxide, *Chemosphere*, 80, 286-292, 2010.
- Anbar, M., and Thomas, J. K.: Pulse radiolysis studies of aqueous sodium chloride solutions, *J. Phys. Chem.*, 68, 3829-3835, doi:10.1021/j100794a050, 1964.
- Andreae, M. O.: Ocean-atmosphere interactions in the global biogeochemical sulfur cycle, *Mar. Chem.*, 30, 1-29, doi:10.1016/0304-4203(90)90059-L, 1990.
- Andreae, M. O., and Merlet, P.: Emission of trace gases and aerosols from biomass burning, *Glob. Biogeochem. Cycles*, 15, 955-966, doi:10.1029/2000GB001382, 2001.
- Andreae, M. O., Jones, C. D., and Cox, P. M.: Strong present-day aerosol cooling implies a hot future, *Nature*, 435, 1187-1190, doi:10.1038/nature03671, 2005.
- Andreozzi, R., Caprio, V., Insola, A., and Marotta, R.: Advanced oxidation processes (AOP) for water purification and recovery, *Catal. Today*, 53, 51-59, doi:10.1016/S0920-5861(99)00102-9, 1999.
- Aneja, V. P., and Cooper, W. J.: Biogenic sulfur emissions, in: *Biogenic Sulfur in the Environment*, ACS Symposium Series, American Chemical Society, 2-13, 1989.
- Ångström, A.: Atmospheric turbidity, global illumination and planetary albedo of the earth, *Tellus*, 14, 435-450, doi:10.1111/j.2153-3490.1962.tb01356.x, 1962.
- Anslyn, E. V., and Dougherty, D. A.: *Modern physical organic chemistry*, University Science, 2006.
- Ariyananda, L. M. D., and Norman, R. E.: Tris(2,2'-bipyridyl-N,N')iron(II) bis[tetrachloroferrate(III)], *Acta Crystallographica Section E*, 58, m775-m776, doi:10.1107/S1600536802021773, 2002.
- Atkinson, R., Aschmann, S. M., Carter, W. P. L., and Pitts, J. N.: Rate constants for the gas-phase reaction of OH radicals with a series of ketones at 299 ± 2 K, *Int. J. Chem. Kinet.*, 14, 839-847, doi:10.1002/kin.550140804, 1982.
- Atkinson, R., Aschmann, S. M., and Carter, W. P. L.: Kinetics of the reactions of O₃ and OH radicals with furan and thiophene at 298 ± 2 K, *Int. J. Chem. Kinet.*, 15, 51-61, doi:10.1002/kin.550150106, 1983.
- Atkinson, R., Pitts, J. N., and Aschmann, S. M.: Tropospheric reactions of dimethyl sulfide with nitrogen oxide (NO₃) and hydroxyl radicals, *J. Phys. Chem.*, 88, 1584-1587, doi:10.1021/j150652a029, 1984.
- Atkinson, R.: Kinetics and mechanisms of the gas-phase reactions of the hydroxyl radical with organic compounds under atmospheric conditions, *Chem. Rev.*, 86, 69-201, doi:10.1021/cr00071a004, 1986.

- Atkinson, R., and Aschmann, S. M.: Rate constants for the gas-phase reactions of the OH radical with a series of aromatic hydrocarbons at 296 ± 2 K, *Int. J. Chem. Kinet.*, 21, 355-365, doi:10.1002/kin.550210506, 1989.
- Atkinson, R., Aschmann, S. M., Arey, J., and Carter, W. P. L.: Formation of ring-retaining products from the OH radical-initiated reactions of benzene and toluene, *Int. J. Chem. Kinet.*, 21, 801-827, doi:10.1002/kin.550210907, 1989a.
- Atkinson, R., Aschmann, S. M., Tuazon, E. C., Arey, J., and Zielinska, B.: Formation of 3-methylfuran from the gas-phase reaction of OH radicals with isoprene and the rate constant for its reaction with the OH radical, *Int. J. Chem. Kinet.*, 21, 593-604, doi:10.1002/kin.550210709, 1989b.
- Atkinson, R.: Gas-phase tropospheric chemistry of volatile organic compounds: 1. Alkanes and alkenes, *J. Phys. Chem. Ref. Data*, 26, 215-290, doi:10.1063/1.556012, 1997.
- ATSDR: Toxicological profile for toluene, US Department of Health and Human Services, Agency for Toxic Substances and Disease Registry, Atlanta, 2000.
- Aust, S. D., Morehouse, L. A., and Thomas, C. E.: Role of metals in oxygen radical reactions, *Free Radical. Bio. Med.*, 1, 3-25, doi:10.1016/0748-5514(85)90025-X, 1985.
- Barb, W. G., Baxendale, J. H., George, P., and Hargrave, K. R.: Reactions of ferrous and ferric ions with hydrogen peroxide. Part II.-The ferric ion reaction, *Trans. Faraday Soc.*, 47, 591-616, doi:10.1039/TF9514700591, 1951.
- Barcellos da Rosa, M.: Untersuchungen heterogener troposphärenrelevanter Reaktionen von Schwefel- und Halogenverbindungen, PhD thesis, 2003.
- Barker, J. P., Patrick, G. C., and Major, D.: Natural attenuation of aromatic hydrocarbons in a shallow sand aquifer, *Ground Water Monit. Rem.*, 7, 64-71, doi:10.1111/j.1745-6592.1987.tb01063.x, 1987.
- Barton, A. F. M., Tjandra, J., and Nicholas, P. G.: Chemical evaluation of volatile oils in Eucalyptus species, *J. Agric. Food. Chem.*, 37, 1253-1257, doi:10.1021/jf00089a011, 1989.
- Barton, D. H. R., Hu, B., Taylor, D. K., and Wahl, R. U. R.: The selective functionalization of saturated hydrocarbons. Part 32. Distinction between the Fe-Fe and Fe-Fe manifolds in Gif chemistry. The importance of carboxylic acids for alkane activation. Evidence for a dimeric iron species involved in Gif-type chemistry, *J. Chem. Soc. Perk. T. 2*, 1031-1041, doi:10.1039/P29960001031, 1996.
- Basco, N., and Norrish, R. G. W.: Vibrational dis-equilibrium in reactions between atoms and molecules, *Can. J. Chem.*, 38, 1769-1779, doi:10.1139/v60-242, 1960.
- Bautz, J., Comba, P., Lopez de Laorden, C., Menzel, M., and Rajaraman, G.: Biomimetic high-valent non-heme iron oxidants for the cis-dihydroxylation and epoxidation of olefins, *Angew. Chem. Int. Edit.*, 46, 8067-8070, doi:10.1002/anie.200701681, 2007.
- Becker, K. H., Brockmann, K. J., and Bechara, J.: Production of hydrogen peroxide in forest air by reaction of ozone with terpenes, *Nature*, 346, 256-258, doi:10.1038/346256a0, 1990.
- Benk, S.: Untersuchung leichtflüchtiger Kohlenwasserstoffe in südwestaustralischen Salzseen mittels GC-FID, Master thesis, 2013.
- Benson, B. B., and Krause Jr, D.: The concentration and isotopic fractionation of oxygen dissolved in freshwater and seawater in equilibrium with the atmosphere, *Limnol. Oceanogr.*, 29, 620-632, 1984.

- Bentor, Y. K.: Some geochemical aspects of the Dead Sea and the question of its age, *Geochim. Cosmochim. Acta*, 25, 239-260, 1961.
- Berndt, T., Böge, O., and Rolle, W.: Products of the gas-phase reactions of NO₃ radicals with furan and tetramethylfuran, *Environ. Sci. Technol.*, 31, 1157-1162, doi:10.1021/es960669z, 1997.
- Berndt, T., and Boge, O.: Gas-phase reaction of OH radicals with benzene: products and mechanism, *Phys. Chem. Chem. Phys.*, 3, 4946-4956, doi:10.1039/B106667F, 2001.
- Bierbach, A., Barnes, I., and Becker, K. H.: Rate coefficients for the gas-phase reactions of hydroxyl radicals with furan, 2-methylfuran, 2-ethylfuran and 2,5-dimethylfuran at 300 ± 2 K, *Atmos. Environ. a-Gen.*, 26, 813-817, doi:10.1016/0960-1686(92)90241-C, 1992.
- Bierbach, A., Barnes, I., and Becker, K. H.: Product and kinetic study of the OH-initiated gas-phase oxidation of furan, 2-methylfuran and furanaldehydes at ≈ 300 K, *Atmos. Environ.*, 29, 2651-2660, doi:10.1016/1352-2310(95)00096-H, 1995.
- Borowitzka, L. J., and Borowitzka, M. A.: Commercial production of β-carotene by *Dunaliella salina* in open ponds, *Bull. Mar. Sci.*, 47, 244-252, 1990.
- Börzel, H., Comba, P., Hagen, K. S., Lampeka, Y. D., Lienke, A., Linti, G., Merz, M., Pritzkow, H., and Tsymbal, L. V.: Iron coordination chemistry with tetra-, penta- and hexadentate bispidine-type ligands, *Inorg. Chim. Acta*, 337, 407-419, doi:10.1016/S0020-1693(02)01100-3, 2002.
- Bowen, B. B., and Benison, K. C.: Geochemical characteristics of naturally acid and alkaline saline lakes in southern Western Australia, *Appl. Geochem.*, 24, 268-284, doi:10.1016/j.apgeochem.2008.11.013, 2009.
- Bozau, E.: Prozessmodellierung hochsalinärer Wässer mit einem erweiterten PHREEQC-Datensatz, *Grundwasser*, 18, 93-98, doi:10.1007/s00767-013-0222-8, 2013.
- Braimbridge, M., and Commander, P.: The Wheatbelt's ancient rivers, *Water notes*, 34, 2005.
- Bravo-Linares, C. M., Mudge, S. M., and Loyola-Sepulveda, R. H.: Occurrence of volatile organic compounds (VOCs) in Liverpool Bay, Irish Sea, *Mar. Pollut. Bull.*, 54, 1742-1753, doi:10.1016/j.marpolbul.2007.07.013, 2007.
- Bray, W. C., and Liebafsky, H. A.: Reactions involving hydrogen peroxide, iodine and iodate ion. I. Introduction, *J. Am. Chem. Soc.*, 53, 38-44, doi:10.1021/ja01352a006, 1931.
- Bray, W. C., and Gorin, M. H.: Ferryl ion, a compound of tetravalent iron, *J. Am. Chem. Soc.*, 54, 2124-2125, doi:10.1021/ja01344a505, 1932.
- Bukowski, M. R., Comba, P., Lienke, A., Limberg, C., de Laorden, C. L., Mas-Balleste, R., Merz, M., and Que, L.: Catalytic epoxidation and 1,2-dihydroxylation of olefins with bispidine-iron(II)/H₂O₂ systems, *Angew. Chem. Int. Edit.*, 45, 3446-3449, doi:10.1002/anie.200504357, 2006.
- Cabañas, B., Villanueva, F., Martín, P., Baeza, M. T., Salgado, S., and Jiménez, E.: Study of reaction processes of furan and some furan derivatives initiated by Cl atoms, *Atmos. Environ.*, 39, 1935-1944, doi:10.1016/j.atmosenv.2004.12.013, 2005.
- Cai, X., and Griffin, R. J.: Secondary aerosol formation from the oxidation of biogenic hydrocarbons by chlorine atoms, *J. Geophys. Res.-Atmos.*, 111, D14206, doi:10.1029/2005JD006857, 2006.

- Cai, X., Ziemba, L. D., and Griffin, R. J.: Secondary aerosol formation from the oxidation of toluene by chlorine atoms, *Atmos. Environ.*, 42, 7348-7359, doi:10.1016/j.atmosenv.2008.07.014, 2008.
- Camilli, R., Reddy, C. M., Yoerger, D. R., Van Mooy, B. A. S., Jakuba, M. V., Kinsey, J. C., McIntyre, C. P., Sylva, S. P., and Maloney, J. V.: Tracking hydrocarbon plume transport and biodegradation at Deepwater Horizon, *Science*, 330, 201-204, doi:10.1126/science.1195223, 2010.
- Carlton, A. G., Wiedinmyer, C., and Kroll, J. H.: A review of secondary organic aerosol (SOA) formation from isoprene, *Atmos. Chem. Phys.*, 9, 4987-5005, doi:10.5194/acp-9-4987-2009, 2009.
- Carpenter, L. J., Sturges, W. T., Penkett, S. A., Liss, P. S., Alicke, B., Hebestreit, K., and Platt, U.: Short-lived alkyl iodides and bromides at Mace Head, Ireland: Links to biogenic sources and halogen oxide production, *J. Geophys. Res.-Atmos.*, 104, 1679-1689, doi:10.1029/98JD02746, 1999.
- Carter, W. P. L.: Updated maximum incremental reactivity scale and hydrocarbon bin reactivities for regulatory applications, California Air Resources Board Contract 07-339, 2009.
- Chapuis-Lardy, L., Contour-Ansel, D., and Bernhard-Reversat, F.: High-performance liquid chromatography of water-soluble phenolics in leaf litter of three Eucalyptus hybrids (Congo), *Plant Sci.*, 163, 217-222, doi:10.1016/S0168-9452(02)00099-7, 2002.
- Charlson, R. J., Lovelock, J. E., Andreae, M. O., and Warren, S. G.: Oceanic phytoplankton, atmospheric sulphur, cloud albedo and climate, *Nature*, 326, 655-661, doi:10.1038/326655a0, 1987.
- Charlson, R. J., Schwartz, S. E., Hales, J. M., Cess, R. D., Coakley, J. A., Hansen, J. E., and Hofmann, D. J.: Climate forcing by anthropogenic aerosols, *Science*, 255, 423-430, doi:10.1126/science.255.5043.423, 1992.
- Chatfield, R. B.: Anomalous HNO₃/NO_x ratio of remote tropospheric air: Conversion of nitric acid to formic acid and NO_x?, *Geophys. Res. Lett.*, 21, 2705-2708, doi:10.1029/94GL02659, 1994.
- Chebуркин, A. K., Frei, R., and Shotyk, W.: An energy-dispersive miniprobe multielement analyzer (EMMA) for direct analysis of trace elements and chemical age dating of single mineral grains, *Chem. Geol.*, 135, 75-87, doi:10.1016/S0009-2541(96)00105-2, 1997.
- Chebуркин, A. K., and Shotyk, W.: Energy-dispersive XRF spectrometer for Ti determination (TITAN), *X-Ray Spectrom.*, 34, 69-72, doi:10.1002/xrs.766, 2005.
- Christian, T. J., Kleiss, B., Yokelson, R. J., Holzinger, R., Crutzen, P. J., Hao, W. M., Saharjo, B. H., and Ward, D. E.: Comprehensive laboratory measurements of biomass-burning emissions: 1. Emissions from Indonesian, African, and other fuels, *J. Geophys. Res.-Atmos.*, 108, 4719, doi:10.1029/2003JD003704, 2003.
- Claeys, M., Graham, B., Vas, G., Wang, W., Vermeylen, R., Pashynska, V., Cafmeyer, J., Guyon, P., Andreae, M. O., Artaxo, P., and Maenhaut, W.: Formation of secondary organic aerosols through photooxidation of isoprene, *Science*, 303, 1173-1176, doi:10.1126/science.1092805, 2004.
- Comba, P., Rajaraman, G., and Rohwer, H.: A density functional theory study of the reaction of the biomimetic iron(II) complex of a tetradentate bispidine ligand with H₂O₂, *Inorganic Chem.*, 46, 3826-3838, doi:10.1021/ic061129y, 2007.

- Comba, P., Maurer, M., and Vadivelu, P.: Oxidation of cyclohexane by a high-valent iron bispidine complex: A combined experimental and computational mechanistic study, *J. Phys. Chem. A*, 112, 13028-13036, doi:10.1021/jp8037895, 2008.
- Comba, P., Maurer, M., and Vadivelu, P.: Oxidation of cyclohexane by high-valent iron bispidine complexes: Tetradentate versus pentadentate ligands, *Inorganic Chem.*, 48, 10389-10396, doi:10.1021/ic901702s, 2009.
- Comba, P., Fukuzumi, S., Kotani, H., and Wunderlich, S.: Electron-transfer properties of an efficient nonheme iron oxidation catalyst with a tetradentate bispidine ligand, *Angew. Chem. Int. Edit.*, 49, 2622-2625, doi:10.1002/anie.200904427, 2010.
- Comba, P., and Wunderlich, S.: Iron-catalyzed halogenation of alkanes: Modeling of nonheme halogenases by experiment and DFT calculations, *Chem. Eur. J.*, 16, 7293-7299, doi:10.1002/chem.201000092, 2010.
- Comba, P., Wadepohl, H., and Wunderlich, S.: Oxidation versus dioxygenation of catechol: The iron-bispidine system, *Eur. J. Inorg. Chem.*, 2011, 5242-5249, doi:10.1002/ejic.201100802, 2011.
- Connick, R. E.: The interaction of hydrogen peroxide and hypochlorous acid in acidic solutions containing chloride ion, *J. Am. Chem. Soc.*, 69, 1509-1514, doi:10.1021/ja01198a074, 1947.
- Cooper, W. J., Zika, R. G., Petasne, R. G., and Plane, J. M. C.: Photochemical formation of hydrogen peroxide in natural waters exposed to sunlight, *Environ. Sci. Technol.*, 22, 1156-1160, doi:10.1021/es00175a004, 1988.
- Copper, C. L., and Koubek, E.: A kinetics experiment to demonstrate the role of a catalyst in a chemical reaction: A versatile exercise for general or physical chemistry students, *J. Chem. Educ.*, 75, 87, doi:10.1021/ed075p87, 1998.
- Corchnoy, S. B., and Atkinson, R.: Kinetics of the gas-phase reactions of hydroxyl and nitrogen oxide (NO₃) radicals with 2-carene, 1,8-cineole, p-cymene, and terpinolene, *Environ. Sci. Technol.*, 24, 1497-1502, doi:10.1021/es00080a007, 1990.
- Davies, C. W.: Ion association, Butterworths, London, 1962.
- Debye, P., and Hückel, E.: Zur Theorie der Elektrolyte. I. Gefrierpunktserniedrigung und verwandte Erscheinungen, *Phys. Z.*, 24, 185-206, 1923.
- Degens, B., and Shand, P.: Assessment of acidic saline groundwater hazard in the Western Australian Wheatbelt: Yarra Yarra, Blackwood and South Coast, CSIRO: Water for a Healthy Country National Research Flagship., Perth, 2010.
- Dencher, N. A.: The five retinal-protein pigments of Halobacteria: bacteriorhodopsin, halorhodopsin, P 565, P 370, and slow-cycling rhodopsin, *Photoch. Photobio. Sci.*, 38, 753-768, doi:10.1111/j.1751-1097.1983.tb03611.x, 1983.
- Deng, Y., and Zuo, Y.: Factors affecting the levels of hydrogen peroxide in rainwater, *Atmos. Environ.*, 33, 1469-1478, doi:10.1016/S1352-2310(98)00239-8, 1999.
- Department of Water: Waterway assessment of the upper Lockhart River: Camm River confluence to Newdegate, Water resource management series, WRM 58, 2009a.
- Department of Water: Waterway assessment of the Camm River: Lockhart River confluence to Hyden, Water resource management series, WRM 57, 2009b.
- Draper, W., and Crosby, D.: The photochemical generation of hydrogen peroxide in natural waters, *Arch. Environ. Contam. Toxicol.*, 12, 121-126, doi:10.1007/BF01055010, 1983.

- Drobner, E., Huber, H., Wächtershäuser, G., Rose, D., and Stetter, K. O.: Pyrite formation linked with hydrogen evolution under anaerobic conditions, *Nature*, 346, 742-744, doi:10.1038/346742a0, 1990.
- Dumdei, B. E., Kenny, D. V., Shepson, P. B., Kleindienst, T. E., Nero, C. M., Cupitt, L. T., and Claxton, L. D.: MS/MS analysis of the products of toluene photooxidation and measurement of their mutagenic activity, *Environ. Sci. Technol.*, 22, 1493-1498, doi:10.1021/es00177a017, 1988.
- Durmusoglu, E., Taspinar, F., and Karademir, A.: Health risk assessment of BTEX emissions in the landfill environment, *J. Hazard. Mater.*, 176, 870-877, doi:10.1016/j.jhazmat.2009.11.117, 2010.
- Easterling, D. R., Meehl, G. A., Parmesan, C., Changnon, S. A., Karl, T. R., and Mearns, L. O.: Climate extremes: Observations, modelling, and impacts, *Science*, 289, 2068-2074, doi:10.1126/science.289.5487.2068, 2000.
- Edwards, E. A., Wills, L. E., Reinhard, M., and Grbicgalic, D.: Anaerobic degradation of toluene and xylene by aquifer microorganisms under sulfate-reducing conditions, *Appl. Environ. Microbiol.*, 58, 794-800, 1992.
- Emmerich, M., Bhansali, A., Lösekann-Behrens, T., Schröder, C., Kappler, A., and Behrens, S.: Abundance, Distribution, and Activity of Fe(II)-Oxidizing and Fe(III)-Reducing Microorganisms in Hypersaline Sediments of Lake Kasin, Southern Russia, *Appl. Environ. Microbiol.*, 78, 4386-4399, doi:10.1128/aem.07637-11, 2012.
- Enzel, Y., Bookman, R., Sharon, D., Gvirtzman, H., Dayan, U., Ziv, B., and Stein, M.: Late Holocene climates of the Near East deduced from Dead Sea level variations and modern regional winter rainfall, *Quaternary Res.*, 60, 263-273, 2003.
- Esau, I. N., and Lyons, T. J.: Effect of sharp vegetation boundary on the convective atmospheric boundary layer, *Agr. Forest Meteorol.*, 114, 3-13, doi:10.1016/S0168-1923(02)00154-5, 2002.
- España, J. S., and Ercilla, M. D.: Geochemical modeling of concentrated mine waters: A comparison of the Pitzer ion-interaction theory with the ion-association model for the study of melanterite solubility in San Telmo mine, in: *Geochemistry Research Advances*, edited by: Stefánsson, Ó., Nova Science Publishers, Inc., New York, 31-55, 2008.
- Evans, M. G., Hush, N. S., and Uri, N.: The energetics of reactions involving hydrogen peroxide, its radicals, and its ions, *Q. Rev. Chem. Soc.*, 6, 186-196, doi:10.1039/QR9520600186 1952.
- Fahimi, I. J., Keppler, F., and Schöler, H. F.: Formation of chloroacetic acids from soil, humic acid and phenolic moieties, *Chemosphere*, 52, 513-520, doi:10.1016/S0045-6535(03)00212-1, 2003.
- Falkowski, P., Scholes, R. J., Boyle, E., Canadell, J., Canfield, D., Elser, J., Gruber, N., Hibbard, K., Höglberg, P., Linder, S., Mackenzie, F. T., Moore Iii, B., Pedersen, T., Rosenthal, Y., Seitzinger, S., Smetacek, V., and Steffen, W.: The global carbon cycle: A test of our knowledge of Earth as a system, *Science*, 290, 291-296, doi:10.1126/science.290.5490.291, 2000.
- Faust, B. C., Anastasio, C., Allen, J. M., and Arakaki, T.: Aqueous-phase photochemical formation of peroxides in authentic cloud and fog waters, *J. Geophys. Res.-Atmos.*, 260, 73-75, doi:10.1126/science.8465202, 1993.

- Fenton, H. J. H.: LXXIII.-Oxidation of tartaric acid in presence of iron, *J. Chem. Soc. Faraday T.*, 65, 899-910, doi:10.1039/CT8946500899, 1894.
- Finkelstein, H.: Darstellung organischer Jodide aus den entsprechenden Bromiden und Chloriden, *Ber. Dtsch. Chem. Ges.*, 43, 1528-1532, doi:10.1002/cber.19100430257, 1910.
- Fitzpatrick, R., and Shand, P.: Inland acid sulfate soil systems across Australia, CRC LEME Open File Report, CRC LEME, Perth, 2008.
- Fofonoff, N. P., and Millard Jr, R. C.: Calculation of physical properties of seawater, *WHP Operations and Methods*, 1-15, 1991.
- Foti, M., Sorokin, D. Y., Lomans, B., Mussman, M., Zacharova, E. E., Pimenov, N. V., Kuenen, J. G., and Muyzer, G.: Diversity, activity, and abundance of sulfate-reducing bacteria in saline and hypersaline soda lakes, *Appl. Environ. Microbiol.*, 73, 2093-2100, doi:10.1128/aem.02622-06, 2007.
- Franco, M., Chairez, I., Poznyak, T., and Poznyak, A.: BTEX decomposition by ozone in gaseous phase, *J. Environ. Manage.*, 95, Supplement, S55-S60, doi:10.1016/j.jenvman.2011.09.009, 2012.
- Frieß, U., Hollwedel, J., König-Langlo, G., Wagner, T., and Platt, U.: Dynamics and chemistry of tropospheric bromine explosion events in the Antarctic coastal region, *J. Geophys. Res.-Atmos.*, 109, doi:10.1029/2003JD004133, 2004.
- Fudge, A. J., and Sykes, K. W.: 25. The reaction between ferric and iodide ions. Part I. Kinetics and mechanism, *J. Chem. Soc.*, 119-124, doi:10.1039/JR9520000119, 1952.
- Furchner, M.: Charakterisierung des Brenner Moores Bad Oldesloe hinsichtlich seiner chemischen Zusammensetzung und mit Hinblick auf natürlich abiotisch gebildete Organohalogenverbindungen, Bachelor thesis, 2011.
- Fuson, R. C., and Bull, B. A.: The haloform reaction, *Chem. Rev.*, 15, 275-309, doi:10.1021/cr60052a001, 1934.
- Galloway, P.: Agricultural sub-regions of the Avon River Basin, Resource Management Technical Report 284, Department of Agriculture, 2004.
- Gardner, L. K., and Lawrence, G. D.: Benzene production from decarboxylation of benzoic acid in the presence of ascorbic acid and a transition-metal catalyst, *J. Agric. Food. Chem.*, 41, 693-695, doi:10.1021/jf00029a001, 1993.
- Geddes, M. C., Deckker, P., Williams, W. D., Morton, D. W., and Topping, M.: 17. On the chemistry and biota of some saline lakes in Western Australia, *Hydrobiologia*, 81-82, 201-222, doi:10.1007/BF00048717, 1981.
- Ghuri, S.: Groundwater trends in the central agricultural region, Resource Management Technical Report 269, Department of Agriculture, 2004.
- Goldstein, S., Meyerstein, D., and Czapski, G.: The Fenton reagents, *Free Radic. Biol. Med.*, 15, 435-445, doi:10.1016/0891-5849(93)90043-T, 1993.
- Goldstein, S., and Meyerstein, D.: Comments on the mechanism of the "Fenton-Like" reaction, *Acc. Chem. Res.*, 32, 547-550, doi:10.1021/ar9800789, 1999.
- Gómez Alvarez, E., Borrás, E., Viidanoja, J., and Hjorth, J.: Unsaturated dicarbonyl products from the OH-initiated photo-oxidation of furan, 2-methylfuran and 3-methylfuran, *Atmos. Environ.*, 43, 1603-1612, doi:10.1016/j.atmosenv.2008.12.019, 2009.

- Gossett, J. M.: Measurement of Henry's law constants for C1 and C2 chlorinated hydrocarbons, *Environ. Sci. Technol.*, 21, 202-208, doi:10.1021/es00156a012, 1987.
- Gozzo, F.: Radical and non-radical chemistry of the Fenton-like systems in the presence of organic substrates, *J. Mol. Catal. A-Chem.*, 171, 1-22, doi:10.1016/S1381-1169(01)00099-1, 2001.
- Grathoff, G. H., Baham, J. E., Easterly, H. R., Gassman, P., and Hugo, R. C.: Mixed-valent Fe Films ('Schwimmeisen') on the surface of reduced ephemeral pools, *Clays Clay Miner.*, 55, 635-643, doi:10.1346/ccmn.2007.0550610, 2007.
- Gratzel, M., and Halmann, M.: Photosensitized oxidation of bromide in dead sea water, *Mar. Chem.*, 29, 169-182, 1990.
- Grebel, J. E., Pignatello, J. J., and Mitch, W. A.: Effect of halide ions and carbonates on organic contaminant degradation by hydroxyl radical-based advanced oxidation processes in saline waters, *Environ. Sci. Technol.*, 44, 6822-6828, doi:10.1021/es1010225, 2010.
- Gribble, G. W.: Naturally occurring organohalogen compounds - a comprehensive update, Springer-Verlag Wien, 2009.
- Gribble, G. W.: Naturally occurring organohalogen compounds - a comprehensive survey, *Fortschritte der Chemie organischer Naturstoffe / Progress in the Chemistry of Organic Natural Products*, edited by: A. D. Kinghorn, H. Falk, J. Kobayashi, and W. Herz, Springer Vienna, Vienna, 1-613 pp., 2010.
- Grossweiner, L. I., and Matheson, M. S.: The kinetics of the dihalide ions from the flash photolysis of aqueous alkali halide solutions, *J. Phys. Chem.*, 61, 1089-1095, doi:10.1021/j150554a013, 1957.
- Gu, C. L., Rynard, C. M., Hendry, D. G., and Mill, T.: Hydroxyl radical oxidation of isoprene, *Environ. Sci. Technol.*, 19, 151-155, doi:10.1021/es00132a007, 1985.
- Guenther, A., Karl, T., Harley, P., Wiedinmyer, C., Palmer, P. I., and Geron, C.: Estimates of global terrestrial isoprene emissions using MEGAN (Model of Emissions of Gases and Aerosols from Nature), *Atmos. Chem. Phys.*, 6, 3181-3210, doi:10.5194/acp-6-3181-2006, 2006.
- Haber, F., and Weiss, J.: Über die Katalyse des Hydroperoxydes, *Naturwissenschaften*, 20, 948-950, doi:10.1007/BF01504715, 1932.
- Hamilton, J. F., Webb, P. J., Lewis, A. C., and Reviejo, M. M.: Quantifying small molecules in secondary organic aerosol formed during the photo-oxidation of toluene with hydroxyl radicals, *Atmos. Environ.*, 39, 7263-7275, doi:10.1016/j.atmosenv.2005.09.006, 2005.
- Hanson, D. R., Ravishankara, A. R., and Lovejoy, E. R.: Reaction of BrONO₂ with H₂O on submicron sulfuric acid aerosol and the implications for the lower stratosphere, *J. Geophys. Res.-Atmos.*, 101, 9063-9069, doi:10.1029/96JD00347, 1996.
- Harrison, R. M., Peak, J. D., and Collins, G. M.: Tropospheric cycle of nitrous acid, *J. Geophys. Res.-Atmos.*, 101, 14429-14439, doi:10.1029/96JD00341, 1996.
- Hassoun, B. S., Palmer, I. S., and Dwivedi, C.: Selenium detoxification by methylation, *Res. Commun. Mol. Path.*, 90, 133-142, 1995.
- Haylock, M., and Nicholls, N.: Trends in extreme rainfall indices for an updated high quality data set for Australia, 1910–1998, *Int. J. Climatol.*, 20, 1533-1541, doi:10.1002/1097-0088(20001115)20:13<1533::AID-JOC586>3.0.CO;2-J, 2000.

- Hebestreit, K., Stutz, J., Rosen, D., Matveiv, V., Peleg, M., Luria, M., and Platt, U.: DOAS measurements of tropospheric bromine oxide in mid-latitudes, *Science*, 283, 55-57, doi:10.1126/science.283.5398.55, 1999.
- Heiden, A. C., Kobel, K., Komenda, M., Koppmann, R., Shao, M., and Wildt, J.: Toluene emissions from plants, *Geophys. Res. Lett.*, 26, 1283-1286, doi:10.1029/1999GL900220, 1999.
- Hempfling, R., and Schulten, H. R.: Chemical characterization of the organic matter in forest soils by Curie point pyrolysis-GC/MS and pyrolysis-field ionization mass spectrometry, *Org. Geochem.*, 15, 131-145, doi:10.1016/0146-6380(90)90078-E, 1990.
- Hjorth, T.: Effects of freeze-drying on partitioning patterns of major elements and trace metals in lake sediments, *Analytica Chimica Acta*, 526, 95-102, doi:10.1016/j.aca.2004.08.007, 2004.
- Hoekstra, E. J., de Leer, E. W. B., and Brinkman, U. A. T.: Findings supporting the natural formation of trichloroacetic acid in soil, *Chemosphere*, 38, 2875-2883, doi:10.1016/S0045-6535(98)00487-1, 1999.
- Hoffmann, A.: Boden- und Wasserchemie des Brenner Moors sowie die Bildung von abiotisch halogenierten Kohlenwasserstoffen Bachelor thesis, 2011.
- Holla, R.: Reactive halogen species above salt lakes and salt pans PhD thesis, 2013.
- Hookey, G. R.: Prediction of delays in groundwater response to catchment clearing, *J. Hydrol.*, 94, 181-198, doi:10.1016/0022-1694(87)90039-4, 1987.
- Huang, C. P., Dong, C., and Tang, Z.: Advanced chemical oxidation: Its present role and potential future in hazardous waste treatment, *Waste Manage.*, 13, 361-377, doi:10.1016/0956-053X(93)90070-D, 1993.
- Huber, S. G., Kilian, G., and Schöler, H. F.: Carbon suboxide, a highly reactive intermediate from the abiotic degradation of aromatic compounds in soil, *Environ. Sci. Technol.*, 41, 7802-7806, doi:10.1021/es071530z, 2007.
- Huber, S. G., Kotte, K., Schöler, H. F., and Williams, J.: Natural abiotic formation of trihalomethanes in soil: Results from laboratory studies and field samples, *Environ. Sci. Technol.*, 43, 4934-4939, doi:10.1021/es8032605, 2009.
- Huber, S. G.: Formation of volatile organic compounds by natural oxidation processes in soil PhD thesis, 2010.
- Huber, S. G., Wunderlich, S., Schöler, H. F., and Williams, J.: Natural abiotic formation of furans in soil, *Environ. Sci. Technol.*, 44, 5799-5804, doi:10.1021/es100704g, 2010.
- Hunsdiecker, H., and Hunsdiecker, C.: Über den Abbau der Salze aliphatischer Säuren durch Brom, *Ber. Dtsch. Chem. Ges. (A and B Series)*, 75, 291-297, doi:10.1002/cber.19420750309, 1942.
- Hurley, M. D., Sokolov, O., Wallington, T. J., Takekawa, H., Karasawa, M., Klotz, B. r., Barnes, I., and Becker, K. H.: Organic aerosol formation during the atmospheric degradation of toluene, *Environ. Sci. Technol.*, 35, 1358-1366, doi:10.1021/es0013733, 2001.
- Hynes, A. J., Wine, P. H., and Nicovich, J. M.: Kinetics and mechanism of the reaction of hydroxyl with carbon disulfide under atmospheric conditions, *J. Phys. Chem.*, 92, 3846-3852, doi:10.1021/j100324a034, 1988.
- Isidorov, V., and Jdanova, M.: Volatile organic compounds from leaves litter, *Chemosphere*, 48, 975-979, doi:10.1016/S0045-6535(02)00074-7, 2002.

- Isidorov, V. A., Zenkevich, I. G., and Ioffe, B. V.: Volatile organic compounds in the atmosphere of forests, *Atmos. Environ.* (1967), 19, 1-8, doi:10.1016/0004-6981(85)90131-3, 1985.
- Jacob, M., Comba, P., Maurer, M., Vadivelu, P., and Venuvanalingam, P.: A combined experimental and computational study on the sulfoxidation by high-valent iron bispidine complexes, *Dalton Trans.*, 40, 11276-11281, doi:10.1039/C1DT11533B, 2011.
- Jang, M., and Kamens, R. M.: Atmospheric secondary aerosol formation by heterogeneous reactions of aldehydes in the presence of a sulfuric acid aerosol catalyst, *Environ. Sci. Technol.*, 35, 4758-4766, doi:10.1021/es010790s, 2001.
- Jang, M., Czoschke, N. M., Lee, S., and Kamens, R. M.: Heterogeneous atmospheric aerosol production by acid-catalyzed particle-phase reactions, *Science*, 298, 814-817, doi:10.1126/science.1075798, 2002.
- Jayson, G. G., Parsons, B. J., and Swallow, A. J.: Some simple, highly reactive, inorganic chlorine derivatives in aqueous solution. Their formation using pulses of radiation and their role in the mechanism of the Fricke dosimeter, *J. Chem. Soc. Farad. T. 1*, 69, 1597-1607, doi:10.1039/F19736901597 1973.
- Jimenez, J. L., Bahreini, R., Cocker, D. R., Zhuang, H., Varutbangkul, V., Flagan, R. C., Seinfeld, J. H., O'Dowd, C. D., and Hoffmann, T.: New particle formation from photooxidation of diiodomethane (CH₂I₂), *J. Geophys. Res.-Atmos.*, 108, 2003.
- Johnson, G. R. A., Nazhat, N. B., and Saadalla-Nazhat, R. A.: Reaction of the aquocopper(I) ion with hydrogen peroxide: evidence against hydroxyl free radical formation, *J. Chem. Soc. Chem. Comm.*, 407-408, doi:10.1039/C39850000407, 1985.
- Jones, B. M. R., Cox, R. A., and Penkett, S. A.: Atmospheric chemistry of carbon disulphide, *J. Atmos. Chem.*, 1, 65-86, doi:10.1007/BF00113980, 1983.
- Jones, C., Crowe, S. A., Sturm, A., Leslie, K. L., MacLean, L. C. W., Katsev, S., Henny, C., Fowle, D. A., and Canfield, D. E.: Biogeochemistry of manganese in ferruginous Lake Matano, Indonesia, *Biogeosciences*, 8, 2977-2991, 2011.
- Jordan, E. D., Hsieh, T. C. Y., and Fischer, N. H.: Volatiles from litter and soil associated with *Ceratiola ericoides*, *Phytochemistry*, 33, 299-302, doi:10.1016/0031-9422(93)85507-N, 1993.
- Junkermann, W., Hacker, J., Lyons, T., and Nair, U.: Land use change suppresses precipitation, *Atmos. Chem. Phys.*, 9, 6531-6539, doi:10.5194/acp-9-6531-2009, 2009.
- Kamilli, K., Ofner, J., Sattler, T., Krause, T., Zetzsch, C., and Held, A.: Particle formation above natural and simulated salt lakes, *Geophys. Res. Abstr. - EGU General Assembly 2013*, 15, 2013.
- Kamilli, K., Ofner, J., Sattler, T., Krause, T., and Held, A.: Particle formation above natural and simulated salt lakes, *Geophysical Research Abstracts - EGU General Assembly 2014*, 2014.
- Karlsson, R. S., Szente, J. J., Ball, J. C., and Maricq, M. M.: Homogeneous aerosol formation by the chlorine atom initiated oxidation of toluene, *J. Phys. Chem. A*, 105, 82-96, doi:10.1021/jp001831u, 2000.
- Katritzky, A. R., Lobanov, V. S., and Karelson, M.: Normal boiling points for organic compounds: Correlation and prediction by a quantitative structure–property relationship, *J. Chem. Inf. Comput. Sci.*, 38, 28-41, doi:10.1021/ci970029v, 1998.

- Kellogg, W. W., Cadle, R. D., Allen, E. R., Lazrus, A. L., and Martell, E. A.: The sulfur cycle, *Science*, 175, 587-596, doi:10.1126/science.175.4022.587, 1972.
- Keppler, F., Eiden, R., Niedan, V., Pracht, J., and Schöler, H. F.: Halocarbons produced by natural oxidation processes during degradation of organic matter, *Nature*, 403, 298-301, doi:10.1038/35002055, 2000.
- Keppler, F., Borchers, R., Pracht, J., Rheinberger, S., and Schöler, H. F.: Natural formation of vinyl chloride in the terrestrial environment, *Environ. Sci. Technol.*, 36, 2479-2483, doi:10.1021/es0156111, 2002.
- Keppler, F., Borchers, R., Elsner, P., Fahimi, I., Pracht, J., and Schöler, H. F.: Formation of volatile iodinated alkanes in soil: results from laboratory studies, *Chemosphere*, 52, 477-483, doi:10.1016/S0045-6535(03)00198-X, 2003.
- Keppler, F., Borchers, R., Hamilton, J. T. G., Kilian, G., Pracht, J., and Schöler, H. F.: De novo formation of chloroethyne in soil, *Environ. Sci. Technol.*, 40, 130-134, doi:10.1021/es0513279, 2006.
- Kesner, M.: Bromine and bromine compounds from the Dead Sea, Israel - Products in the service of people, edited by: Simons, J., and Ram, S., The Department of Science and Teaching, The Weizmann Institute of Science, 1999.
- Kesselmeier, J., and Staudt, M.: Biogenic volatile organic compounds (VOC): An overview on emission, physiology and ecology, *J. Atmos. Chem.*, 33, 23-88, doi:10.1023/A:1006127516791, 1999.
- Kessick, M. A., and Morgan, J. J.: Mechanism of autoxidation of manganese in aqueous solution, *Environ. Sci. Technol.*, 9, 157-159, doi:10.1021/es60100a008, 1975.
- Khain, A., Rosenfeld, D., and Pokrovsky, A.: Aerosol impact on the dynamics and microphysics of deep convective clouds, *Q. J. Roy. Meteor. Soc.*, 131, 2639-2663, doi:10.1256/qj.04.62, 2005.
- Khalil, M. A. K., and Rasmussen, R. A.: Global sources, lifetimes and mass balances of carbonyl sulfide (OCS) and carbon disulfide (CS₂) in the earth's atmosphere, *Atmos. Environ.* (1967), 18, 1805-1813, doi:10.1016/0004-6981(84)90356-1, 1984.
- Kiehl, J. T., and Briegleb, B. P.: The relative roles of sulfate aerosols and greenhouse gases in climate forcing, *Science*, 260, 311-314, doi:10.1126/science.260.5106.311, 1993.
- Kim, S.-M., and Vogelpohl, A.: Degradation of organic pollutants by the photo-Fenton-process, *Chemical Engineering & Technology*, 21, 187-191, doi:10.1002/(SICI)1521-4125(199802)21:2<187::AID-CEAT187>3.0.CO;2-H, 1998.
- Kind, I., Berndt, T., Böge, O., and Rolle, W.: Gas-phase rate constants for the reaction of NO₃ radicals with furan and methyl-substituted furans, *Chem. Phys. Lett.*, 256, 679-683, doi:10.1016/0009-2614(96)00513-1, 1996.
- Kiwi, J., Lopez, A., and Nadochenko, V.: Mechanism and Kinetics of the OH-Radical Intervention during Fenton Oxidation in the Presence of a Significant Amount of Radical Scavenger (Cl⁻), *Environ. Sci. Technol.*, 34, 2162-2168, doi:10.1021/es991406i, 2000.
- Klein, C., and Flohn, H.: Contributions to the knowledge of the fluctuations of the Dead Sea level, *Theor. Appl. Climatol.*, 38, 151-156, 1987.
- Koenigs, J.: Production of hydrogen peroxide by wood-rotting fungi in wood and its correlation with weight loss, depolymerization, and pH changes, *Arch. Microbiol.*, 99, 129-145, doi:10.1007/BF00696229, 1974.

- Kogel, J. E., and Society for Mining Metallurgy and Exploration: Industrial minerals & rocks: Commodities, markets, and uses, Society for Mining, Metallurgy, and Exploration, 2006.
- Kok, G. L., Darnall, K. R., Winer, A. M., Pitts, J. N., and Gay, B. W.: Ambient air measurements of hydrogen peroxide in the California South Coast Air Basin, *Environ. Sci. Technol.*, 12, 1077-1080, doi:10.1021/es60145a011, 1978.
- Kok, G. L.: Measurements of hydrogen peroxide in rainwater, *Atmos. Environ.* (1967), 14, 653-656, doi:10.1016/0004-6981(80)90048-7, 1980.
- Kotte, K., Löw, F., Huber, S. G., Krause, T., Mulder, I., and Schöler, H. F.: Organohalogen emissions from saline environments - spatial extrapolation using remote sensing as most promising tool, *Biogeosciences*, 9, 1225-1235, doi:10.5194/bg-9-1225-2012, 2012.
- Krause, T., and Sattler, T.: Geochemical inventory and emission from selected Australian salt lakes, Fall Meeting of the Research Unit 763, Annweiler/Palatinate, 2013.
- Krause, T., Tubbesing, C., Benzing, K., and Schöler, H. F.: Model reactions and natural occurrence of furans from hypersaline environments, *Biogeosciences Discuss.*, 10, 17439-17468, doi:10.5194/bgd-10-17439-2013, 2013.
- Kroll, J. H., and Seinfeld, J. H.: Chemistry of secondary organic aerosol: Formation and evolution of low-volatility organics in the atmosphere, *Atmos. Environ.*, 42, 3593-3624, doi:10.1016/j.atmosenv.2008.01.003, 2008.
- Krupa, S. V., and Manning, W. J.: Atmospheric ozone: Formation and effects on vegetation, *Environ. Pollut.*, 50, 101-137, doi:10.1016/0269-7491(88)90187-X, 1988.
- Krupp, L.: Untersuchung der Ionengehalte in Wasserproben australischer Salzseen Bachelor thesis, 2013.
- Küpper, F. C., Müller, D. G., Peters, A. F., Kloareg, B., and Potin, P.: Oligoalginate recognition and oxidative burst play a key role in natural and induced resistance of sporophytes of laminariales, *J. Chem. Ecol.*, 28, 2057-2081, doi:10.1023/A:1020706129624, 2002.
- Küpper, F. C., Carpenter, L. J., McFiggans, G. B., Palmer, C. J., Waite, T. J., Boneberg, E.-M., Woitsch, S., Weiller, M., Abela, R., Grolimund, D., Potin, P., Butler, A., Luther, G. W., Kroneck, P. M. H., Meyer-Klaucke, W., and Feiters, M. C.: Iodide accumulation provides kelp with an inorganic antioxidant impacting atmospheric chemistry, *Proc. Natl. Acad. Sci. USA*, 105, 6954-6958, doi:10.1073/pnas.0709959105, 2008.
- Lal, R., Hall, G. F., and Miller, F. P.: Soil degradation: I. Basic processes, *Land Degrad. Dev.*, 1, 51-69, doi:10.1002/ldr.3400010106, 1989.
- Landolt, H.: Ueber die Zeitdauer der Reaction zwischen Jodsäure und schwefliger Säure, *Ber. Dtsch. Chem. Ges.*, 19, 1317-1365, doi:10.1002/cber.188601901293, 1886.
- Landolt, H.: Ueber die Zeitdauer der Reaction zwischen Jodsäure und schwefliger Säure, *Ber. Dtsch. Chem. Ges.*, 20, 745-760, doi:10.1002/cber.188702001173, 1887.
- Larson, R. A., and Rockwell, A. L.: Chloroform and chlorophenol production by decarboxylation of natural acids during aqueous chlorination, *Environ. Sci. Technol.*, 13, 325-329, doi:10.1021/es60151a014, 1979.
- Lashof, D. A., and Ahuja, D. R.: Relative contributions of greenhouse gas emissions to global warming, *Nature*, 344, 529-531, doi:10.1038/344529a0, 1990.
- Lee, A., Goldstein, A. H., Kroll, J. H., Ng, N. L., Varutbangkul, V., Flagan, R. C., and Seinfeld, J. H.: Gas-phase products and secondary aerosol yields from the photooxidation of

- 16 different terpenes, *J. Geophys. Res.-Atmos.*, 111, D17305, doi:10.1029/2006JD007050, 2006.
- Leff, J. W., and Fierer, N.: Volatile organic compound (VOC) emissions from soil and litter samples, *Soil Biol. Biochem.*, 40, 1629-1636, doi:10.1016/j.soilbio.2008.01.018, 2008.
- Levy, H.: Normal atmosphere: Large radical and formaldehyde concentrations predicted, *Science*, 173, 141-143, doi:10.1126/science.173.3992.141, 1971.
- Li, L., Chen, Z. M., Zhang, Y. H., Zhu, T., Li, J. L., and Ding, J.: Kinetics and mechanism of heterogeneous oxidation of sulfur dioxide by ozone on surface of calcium carbonate, *Atmos. Chem. Phys.*, 6, 2453-2464, doi:10.5194/acp-6-2453-2006, 2006.
- Lillicrap, A., and George, R.: The distribution and origins of acid groundwaters in the South West Agricultural Area, Resource Management Technical Report, Department of Agriculture and Food, Perth, 2010.
- Lin, J. L., and Bent, B. E.: Carbon-halogen bond dissociation on copper surfaces: effect of alkyl chain length, *J. Phys. Chem.*, 96, 8529-8538, doi:10.1021/j100200a059, 1992.
- Lippe, S.: Charakterisierung des Brenner Moors hinsichtlich seiner chemischen Zusammensetzung und natürlich gebildeter Organohalogenverbindungen, Bachelor thesis, 2011.
- Logan, J. A.: Nitrogen oxides in the troposphere: Global and regional budgets, *J. Geophys. Res.-Oceans*, 88, 10785-10807, doi:10.1029/JC088iC15p10785, 1983.
- Lovley, D. R.: Organic matter mineralization with the reduction of ferric iron: A review, *Geomicrobiol. J.*, 5, 375-399, 1987.
- Lovley, D. R.: Potential for anaerobic bioremediation of BTEX in petroleum-contaminated aquifers, *J. Ind. Microbiol. Biot.*, 18, 75-81, doi:10.1038/sj.jim.2900246, 1997.
- Lyons, T. J., Xinmei, H., Schwerdtfeger, P., Hacker, J. M., Foster, I. J., and Smith, R. C. G.: Land-atmosphere interaction in a semiarid region: the Bunny Fence experiment, *Bull. Am. Meteorol. Soc.*, 74, 1327-1334, doi:10.1175/1520-0477(1993)074<1327:LIIASR>2.0.CO;2, 1993.
- Lyons, T. J., Smith, R. C. G., and Xinmei, H.: The Impact of clearing for agriculture on the surface energy budget, *Int. J. Climatol.*, 16, 551-558, doi:10.1002/(SICI)1097-0088(199605)16:5<551::AID-JOC25>3.0.CO;2-9 1996.
- Lyons, T. J.: Clouds prefer native vegetation, *Meteorol. Atmos. Phys.*, 80, 131-140, doi:10.1007/s007030200020, 2002.
- M'Hemdi, A., Dbira, B., Abdelhedi, R., Brillas, E., and Ammar, S.: Mineralization of catechol by Fenton and photo-Fenton processes, *CLEAN – Soil, Air, Water*, 40, 878-885, doi:10.1002/clen.201100376, 2012.
- Machulek Jr, A., Moraes, J. E. F., Okano, L. T., Silverio, C. A., and Quina, F. H.: Photolysis of ferric ions in the presence of sulfate or chloride ions: implications for the photo-Fenton process, *Photoch. Photobio. Sci.*, 8, 985-991, doi:10.1039/B900553F, 2009.
- Malin, G., and Erst, G. O.: Algal production of dimethyl sulfide and its atmospheric role, *J. Phycol.*, 33, 889-896, doi:10.1111/j.0022-3646.1997.00889.x, 1997.
- Mann, A. W.: Hydrogeochemistry and weathering on the Yilgarn Block, Western Australia - ferrollysis and heavy metals in continental brines, *Geochim. Cosmochim. Acta*, 47, 181-190, doi:10.1016/0016-7037(83)90131-X, 1983.

- Markert, F., and Nielsen, O. J.: The reactions of OH radicals with chloroalkanes in the temperature range 295-360 K, *Chem. Phys. Lett.*, 194, 123-127, doi:10.1016/0009-2614(92)85753-W, 1992.
- Martinez, R. I., Herron, J. T., and Huie, R. E.: The mechanism of ozone-alkene reactions in the gas phase. A mass spectrometric study of the reactions of eight linear and branched-chain alkenes, *J. Am. Chem. Soc.*, 103, 3807-3820, doi:10.1021/ja00403a031, 1981.
- Matheson, M. S., Mulac, W. A., Weeks, J. L., and Rabani, J.: The pulse radiolysis of deaerated aqueous bromide solutions, *J. Phys. Chem.*, 70, 2092-2099, doi:10.1021/j100879a004, 1966.
- Matveev, V., Peleg, M., Rosen, D., Tov-Alper, D. S., Hebestreit, K., Stutz, J., Platt, U., Blake, D., and Luria, M.: Bromine oxide—ozone interaction over the Dead Sea, *J. Geophys. Res.-Atmos.*, 106, 10375-10387, doi:10.1029/2000JD900611, 2001.
- McArthur, J. M., Turner, J. V., Lyons, W. B., Osborn, A. O., and Thirlwall, M. F.: Hydrochemistry on the yilgarn block, Western Australia: Ferrollysis and mineralisation in acidic brines, *Geochim. Cosmochim. Acta*, 55, 1273-1288, doi:10.1016/0016-7037(91)90306-P, 1991.
- McBee, E. T., Hass, H. B., Neher, C. M., and Strickland, H.: Chlorination of methane, *Ind. Eng. Chem. Fund.*, 34, 296-300, doi:10.1021/ie50387a009, 1942.
- McCormick, R. A., and Ludwig, J. H.: Climate modification by atmospheric aerosols, *Science*, 156, 1358-1359, doi:10.1126/science.156.3780.1358, 1967.
- Merz, J. H., and Waters, W. A.: A.-Electron-transfer reactions. The mechanism of oxidation of alcohols with Fenton's reagent, *Discuss. Faraday Soc.*, 2, 179-188, doi:10.1039/DF9470200179, 1947.
- Messer, R., Fuhrer, C. A., and Häner, R.: Natural product-like libraries based on non-aromatic, polycyclic motifs, *Current Opinion in Chemical Biology*, 9, 259-265, doi:10.1016/j.cbpa.2005.04.002, 2005.
- Millero, F. J.: The effect of ionic interactions on the oxidation of metals in natural waters, *Geochim. Cosmochim. Acta*, 49, 547-553, doi:10.1016/0016-7037(85)90046-8, 1985.
- Millero, F. J.: Effect of ionic interactions on the oxidation of Fe(II) and Cu(I) in natural waters, *Mar. Chem.*, 28, 1-18, doi:10.1016/0304-4203(89)90183-7, 1989.
- Millero, F. J., Yao, W., and Aicher, J.: The speciation of Fe(II) and Fe(III) in natural waters, *Mar. Chem.*, 50, 21-39, doi:10.1016/0304-4203(95)00024-L, 1995.
- Min, D. B., Callison, A. L., and Lee, H. O.: Singlet oxygen oxidation for 2-pentylfuran and 2-pentenylfuran formation in soybean oil, *J. Food Sci.*, 68, 1175-1178, doi:10.1111/j.1365-2621.2003.tb09620.x, 2003.
- Minisci, F., and Fontana, F.: Mechanism of the Gif-Barton type alkane functionalization by halide and pseudohalide ions, *Tetrahedron Lett.*, 35, 1427-1430, doi:10.1016/S0040-4039(00)76237-X, 1994.
- Mossinger, J. C., Shallcross, D. E., and Cox, R. A.: UV-VIS absorption cross-sections and atmospheric lifetimes of CH₂Br₂, CH₂I₂ and CH₂BrI, *J. Chem. Soc. Faraday T.*, 94, 1391-1396, doi:10.1039/A709160E, 1998.
- Mulder, I., Huber, S. G., Krause, T., Zetzsch, C., Kotte, K., Dultz, S., and Schöler, H. F.: A new purge and trap headspace technique to analyse low volatile compounds from fluid

- inclusions of rocks and minerals, *Chem. Geol.*, 358, 148-155, doi:10.1016/j.chemgeo.2013.09.003, 2013.
- Müller, D.: Kinetic model of atmospheric SO₂ oxidation based on published data, *Atmos. Environ.* (1967), 14, 1067-1076, doi:10.1016/0004-6981(80)90037-2, 1980.
- Müller, G., and Gastner, M.: The 'Karbonat-Bombe', a simple device for the determination of carbonate content in sediment, soils, and other materials, *Neues JB Miner. Monat.*, 10, 466-469, doi:10013/epic.27884, 1971.
- Nadtochenko, V., and Kiwi, J.: Primary Photochemical Reactions in the Photo-Fenton System with Ferric Chloride. 1. A Case Study of Xylidine Oxidation as a Model Compound, *Environ. Sci. Technol.*, 32, 3273-3281, doi:10.1021/es970962e, 1998a.
- Nadtochenko, V. A., and Kiwi, J.: Photolysis of FeOH²⁺ and FeCl²⁺ in aqueous solution. Photodissociation kinetics and quantum yields, *Inorganic Chem.*, 37, 5233-5238, doi:10.1021/ic9804723, 1998b.
- National Institute of Oceanography of Great Britain and UNESCO: International Oceanographic Tables, 2, 1973.
- Neyens, E., and Baeyens, J.: A review of classic Fenton's peroxidation as an advanced oxidation technique, *J. Hazard. Mater.*, 98, 33-50, doi:10.1016/S0304-3894(02)00282-0, 2003.
- Ng, N. L., Kroll, J. H., Chan, A. W. H., Chhabra, P. S., Flagan, R. C., and Seinfeld, J. H.: Secondary organic aerosol formation from m-xylene, toluene, and benzene, *Atmos. Chem. Phys.*, 7, 3909-3922, doi:10.5194/acp-7-3909-2007, 2007.
- Nicovich, J. M., Shackelford, C. J., and Wine, P. H.: Kinetics and thermochemistry of reversible adduct formation in the reaction of atomic chlorine with carbon disulfide, *J. Phys. Chem.*, 94, 2896-2903, doi:10.1021/j100370a031, 1990.
- Niedan, V., and Schöler, H. F.: Natural formation of chlorobenzoic acids (CBA) and distinction between PCB-degraded CBA, *Chemosphere*, 35, 1233-1241, doi:10.1016/S0045-6535(97)00205-1, 1997.
- Novakov, T., and Penner, J. E.: Large contribution of organic aerosols to cloud-condensation-nuclei concentrations, *Nature*, 365, 823-826, doi:10.1038/365823a0, 1993.
- Nozière, B., and Riemer, D. D.: The chemical processing of gas-phase carbonyl compounds by sulfuric acid aerosols: 2,4-pentanedione, *Atmos. Environ.*, 37, 841-851, doi:10.1016/S1352-2310(02)00934-2, 2003.
- Nulsen, R. A., and Catchment Hydrology Group: Groundwater trends in the agricultural area of Western Australia, Resource Management Technical Report No.173, Agriculture Western Australia, 1998.
- Nutmagul, W., and Cronn, D. R.: Determination of selected atmospheric aromatic hydrocarbons at remote continental and oceanic locations using photoionization/flame-ionization detection, *J. Atmos. Chem.*, 2, 415-433, doi:10.1007/BF00130752, 1985.
- O'Dowd, C. D., Jimenez, J. L., Bahreini, R., Flagan, R. C., Seinfeld, J. H., Hameri, K., Pirjola, L., Kulmala, M., Jennings, S. G., and Hoffmann, T.: Marine aerosol formation from biogenic iodine emissions, *Nature*, 417, 632-636, doi:10.1038/nature00775, 2002.
- Oeste, F. D.: Bestimmung der Redox-Milieuzonierung mit gM-Redox-Milieu-Detektorband (RMD), DECHEMA Symposium Strategien zur Boden- und Grundwassersanierung, Frankfurt am Main, 2010.

- Ofner, J., Balzer, N., Buxmann, J., Grothe, H., Schmitt-Kopplin, P., Platt, U., and Zetzsch, C.: Halogenation processes of secondary organic aerosol and implications on halogen release mechanisms, *Atmos. Chem. Phys.*, 12, 5787-5806, doi:10.5194/acp-12-5787-2012, 2012.
- Ofner, J., Kamilli, K. A., Held, A., Lendl, B., and Zetzsch, C.: Halogen-induced organic aerosol (XOA): a study on ultra-fine particle formation and time-resolved chemical characterization, *Faraday Discuss.*, doi:10.1039/C3FD00093A, 2013.
- Ohta, T.: Furan ring formation in OH-initiated photooxidation of 1, 3-butadiene and cis-1, 3-pentadiene, *B. Chem. Soc. Jpn.*, 57, 960-966, 1984.
- Olszyna, K. J., Meagher, J. F., and Bailey, E. M.: Gas-phase, cloud and rain-water measurements of hydrogen peroxide at a high-elevation site, *Atmos. Environ. (1967)*, 22, 1699-1706, doi:10.1016/0004-6981(88)90398-8, 1988.
- Palin, A. T.: The determination of free and combined chlorine in water by the use of diethyl-p-phenylene diamine, *J. Am. Water Works Assoc.*, 49, 873-880, 1957.
- Pallmer, N.: Bodenanalyse dreier Bodenprofile aus Teneriffa, Bachelor thesis, 2010.
- Papagni, C., Arey, J., and Atkinson, R.: Rate constants for the gas-phase reactions of a series of C3-C6 aldehydes with OH and NO₃ radicals, *Int. J. Chem. Kinet.*, 32, 79-84, doi:10.1002/(SICI)1097-4601(2000)32:2<79::AID-KIN2>3.0.CO;2-A, 2000.
- Paraskevopoulos, G., and Cvetanović, R. J.: Relative rate of reaction of O(¹D₂) with H₂O, *Chem. Phys. Lett.*, 9, 603-605, doi:10.1016/0009-2614(71)85139-4, 1971.
- Pardieck, D. L., Bouwer, E. J., and Stone, A. T.: Hydrogen peroxide use to increase oxidant capacity for in situ bioremediation of contaminated soils and aquifers: A review, *J. Contam. Hydrol.*, 9, 221-242, doi:10.1016/0169-7722(92)90006-Z, 1992.
- Paul, C., and Pohnert, G.: Production and role of volatile halogenated compounds from marine algae, *Nat. Prod. Rep.*, 28, 186-195, doi:10.1039/C0NP00043D, 2011.
- Peard, M. G., and Cullis, C. F.: A periodic chemical reaction. The reaction between hydrogen peroxide and iodic acid, *Trans. Faraday Soc.*, 47, 616-630, doi:10.1039/TF9514700616, 1951.
- Pease, R. N., and Walz, G. F.: Kinetics of the thermal chlorination of methane, *J. Am. Chem. Soc.*, 53, 3728-3737, doi:10.1021/ja01361a016, 1931.
- Peleg, M., Matveev, V., Tas, E., and Luria, M.: Bromine oxide formation over the Dead Sea valley, Israel, 13th World Clean Air and Environmental Protection Congress and Exhibition, London, 2004.
- Petasne, R. G., and Zika, R. G.: Fate of superoxide in coastal sea water, *Nature*, 325, 516-518, doi:10.1038/325516a0, 1987.
- Pham, A. N., Xing, G., Miller, C. J., and Waite, T. D.: Fenton-like copper redox chemistry revisited: Hydrogen peroxide and superoxide mediation of copper-catalyzed oxidant production, *J. Catalysis*, 301, 54-64, doi:10.1016/j.jcat.2013.01.025, 2013.
- Pierce, J. R., and Adams, P. J.: Efficiency of cloud condensation nuclei formation from ultrafine particles, *Atmos. Chem. Phys.*, 7, 1367-1379, doi:10.5194/acp-7-1367-2007, 2007.
- Pitzer, K. S.: Thermodynamics of electrolytes. I. Theoretical basis and general equations, *J. Phys. Chem.*, 77, 268-277, doi:10.1021/j100621a026, 1973.
- Platt, U., and Hönninger, G.: The role of halogen species in the troposphere, *Chemosphere*, 52, 325-338, doi:10.1016/S0045-6535(03)00216-9, 2003.

- Plummer, L. N., Parkhurst, D. L., Fleming, G. W., and Dunkle, S. A.: A computer program incorporating Pitzer's equations for calculation of geochemical reactions in brines, Water-Resources Investigations Report 88-4153, U.S. Geological Survey Reston, 1988.
- Postma, D.: Concentration of Mn and separation from Fe in sediments--I. Kinetics and stoichiometry of the reaction between birnessite and dissolved Fe(II) at 10°C, *Geochim. Cosmochim. Acta*, 49, 1023-1033, doi:10.1016/0016-7037(85)90316-3, 1985.
- Potter, F. J., and Roth, J. A.: Oxidation of chlorinated phenols using Fenton's reagent, *Hazard. Waste Hazard. Mater.*, 10, 151-170, doi:10.1089/hwm.1993.10.151, 1993.
- Pracht, J., Boenigk, J., Isenbeck-Schröter, M., Keppler, F., and Schöler, H. F.: Abiotic Fe(III) induced mineralization of phenolic substances, *Chemosphere*, 44, 613-619, doi:10.1016/S0045-6535(00)00490-2, 2001.
- Prithiviraj, B., Vikram, A., Kushalappa, A. C., and Yaylayan, V.: Volatile metabolite profiling for the discrimination of onion bulbs infected by *Erwinia carotovora* ssp. *carotovora*, *Fusarium oxysporum* and *Botrytis allii*, *Eur. J. Plant Pathol.*, 110, 371-377, doi:10.1023/B:EJPP.0000021058.81491.f8, 2004.
- Rattigan, O. V., Shallcross, D. E., and Cox, R. A.: UV absorption cross-sections and atmospheric photolysis rates of CF₃I, CH₃I, C₂H₅I and CH₂ClI, *J. Chem. Soc. Faraday T.*, 93, 2839-2846, doi:10.1039/A701529A, 1997.
- Ravishankara, A. R.: Heterogeneous and multiphase chemistry in the troposphere, *Science*, 276, 1058-1065, doi:10.1126/science.276.5315.1058, 1997.
- Reissell, A., Arey, J., and Atkinson, R.: Atmospheric chemistry of camphor, *Int. J. Chem. Kinet.*, 33, 56-63, doi:10.1002/1097-4601(20010101)33:1<56::AID-KIN7>3.0.CO;2-Y, 2001.
- Remucal, C. K., and Sedlak, D. L.: The Role of iron coordination in the production of reactive oxidants from ferrous iron oxidation by oxygen and hydrogen peroxide, in: *Aquatic Redox Chemistry*, ACS Symposium Series, American Chemical Society, 177-197, 2011.
- Risholm-Sundman, M., Lundgren, M., Vestin, E., and Herder, P.: Emissions of acetic acid and other volatile organic compounds from different species of solid wood, *Holz als Roh- und Werkstoff*, 56, 125-129, doi:10.1007/s001070050282, 1998.
- Roberts, I., and Kimball, G. E.: The halogenation of ethylenes, *J. Am. Chem. Soc.*, 59, 947-948, doi:10.1021/ja01284a507, 1937.
- Roehl, C. M., Burkholder, J. B., Moortgat, G. K., Ravishankara, A. R., and Crutzen, P. J.: Temperature dependence of UV absorption cross sections and atmospheric implications of several alkyl iodides, *J. Geophys. Res.-Atmos.*, 102, 12819-12829, doi:10.1029/97JD00530, 1997.
- Rogers, S., and George, R.: WA Wheatbelt drainage - acidic groundwater, not just a salt issue, *Focus on Salt* 33, 8-9, 2005.
- Rogge, W. F., Hildemann, L. M., Mazurek, M. A., Cass, G. R., and Simoneit, B. R. T.: Sources of fine organic aerosol. 1. Charbroilers and meat cooking operations, *Environ. Sci. Technol.*, 25, 1112-1125, doi:10.1021/es00018a015, 1991.
- Ross, P. L., and Johnston, M. V.: Excited state photochemistry of iodoalkanes, *J. Phys. Chem.*, 99, 4078-4085, doi:10.1021/j100012a031, 1995.
- Rowland, F. S.: Stratospheric ozone depletion, *Phil. Trans. R. Soc. B*, 361, 769-790, doi:10.1098/rstb.2005.1783, 2006.

- Ruasse, M. F.: Bromonium ions or .beta.-bromocarocations in olefin bromination. A kinetic approach to product selectivities, *Acc. Chem. Res.*, 23, 87-93, doi:10.1021/ar00171a006, 1990.
- Rush, J. D., and Bielski, B. H. J.: Pulse radiolytic studies of the reaction of perhydroxyl/superoxide O_2^- with iron(II)/iron(III) ions. The reactivity of HO_2/O_2^- with ferric ions and its implication on the occurrence of the Haber-Weiss reaction, *J. Phys. Chem.*, 89, 5062-5066, doi:10.1021/j100269a035, 1985.
- Saiz-Lopez, A., and von Glasow, R.: Reactive halogen chemistry in the troposphere, *Chem. Soc. Rev.*, 41, 6448-6472, doi:10.1039/C2CS35208G, 2012.
- Sander, R., Keene, W. C., Pszenny, A. A. P., Arimoto, R., Ayers, G. P., Baboukas, E., Caine, J. M., Crutzen, P. J., Duce, R. A., Hönninger, G., Huebert, B. J., Maenhaut, W., Mihalopoulos, N., Turekian, V. C., and Van Dingenen, R.: Inorganic bromine in the marine boundary layer: a critical review, *Atmos. Chem. Phys.*, 3, 1301-1336, 2003.
- Sander, S. P., Golden, D. M., Kurylo, M. J., Moortgat, G. K., Wine, P. H., Ravishankara, A. R., Kolb, C. E., Molina, M. J., Finlayson-Pitts, B. J., and Huie, R. E.: Chemical kinetics and photochemical data for use in atmospheric studies evaluation number 15, 2006.
- Sato, K., Aoki, M., Takagi, J., and Noyori, R.: Organic solvent- and halide-free oxidation of alcohols with aqueous hydrogen peroxide, *J. Am. Chem. Soc.*, 119, 12386-12387, doi:10.1021/ja973412p, 1997.
- Sattler, T.: Analyse bodennaher Luftproben von Salzseen, Master thesis, 2012.
- Schiermeier, Q.: Hot air, *Nature*, 491, 656-658, 2012.
- Schnitker, D., Mayer, L. M., and Norton, S.: Loss of calcareous microfossils from sediments through gypsum formation, *Mar. Geol.*, 36, M35-M44, 1980.
- Schofield, N. J.: Stream salinisation and its amelioration in south-west Western Australia, in: *Regional Characterization of Water Quality*, edited by: Ragone, S., IAHS Publication No. 182, International Association of Hydrological Sciences, Wallingford, 211-220, 1989.
- Schöler, H. F., and Keppler, F.: Abiotic formation of organohalogens during early diagenetic processes, in: *Natural Production of Organohalogen Compounds*, edited by: Gribble, G., *The Handbook of Environmental Chemistry*, Springer Berlin Heidelberg, 63-84, 2003.
- Sehls, B.: Untersuchung der Schwermetallkonzentrationen verschiedener Salzseen in Westaustralien mittels ICP-OES-Analyse, Bachelor thesis, 2013.
- Shand, P., and Degens, B.: Avon Catchment acidic groundwater - geochemical risk assessment, CRC LEME Open File Report, CRC LEME, Bentley, 82pp pp., 2008.
- Sharkey, T. D., and Yeh, S.: Isoprene emission from plants, *Annu. Rev. Plant Physiol. Plant Mol. Biol.*, 52, 407-436, doi:10.1146/annurev.arplant.52.1.407, 2001.
- Sharkey, T. D., Wiberley, A. E., and Donohue, A. R.: Isoprene emission from plants: why and how, *Ann. Bot.*, 101, 5-18, doi:10.1093/aob/mcm240, 2008.
- Shaw, S. L., Gantt, B., and Meskhidze, N.: Production and emissions of marine isoprene and monoterpenes: A review, *Advances in Meteorology*, 2010, doi:10.1155/2010/408696, 2010.
- Shepson, P. B., Edney, E. O., and Corse, E. W.: Ring fragmentation reactions in the photooxidations of toluene and o-xylene, *J. Phys. Chem.*, 88, 4122-4126, doi:10.1021/j150662a053, 1984.

- Sherwood, J. E., Stagnitti, F., Kokkinn, M. J., and Williams, W. D.: Dissolved oxygen concentrations in hypersaline waters, *Limnol. Oceanogr.*, 36, 235-250, 1991.
- Sherwood, J. E., Stagnitti, F., Kokkinn, M. J., and Williams, W. D.: A standard table for predicting equilibrium dissolved oxygen concentrations in Salt Lakes dominated by sodium chloride, *Int. J. Salt Lake Res.*, 1, 1-6, 1992.
- Silverman, M. P., Ehrlich, H. L., and Wayne, W. U.: Microbial formation and degradation of minerals, in: *Advances in Applied Microbiology*, Academic Press, 153-206, 1964.
- Sivagurunathan, M., Sumithra Devi, G., and Ramasamy, K.: Allelopathic compounds in *Eucalyptus* spp., *Alleopath. J.*, 4, 313-320, 1997.
- SkudaeV, V. I., Solomonov, A. B., Morozovskii, A. I., and Isakov, N. A.: Oxidation of hydrogen chloride with hydrogen peroxide in aqueous solution, *Russ. J. Appl. Chem.*, 81, 14-16, doi:10.1134/S1070427208010035, 2008.
- Smith, J., and Melville, M. D.: Iron monosulfide formation and oxidation in drain-bottom sediments of an acid sulfate soil environment, *Appl. Geochem.*, 19, 1837-1853, doi:10.1016/j.apgeochem.2004.04.004, 2004.
- Smoydzin, L., and von Glasow, R.: Modelling chemistry over the Dead Sea: bromine and ozone chemistry, *Atmos. Chem. Phys.*, 9, 5057-5072, doi:10.5194/acp-9-5057-2009, 2009.
- Solomon, S.: Stratospheric ozone depletion: A review of concepts and history, *Rev. Geophys.*, 37, 275-316, doi:10.1029/1999RG900008, 1999.
- Solyanikov, V. M., and Denisov, E. T.: Formation of radicals in the reaction of hydrogen peroxide with the bromide anion, *B. Acad. Sci. USSR, Div. Chem. Sci.*, 17, 1415-1418, doi:10.1007/BF00907836, 1968.
- Sparks, D. L.: 8 - Redox chemistry of soils, in: *Environmental Soil Chemistry (Second Edition)*, Academic Press, Burlington, 245-265, 2003.
- Spicer, C. W., Chapman, E. G., Finlayson-Pitts, B. J., Plastridge, R. A., Hubbe, J. M., Fast, J. D., and Berkowitz, C. M.: Unexpectedly high concentrations of molecular chlorine in coastal air, *Nature*, 394, 353-356, doi:10.1038/28584, 1998.
- Spivakovsky, C. M., Logan, J. A., Montzka, S. A., Balkanski, Y. J., Foreman-Fowler, M., Jones, D. B. A., Horowitz, L. W., Fusco, A. C., Brenninkmeijer, C. A. M., Prather, M. J., Wofsy, S. C., and McElroy, M. B.: Three-dimensional climatological distribution of tropospheric OH: Update and evaluation, *J. Geophys. Res.-Atmos.*, 105, 8931-8980, doi:10.1029/1999JD901006, 2000.
- Stadtman, T. C.: Selenocysteine, *Annu. Rev. Biochem.*, 65, 83-100, doi:10.1146/annurev.bi.65.070196.000503, 1996.
- Steinhorn, I., Assaf, G., Gat, J. R., Nishry, A., Nissenbaum, A., Stiller, M., Beyth, M., Neev, D., Garber, R., Friedman, G. M., and Weiss, W.: The Dead Sea: Deepening of the Mixolimnion signifies the overture to overturn of the water column, *Science*, 206, 55-57, doi:10.1126/science.206.4414.55, 1979.
- Stickel, R. E., Nicovich, J. M., Wang, S., Zhao, Z., and Wine, P. H.: Kinetic and mechanistic study of the reaction of atomic chlorine with dimethyl sulfide, *J. Phys. Chem.*, 96, 9875-9883, doi:10.1021/j100203a055, 1992.
- Stoeckenius, W., and Bogomolni, R. A.: Bacteriorhodopsin and related pigments of halobacteria, *Annu. Rev. Biochem.*, 51, 587-616, doi:10.1146/annurev.bi.51.070182.003103, 1982.

- Strlič, M., Kolar, J., Šelih, V.-S., Kočar, D., and Pihlar, B.: A comparative study of several transition metals in Fenton-like reaction systems at circum-neutral pH, *Acta Chim. Slov.*, 50, 619-632, 2003.
- Studenroth, S., Huber, S. G., Kotte, K., and Schöler, H. F.: Natural abiotic formation of oxalic acid in soils: Results from aromatic model compounds and soil samples, *Environ. Sci. Technol.*, 47, 1323-1329, doi:10.1021/es304208a, 2013.
- Stumm, W., and Lee, G. F.: Oxygenation of ferrous iron, *Ind. Eng. Chem. Fund.*, 53, 143-146, doi:10.1021/ie50614a030, 1961.
- Stumm, W., and Sulzberger, B.: The cycling of iron in natural environments: Considerations based on laboratory studies of heterogeneous redox processes, *Geochim. Cosmochim. Acta*, 56, 3233-3257, doi:10.1016/0016-7037(92)90301-X, 1992.
- Stutz, J., Hebestreit, K., Alicke, B. r., and Platt, U.: Chemistry of halogen oxides in the troposphere: Comparison of model calculations with recent field data, *J. Atmos. Chem.*, 34, 65-85, doi:10.1023/A:1006245802825, 1999.
- Stutz, J., Ackermann, R., Fast, J. D., and Barrie, L.: Atmospheric reactive chlorine and bromine at the Great Salt Lake, Utah, *Geophys. Res. Lett.*, 29, 18-11-18-14, doi:10.1029/2002GL014812, 2002.
- Suppiah, R., and Hennessy, K. J.: Trends in total rainfall, heavy rain events and number of dry days in Australia, 1910–1990, *Int. J. Climatol.*, 18, 1141-1164, doi:10.1002/(SICI)1097-0088(199808)18:10<1141::AID-JOC286>3.0.CO;2-P, 1998.
- Switzer Blum, J., Stolz, J. F., Oren, A., and Oremland, R. S.: *Selenihalanaerobacter shriftii* gen. nov., sp. nov., a halophilic anaerobe from Dead Sea sediments that respire selenate, *Arch. Microbiol.*, 175, 208-219, doi:10.1007/s002030100257, 2001.
- Tang, T., and McConnell, J. C.: Autocatalytic release of bromine from Arctic snow pack during polar sunrise, *Geophys. Res. Lett.*, 23, 2633-2636, doi:10.1029/96GL02572, 1996.
- Tang, W. Z., and Huang, C. P.: The effect of chlorine position of chlorinated phenols on their dechlorination kinetics by Fenton's reagent, *Waste Manage.*, 15, 615-622, doi:10.1016/0956-053X(96)00022-0, 1995.
- Tarbell, D. S., and Bartlett, P. D.: The Mechanism of Addition Reactions. Chloro- and Bromo-Beta-Lactones from Dimethylmaleic and Dimethylfumaric Acids, *J. Am. Chem. Soc.*, 59, 407-410, doi:10.1021/ja01281a056, 1937.
- Tas, E., Peleg, M., Matveev, V., Zingler, J., and Luria, M.: Frequency and extent of bromine oxide formation over the Dead Sea, *J. Geophys. Res.-Atmos.*, 110, D11304, doi:10.1029/2004JD005665, 2005.
- Tas, E., Peleg, M., Pedersen, D. U., Matveev, V., Pour Biazar, A., and Luria, M.: Measurement-based modeling of bromine chemistry in the boundary layer: 1. Bromine chemistry at the Dead Sea, *Atmos. Chem. Phys.*, 6, 5589-5604, doi:10.5194/acp-6-5589-2006, 2006.
- Taylor, S. R.: Abundance of chemical elements in the continental crust: a new table, *Geochim. Cosmochim. Acta*, 28, 1273-1285, doi:10.1016/0016-7037(64)90129-2, 1964.
- Thauer, R. K.: Biochemistry of methanogenesis: a tribute to Marjory Stephenson:1998 Marjory Stephenson Prize Lecture, *Microbiology*, 144, 2377-2406, doi:10.1099/00221287-144-9-2377, 1998.

- Timerghazin, Q. K., and Ariya, P. A.: Kinetics of the gas-phase reaction of atomic chlorine with selected monoterpenes, *Phys. Chem. Chem. Phys.*, 3, 3981-3986, doi:10.1039/B101380G, 2001.
- Timms, B. V.: Study of the saline lakes of the Esperance Hinterland, Western Australia, with special reference to the roles of acidity and episodicity, *Nat. Resour. Env. Iss.*, 15, 215-225, 2009.
- Trapp, J. M., and Millero, F.: The Oxidation of Iron(II) with Oxygen in NaCl Brines, *J. Solution Chem.*, 36, 1479-1493, doi:10.1007/s10953-007-9192-8, 2007.
- Tung, H. C., Kang, C., and Sawyer, D. T.: Nature of the reactive intermediates from the iron-induced activation of hydrogen peroxide: agents for the ketonization of methylenic carbons, the monooxygenation of hydrocarbons, and the dioxygenation of aryl olefins, *J. Am. Chem. Soc.*, 114, 3445-3455, doi:10.1021/ja00035a043, 1992.
- Turpin, B. J., and Huntzicker, J. J.: Secondary formation of organic aerosol in the Los Angeles basin: A descriptive analysis of organic and elemental carbon concentrations, *Atmos. Environ. a-Gen.*, 25, 207-215, doi:10.1016/0960-1686(91)90291-E, 1991.
- Twomey, S.: Pollution and the planetary albedo, *Atmos. Environ.* (1967), 8, 1251-1256, doi:10.1016/0004-6981(74)90004-3, 1974.
- Twomey, S.: The influence of pollution on the shortwave albedo of clouds, *Journal of the Atmospheric Sciences*, 34, 1149-1152, doi:10.1175/1520-0469(1977)034<1149:TIOPOT>2.0.CO;2, 1977.
- U.S. Climate Change Science Program: Strategic plan for the U.S. Climate Change Science Program, Washington, D.C, 2003.
- U.S. Geological Survey: Change to solubility equations for oxygen in water Quality of Water Branch Technical Memorandum 11.03, 2011.
- U.S. Geological Survey: Mineral commodity summaries 2013, 34-35, 2013.
- UN: United Nations Framework Convention on Climate Change, New York, 1992,
- UN: Kyoto Protocol to the United Nations Framework Convention on Climate Change, Kyoto, 1997,
- UNEP: Handbook for the Montreal Protocol on substances that deplete the ozone layer, 8th ed., Nairobi, 2009.
- Verink, E. D.: Simplified procedure for constructing Pourbaix diagrams, in: Uhlig's Corrosion Handbook, edited by: Revie, R. W., John Wiley & Sons, Inc., 93-101, 2000.
- Villanueva, F., Cabañas, B., Monedero, E., Salgado, S., Bejan, I., and Martín, P.: Atmospheric degradation of alkylfurans with chlorine atoms: Product and mechanistic study, *Atmos. Environ.*, 43, 2804-2813, doi:10.1016/j.atmosenv.2009.02.030, 2009.
- Voelker, B. M., Morel, F. M. M., and Sulzberger, B.: Iron redox cycling in surface waters: Effects of humic substances and light, *Environ. Sci. Technol.*, 31, 1004-1011, doi:10.1021/es9604018, 1997.
- Vogt, R., Crutzen, P. J., and Sander, R.: A mechanism for halogen release from sea-salt aerosol in the remote marine boundary layer, *Nature*, 383, 327-330, doi:10.1038/383327a0, 1996.

- Vogt, R., Sander, R., von Glasow, R., and Crutzen, P.: Iodine chemistry and its role in halogen activation and ozone loss in the marine boundary layer: A model study, *J. Atmos. Chem.*, 32, 375-395, doi:10.1023/A:1006179901037, 1999.
- von Glasow, R., and Crutzen, P. J.: Model study of multiphase DMS oxidation with a focus on halogens, *Atmos. Chem. Phys.*, 4, 589-608, doi:10.5194/acp-4-589-2004, 2004.
- Von Gunten, U., and Oliveras, Y.: Kinetics of the reaction between hydrogen peroxide and hypobromous acid: Implication on water treatment and natural systems, *Water Res.*, 31, 900-906, doi:10.1016/S0043-1354(96)00368-5, 1997.
- Wallington, T. J., Skewes, L. M., and Siegl, W. O.: Kinetics of the gas phase reaction of chlorine atoms with a series of alkenes, alkynes and aromatic species at 295 K, *J. Photoch. Photobio. A*, 45, 167-175, doi:10.1016/1010-6030(88)80126-6, 1988.
- Wang, Z., Fingas, M., Landriault, M., Sigouin, L., and Xu, N.: Identification of alkylbenzenes and direct determination of BTEX and BTEX + C3-benzenes in oils by GC/MS, *Anal. Chem.*, 67, 3491-3500, doi:10.1021/ac00115a018, 1995.
- Warneck, P.: *Chemistry of the natural atmosphere*, Elsevier Science, 1999.
- Warneck, P., and Williams, J.: *The atmospheric chemist's companion: Numerical data for use in the atmospheric sciences*, Springer, 2012.
- Watts, S. F.: The mass budgets of carbonyl sulfide, dimethyl sulfide, carbon disulfide and hydrogen sulfide, *Atmos. Environ.*, 34, 761-779, doi:10.1016/S1352-2310(99)00342-8, 2000.
- Weiss, J.: Elektronenübergangsprozesse im Mechanismus von Oxydations- und Reduktionsreaktionen in Lösungen, *Naturwissenschaften*, 23, 64-69, doi:10.1007/BF01497021, 1935.
- Weiss, J.: Reaction mechanism of the enzymes catalase and peroxidase in the light of the theory of chain reactions, *J. Phys. Chem.*, 41, 1107-1116, doi:10.1021/j150386a008, 1937.
- Weiss, R.: Tenth report of the joint panel on oceanographic tables and standards, *UNESCO Technical Papers in Marine Science*, 36, 22, 1980.
- Weiss, R. F.: The solubility of nitrogen, oxygen and argon in water and seawater, *Deep-Sea Res. Oceanogr. Abstr.*, 17, 721-735, 1970.
- Weissflog, L., Lange, C. A., Pfennigsdorff, A., Kotte, K., Elansky, N., Lisitzyna, L., Putz, E., and Krueger, G.: Sediments of salt lakes as a new source of volatile highly chlorinated C1/C2 hydrocarbons, *Geophys. Res. Lett.*, 32, L01401, doi:10.1029/2004GL020807, 2005.
- Welch, K. D., Davis, T. Z., and Aust, S. D.: Iron autoxidation and free radical generation: Effects of buffers, ligands, and chelators, *Arch. Biochem. Biophys.*, 397, 360-369, doi:10.1006/abbi.2001.2694, 2002.
- Westerhoff, P., Chao, P., and Mash, H.: Reactivity of natural organic matter with aqueous chlorine and bromine, *Water Res.*, 38, 1502-1513, doi:10.1016/j.watres.2003.12.014, 2004.
- WHO: Toluene, Environmental Health Criteria 52, World Health Organization, Geneva, 1985.
- WHO: Indoor air quality: organic pollutants, Euro Reports and Studies No. 111, World Health Organisation, Regional Office for Europe, Copenhagen, 1989.
- WHO: Benzene, Environmental Health Criteria 150, World Health Organization, Geneva, 1993.

- WHO: Ethylbenzene, Environmental Health Criteria 186, World Health Organization, Geneva, 1996.
- WHO: Xylenes, Environmental Health Criteria 190, World Health Organization, Geneva, 1997.
- Williams, W. D., and Sherwood, J. E.: Definition and measurement of salinity in salt lakes, *Int. J. Salt Lake Res.*, 3, 53-63, 1994.
- Williams, W. D.: Anthropogenic salinisation of inland waters, *Hydrobiologia*, 466, 329-337, doi:10.1023/A:1014598509028, 2001.
- Wine, P. H., Kreutter, N. M., Gump, C. A., and Ravishankara, A. R.: Kinetics of hydroxyl radical reactions with the atmospheric sulfur compounds hydrogen sulfide, methanethiol, ethanethiol, and dimethyl disulfide, *J. Phys. Chem.*, 85, 2660-2665, doi:10.1021/j150618a019, 1981.
- Winning, I. H.: The kinetics of the photo-chlorination of chloroform vapour, *Trans. Faraday Soc.*, 47, 1084-1088, doi:10.1039/TF9514701084, 1951.
- Wirth, C.: Geochemie und Kohlenstoffgehalt von sauren und alkalischen Salzseen in Westaustralien, Bachelor thesis, 2013.
- Wu, D., Wong, D., and Di Bartolo, B.: Evolution of Cl_2^- in aqueous NaCl solutions, *J. Photochem.*, 14, 303-310, doi:10.1016/0047-2670(80)85102-1, 1980.
- Xinmei, H., Lyons, T. J., and Smith, R. C. G.: Meteorological impact of replacing native perennial vegetation with annual agricultural species, *Hydrol. Process.*, 9, 645-654, doi:10.1002/hyp.3360090512, 1995.
- Yamazaki, I., and Piette, L. H.: EPR spin-trapping study on the oxidizing species formed in the reaction of the ferrous ion with hydrogen peroxide, *J. Am. Chem. Soc.*, 113, 7588-7593, doi:10.1021/ja00020a021, 1991.
- Yechieli, Y., Gavrieli, I., Berkowitz, B., and Ronen, D.: Will the Dead Sea die?, *Geology*, 26, 755-758, doi:10.1130/0091-7613(1998)026<0755:wtdsd>2.3.co;2, 1998.
- Yocis, B. H., Kieber, D. J., and Mopper, K.: Photochemical production of hydrogen peroxide in Antarctic Waters, *Deep-Sea Res. Oceanogr.*, A, 47, 1077-1099, doi:10.1016/S0967-0637(99)00095-3, 2000.
- Yoshizumi, K., Aoki, K., Nouchi, I., Okita, T., Kobayashi, T., Amakura, S. K., and Tajima, M.: Measurements of the concentration in rainwater and of the Henry's law constant of hydrogen peroxide, *Atmos. Environ.* (1967), 18, 395-401, doi:10.1016/0004-6981(84)90114-8, 1984.
- Yu, X.-Y., and Barker, J. R.: Hydrogen peroxide photolysis in acidic aqueous solutions containing chloride ions. I. Chemical mechanism, *J. Phys. Chem. A*, 107, 1313-1324, doi:10.1021/jp0266648, 2003.
- Zazo, J. A., Casas, J. A., Mohedano, A. F., Gilarranz, M. A., and Rodríguez, J. J.: Chemical pathway and kinetics of phenol oxidation by Fenton's reagent, *Environ. Sci. Technol.*, 39, 9295-9302, doi:10.1021/es050452h, 2005.
- Zhang, H.-Z., Kasibhatla, S., Kuemmerle, J., Kemnitzer, W., Ollis-Mason, K., Qiu, L., Crogan-Grundy, C., Tseng, B., Drewe, J., and Cai, S. X.: Discovery and structure-activity relationship of 3-aryl-5-aryl-1,2,4-oxadiazoles as a new series of apoptosis inducers and potential anticancer agents, *J. Med. Chem.*, 48, 5215-5223, doi:10.1021/jm050292k, 2005.

Zhang, R., Leu, M.-T., and Keyser, L. F.: Heterogeneous chemistry of HONO on liquid sulfuric acid: A new mechanism of chlorine activation on stratospheric sulfate aerosols, *J. Phys. Chem.*, 100, 339-345, doi:10.1021/jp952060a, 1996.

Zhang, W., and Du, B.: Products and mechanism of the Cl-initiated atmospheric oxidation of furan: A theoretical study, *Comput. Theor. Chem.*, 963, 348-356, doi:10.1029/2004JD004993, 2011.

Zingler, J., and Platt, U.: Iodine oxide in the Dead Sea Valley: Evidence for inorganic sources of boundary layer IO, *J. Geophys. Res.-Atmos.*, 110, D07307, doi:10.1029/2004JD004993, 2005.

Zuo, Y., and Deng, Y.: Evidence for the production of hydrogen peroxide in rainwater by lightning during thunderstorms, *Geochim. Cosmochim. Acta*, 63, 3451-3455, doi:10.1016/S0016-7037(99)00274-4, 1999.

Zytner, R. G.: Sorption of benzene, toluene, ethylbenzene and xylenes to various media, *J. Hazard. Mater.*, 38, 113-126, doi:10.1016/0304-3894(94)00027-1, 1994.

Appendix A – GC-MS calibration data

Table 22. GC-MS calibration data.

Concentration (ng)	Benzene	Toluene	Ethylbenzene	X-Xylenes	Y-Xylene	Chlorobenzene	Isoprene	a-Pinene	Camphor	3-Carene	Sabinene	p-Cymene
0.05			104	84	104	222	517					
0.1	645	1756	346	166	332	526			70			444
0.5	2794	8982	1660	1620	1663	1820	3637	55	741			288
1	8380	11062	4193	4094	4196	5642	5110	291		335	212	1369
5	25930	32941	15051	15035	15060		29828	2909	2218	1561		1671
50		444410		342860			181743	51389	28569	10612	472	15311
500		3413469					1841981	540691	318082	114773	15689	258530
1000							3195039	828759	449318	158268	67948	345736

Concentration (ng)	Limonene	Eucalyptol	Furan	3-Methylfuran	2-Methylfuran	2-Ethylfuran	2-Propylfuran	2-Butylfuran	2-Pentylfuran	2,3-Dimethylfuran	2,4-Dimethylfuran	2,5-Dimethylfuran
0.05			76	272	273	199	310	312	194	255	205	305
0.1			159	437	437	443	430	526	1068	409	344	474
0.5			540	1675	1677	2024	1964	995	4423	1745	1456	2033
1	158	502	1359	3838		4407	3809	1628	8439	4006	3164	4847
5	463	1857	5551	17051	15002	19528	22040	11100	41737	19388	14088	20173
50	3445	21455	49761	215357	156222	205145			548555			
500	48544	130184										
1000	56905											

Concentration (ng)	3-Chlorofuran	3-Bromofuran	Carbon disulfide	Dimethyl sulfide	Dimethyl selenide	Dimethyl disulfide	Dimethyl diselenide	Thiophene	2-Methylthiophene	3-Methylthiophene	Chloromethane	Dichloromethane
0.05		254	182	150	155			259	250	257	65	524
0.1	110	435	599	202	240	242		731	649	806	649	716
0.5		1675	1186	606	747	1617		1886	2042	2021	1992	1832
1	1119	3560	3813	1818	1916	4465	245	6595	6350	6545	5229	2492
5	4707		14202	7569	7158	20255	1349	24721	29596	28574	16017	6983
50			102081	63647		214859	19392				98808	96152
100				76557		445170						
500			1446495	426169		1767206					619980	
1000			2144384	761411							1382878	

Continuation of: **Table 22.** GC-MS calibration data.

Concentration (ng)	Trichloromethane	Tetrachloromethane	Chloroethane	1-Chloropropane	1-Chlorobutane	1-Chloropentane	1-Chlorohexane	1-Chloroheptane	1-Chlorooctane	1,1-Dichloroethane	1,2-Dichloroethane	1,1,1-Trichloroethane
	mean peak area (counts)											
0.05	124	108			39	112		43		289	244	307
0.1	530	293	95		199	193	108	86	392	464	425	725
0.5	1993	1759	239	102	704	910	468	614	1531	858	1403	1614
1	5281	5310	470	293	2218	2125		1809	3034	4503	3882	
5	23787	16158	1371	676	7285	7251	3041		16821	9399		
10					14383	15629	6860					
50		315917	9272	6648				14833	174112			
100					147859	146990						
500						2796096	2919453	2375182				
1000								7948110				

Concentration (ng)	1,2-Dichloropropane	1,3-Dichloropropane	2-Chlorobutane	Chloroethene	1,1-Dichloroethene	trans-1,2-Dichloroethene	Trichloroethene	Tetrachloroethene	Bromomethane	Dibromomethane	Tribromomethane	Iodomethane
	mean peak area (counts)											
0.05				251	133	209	116	35	44		102	115
0.1	440	188	167	549	567	467	431	224	213	210	185	280
0.5	1417	684	618	1724	1872	1234	1745	625	1047	649	548	1097
1	3758	1925	2383	5146	5010	4345		1683	1040	1664	1198	2971
5	15134	8001	6582	13528	10516	9474		4243	7784		5175	7924
50												60049

Concentration (ng)	Diiodomethane	Iodoethane	1-Iodopropane	2-Iodopropane	1-Iodobutane	2-Iodobutane	Bromochloromethane	Bromodichloromethane	Dibromochloromethane	1-Bromo-2-chloroethane
	mean peak area (counts)									
0.05	53							265	196	234
0.1	115	237	69		56	95	157	537	485	269
0.5	421	795	259	65	99	106	503	1875	1881	1178
1	556	2255	655	151	227	94	1504	5145	2365	2424
5	3199						5417	20401	10945	9883
10		27080	7531	1614	2597	463				

Appendix B – Locations and pH of Western Australian salt lakes

Table 23. Geographical position and pH of salt lakes in Western Australia.

Salt lake	Year	pH	Geographical position		Sampling site	Year	pH	Geographical position	
Stennets L.	2012	8.1	-33.200260°	119.989088°	L. Nelson	2011	6.0	-32.473419°	119.154679°
L. Hatter Hill*	2013	8.0	-33.099081°	119.842574°	L. Homestead Road*	2012	5.9	-33.007168°	118.938132°
Stennets L.	2013	7.8	-33.200260°	119.989088°	L. Fox SE	2012	5.9	-32.882158°	119.523119°
L. Hatter Hill*	2012	7.5	-33.099081°	119.842574°	L. Emu*	2012	5.6	-33.159325°	119.655523°
L. Walker*	2012	7.4	-33.053173°	118.953010°	Hyden Pool*	2012	5.6	-32.434264°	118.906424°
L. Muncaster*	2012	7.4	-33.219541°	119.928310°	L. Tay	2011	5.5	-33.005308°	120.735264°
L. Strawbridge*	2012	7.3	-32.848018°	119.396998°	L. Kathleen	2011	5.5	-32.984241°	119.694444°
L. Muncaster*	2013	7.3	-33.219541°	119.928310°	L. Newton	2011	5.5	-32.965979°	119.615020°
L. Parson	2012	7.3	-33.170655°	119.067834°	L. Carmody	2011	5.5	-32.516601°	119.325312°
L. Strawbridge*	2013	7.2	-32.848018°	119.396998°	L. Spiked Ball*	2013	5.1	-33.065724°	119.623889°
L. Sand North	2013	7.2	-33.047762°	119.596167°	L. Golf*	2011	5.0	-32.814024°	119.515873°
L. Will-Rock*	2012	7.2	-33.063374°	118.934303°	L. Mirror*	2012	5.0	-33.161005°	119.663714°
DK's Pit	2012	7.2	-33.201086°	119.081622°	L. Crack*	2012	5.0	-32.644468°	119.429868°
L. Bean*	2013	7.1	-33.161294°	119.744744°	L. Fox Road*	2012	4.9	-32.886857°	119.529571°
L. Monday*	2012	7.1	-33.049237°	118.967175°	L. Golf*	2012	4.7	-32.814024°	119.515873°
L. Stubbs	2012	7.1	-33.062790°	119.015450°	L. Vernom*	2012	4.7	-32.758752°	119.381395°
L. Hill*	2012	7.1	-33.119506°	119.106541°	L. Orange*	2012	4.4	119.161999°	119.095888°
L. Road*	2012	7.1	-32.878682°	119.546204°	L. Whurr*	2011	4.2	-33.042975°	119.012466°
L. Dillon*	2011	7.0	-32.932642°	118.860942°	L. Birdy*	2012	4.2	-33.148285°	119.663169°
L. Stubbs	2011	7.0	-33.062790°	119.015450°	L. Gulson - Salt Pan*	2012	4.2	-32.766019°	119.398892°
L. Kathleen	2013	7.0	-32.984241°	119.694444°	L. Quarry*	2012	4.2	-32.648702°	119.440032°
L. Austral	2012	7.0	-33.002271°	118.889275°	L. Orr*	2011	4.0	-33.148051°	119.161199°
L. Days Road*	2012	7.0	-33.121582°	119.687893°	L. Hound*	2012	4.0	-32.799632°	119.490641°
L. Burns*	2011	7.0	-32.960841°	118.887130°	L. Marble*	2012	4.0	-32.582448°	119.426662°
L. Strawbridge*	2011	7.0	-32.848018°	119.396998°	L. Springfield*	2011	3.9	-32.460839°	119.165660°
L. Burkett	2012	6.9	-33.095713°	119.038995°	Hyden Pool*	2011	3.9	-32.434264°	118.906424°
L. Fleay	2012	6.9	-33.193300°	119.076839°	L. Sand South*	2013	3.8	-33.048308°	119.598288°
L. Void*	2012	6.9	-32.660078°	119.431589°	Sip Ford*	2012	3.8	-32.474880°	119.030960°
L. King	2011	6.8	-33.089109°	119.592649°	L. Magic	2012	3.8	-32.431246°	118.906000°
L. Muncaster*	2011	6.8	-33.219541°	119.928310°	L. Morgan	2013	3.7	-33.461863°	119.246552°
L. Ottaway	2013	6.8	-33.199386°	119.069249°	L. Dune*	2012	3.7	-33.084896°	119.637903°
L. Kathleen	2012	6.8	-32.984241°	119.694444°	L. Eukalyptus*	2012	3.6	-33.147746°	119.645759°
L. Mud*	2012	6.8	-32.890684°	119.538376°	L. Winchcombe*	2012	3.6	-32.762925°	119.390091°
Gulson Downs*	2012	6.8	-32.762340°	119.418896°	L. Springfield*	2012	3.6	-32.460839°	119.165660°
L. Friday*	2013	6.7	-33.063005°	119.631039°	L. Whurr*	2012	3.6	-33.042975°	119.012466°
L. Cobham	2013	6.7	-33.440175°	119.279143°	L. Orr*	2012	3.6	-33.148051°	119.161199°
L. King	2012	6.7	-33.089109°	119.592649°	L. Smerdon*	2012	3.5	-33.165383°	119.751668°
L. Gregson*	2012	6.7	-32.649027°	119.426251°	L. Lucky*	2012	3.5	-32.803466°	119.493182°
L. Stubbs	2013	6.6	-33.062790°	119.015450°	L. Needle*	2012	3.5	-32.809276°	119.422920°
L. Bidy	2012	6.6	-33.013998°	118.942529°	L. Acid*	2012	3.5	-32.812620°	119.427910°
Eclipse L.	2011	6.5	-32.951638°	118.835514°	L. Shot*	2013	3.5	-33.047973°	119.610159°
L. Hatter Hill*	2011	6.5	-33.099081°	119.842574°	L. Orr*	2011	3.5	-33.148051°	119.161199°
L. Morris	2013	6.5	-33.472128°	119.237592°	L. Wind*	2013	3.4	-33.053119°	119.604606°
L. Mission*	2012	6.5	-33.108759°	119.093278°	L. Whurr*	2013	3.4	-33.042975°	119.012466°
L. Lee*	2012	6.5	-33.132155°	119.133003°	L. Rodger*	2012	3.4	-33.045184°	118.960887°
L. Camm	2012	6.5	-32.960170°	119.559751°	L. Farm*	2012	3.4	-32.807297°	119.494150°
L. Rabbit*	2012	6.5	-32.793437°	119.488364°	L. Karrigan*	2012	3.4	-32.432275°	118.931442°
L. Newman*	2012	6.3	-33.142869°	119.133342°	L. Wave Rock*	2012	3.4	-32.436276°	118.930648°
L. Nature Reserve*	2012	6.3	-32.810530°	119.462223°	L. Sheoak*	2012	3.3	-33.061309°	118.942560°
L. Shapes*	2012	6.3	-32.459767°	119.094205°	L. Valley*	2012	3.3	-33.055975°	118.949105°
L. Gulson	2012	6.2	-32.788847°	119.404131°	L. Trash*	2012	3.3	-33.143318°	119.161999°
L. Newton	2012	6.2	-32.965979°	119.615020°	L. Bobtail*	2012	3.2	-32.887975°	119.534392°
L. Austral	2011	6.1	-33.002271°	118.889275°	L. Chlorine*	2011	3.2	-32.653062°	119.422726°
Stennets L.	2011	6.0	-33.200260°	119.989088°	L. Holt Rock*	2011	3.2	-32.649258°	119.433930°
L. Camm	2011	6.0	-32.960170°	119.559751°	L. Field*	2012	3.1	-33.163669°	119.681878°
Gulson Downs*	2011	6.0	-32.762340°	119.418896°	L. Bunche*	2011	3.0	-32.982874°	118.914506°

Appendix B – Locations and pH of Western Australian salt lakes

Continuation of: **Table 23.** Geographical position and pH of salt lakes in Western Australia..

Salt Lake	Year	pH	Geographical position		Sampling site	Year	pH	Geographical position	
L. Harvey*	2011	3.0	-32.601458°	119.464103°	Sleeping Kangaroo*	2012	2.8	-33.162146°	119.691262°
L. Modesty*	2011	3.0	-32.600308°	119.475420°	L. Homestead Rail*	2011	2.8	-33.004226°	118.939858°
L. Yellow*	2011	3.0	-32.498005°	119.366397°	L. Homestead Rail*	2012	2.7	-33.004226°	118.939858°
L. Cuthulhu*	2013	3.0	-33.064269°	119.620954°	L. Modesty*	2012	2.7	-32.600308°	119.475420°
L. Roystone	2013	2.9	-33.453585°	119.247573°	L. Harvey*	2012	2.7	-32.601458°	119.464103°
L. Holland*	2012	2.9	-32.549540°	119.341360°	L. Yellow*	2012	2.7	-32.498005°	119.366397°
L. Dune*	2013	2.9	-33.084896°	119.637903°	L. Boats*	2013	2.7	-33.068538°	119.636983°
L. Crusty*	2012	2.8	-32.484355°	119.303575°	L. Holt Rock*	2012	2.6	-32.649258°	119.433930°
L. Crusty*	2011	2.8	-32.484355°	119.303575°	L. Boats*	2012	2.6	-33.068538°	119.636983°
L. Magic	2011	2.8	-32.431246°	118.906000°	L. Dune*	2011	2.5	-33.084896°	119.637903°
					L. Chlorine*	2012	2.4	-32.653062°	119.422726°

* No official sample site name.

Appendix C – Soil/sediment sampling locations

Table 24. Parameters of Australian sediments of 2011.

Sampling sites	Layer (cm)	Geographical position		Iron (w%)	pH	Organic carbon (w%)
Lake Magic I	0-2	S32.432488°	E118.905544°	1.0	5.0	0.9
Lake Magic II	14-22	S32.432970°	E118.905360°	1.6	5.0	0.1
Lake Springfield*	0-2	S32.461780°	E119.166200°	1.5	5.1	2.2
	2-4			2.1	5.8	2.8
	4-6			2.0	6.4	1.3
Lake Tay	0-0.5	S33.031390°	E120.740700°	0.5	6.4	0.9
Lake Orr* I	0-4	S33.148681°	E119.163755°	1.0	5.9	0.5
	4-6			0.7	5.4	0.5
	6-10			1.3	5.4	0.4
Lake Orr* II	0-0.5	S33.150270°	E119.160960°	1.2	5.7	0.4
	0.5-2			1.9	5.8	1.5
	2-4			2.0	6.3	1.4
	4-6			1.7	6.6	1.2
Lake Hatter Hill*	6-8	S33.099221°	E119.839868°	1.0	6.6	0.2
	0-2			1.1	7.6	4.7
	2-4			1.3	8.4	2.0
Lake King I	4-6	S33.089010°	E119.618810°	1.6	8.4	0.5
	0-0.5			0.5	7.1	0.6
	0.5-2			0.8	7.9	0.8
Lake King II	2-4	S33.090780°	E119.617690°	0.9	8.0	0.6
	4-6			0.8	7.9	0.3
	26-28			0.8	7.9	0.2
	0-2			0.6	7.6	0.5
	2-4			0.5	7.9	0.2
Lake Dune*	4-6	S33.082940°	E119.638370°	0.6	7.6	0.3
	0-0.5			2.1	7.9	0.8
	0.5-1.5			0.8	7.4	0.2
	1.5-3.5			2.5	6.0	1.3
Lake Strawbridge*	3.5-6	S32.844030°	E119.397990°	2.4	5.6	2.1
	0-2			1.4	8.1	1.3
	2-4			1.6	8.1	1.4
	4-6			1.6	8.1	2.1
Lake Golf*	6-8	S32.810020°	E119.519620°	1.2	8.3	0.7
	0-2			3.6	7.5	2.0
	2-4			1.9	7.5	0.6
Lake Stubbs I	4-6	S33.060340°	E118.996750°	3.1	6.7	0.2
	0-0.5			0.8	7.3	0.6
	0.5-10			1.5	8.0	1.0
Lake Stubbs II	>10	S33.060360°	E119.000350°	3.0	8.2	1.1
	0-20			1.6	8.2	0.8
Lake Stubbs III	0-2	S33.060250°	E118.996610°	1.1	8.1	0.7
	2-4			1.1	8.3	0.5
	4-6			1.0	8.2	1.1
	6-8			1.6	8.2	0.6
Lake Whurr*	0-1	S33.043120°	E119.008820°	2.4	4.8	0.8
	1-2			2.0	5.2	1.4
	2-6			1.7	5.8	1.6
	6-7			0.8	5.9	0.5
	>7			2.4	5.4	0.5

* No official sample site name.

Table 25. Parameters of Australian sediments of 2012.

Sampling sites	Layer (cm)	Geographical position		Iron (w%)	pH	Organic carbon (w%)
Lake Emu*	0-2	S33.160990°	E119.655110°	1.2	6.9	1.7
	2-4			0.8	7.8	1.5
Stennets Lake	0-2	S33.202230°	E119.979520°	0.8	7.3	2.7
Lake Strawbridge*	0-4	S32.844550°	E119.397750°	1.6	7.6	1.5
	4-6			1.3	7.9	0.1
Lake Gulson I	0-2	S32.772020°	E119.399680°	0.7	7.8	0.7
	2-4			0.6	8.2	0.2
	4-6			0.6	7.8	0.2
Lake Gulson II	0-0.5	S32.7685°	E119.39834°	0.5	7.6	0.5
Lake Boats Claypan*	0-2	S33.06899°	E119.63868°	2.5	4.3	5.9
	2-4			2.7	4.5	4.0
	4-6			2.6	4.5	3.7
Lake Boats*	0-2	S33.069214°	E119.637771°	1.0	4.7	1.0
	2-4			1.2	4.2	3.2
	4-6			0.9	4.6	0.9
Lake Whurr*	0-1	S33.041650°	E119.010200°	1.9	6.9	0.7
	1-4			2.1	6.2	1.6
	4-6			2.0	5.6	1.6
Lake Orr*	crust	S33.148180°	E119.165160°	1.0	5.0	0.2
	0-2			1.5	5.9	0.5
	2-4			1.6	5.2	0.7
	4-6			1.5	4.9	0.8
Lake Dune*	0-2	S33.083720°	E119.639450°	0.7	4.8	0.1
	2-4			0.8	5.4	0.2
	4-6			0.7	5.6	0.5
Lake Newton I	0-2	S32.960670°	E119.611770°	0.6	7.5	0.5
	2-4			0.5	7.6	0.3
	4-6			0.8	7.6	0.2
Lake Newton II	0-0.5	S32.960486°	E119.611766°	0.5	6.8	1.1
	0.5-2			0.5	7.7	0.5

* No official sample site name.

Table 26. Parameters of Dead Sea sediments of 2012.

Sampling sites	Layer (cm)	Geographical position		Iron (w%)	pH	Organic carbon (w%)
Sodom* I	crust	N30.96472°	E35.36380°	1.3	7.9	0.0
	0-2			1.5	7.9	0.2
	2-4			1.6	8.0	0.5
	4-6			1.7	8.0	0.6
	6-8			1.8	8.1	0.4
Sodom* II	crust	N30.96456°	E35.36388°	1.4	7.7	0.4
	0-2			1.2	8.0	0.4
	2-4			1.3	7.9	0.4
	4-6			1.6	7.9	0.3
Sodom* Plant	crust	N30.96424°	E35.36335°	1.3	7.9	0.6
	0-2			1.5	7.8	0.5
	2-4			1.5	7.8	0.4
	4-6			1.5	7.9	0.4

* No official sample site name.

Appendix D – Water sampling locations

Table 27. Properties of the Australian water samples of 2011.

Sampling sites		Geographical position		Iron (mg/L)	pH	Organic carbon (mg/L)
Lake Orr*	groundwater	S33.148681°	E119.163755°	13.6	3.1	53
Lake Springfield*	surface water	S32.461780°	E119.166200°	84.0	3.4	89
Lake Dune*	surface water	S33.083083°	E119.639139°	24.0	2.6	55
Lake Golf*	groundwater	S32.810390°	E119.518654°	18.0	5.1	39
Lake Strawbridge*	groundwater	S32.844030°	E119.397990°	0.64	7.1	107
Lake Hatter Hill*	groundwater	S33.099221°	E119.839868°	0.22	7.2	1266
Lake King	surface water	S33.089010°	E119.618810°	0.66	7.4	104
Lake Stubbs	groundwater	S33.060340°	E118.996750°	2.26	7.2	26

* No official sample site names.

Table 28. Properties of the Australian water samples of 2012.

Sampling sites		Geographical position		Iron (mg/L)	pH	Organic carbon (mg/L)
Lake Newton	groundwater	S32.960670°	E119.611770°	2.88	6.3	86
Lake Strawbridge*	surface water	S32.844550°	E119.397750°	0.47	7.4	280
Lake Boats*	surface water	S33.069214°	E119.637771°	173	2.4	101
Stennets Lake	surface water	S33.202230°	E119.979520°	-	8.7	44
Lake Dune*	surface water	S33.085950°	E119.637450°	1.77	3.5	26
Lake Orr*	surface water	S33.148180°	E119.165160°	7.41	3.1	34
Lake Emu*	surface water	S33.160990°	E119.655110°	-	5.7	65
Lake Whurr*	surface water	S33.041650°	E119.010200°	65.5	3.1	37

* No official sample site names.

Table 29. Properties of the Dead Sea water samples of 2012.

Sampling sites		Geographical position		Iron (mg/L)	pH	Organic carbon (mg/L)
South End* I	surface water	N30.965436°	E35.366744°	-	5.1	-
South End* II	surface water	N30.965436°	E35.366744°	-	5.1	-
Sodom* I	groundwater	N30.964397°	E35.363672°	-	6.5	-
Sodom* II	groundwater	N30.964583°	E35.363028°	-	6.5	-
Sodom* Plant	groundwater	N30.964553°	E35.362258°	-	6.5	-
En Gedi	surface water	N31.467156°	E35.398942°	-	6.0	-
En Bokek	surface water	N31.201047°	E35.366775°	-	6.0	-

* No official sample site names.

Appendix E – Selected emission data
Table 30. Emission data for BTEX and chlorobenzene from water samples.

Sampling sites	Benzene (ng/mL)	Toluene (ng/mL)	Ethylbenzene (ng/mL)	X-Xylenes (ng/mL)	Y-Xylene (ng/mL)	Chlorobenzene (ng/mL)
L. Orr 2011	0.004	-	0.016	-	-	0.007
L. Springfield 2011	-	-	0.010	-	-	0.004
L. Golf 2011	-	0.024	0.024	-	0.031	0.004
L. Strawberry 2011	-	0.021	-	-	-	-
L. Hatter Hill 2011	-	0.037	0.037	0.035	0.011	0.008
L. King 2011	-	0.047	0.024	-	-	0.006
L. Stubbs 2011	-	0.036	0.026	-	-	0.008
L. Newton 2012	0.004	0.075	0.104	0.056	-	-
L. Strawbridge 2012	-	0.091	0.097	0.035	-	-
L. Boats Inlet 2012	-	0.047	0.012	0.048	-	-
L. Boats 2012	-	0.031	-	-	-	0.006
Stennets Lake 2012	-	0.033	0.047	-	-	-
L. Orr 2 2012	-	-	0.037	-	-	0.005
L. Emu 2012	-	-	0.078	0.017	-	-
L. Whurr 2012	-	-	0.061	-	-	-
Sodom I	0.058	12.245	0.173	0.339	0.155	0.006
Sodom II	0.018	12.564	0.158	0.371	0.156	0.005
Sodom Plant	0.019	27.037	0.136	0.421	0.236	0.006
En Bokek	-	0.224	0.049	0.157	0.039	0.006
En Gedi	-	0.163	0.027	0.077	0.012	0.004
South End I	-	0.172	0.038	0.126	-	0.006
South End II	-	1.965	0.025	0.078	0.012	0.004

Table 31. Emission data for VSC/VSeC from water samples.

Sampling sites	pH	Carbon disulfide (ng/mL)	Dimethyl sulfide (ng/mL)	Dimethylselenide (ng/mL)	Dimethyl disulfide (ng/mL)	Dimethyl selenenyl sulfide (counts/mL)	Dimethyl diselenide (ng/mL)	Thiophene (ng/mL)	2-Methylthiophene (ng/mL)	3-Methylthiophene (ng/mL)
Stennets Lake 2012	8.7	0.020	0.102	-	0.011	-	-	-	-	-
L. King 2011	7.4	0.037	0.138	-	0.005	-	-	0.005	-	-
L. Strawbridge 2012	7.4	0.288	0.441	0.019	0.007	-	-	0.011	0.025	0.058
L. Stubbs 2011	7.2	-	-	-	-	-	-	-	-	-
L. Hatter Hill 2011	7.2	0.016	0.106	-	0.005	-	-	0.028	0.007	0.007
L. Strawbridge 2011	7.1	-	-	-	0.016	-	-	0.007	0.015	-
L. Newton 2012	6.3	0.017	0.039	-	0.005	-	-	0.014	0.021	0.022
L. Emu 2012	5.7	-	0.012	-	-	-	-	-	-	-
L. Golf 2011	5.1	-	0.090	-	0.005	-	-	-	-	-
L. Boats GW 2012	3.6	1.092	-	0.018	0.415	-	-	0.019	0.027	0.007
L. Dune 2012	3.5	-	0.077	-	-	-	-	-	-	-
L. Springfield 2011	3.4	0.085	0.464	-	0.014	-	-	0.016	0.006	-
Hyden Pool 2011	3.3	-	0.029	0.134	-	-	-	-	-	-
L. Whurr 2012	3.1	-	3.109	-	0.007	-	-	-	-	-
L. Orr 2011	3.1	-	0.059	-	-	-	-	-	-	-
L. Orr 2012	3.1	0.004	0.030	-	-	-	-	-	-	-
L. Boats Inlet 2012	3.0	0.093	0.473	-	0.077	-	-	0.011	0.013	0.005
L. Dune 2011	2.6	-	0.033	-	-	-	-	-	-	-
L. Boats 2012	2.4	0.019	0.082	-	0.037	-	-	0.008	0.005	-
Sodom I	6.5	0.014	-	-	0.010	-	-	-	-	-
Sodom II	6.5	0.021	-	-	-	-	-	-	-	-
Sodom Plant	6.5	0.028	-	0.015	-	-	-	-	-	-
En Bokek	6.0	0.057	-	-	0.005	-	-	0.017	0.020	0.005
En Gedi	6.0	0.006	-	-	-	-	-	-	-	-
South End I	5.1	-	-	-	-	-	-	-	-	-
South End II	5.1	-	-	-	-	-	-	-	-	-

Table 35. Emission data for chloroalkanes and chloroalkenes from Israeli soils.

Sampling sites	Layer (cm)	2-Chlorobutane (ng/g)	1,1,1-Trichloroethane (ng/g)	1,2-Dichloroethane (ng/g)	1,3-Dichlorobutane (counts/g)	1-Chloro-5-methylhexane (ng/g)	Chloroethene (ng/g)	1,1-Dichloroethene (ng/g)	trans-1,2-Dichloroethene (ng/g)	1-Chloro-2-methyl-1-propene (counts/g)	1,1-Dichloro-propene (counts/g)
Israel Sodom I	4-6	-	-	-	-	1087	-	-	-	-	-
Sodom I	6-8	-	-	-	-	1522	-	-	-	-	-
Sodom Plant	0-2	0.12	-	-	-	-	-	-	-	-	-

Table 32. Emission data for chloroalkanes and chloroalkenes from Australian sediments.

Sampling sites	Layer (cm)	2-Chlorobutane	Trichloroethane 1,1,1-	1,2-Dichloroethane	Dichlorobutane 1,3-	1-Chloro-5- methylhexane	Chloroethene	1,1-Dichloroethene	trans-1,2- Dichloroethene	1-Chloro-2- methyl-1-propene	1,1-Dichloro- propene		
		(ng/g)	(ng/g)	(ng/g)	(counts/g)	(ng/g)	(ng/g)	(ng/g)	(ng/g)	(counts/g)	(counts/g)		
Australia 2011	L. Springfield	0-2	1.54	-	0.12	537	6302	-	-	-	300	-	
	L. Springfield	2-4	4.72	-	-	1614	12280	-	-	-	889	264	
	L. Springfield	4-6	2.20	0.06	0.21	1763	5322	-	3.79	-	350	-	
	L. Orr II	0-0.5	-	-	0.06	-	-	-	-	-	-	-	-
	L. Orr II	0.5-2	1.16	-	0.17	1931	8385	-	-	-	-	-	-
	L. Orr II	2-4	1.83	0.04	0.38	5776	11643	-	-	-	197	-	-
	L. Orr II	4-6	1.83	0.09	0.77	4550	11679	-	-	-	257	-	-
	L. Orr II	6-8	-	-	-	-	4236	-	-	-	-	-	-
	L. Hatter Hill	0-2	12.56	-	-	-	10711	-	-	-	910	458	-
	L. Hatter Hill	2-4	5.84	-	-	355	7373	-	-	-	569	132	-
	L. King I	0-0.5	-	-	-	-	142	-	-	-	-	-	-
	L. King I	0.5-2	-	-	-	-	4647	-	-	-	-	-	-
	L. King I	2-4	0.23	-	-	-	3020	-	-	-	-	-	-
	L. King I	4-6	-	-	-	-	453	-	0.37	-	-	-	-
	L. King II	0-2	-	-	-	-	930	-	-	-	-	-	-
	L. King II	4-6	-	-	-	-	-	0.41	-	-	-	-	-
	L. Dune	0-0.5	0.27	-	0.09	914	16368	-	-	-	-	-	-
	L. Dune	1-5-3.5	1.12	0.09	0.98	3125	-	-	-	-	-	-	-
	L. Dune	3.5-6	1.57	0.20	1.11	3561	11159	-	-	-	-	-	-
	L. Strawbridge	0-2	0.59	-	-	376	6027	-	0.33	-	-	-	-
	L. Strawbridge	2-4	0.49	-	-	543	5514	-	-	-	-	-	-
	L. Strawbridge	4-6	1.04	-	-	482	5629	-	-	-	-	-	214
	L. Strawbridge	6-8	-	-	-	-	-	-	-	-	-	-	-
	L. Golf	0-2	6.41	0.06	0.46	7705	24452	-	-	-	2035	673	-
	L. Golf	2-4	1.31	-	0.18	1212	8013	-	-	-	-	-	-
	L. Golf	4-6	0.36	-	0.12	-	-	-	-	-	-	-	-
	L. Stubbs III	0-2	0.31	-	-	-	2401	-	-	-	-	-	-
	L. Stubbs III	2-4	0.11	-	-	-	1002	0.09	-	-	-	-	-
	L. Stubbs III	4-6	2.27	-	0.05	386	2888	-	-	-	421	178	-
	L. Whurr	0-1	0.59	-	0.07	-	-	-	-	-	-	-	-
L. Whurr	1-2	0.82	-	0.07	-	8262	-	-	-	197	-	-	
L. Whurr	2-6	0.38	-	0.05	-	8295	-	-	-	-	-	-	
L. Whurr	6-7	-	-	0.21	-	-	-	-	-	-	-	-	
L. Whurr	> 7	1.37	-	0.06	-	-	-	-	-	-	-	-	
L. Emu	0-2	-	-	-	-	12642	-	-	-	-	-	-	
Stennets Lake	0-2	0.47	-	-	-	-	-	-	-	-	-	-	
L. Strawbridge	0-4	4.65	-	0.12	2078	11258	-	-	0.21	763	425	-	
L. Strawbridge	4-6	-	-	-	-	1608	-	-	-	-	-	-	
L. Gulson	0-2	-	-	-	-	672	-	-	-	-	-	-	
Australia 2012	L. Boats Claypan	0-2	1.83	0.04	0.61	-	-	-	2.60	-	-	-	
	L. Boats Claypan	2-4	2.51	0.04	0.58	-	-	-	2.84	-	-	-	
	L. Boats Claypan	4-6	1.80	-	0.64	-	-	-	1.61	-	-	-	
	L. Boats	0-2	0.14	0.05	0.13	-	-	-	-	-	-	-	
	L. Boats	2-4	0.47	-	0.16	-	-	-	-	-	-	-	
	L. Boats	4-6	0.14	-	0.06	-	-	-	-	-	-	-	
	L. Whurr	0-1	-	-	-	-	3550	-	-	-	-	-	
	L. Whurr	1-4	3.53	-	0.48	2300	4213	-	-	0.05	-	-	-
	L. Whurr	4-6	0.69	-	0.18	996	6454	-	-	-	-	-	-
	L. Orr	0-2	0.86	-	0.26	664	5962	-	-	0.12	-	-	-
	L. Orr	2-4	1.01	-	0.36	969	-	-	-	0.16	-	-	-
	L. Orr	4-6	0.71	-	0.21	1092	8168	-	-	0.09	-	-	-

Table 33. Emission data for chloroalkanes from water samples.

Sampling sites	Chloromethane	Dichloromethane	Trichloromethane	Tetrachloromethane	Chloroethane	1-Chlorobutane	(ng/mL)							
							1-Chloropentane	1-Chlorohexane	1-Chlorooctane	1,1-Dichloroethane	1,2-Dichloroethane	1,2-Dichloropropane	1,3-Dichloropropane	2-Chlorobutane
L. Orr 2011	-	0.008	0.128	-	-	0.032	0.400	0.366	0.012	0.017	0.029	0.012	-	0.090
L. Springfield 2011	0.080	-	-	-	-	0.016	0.039	-	-	-	0.010	-	-	0.025
Hyden Pool 2011	-	-	-	-	-	0.017	-	-	-	-	0.010	-	-	0.093
L. Dune 2011	0.049	-	-	-	-	0.004	-	-	-	-	0.009	-	-	0.066
L. Golf 2011	-	-	0.009	-	-	-	-	-	-	-	0.010	-	-	-
L. Strawbridge 2011	-	-	-	-	-	-	-	-	-	-	0.010	-	-	-
L. Hatter Hill 2011	-	-	-	-	-	-	-	-	-	-	0.011	-	-	-
L. King 2011	-	-	-	-	-	-	-	-	0.009	-	0.012	-	-	-
L. Stubbs 2011	-	0.077	-	-	-	-	-	-	-	-	0.010	-	-	-
L. Newton 2012	-	-	-	-	-	-	-	-	-	0.023	0.006	-	0.005	-
L. Strawbridge 2012	-	-	-	-	-	-	-	-	-	-	0.006	-	0.005	-
L. Boats Inlet 2012	0.491	0.035	0.112	0.133	-	-	0.122	0.057	-	0.016	0.006	-	-	0.072
L. Boats GW 2012	-	-	0.055	-	-	-	-	-	-	-	-	-	-	-
L. Boats 2012	1.166	0.068	0.017	0.008	0.387	-	0.450	0.178	0.005	0.034	0.009	0.006	-	0.210
Stennets Lake 2012	-	-	-	-	-	-	-	-	-	-	-	-	-	-
L. Dune 2012	-	-	-	-	-	-	0.048	0.086	-	-	-	-	-	-
L. Orr 2 2012	0.103	-	-	-	-	-	0.081	-	-	-	-	-	-	0.038
L. Emu 2012	-	-	-	-	-	-	-	-	-	-	0.004	-	0.006	-
L. Whurr 2012	-	-	-	-	-	-	0.061	-	-	-	-	-	0.006	0.022
Sodom I	-	-	-	-	-	-	-	-	-	-	-	-	-	-
Sodom II	-	-	-	-	-	-	-	-	-	-	-	-	-	-
Sodom Plant	-	-	-	-	-	-	-	0.045	-	-	-	-	-	-
En Bokek	-	-	0.005	-	-	-	0.072	0.069	0.023	-	-	-	-	-
En Gedi	-	-	-	-	-	-	0.046	-	0.010	-	-	-	-	-
South End I	-	-	1.143	-	-	-	0.078	0.036	0.014	-	0.023	-	-	-
South End II	-	-	0.781	-	-	-	-	-	0.011	-	0.040	-	-	-

Table 34. Emission data for chloroalkenes from water samples.

Sampling sites	Chloroethene	trans-1,2-Dichloroethene	Trichloroethene	Tetrachloroethene
	(ng/mL)	(ng/mL)	(ng/mL)	(ng/mL)
L. Orr 2011	-	-	-	0.01
Hyden Pool 2011	-	-	0.01	0.03
L. Dune 2011	-	-	-	0.01
L. Golf 2011	-	-	-	0.05
L. Strawbridge 2011	-	-	0.00	0.05
L. Hatter Hill 2011	-	-	0.01	0.05
L. King 2011	-	-	0.01	0.06
L. Stubbs 2011	-	-	0.01	0.04
L. Strawbridge 2012	-	-	-	0.04
L. Boats Inlet 2012	-	0.01	-	-
L. Boats 2012	0.01	0.01	-	-
Stennets Lake 2012	-	0.02	-	-
L. Dune 2012	-	0.01	-	-
L. Orr 2012	-	0.02	-	-
L. Emu 2012	-	0.02	-	-
L. Whurr 2012	-	0.02	-	-

Table 35. Emission data for mixed halogenated alkanes from soils/sediments.

Sampling sites	Layer	Bromochloromethane (ng/g)	Bromodichloromethane (ng/g)	1-Bromo-2-chloroethane (ng/g)	2-Bromo-1-chloropropane (counts/g)	Dibromochloromethane (ng/g)	Dichloroiodomethane (counts/g)	1,2-Chloroiodoethane (counts/g)	
									(cm)
Australia 2011	Springfield	0-2	-	-	-	0.13	-	-	
	Springfield	2-4	-	-	-	0.07	-	-	
	Springfield	4-6	0.31	-	-	0.12	-	-	
	Orr I	0-4	-	-	-	0.10	-	-	
	Orr I	4-6	-	-	-	0.08	-	-	
	Orr II	0-2	0.13	-	-	0.09	-	-	
	Orr II	2-4	0.26	-	0.20	-	0.22	-	
	Orr II	4-6	0.65	-	0.32	-	0.24	-	
	Dune	0-0.5	-	-	-	-	0.21	-	-
	Dune	1.5-3.5	1.98	2.77	0.41	651	4.90	-	-
	Dune	3.5-6	1.38	0.89	0.53	-	2.14	-	-
	Golf	0-2	0.59	0.15	-	-	0.17	-	-
	Golf	2-4	-	0.38	-	-	0.53	-	-
	Golf	4-6	-	0.14	-	-	0.19	-	-
	Stubbs III	0-2	-	0.08	-	-	0.09	65	-
	Stubbs III	4-6	-	-	-	-	0.04	-	-
	Whurr	0-1	-	0.24	-	-	0.11	-	-
	Whurr	6-7	-	-	-	-	0.08	-	-
	Whurr	>7	-	0.27	-	-	0.09	-	-
	Australia 2012	Lake Emu	0-2	-	-	-	0.07	-	-
L. Strawbridge		0-4	-	-	-	0.08	-	-	
L. Boats Claypan		0-2	-	0.08	-	-	0.63	-	239
L. Boats Claypan		2-4	-	0.09	-	-	0.56	-	422
L. Boats Claypan		4-6	-	0.09	-	-	0.39	-	332
Lake Boats		0-2	-	-	-	-	0.08	-	-
Lake Boats		2-4	-	-	-	-	0.14	-	-
Lake Boats		4-6	-	-	-	-	0.07	-	-
Lake Whurr		0-1	-	-	-	-	0.05	-	-
Lake Whurr		1-4	-	0.08	-	-	0.29	-	-
Lake Whurr		4-6	-	0.05	-	-	0.25	-	-
Lake Orr		0-2	-	0.11	0.10	-	0.50	-	-
Lake Orr	2-4	-	0.27	0.15	-	1.01	-	-	
Lake Orr	4-6	-	0.05	-	-	0.14	-	-	
Israel	Sodom Ia Kruste	crust	-	-	-	0.10	-	-	
	Sodom I 4-6 cm	4-6	-	-	-	0.06	-	-	
	Sodom I 6-8 cm	6-8	-	-	-	0.05	-	-	
	Sodom II 0-2 cm Kruste	crust	-	0.29	-	-	1.11	-	-
	Sodom II 0-2 cm	0-2	-	-	-	-	0.06	-	-
	Sodom Plant Kruste	crust	-	0.23	-	-	0.91	-	-

Appendix F – Data obtained during PTFE chamber experiments

Lake Boats (S33.06896° E119.63798°), 08.03.2013

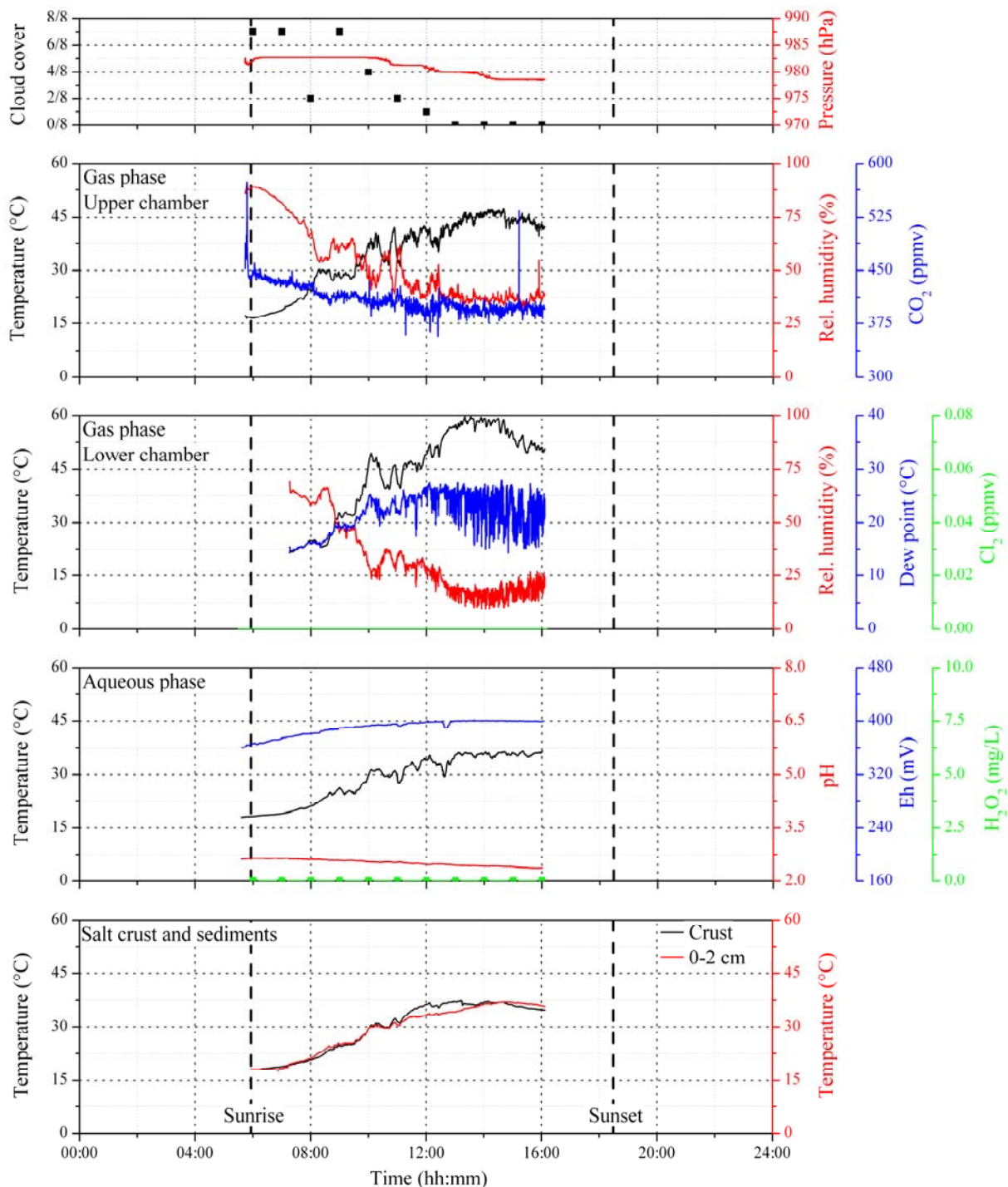


Figure 148. Data obtained during a PTFE chamber experiment at Lake Boats (S33.06896° E119.63798°), 08.03.2013.

Mean free chlorine concentrations 0.13 mg/L.

Mean bound chlorine concentrations 0 mg/L.

Lake Strawbridge (S32.84420° E119.39742°), 09.03.2013

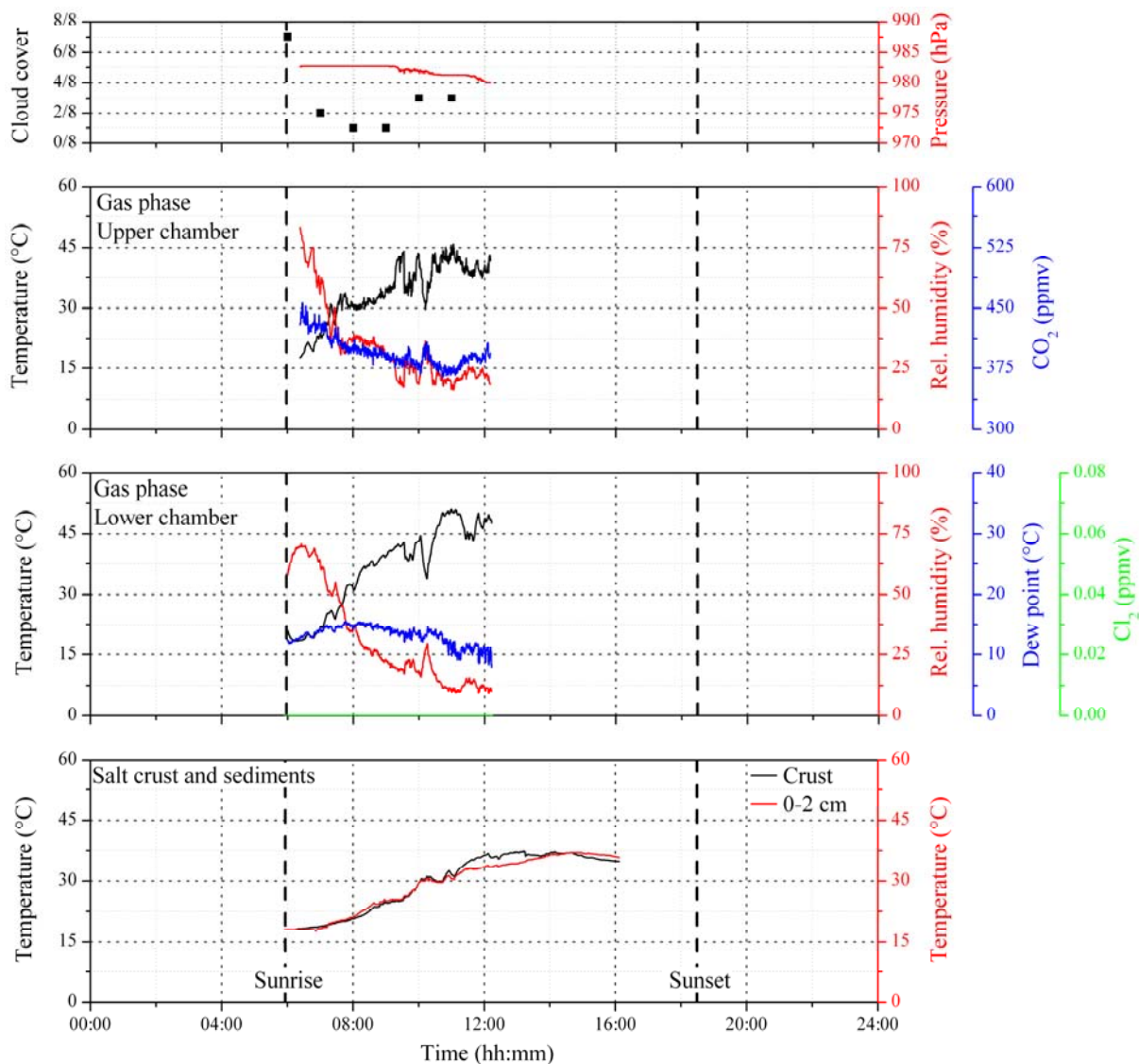


Figure 149. Data obtained during a PTFE chamber experiment at Lake Strawbridge (S32.84420° E119.39742°), 09.03.2013.

Mean free chlorine concentrations 0.24 mg/L.

Mean bound chlorine concentrations 0.01 mg/L.

Lake Dune (S33.08490° E119.63913°), 13.03.2013

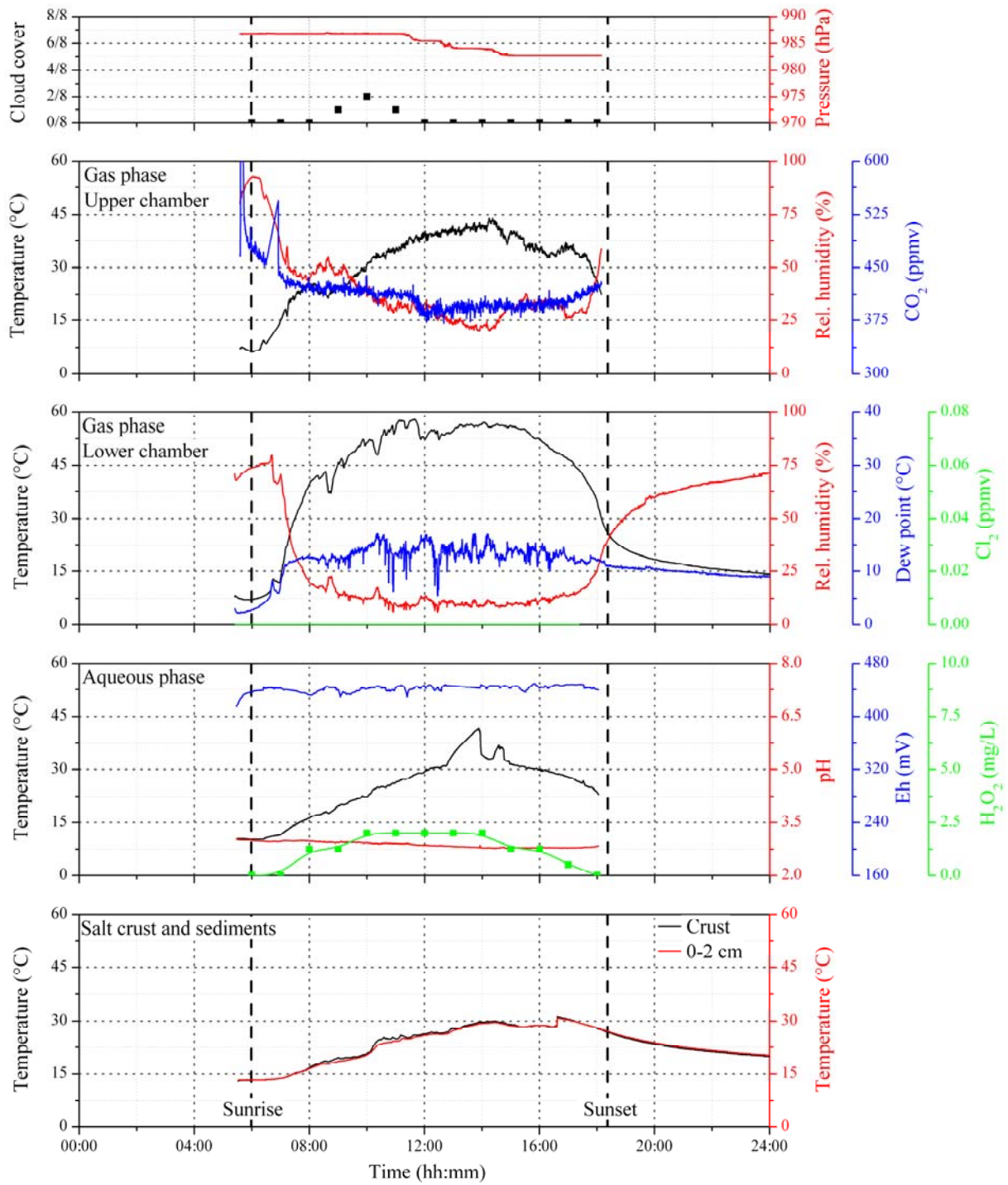


Figure 150. Data obtained during a PTFE chamber experiment at Lake Dune (S33.08490° E119.63913°), 13.03.2013.

Mean free chlorine concentrations 0.14 mg/L.

Mean bound chlorine concentrations 0.12 mg/L.

Lake Dune (S33.08490° E119.63913°), 14.03.2013

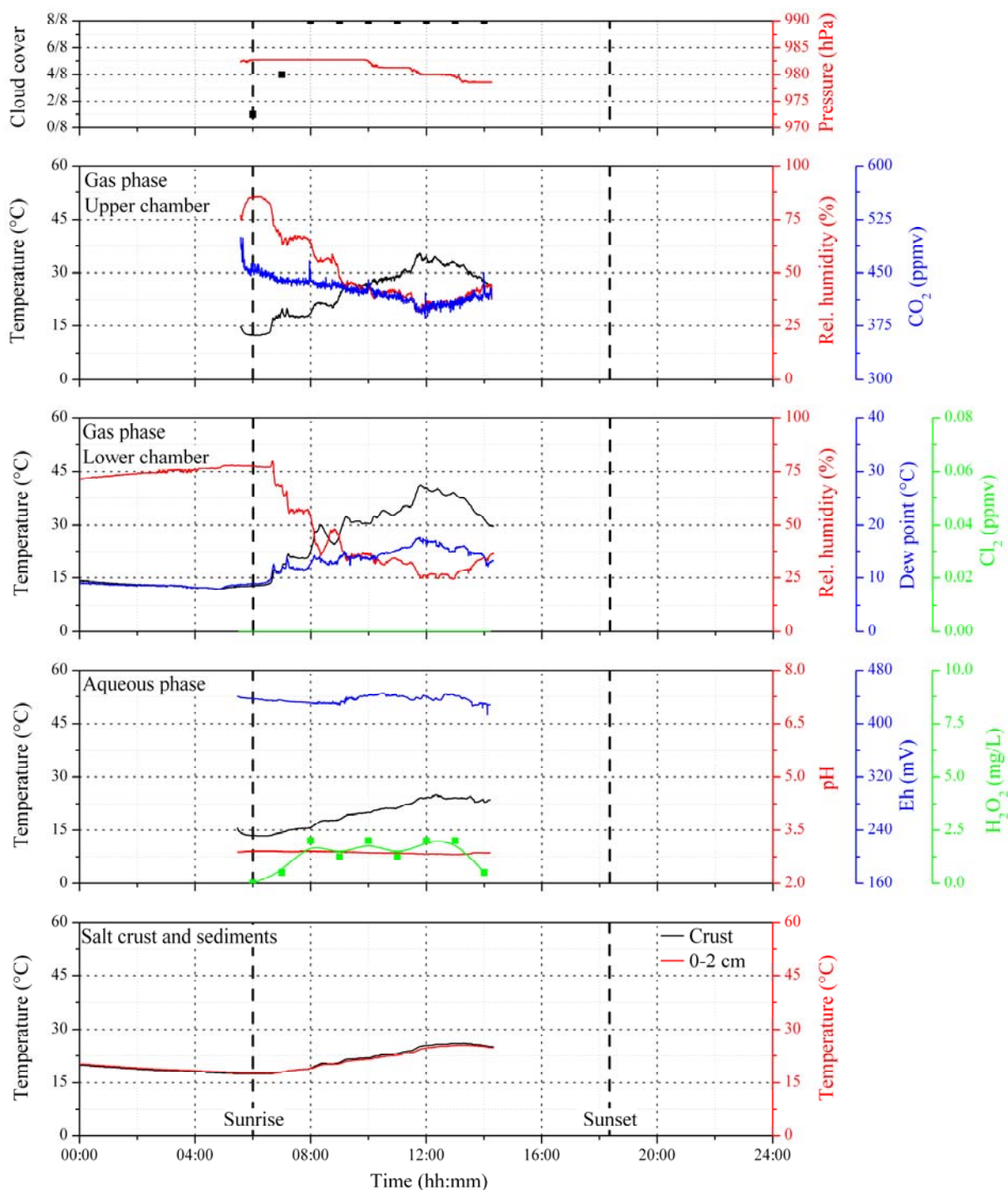


Figure 151. Data obtained during a PTFE chamber experiment at Lake Dune (S33.08490° E119.63913°), 14.03.2013.

Mean free chlorine concentrations 0.13 mg/L.

Mean bound chlorine concentrations 0 mg/L.

Lake Boats (S33.06879° E119.63813°), 18.03.2013

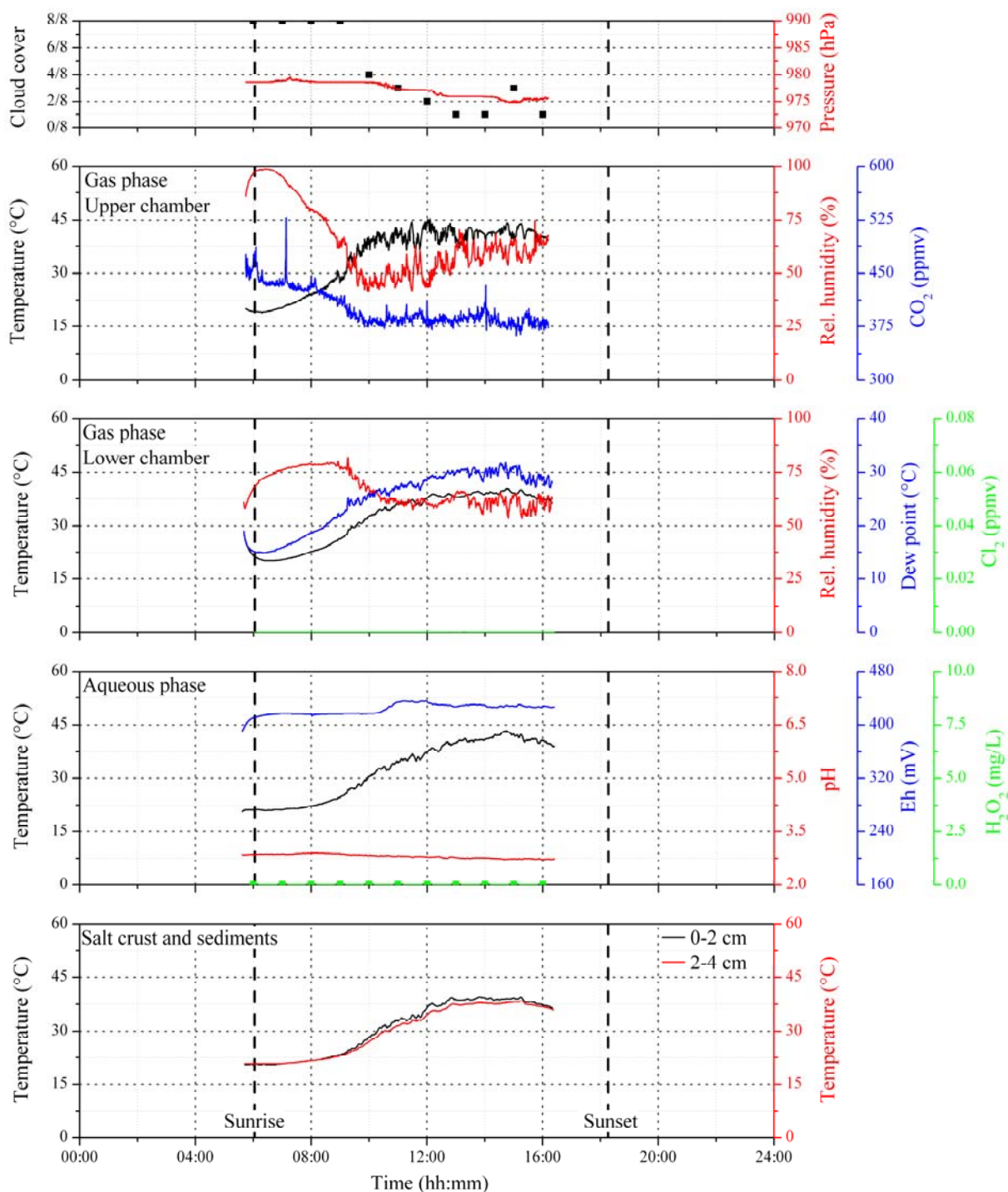


Figure 152. Data obtained during a PTFE chamber experiment at Lake Boats (S33.06879° E119.63813°), 18.03.2013.

Mean free chlorine concentrations 0.08 mg/L.

Mean bound chlorine concentrations 0 mg/L.

Lake Orr (S33.14966° W119.16431°), 19.03.2013

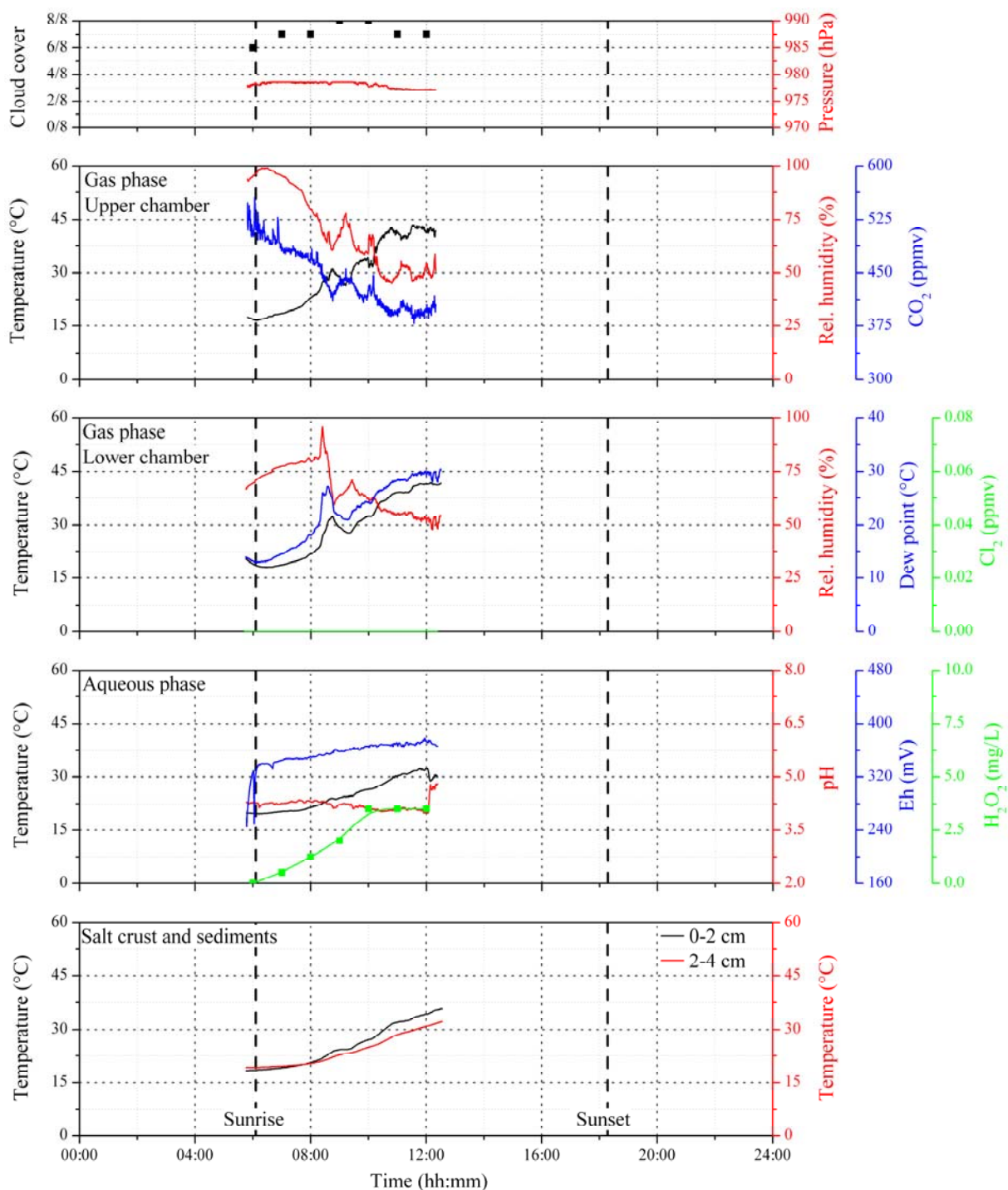


Figure 153. Data obtained during a PTFE chamber experiment at Lake Orr (S33.14966° W119.16431°), 19.03.2013.

Mean free chlorine concentrations 0.04 mg/L.

Mean bound chlorine concentrations 0.01 mg/L.

Lake Shot (S33.04610° E119.60968°), 21.03.2013

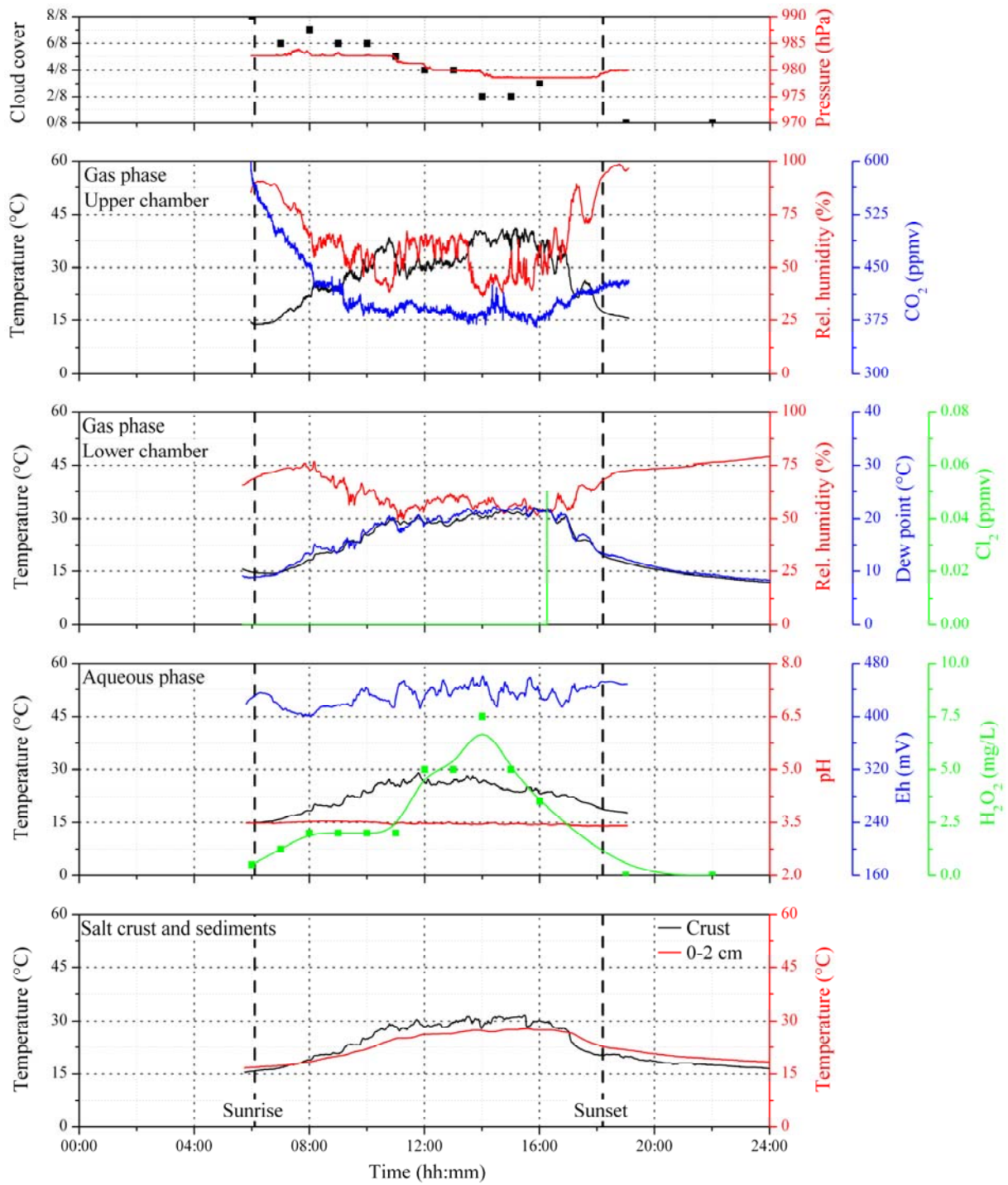


Figure 154. Data obtained during a PTFE chamber experiment at Lake Shot (S33.04610° E119.60968°), 21.03.2013.

Mean free chlorine concentrations 0.16 mg/L.

Mean bound chlorine concentrations 0.09 mg/L.

Lake Shot (S33.04610° E119.60968°), 22.03.2013

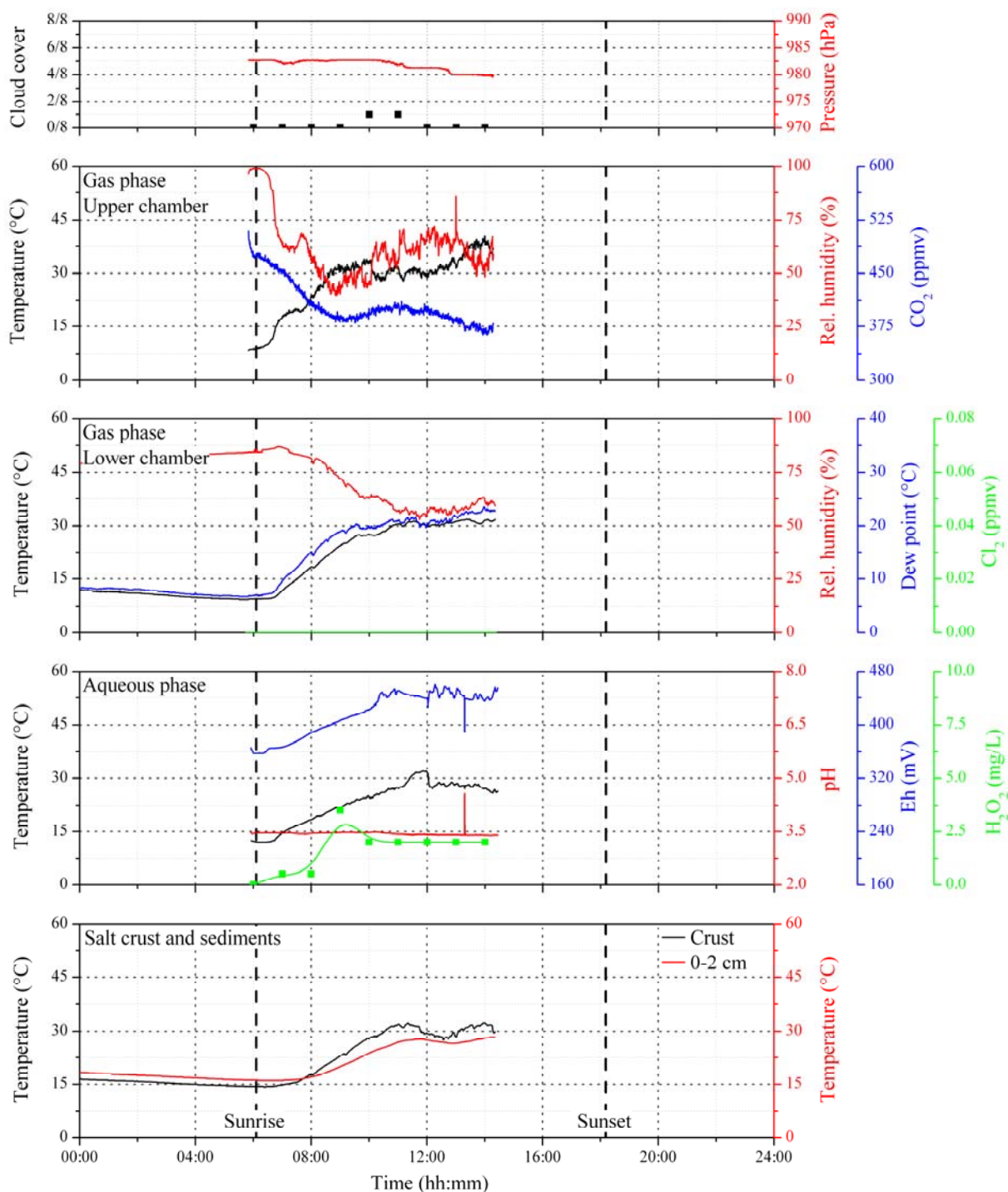


Figure 155. Data obtained during a PTFE chamber experiment at Lake Shot (S33.04610° E119.60968°), 22.03.2013.

Mean free chlorine concentrations 0.14 mg/L.

Mean bound chlorine concentrations 0.1 mg/L.

Lake Dune (S33.08285° E119.63913°), 23.03.2013

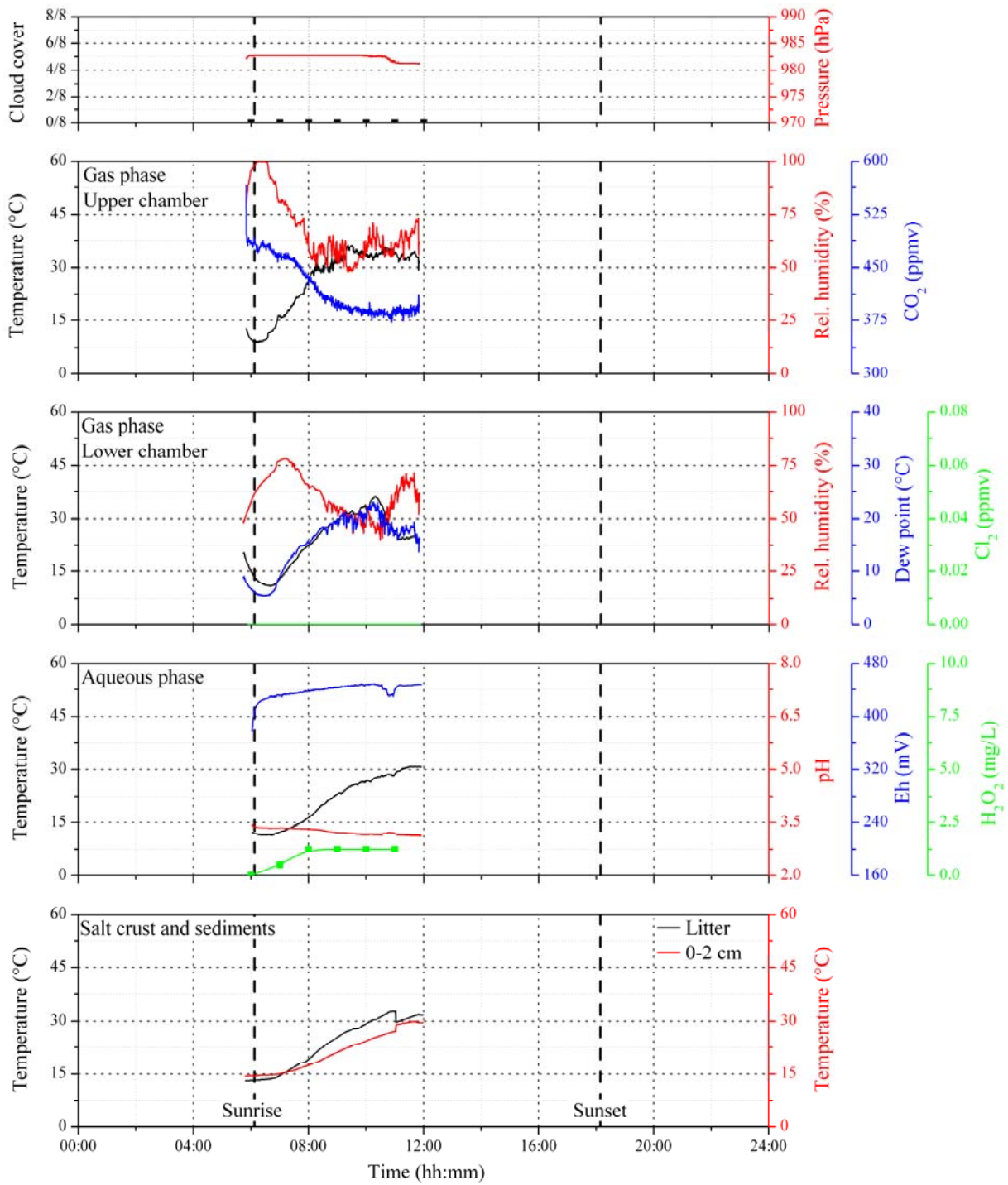


Figure 156. Data obtained during a PTFE chamber experiment at Lake Dune (S33.08285° E119.63913°), 23.03.2013.

Mean free chlorine concentrations 0.13 mg/L.

Mean bound chlorine concentrations 0.11 mg/L.

Lake Kathleen (S32.97411° E119.68320°), 24.03.2013

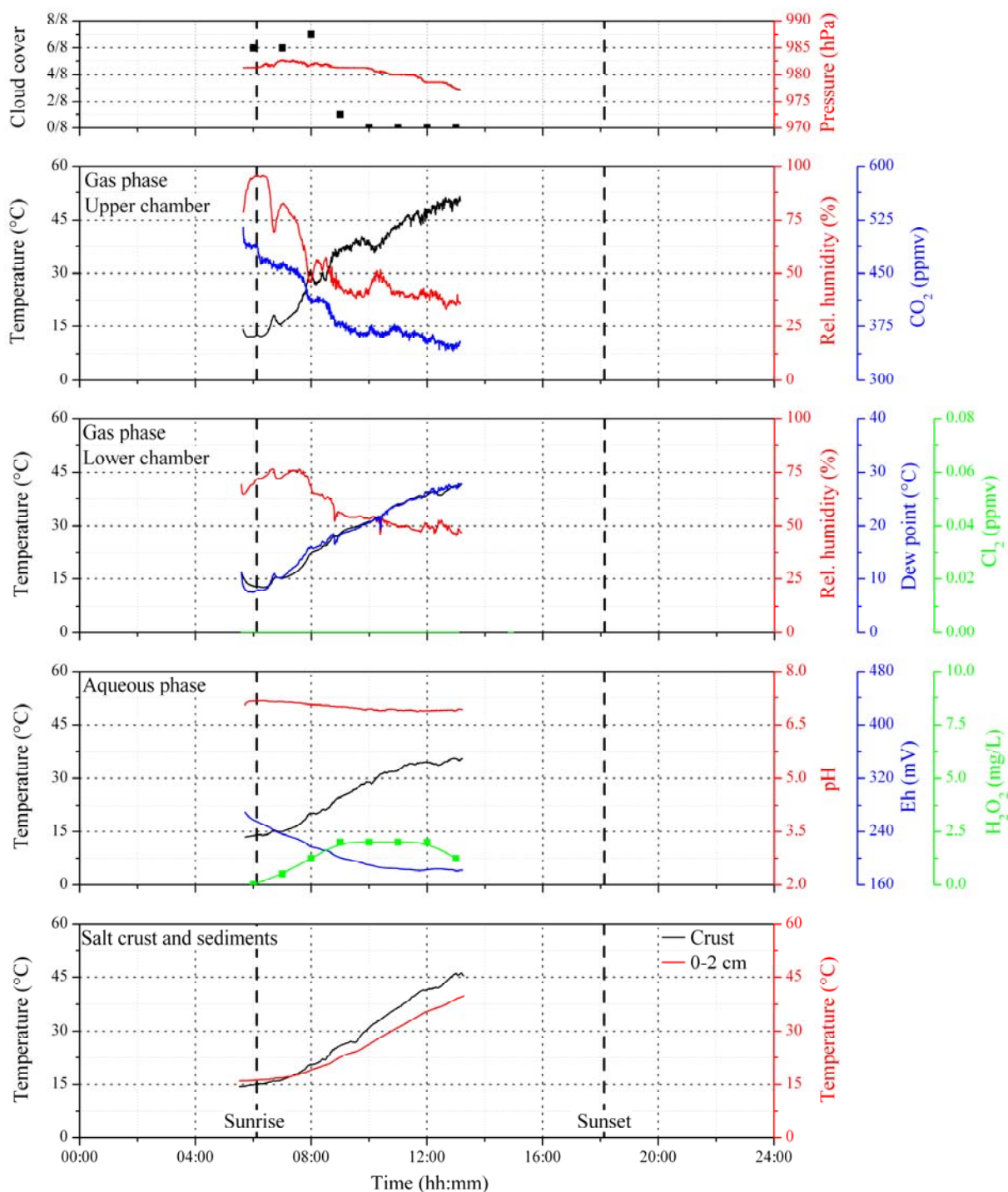


Figure 157. Data obtained during a PTFE chamber experiment at Lake Kathleen (S32.97411° E119.68320°), 24.03.2013.

Mean free chlorine concentrations 0.15 mg/L.

Mean bound chlorine concentrations 0.05 mg/L.

Lake Bean (S33.16311° E119.74404°), 29.03.2013

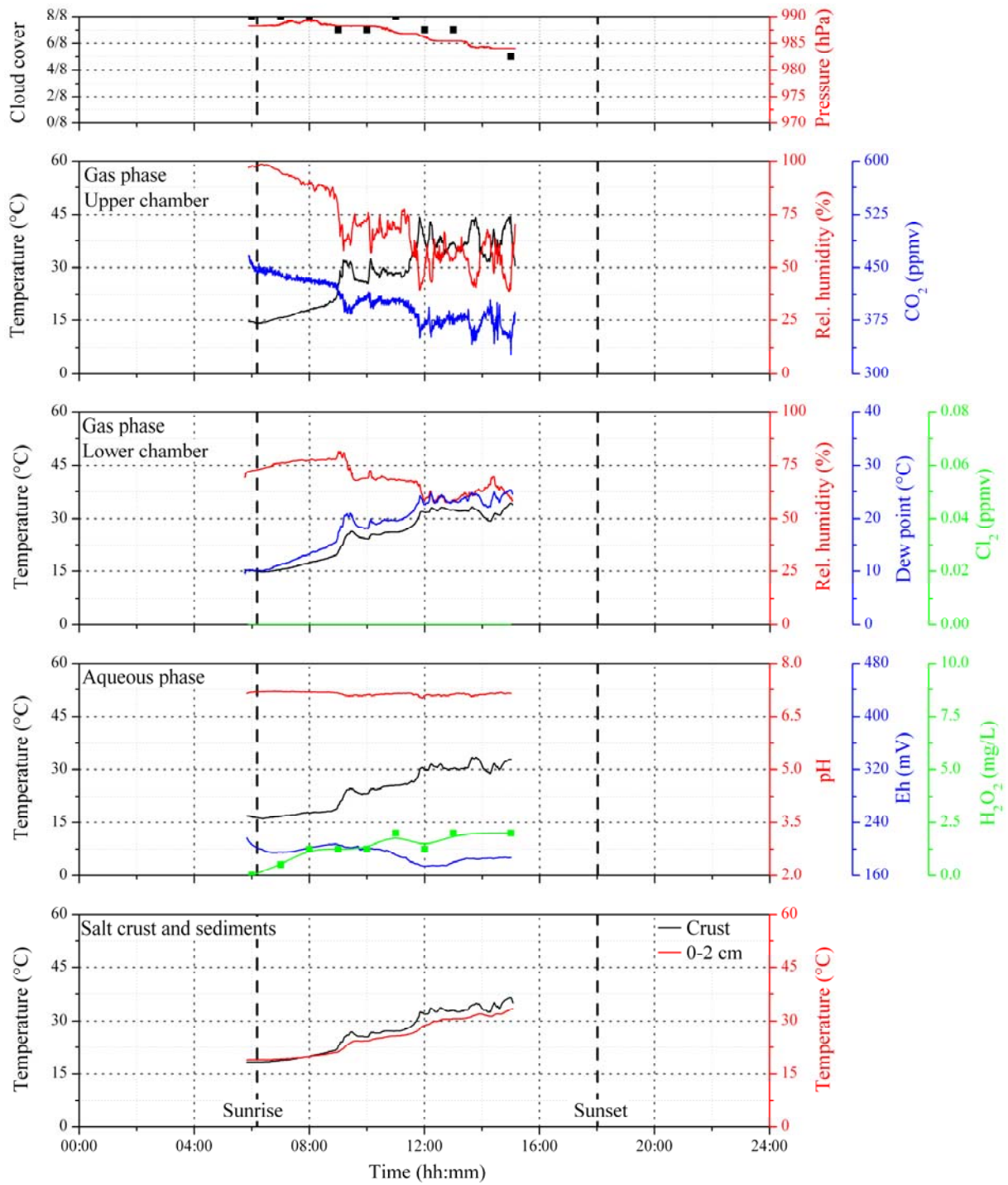


Figure 158. Data obtained during a PTFE chamber experiment at Lake Bean (S33.16311° E119.74404°), 29.03.2013.

Mean free chlorine concentrations 0.98 mg/L.

Mean bound chlorine concentrations 0.05 mg/L.

Acknowledgements

At this point, I want to thank everyone who helped me and worked in the background to make this work possible and as valuable to scientific research on hypersaline ecosystems as it now is.

First of all I thank Prof. Dr. Heinfried Schöler who made this work possible to begin with. He always helped with words and deeds when necessary and his knowledge on gas chromatography was invaluable for this work. Unforgotten will be our good collaboration during the Australian campaigns in 2011, 2012 and 2013, where we collected valuable samples to lay the foundation for this comprehensive study in hand. Furthermore, our discussions on the data triggered various fruitful ideas that led to new experiments and perceptions.

Prof. Dr. Peter Comba I thank for undertaking a second opinion.

I also thank my former and current co-workers. Firstly, I thank Dr. Stefan Huber and Ines Mulder from whom I learned so much on gas chromatography and who participated to create the improved purge and trap system. Dr. Sabine Studenroth I thank for her invaluable discussions on natural mechanisms, sampling and method development as well as IC measurements. I thank Christoph Tubbesing for sample collection at the Dead Sea and subsequent analysis on geochemical parameters. Tobias Sattler, whom I supervised as a student assistance, bachelor and master student I give my thanks for measuring the gas samples at Eliot Atlas in Miami.

Thanks to all of them for helping with processing and analysis of natural samples and revising this work at hand.

Special thanks to Dr. Stefan and Silvia Rheinberger as well as Dr. Christian Scholz for IC, ICP-OES and DOC measurements and their support for other analytical methods.

With regard to sample processing I thank all the involved Bachelor and Master students as well as our student assistances. In alphabetic order, these are Simon Benk, Svenja Bugla, Manuela Dolligkeit, Arnaud Hoffmann, Nadine Krieger, Lisa Krupp, Sabine Lippe, Markus

Merk, Nadine Palmer, Daniel Pfeif, Maik Rudloff, Birgit Sehls, Marcus Schneider, Markus Ubl and Carolin Wirth.

I would like to particularly thank Torsten Hoffman for his support with administration. Special thanks to Andreas Thum, Christian Mächtel and their apprentices from our workshop for constructing vital parts of the GC-MS purge and trap system as well as equipment for the field campaigns.

Within the sphere of HaloProc I give my special thanks to Dr. Stefan Wunderlich, Dr. Marion Kerscher, Kathrin Benzing and Prof. Dr. Peter Comba for providing us with the bispidine Fe^{2+} complex and lively discussions.

Also, unforgettable will be the sampling campaigns in Australia. A very special thanks to Dr. Wolfgang Junkermann and Dr. Jorg Hacker who introduced us to this interesting ecosystem. With this regard I thank Robert Holla, Stefan Schmitt, Dr. Johannes Ofner, Prof. Dr. Cornelius Zetzsch, Katharina Kamilli and Prof. Dr. Andreas Held, from whom I learned a lot about atmospheric chemistry in Australia and Bayreuth at the smog chamber. Also I thank Alexander Rücker, Pascal Weigold, Dr. Sebastian Behrens and Prof. Dr. Andreas Kappler who complemented our work by focusing on microbiologic life in these extreme environments. Furthermore, I give my thanks to all the other former and current HaloProc members not mentioned above as well as our guests at the spring and fall meetings who contributed to the valuable discussions and interpretations of this multifaceted work.

Concluding I give my special thanks to my growing family for all the support I got. In particular I thank my mother, father and brother who raised me to be scientifically interested but also to have a critical and independent mind. Special thanks I owe to my loving wife Marie Sophie for all her support and patience and also my thanks to her family who welcomed me with open arms. I like to thank my dog Lucky who accompanied me through this work and ensured that I had to step out into nature once everyday to refresh my mind. My new born daughter Emma Sophie I finally thank for always managing to bring a smile to my face even when I worked all day.